Faculty of Science and Engineering

Department of Chemical Engineering

Analysis of Natural Gas Hydrates using Inert Gases

Callum Conway Smith

This thesis is presented for the Degree of
Doctor of Philosophy
of
Curtin University

March 2017

To the best of my knowledge and belief this thesis contains no material previously published by any other person except where due acknowledgment has been made.

This thesis contains no material which has been accepted for the award of any other degree or diploma in any university.

Signature:

Date: 17/03/2017

Peer Reviewed Publications

1. Smith, C., Barifcani, A. & Pack, D., 2015. Gas Hydrate Formation And Dissociation Numerical Modelling with Nitrogen and Carbon Dioxide. *Journal of Natural Gas Science and Engineering,* pp. 1118-1128.

2. Smith, C., Barifcani, A. & Pack, D., 2016. Helium Substitution of Natural Gas Hydrocarbons in the Analysis of their Hydrate. *Journal of Natural Gas Science and Engineering,* pp. 1293-1300.

3. Sadeq, D., Iglauer, S., Lebedev, M., Smith, C. & Barifcani, A., 2017. Experimental Determination of Hydrate Phase Equilibrium for different Gas Mixtures containing Methane, Carbon Dioxide and Nitrogen with Motor Current Measurements. *Journal of Natural Gas Science and Engineering,* pp. 59-73.

4. Smith, C., Pack, D. & Barifcani, A., 2017. Propane, n-Butane and i-Butane Stabilization Effects on Methane Gas Hydrates. *The Journal of Chemical Thermodynamics,* pp. 293-301.

Acknowledgements

My earnest gratitude goes to my supervisor, Associate Professor Ahmed Barifcani, for his expert knowledge and continuous encouragement throughout the course of my research. I am extremely grateful for the very rewarding opportunity he has given me and for his dedication and enthusiasm towards our research.

I also wish to acknowledge Associate Professor David Pack, for his help and unfailing support. His guidance, insightful comments, dedicated efforts and knowledge regarding manuscript writing, manuscript preparation and uncertainty analyses have taught me so much about presenting my work professionally.

Shell Australia with their sponsorship and backing of this project have also been extremely influential towards what we've achieved. I wish to offer them my sincerest gratitude for their financial support, constructive feedback and project guidance. Our research would not have been possible otherwise.

Abstract

The presented research includes several individual studies which collectively investigate the hydrate phase behaviour of many natural gas components. All experimental hydrate research was performed using a cylindrical sapphire PVT cell where gas comes into contact with the aqueous phase to promote hydrate formation when subjected to favourable thermodynamic conditions. Pressure transmitters (±0.25 bar) and thermocouples (±0.075 °C) were implemented to measure the gas pressure and temperature respectively. Pressures from 30-200 bar were used for all experiments and the equilibrium temperature corresponding to the set pressure was determined by cooling the PVT cell.

Three experimental studies were performed with the PVT cell: methane-nitrogen/carbon dioxide hydrates, helium substitution of natural gas hydrates and methane-propane/i-butane/n-butane hydrates. The three-phase hydrate equilibria of methane-nitrogen/carbon dioxide demonstrated that nitrogen suppressed the hydrate equilibrium conditions and carbon dioxide promoted them. An empirical correlation was founded and describes the collective dilution and promoting influences of these additives with methane gas. The equilibrium data was applied with the Clausius-Clapeyron equation, giving values for dissociation enthalpies. It was concluded that the gas compressibility had too much of an impact when calculating values for methane – nitrogen hydrates, but enthalpies tended to increase with greater carbon dioxide concentrations. Pure methane hydrates were found to have a dissociation enthalpy of 60.0 (±0.6) kJ/mol. Methane–carbon dioxide hydrates with 7.0, 14.0 and 19.0 mol% carbon dioxide had values of 64.0 (±0.5), 64.7 (±0.7) and 68.1 (±0.4) kJ/mol respectively. The increasing magnitude of the dissociation enthalpy complemented the hydrate promoting behaviour of carbon dioxide with methane.

Hydrate phase equilibrium studies were also performed on a synthetic natural gas with components up to the pentanes. Individual substitution of the natural gas hydrocarbons with helium gave insight into the relative contributions of each component on the three phase hydrate equilibria of the original natural gas. Substitution of i-butane (M3) had the greatest effect on the equilibria, closely followed by propane (M2) – the remaining components had very little effect. A dissociation enthalpy of 120.7 (±0.4) kJ/mol was evaluated for the natural gas, M0. In contrast, the M2 and M3 natural gas had values of 91.5 (±0.4) and 99.9 (±0.8) kJ/mol respectively, indicating reduced stability in the absence of propane or i-butane. An experimental correlation was formulated with the collected equilibria. It established that when

applied to a natural gas with similar constituents, a respectable degree of accuracy could be achieved. Empirical constants were founded for each gas species and are proportional to the average extent of equilibria promotion. The constants were derived from an interpolation procedure, limiting the equation's reliability to the pressure range (30-180 bar) of the experimental data.

Propane, n-butane and i-butane were studied further by performing equilibrium experiments with methane-propane/n-butane/i-butane gas mixtures. Nitrogen was also added to one of each methane-hydrocarbon mixture to observe its dilution effect. Nitrogen's suppression was evident in all three scenarios. 16.0 mol% nitrogen with 5.0 mol% of propane was significant enough to be equivalent to a 4.0 mol% propane in methane mixture. Similarly, 19.0 mol% nitrogen with 4.6 mol% i-butane was equivalent to 4.0 mol% i-butane in methane. Hydrocarbon compositions less than 1 mol% in the presence of methane were tested to estimate when the hydrocarbon begins to contribute to the hydrate phase. The heat of dissociation was used as an indicator, which demonstrated n-butane in methane transitions from sI to sII from 0.5-0.75 mol%. Values had to be approximated for propane and i-butane mixtures because of the gas compositions available with the accessible equipment. Likewise, with the aid of computational equilibria, ranges of 0-0.1 and 0-(<0.1) mol% were approximated for propane and i-butane in methane respectively. Conclusively, i-butane and propane rapidly increase the stability of their hydrate with methane at very low compositions and become less sensitive as their compositions increase, leading to diminishing returns.

Nomenclature

Parameters

a	Empirical constant/Equation of state attraction parameter/core radius
b	Empirical constant/Equation of state repulsion parameter
A	Area/Equation of state factor/ Munck's equation constant
B	Formation volume factor/Equation of state factor/Munck's equation constant
C	Langmuir adsorption constant
d	Collective empirical constant
f	Fugacity
F	Fugacity when saturated
G	Gibb's energy
H	Enthalpy/Hydrate
H_{NG}	Henry constant for natural gas
J	Nucleation rate
k	Boltzmann constant
k_{ij}	Binary interaction parameter for species i with j
K	Kinetic factor
K_H	Henry's volatility constant
l	Fraction of empty lattice cavities
L	Liquid
m	Mass/Equation of state acentric factor contribution
M	Molar mass
n	Number of moles/data points
N	Stoichiometric ratio with respect to water
P	Pressure (or equilibrium pressure)
P_a	Partial pressure
r	Radius

R	Universal gas constant/Cavity radius
R_s	Solution gas-oil ratio
s	Standard deviation
S	Entropy
S_w	Water saturation
t	t-statistic
T	Temperature
V	Vapour/Volume
v	Molar volume/Cavities per mole of water
W	Work
x	Mole fraction of gas
y	Gas composition of water
z	Gas composition of hydrate
Z	Gas compressibility
α	Non-sphericity of gas molecule
γ	Activity coefficient
ε	Maximum Lennard-Jones potential
θ	Angle of contact/Fractional occupation
μ	Chemical potential
σ	Surface energy/Core distance when φ=0
φ	Porosity/fugacity coefficient/Lennard-Jones potential
ω	Acentric factor/ Lennard-Jones-Devonshire potential
Θ	Michelsen's correction factor

Superscripts

0	Reference point
driv	Driving force
eq	Equilibrium
H	Hydrate

P	Products
R	Reactants
sat	Saturation point
T	Total
α	Pure water state
β	Hypothetical empty hydrate lattice state

Subscripts

ave	Average
c	Critical point
C1	Methane gas
C1, ref	Methane gas reference
CO_2	Carbon dioxide gas
CO_2, ref	Carbon dioxide gas reference
d	Dissociation
ef1	Effective 1
ef2	Effective 2
eq,i	Equilibrium of species i
eq,i0	Equilibrium of species i when $x_i=0$
eq,ref	Equilibrium of a reference point
f	Formation
g	Gas
g,stp	Gas at standard temperature and pressure
h	Hydrate
l	Liquid
i,j	Species
N_2	Nitrogen gas
N_2, ref	Nitrogen gas reference
NG	Natural gas

o	Oil
PR	Peng-Robinson
r	Reservoir/Reduced
ref,i	Reference of species i
sol	Solution
SRK	Soave-Redlich-Kwong
sub	Sub-cooling
w	Water

Table of Contents

List of Figures

List of Tables

Chapter 1

1. Introduction

This thesis constitutes three experimental investigations, each with related agendas but are themselves separate works of research pertaining to natural gas hydrates. One study focused on the hydrate of nitrogen, carbon dioxide and methane. Another was associated with the hydrate of helium-substituted gas natural gas mixtures. The final study was concerned with propane, i-butane, n-butane in methane hydrates. The research presented contains new data and insights relating to hydrate stability, correlations and the relative influences of several hydrocarbons in a natural gas mixture on hydrate equilibria and stability.

The importance of natural gas hydrate research is outlined by the increasing frequency of which we now encounter gas hydrates. From process plants, natural gas and oil reservoirs, methane hydrate deposits deep beneath the earth's oceanic surfaces to the hydrates that inhabit comets, hydrate-related research has never been more important. Initially thought to be troublesome and a hindrance in natural gas pipelines, as discovered by Hammerschmidt (1934), researchers have discovered that there is potential for gas hydrates to have beneficial effects, such as natural gas storage (Sloan & Koh, 2008). However, a significant amount of study has been directed towards mitigating and characterising the phase behaviour of gas hydrates. The surge in scientific interest is demonstrated by an exponential increase in gas hydrate related research publications (Figure 1, data acquired from Google Scholar).

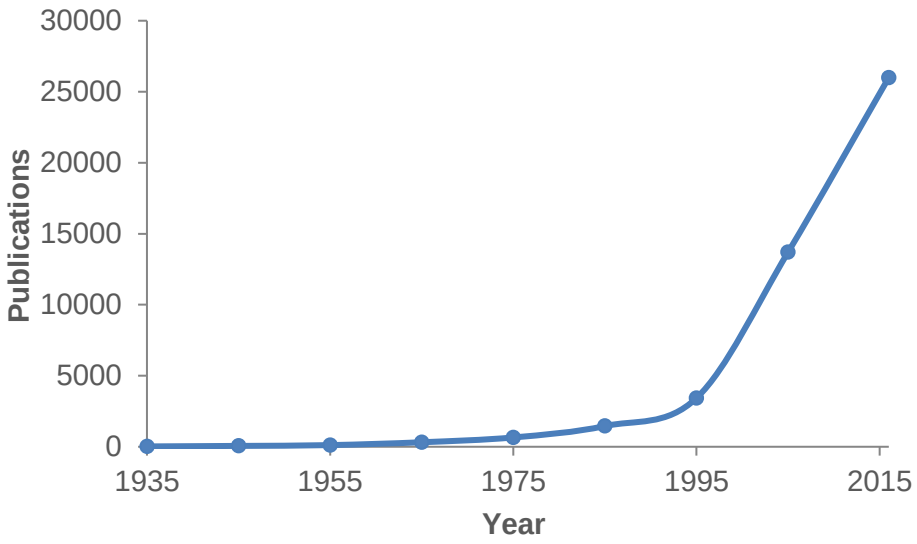

Figure 1 – Increasing Quantity of Gas Hydrate Publications

Gas hydrate research has many areas of study. These include but are not limited to, theoretical thermodynamic modelling, hydrate phase behaviour, thermodynamic, kinetic inhibition and antiagglomerants, hydrate formation and dissociation kinetics, hydrate physical and chemical properties, hydrate as a gas storage medium and many others. Research presented in this thesis is based primarily on hydrate phase behaviour with varying degrees of hydrate physical properties also provided. In particular, values for the dissociation enthalpy, which is an indication of hydrate stability, are given and discussed accordingly. Thermodynamic modelling of hydrate equilibria is mentioned numerous times throughout and is the centrepiece of Chapter 7. Several empirical correlations describing hydrate equilibria are offered as a possible alternative depending on the situation, and discussed with reference to common thermodynamic models.

1.1 Research Objectives

The initial goal of this research project was to focus primarily on the dilution effects of nitrogen and carbon dioxide on methane hydrate phase behaviour. An early completion prompted further study, one which would take a slightly different route and focus on examining which hydrocarbon components are contributing to the observed equilibria of natural gas and to what extent, using helium as a substituent to replace these components. Another phase of the project was introduced after the completion of this examination - one that follows on from the conclusions gathered from the natural gas study. Hydrates of propane, i-butane and n-butane in methane were of interest and ultimately studied.

Studying the dilution of methane with nitrogen and carbon dioxide and the effect on the resulting mixture's hydrate equilibrium profile was the primary interest of the first phase. The hydrate equilibria for all three gases have been well documented under varying conditions with a variety of equipment, but less of it is concerned with mixtures of these gases, particularly methane and nitrogen. The objective of this experimental phase was to observe and quantify the shift in equilibrium conditions upon addition of either nitrogen or carbon dioxide to methane. It would successfully demonstrate that nitrogen suppresses the equilibrium conditions when introduced to methane by reducing its partial pressure and that carbon dioxide is a promotor and helps stabilize the hydrate structure.

The next phase involved the analysis of a synthetic natural gas mixture from a hydrate perspective by substituting hydrocarbons with helium, a gas that is hydrate-inert. By using this substitution, the hydrate phase behaviour of the substituted gas can be

compared with that of the original gas. Substituting a hydrocarbon species with helium would permit the determination of whether that species had any contribution to the hydrate phase. The aim was to substitute all hydrocarbons one at a time and evaluate the components that stabilize and promote the hydrate phase. Additionally, the substitution process would simulate a typical separation process in a natural gas processing plant. It was possible to determine the hydrate phase conditions of the outlet stream using the helium substitution technique. With the collected hydrate equilibria, the stability of the hydrate would be calculated by the dissociation enthalpy, which is representative of stability. The Clausius-Clapeyron equation was used, which has not previously been applied to natural gas hydrates in the determination of their dissociation enthalpies. The final plan for this phase entailed an empirical correlation that summarises the individual contributions of hydrocarbons. Overall, it quantifies hydrate equilibrium temperatures and pressures as a function of initial composition.

The final experimental phase of the hydrate project extends from the conclusions made in the helium substitution study. Hydrates of methane mixed with propane, i-butane or n-butane were the focus and are investigative much like previous project phases. Very low compositions were considered to approximate the required concentration of added hydrocarbon (propane, i-butane, n-butane) to induce a hydrate crystal structure transition. The slope of the Clausius-Clapeyron equation gives an indication whether the structure type has changed, allowing the transition concentration to be approximated. Like the previous studies, the dissociation enthalpies for all methane-hydrocarbon hydrate were calculated to complement the phase equilibria.

1.2 Thesis Outline & Structure

The structure of this thesis constitutes four research-oriented chapters that capture the fundamentals of the research performed throughout the entirety of the research program. All four chapters relate to one another through the general theme of gas hydrate equilibrium. With this common theme, other relatable information was applied analytically, namely dissociation enthalpies, correlations, inhibiting and promoting effects and hydrate structure determinations.

Initially, the inhibiting and promoting influence of nitrogen and carbon dioxide on methane hydrates was of interest. Using an experimental setup to record hydrate equilibrium temperatures, the inhibiting/promoting effects could be quantified and represented empirically. Using this data, dissociation enthalpies were acquired and

provided a means of relating nitrogen/carbon dioxide composition to enthalpy, and therefore hydrate stability.

This process of acquiring equilibrium data and transcribing it to other useful parameters was then applied to natural gas mixtures. Given the greater complexity of such mixtures, it was necessary to develop a method of determining component inhibiting/promoting effects in the gas mixture without changing the relative concentrations of each gas species. Replacing a certain species with an equal concentration of helium (hydrate-inert) permitted the study of said component's influences on the natural gas's hydrate equilibrium state. This method was preferred over the method of determining that particular component's influence with a simple binary gas mixture with methane. Evaluation of a component's promoting/inhibiting effect in natural gas by experimenting with its binary mixture with methane does not involve all the various gas-liquid interactions in natural gas. These interactions are accounted for with helium substitution of a component in a natural gas sample.

Results from the investigation into helium substitution prompted further investigation into the major contributing gas species towards increased natural gas hydrate equilibrium temperatures. Propane, i-butane and n-butane were ultimately studied as binary gas mixtures with methane to establish the extent of their activity towards hydrate formation. The transition from structure I to II hydrate due to propane/i-butane/n-butane addition to methane is discussed and the minimum concentration (range) for a structural transition is investigated. Additionally, the concept of nitrogen dilution with the mentioned binary gas mixtures is discussed in accordance to experimental results.

To aid with interpretations of experimental hydrate equilibrium data, hydrate utilities implemented in Aspen HYSYS and Calsep PVTsim were consulted. The final research-oriented chapter focuses on the methods both programs employ with their respective hydrate utilities and discusses how their differing methods impact their predicted hydrate equilibria. Discrepancies are explored with respect to the selected equation of state, data sources and thermodynamic modelling. Collectively, these are the primary aspects that are referred to throughout the given arguments towards the degree of consistency between HYSYS, PVTsim and the presented experimental results.

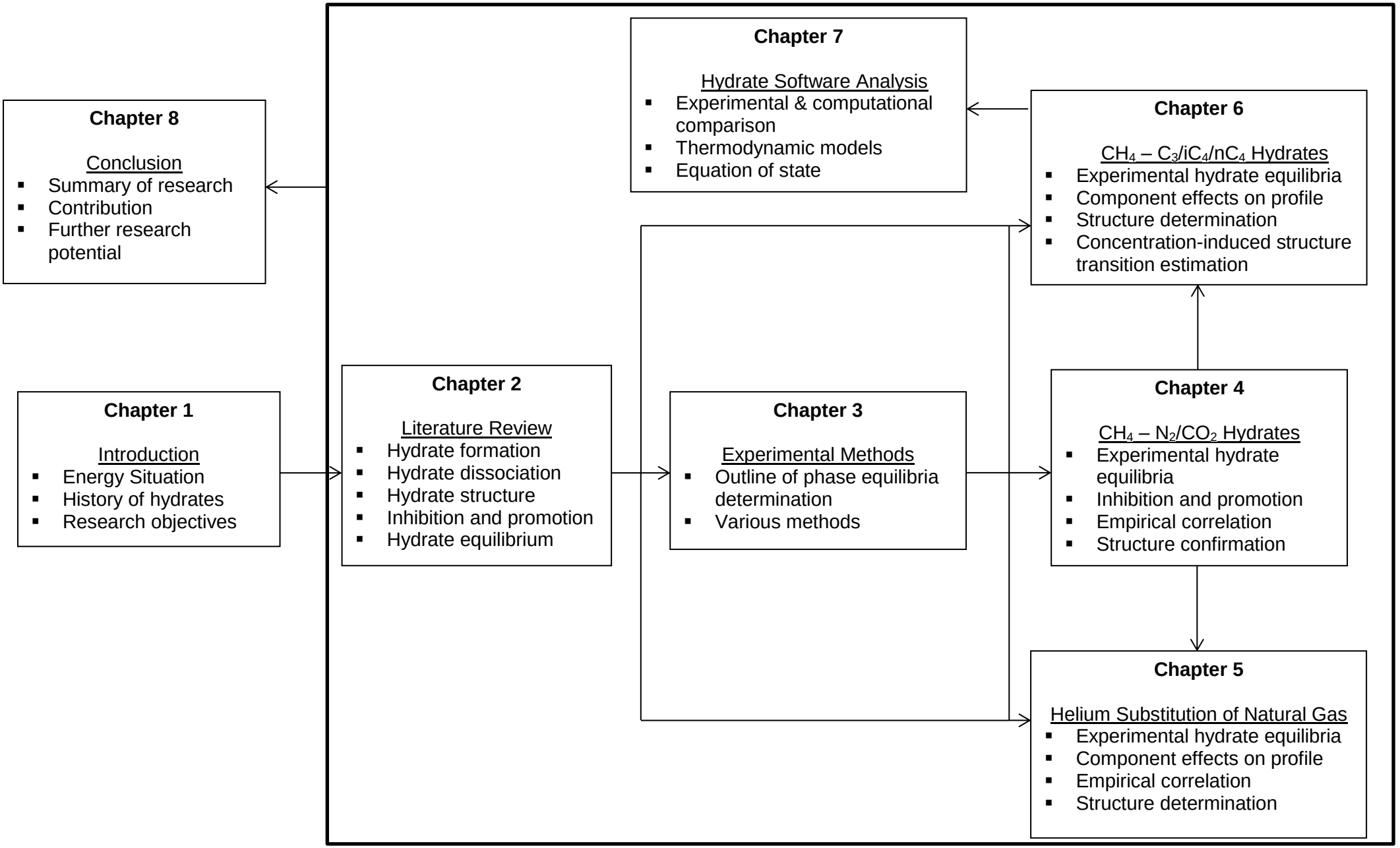
Chapter 7
Hydrate Software Analysis
Experimental & computational comparison
Thermodynamic models
Equation of state
Chapter 8
Conclusion
Summary of research
Contribution
Further research potential
Chapter 6
CH4 – C3/iC4/nC4 Hydrates
Experimental hydrate equilibria
Component effects on profile
Structure determination
Concentration-induced structure transition estimation
Chapter 1
Introduction
Energy Situation
History of hydrates
Research objectives
Chapter 2
Literature Review
Hydrate formation
Hydrate dissociation
Hydrate structure
Inhibition and promotion
Hydrate equilibrium
Chapter 3
Experimental Methods
Outline of phase equilibria determination
Various methods
Chapter 4
CH4 – N2/CO2 Hydrates
Experimental hydrate equilibria
Inhibition and promotion
Empirical correlation
Structure confirmation
Chapter 5
Helium Substitution of Natural Gas
Experimental hydrate equilibria
Component effects on profile
Empirical correlation
Structure determination

Chapter 2

2. Literature Review

2.1 History of Hydrates

Since the early nineteenth century, great efforts by researchers have gone into discovering what compounds form hydrates and what their physical and chemical properties are. The first documented case of clathrate hydrates was in 1810 by Sir Humphrey Davy who made note of chlorine hydrates. In a lecture to the Royal Society, Davy mentions that despite chlorine's capability of condensing and crystalizing at low temperatures, he observed that the freezing of a chlorine gas solution occurred more readily than pure water. Further studies primarily focused on qualitative work on the identification of hydrate-forming species. It was only until 1888 that it was discovered that small hydrocarbons of natural gas were hydrate-forming compounds. Of note are the works of Villard, who discovered that methane, ethane, ethylene, acetylene and propane can form gas hydrates (Villard, 1888; 1890). Table 1 summarizes some prominent hydrate research and findings since the discovery of their existence.

Table 1 – Gas Hydrate Research Milestones

Year	Research
1810	Sir Humphrey Davy discovers hydrates of chorine (Davy, 1811)
1823	The chlorine hydrate formula, $Cl_2.10H_2O$ is proposed by Faraday (Faraday, 1823)
1828	Bromine hydrates are discovered by Löwig (Löwig, 1828)
1829	SO_2 hydrates ($SO_2.7H_2O$) are confirmed
1882	Hydrate of CO_2 is discovered
1877-1882	Discovery of hydrates of various $CO_2 – PH_3$ and $H_2S – PH_3$ mixtures
1884	The change in slope for the pressure-temperature equilibrium line for chlorine hydrates is described at 273 K by Le Chatelier
1888	Villard observes hydrates of methane, ethane, ethylene, acetylene and nitrous oxide (Villard, 1888)
1890	Villard discovers hydrates of propane (Villard, 1890) and advises that the lower quadruple point decreases when the molecular weight of the guest molecule increases.
1896	Villard proposes that nitrogen and oxygen can form hydrates. Measures hydrates of argon (Villard, 1896)
1897	Hydrates of various halohydrocarbons mixed with acetylene, CO_2 and ethane are discovered by de Forcrand and Thomas (deForcrand & Thomas, 1897)
1902	The Clausius-Clapeyron equation is used for the first time to calculate hydrate heats of formation and compositions by de Forcrand (de Forcrand, 1902)
1923	Hydrates of krypton are discovered and measured by de Forcrand (de Forcrand, 1923)
1925	Hydrates of xenon are discovered and measured by de Forcrand (de Forcrand, 1925)
1934	Hammerschmidt discovers natural gas hydrates in transmission lines as the source of pipeline blockage (Hammerschmidt, 1934)
1946	Deaton and Frost detail hydrate equilibrium data for unary and binary gases. Prevention of formation is also presented (Deaton & Frost, 1946)
1951	The structure II hydrate unit crystal is confirmed by von Stackelberg and Müller (von Stackelberg & Müller, 1951)

1952	The structure I hydrate unit crystal is confirmed by Claussen and Polglase (Claussen & Polglase, 1952)
1959	van der Waals and Platteeuw (vdWP) propose a statistical thermodynamic approach in determining hydrate equilibria (van der Waals & Platteeuw, 1959)
1963	McKoy and Sinanoglu implement Kihara potentials into vdWP theory for better accuracy (Mckoy & Sinanoglu, 1963)
1965	Natural Gas hydrates discovered in Siberian permafrost (Makogon, 1965)
1966	First NMR measurements of hydrates performed by Davidson
1969	The first measurements of hydrates in geology are performed by Ginsburg (Ginsburg, 1969)
1972	The vdWP theory is used with natural gases by Parrish and Prausnitz (Parrish & Prausnitz, 1972)
1976	Studies of three and four-phase equilibria with liquid hydrocarbons are performed by Ng and Robinson (Ng & Robinson, 1976b)
1980	The first pulsed NMR measurements of hydrates are conducted by Ripmeester and Davidson (Ripmeester & Davidson, 1980)
1982	Molecular dynamic simulations are performed by Tse and others
1984	Calorimetry studies including heat capacity and heat of dissociation are instigated by Handa and co-workers (Handa, et al., 1984)
1985	The vdWP theory is extended by the premise of coordination shells by John and Holder (John & Holder, 1985)
1987	The new hydrate structure H is discovered by Ripmeester and co-workers (Ripmeester, et al., 1987)
1988	Gas hydrates are measured *in situ* by Makogon (Makogon, 1988)
1994	Mehta and Sloan gather sH hydrate experimental data. Apply the vdWP model to CH_4 + large guest molecule mixtures (Mehta & Sloan, 1994)
1996	Hydrate composition and hydration number, n, is measurements using Raman spectroscopy are performed by Sum
1997	First findings of double cavity occupancy of Nitrogen in $5^{12}6^4$ cage of sII hydrates by Kuhs and co-workers (Kuhs, et al., 1997) A new high pressure (600 Mpa) phase of methane hydrate is discovered by Dyadin et al. (Dyadin, et al., 1997)

1999	Dyadin et al. also discovers that hydrogen and neon form hydrates at very high pressures (Dyadin, et al., 1999)
2006	The first *in situ* Raman spectroscopy measurements are performed off Vancouver Island by Hester et al. (Hester, et al., 2007)
2013	First production of methane gas from deep-water methane hydrate deposits in Japanese waters as part of the MH21 methane hydrate research and development program

Equally important research has been conducted in establishing their equilibria, particularly with today's issues associated with the blocking of pipelines by hydrates and their associated safety hazards. Since Hammerschmidt's discovery of natural gas hydrates in pipelines, work on establishing the thermodynamic conditions that define hydrate formation has been pursued by many researchers. Due to the high transmission pressures and often cold underground and oceanic temperatures, hydrates were and remain a huge problem. The need for data on exact hydrate forming conditions were in demand so that appropriate action could be taken to prevent further issues associated with pipeline blockages caused by hydrates. The experimental work by Deaton and Frost on pure methane, ethane and propane as well as mixtures with heavy components was the first extensive research on pure component hydrate equilibrium conditions (Deaton & Frost, 1946). Such work is still being produced today, particularly with respect to the shift in hydrate equilibrium conditions with doses of thermodynamic inhibitors and various aqueous phases.

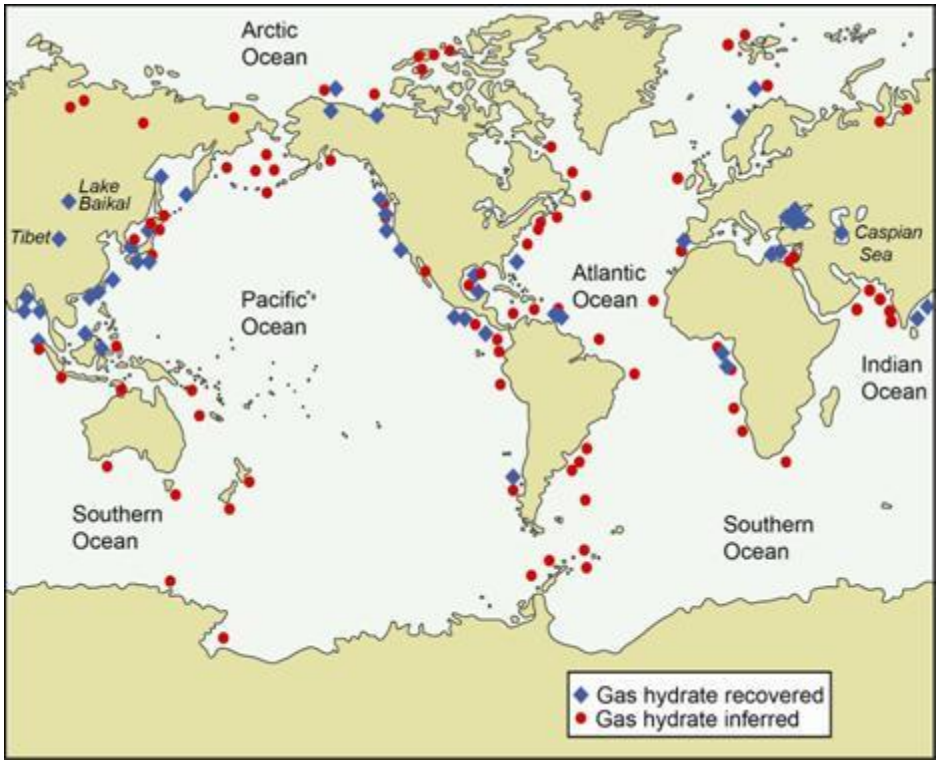

Figure 2 – Locations of Natural Gas Hydrate Deposits (USGS, 2014)

As of fairly recent history, hydrates have been discovered in nature, mostly in permafrost and deep-sea sediments that have likely existed in an unchanged state for many millions of years. Hydrates have since been discovered in other regions of the universe, such as planets and moons (Sloan & Koh, 2008). Hydrates in nature were discovered in 1965 by Makogon in a Siberian permafrost, and were identified as a possible source of energy (Makogon, 1965). It has been discovered that the clear majority of natural gas hydrate deposits compose of methane gas hydrate. Methane gas has now been recovered from many marine sediments all over the globe, particularly in the northern hemisphere amongst the coasts of Europe (Figure 2). Some deposits have also been located onshore. Of note are the sediments beneath large lakes such as Lake Baikal, the world's largest freshwater lake. Discoveries of hydrate are common in permafrosts because they are favourable for the collection of methane hydrate due to their depth below sea which conserves pressure and have cold temperatures, both of which promote hydrate stability. These stable conditions have ensured their formation and existence for millions of years.

2.2 The Current Situation

The demand for energy continues to rapidly rise with the increasing population and economic and social development. Higher energy demands have led to a doubling of world energy production and a 300% increase in natural gas production since the

early 1970s (Figure 3). Natural gas is the fastest growing energy source in the world and is considered the most flexible of all fossil fuels. Its energy can be accessed directly by combustion, or it can be converted to diesel and other carbon products such as petrochemicals, fertilizers, chemicals and paints. The processing of natural gas and the manufacturing of natural gas products is also relatively greener than other fossil fuels, emitting far less greenhouse gases and pollutants. With the increased demand for energy, the fast decline in crude oil reserves and the relatively recent realization of the potential for natural gas, attention towards the recovery and utilization of natural gas is on the rise.

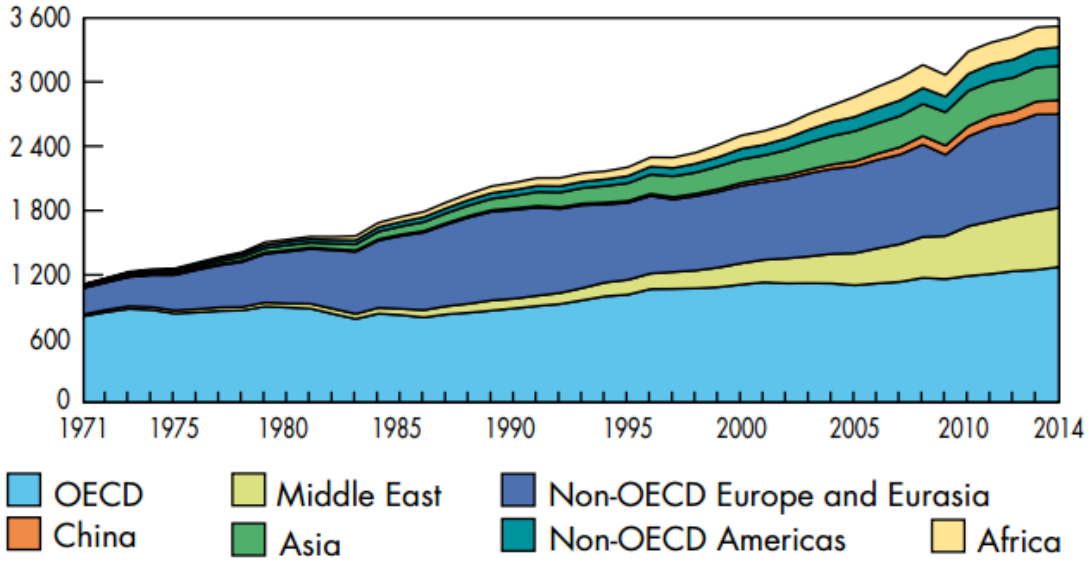

Figure 3 – Natural Gas Production (in billion cubic meters) (IEA, 2015)

Natural gas is constituted primarily of a mixture of light and intermediate hydrocarbon compounds as well as other more complex hydrocarbons. It is commonly believed that natural gas and oil are generated by organic debris that have been embedded deep below the earth's surface. Over the course of millions of years, the organic matter is exposed to intense pressure and temperature conditions, causing the gradual transformation to coal, oil or gas. Methane is by far the most abundant hydrocarbon, and is usually present in compositions between 70 and 90 mol%. Other common hydrocarbon constituents include ethane, propane, isobutane and n-butane, with their compositions often declining based on their molecular weight. In addition to hydrocarbons, natural gas also contains impurities. Commonly encountered impurities include nitrogen, carbon dioxide, hydrogen sulphide and water, all of which have negligible effects on calorific value. Carbon dioxide and water can cause corrosion and hydrogen sulphide is toxic, so it is important that impurities are removed

quickly, for safety and processing purposes. Strictly speaking, natural gas is composed of compounds that remain in the gaseous state at standard temperature and pressure (STP) (Chandra, 2006).

According the United States (U.S.) Energy Information Administration (EIA), the estimated proven natural gas reserves in the world is 6973 trillion cubic meters (tcm) as of 2014. A very large proportion of reserves are located in Eurasia and the Middle East, accounting for approximately 31.2% and 40.3% of the world's reserves respectively. Russia, with proven reserves equating to almost a quarter of global reserves (24.2%), and Iran with 17.1%, are estimated to have the largest proportions, while Asia and Oceania combined hold only 7.7%. However, out of a total 121.3 tcm produced in 2013, Asia and Oceania were associated with 14.6% of the world's production of natural gas. The U.S. and Russia were amongst the biggest producers, totalling 20.1% and 18.3% respectively, despite the U.S.'s mediocre reserves (4.85%). Unsurprisingly, the U.S. is the biggest consumer of natural gas, with an estimated 21.6% of the 121.4 tcm consumed by the world in 2013. Interestingly, Asia and Oceania are almost on par with North America (dominated by the U.S.), consuming 19.5% compared to 26.5% (Table 2).

Table 2 – Global Reserves, Production and Consumption of Natural Gas (EIA, 2015)

	Reserves (2014)		Production (2013)		Consumption (2013)	
	tcm	%	bcm	%	bcm	%
North America	422	6.05	31103	25.64	32103	26.45
Central & South America	278	3.98	5944	4.90	5519	4.55
Europe	136	1.95	9982	8.23	18512	15.25
Eurasia	2178	31.24	29357	24.21	21945	18.08
Middle East	2813	40.34	19831	16.35	15078	12.43
Africa	606	8.69	7328	6.04	4573	3.77
Asia & Oceania	540	7.75	17738	14.63	23627	19.47
Total	6973	100	121283	100	121357	100

Recent estimates indicate that natural gas is responsible for roughly 23% of the world's energy consumption (Wang & Economides, 2009). With the world relying heavily on natural gas energy, it is vital that its transportation and distribution meet the global demand as safely and effectively as possible without exposing the environment to unnecessary risk. Transporting natural gas is still one of the primary challenges in natural gas production today, where the transmission of gas over very long distances is required. There are two primary methods of transportation: pipeline networks and as liquefied natural gas (LNG), with pipelines accounting for 70% of natural gas transmission (Wang & Economides, 2009). Pipelines may be referred to as onshore, where they can be laid above ground or buried underground, or as offshore pipelines, in which the pipeline system is submerged underwater.

2.3 Pipeline Failure

Transportation of natural gas via transmission pipelines is safer than other methods of transport. However, failure of a pipeline can have disastrous consequences. Such a failure can result in loss of life, environmental damage, personal injury, property damage and loss of product. Natural gas pipeline failure incidents are relatively infrequent considering the complexity, mileage and scope of transmission networks. In the U.S. during the 3-year period from 1999 – 2001, natural gas pipeline accidents resulted in an annual average of 6 deaths, 10 injuries and $20 million in property damage (TRB, 2004). The European gas transmission network, which totalled almost

90,000 miles as of 2011, experienced 1,246 incidents throughout the 40-year period 1970 – 2010 (EGIG, 2011). Only 7 of these incidents involved fatalities, 2 of which were associated with the public. Although pipeline failures can result in serious injury or death, such events are relatively rare.

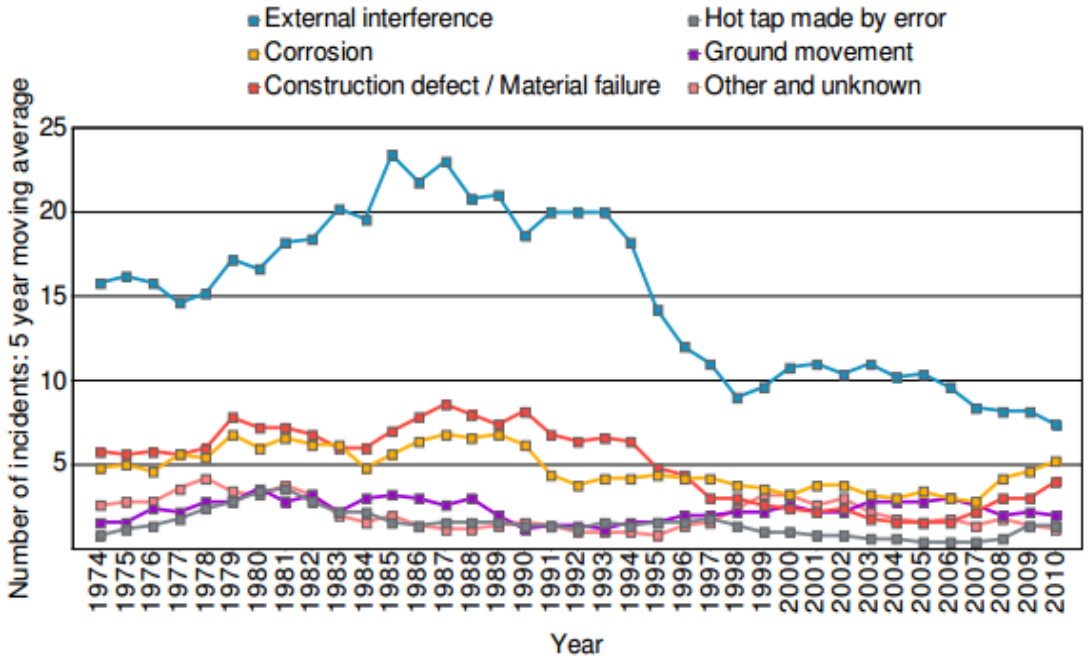

Figure 4 – Natural Gas Transmission Pipeline Incidents in Europe (EGIG, 2011)

These incidents were attributed to external interferences, accounting for roughly 50% of all cases, as depicted in Figure 4. Third party external interferences are more difficult to prevent because they are not associated with the technical design of a pipeline like so many other causes of failure are. For example: events such as vandalism, bulldozing, excavating and digging are all capable of causing damage to a pipeline, and are difficult to control. Incidents caused by external influences have declined in the 20 years, but remain the primary cause. Other sources of accidents have remained relatively constant, with construction defects and material failures declining. Because of the exponential growth in technology and scientific advances, more reliable and efficient design procedures, practises and testing ensure better quality manufacturing and construction.

2.3.1 Hydrate-Facilitated Corrosion

The corrosion of pipelines is also a major source of failure, and occurs internally and externally, causing thinning of the pipe wall making it vulnerable to cracking and bursting. Corrosion can be defined as the degradation of a material (usually of a

metallic nature) or of its functional properties through a chemical reaction with the environment (Landolt, 2007). The environments where pipelines are installed are often corrosion-inducing, and range from the highly corrosive medium in the upstream gas pipelines, where hydrogen sulphide and carbon dioxide are dissolved in multi-phase fluids, to the milder external environments where soil and coating properties influence the severity of corrosion (Cheng, 2015). Recent developments indicate that the presence of enclathrated methane, carbon dioxide and hydrogen sulphide in the form of early-stage hydrate formations have the ability to participate in the corrosion of the pipeline's internal surface (Obanijesu, et al., 2011); (Obanijesu, et al., 2011). Obanijesu and co-workers constructed a model, and calculated that the corrosion rate due to hydrates could be as high as 174 mm/yr (0.48 mm/day), which would cause wall rupture within days (Obanijesu, 2012). Corrosion is therefore of paramount importance in the design of natural gas pipelines.

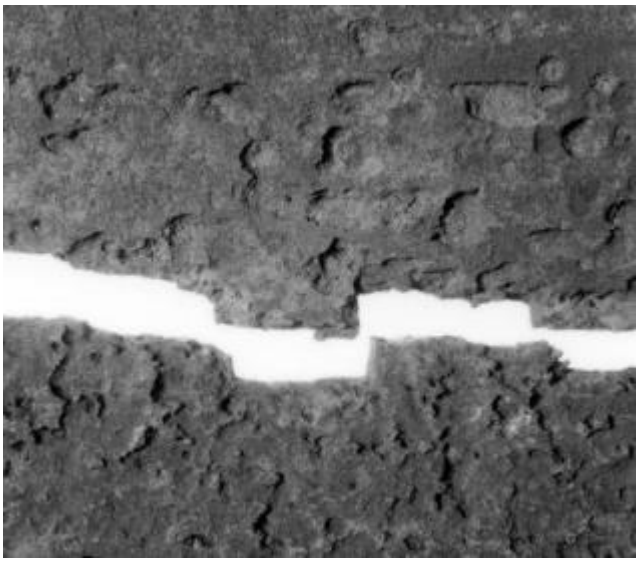

Figure 5 – Internal Surface of Pipeline from Corrosion (Dahlberg & Bruno, 1985)

Internal corrosion typically attacks the base of the pipeline surface due to gravity, although water may condense on the top of the pipeline, causing top-line corrosion. Figure 5 is an example of the extensive damage pitting corrosion inflicts on pipeline walls, where the thickness of the pipe wall is observably reduced. In this instance, the pipeline failed soon after the operating pressure of the system was elevated (Dahlberg & Bruno, 1985).

There are several approaches towards the mitigation of pipeline corrosion. By far the most common preventative measure is the selection of the appropriate materials. The

majority of pipelines utilize some form of carbon steel, although alloy steels are sometimes implemented in some environments as well as cast iron. In recent times, non-metallic materials have even been employed in the construction of pipelines, and have proven to be effective as liners in the restoration of failed piping instead of trenching and replacement (Garverick, 1994). Another effective means of prevention is the use of protective coatings and linings. Coatings are commonly dielectric materials and usually have properties which provide electrical insulation and/or act as a moisture barrier, thereby preventing the electrolytic discharge of current from the metal pipe (Hatley, 1969).

Hydrate inhibitor chemicals may also be injected into the pipeline to reduce the possibility of hydrate-induced corrosion occurring. Without flowing hydrate formations, internal corrosion of the pipeline via hydrate cannot occur (Obanijesu, 2012). Obanijesu et al. also demonstrated that some corrosion inhibitors exhibited tendencies to aid the formation of hydrates. Inhibitors including 2-mercapto pyrimidine (MP), Cetylpyridinium chloride (CPC), Dodecylpyridinium chloride (DPC), Thiobenzamide (TB) and Benzyl dimethyl hexadecylammonium chloride (BDHC) were investigated as hydrate promoters. All the mentioned chemicals are surfactants which generally tend to behave as hydrate promoters. Apart from DPC, at 500 ppm in pure water, each corrosion inhibitor elevated the hydrate equilibrium temperature from 0.5-0.8 °C. DPC was a more efficient promoter and increased hydration conditions by approximately 1.5 °C. Given the unfortunate relationship between some corrosion inhibitors and the promotion of hydrates from an aqueous phase, this is more reason to investigate alternative methods for their inhibition, and dissociation in the event of their formation.

2.3.2 Material Failure

There are over 1.8 million km of natural gas pipelines currently transporting natural gas supplies to all corners of the world (CIA, 2013). Statistically speaking, it is not surprising that some may experience material failure, of which there are several factors that may be responsible. One of the primary causes of material failure is the construction quality, which when left unchecked or unnoticed during testing, ultimately leads to that particular component's failure. Defects of a component or pipe body are almost always discovered during the testing stages or upon inspection, but should they remain under the radar, failure is almost certain not long after installation.

Material failure due to internal corrosion, induced by the introduction of unwanted liquids into the pipeline as well as particulate matter and foreign particles causing

internal erosion can also occur. Pipeline bends in particular are at risk of eroding because of the constantly impacting solid particles that occur at non-linear pipeline sections. Unwanted fluids and particles can come from dehydration liquids, compressor sealant, process plant upset conditions and sand/dirt produced with the reservoir fluid. Control of these influences on the integrity of pipelines is of paramount importance, as the consequences of pipeline and material failure are great.

Figure 6 – Devastation from Material Failure of a Pipeline (Wittenstein & Wolfson, 2010)

In 2010, a PG&E natural gas pipeline in San Bruno, California, ruptured causing a large explosion resulting in a fireball that rose 30 meters from the blast site (Figure 6). The resulting fire burned over 10 acres of land, destroyed over 50 homes and caused the death of 8 people with many more injured (Wittenstein & Wolfson, 2010). It was discovered that there were at least 26 leaks on the Milpitas-to-San Francisco pipeline from 1951 to 2009, none of which were confirmed or rectified by PG&E. After investigation of the incident, many of the leaks were found to be caused by defective welds on longitudinal seams (Peekma, 2013). PG&E only conducted tests that involved cheap methods, which were best suited at detecting corrosion rather than leaks. Longitudinal seam defects remained in service from 1948, adding to the risk of failure. This is a prime example of how material defects and human error largely contribute to pipeline incidents and the importance of professional testing, inspection and maintenance procedures.

Material failure due to hydrate formation is also a real possibility given the presence of free water. Free water is unfortunately a common occurrence in the recovery of

petroleum fluids and can prove to be extremely hazardous on a number of levels. The major consequences of free water production include a reduced natural gas recovery rate (which is largely unavoidable), internal corrosion acceleration and the risk of natural gas hydrate formation. Gas hydrate formation in pipelines is particularly dangerous because of their tendency to agglomerate and form larger solids that hamper production and plug the pipeline. Valves and instrumentation are particularly vulnerable – damaging them can lead to equipment failure and ultimately result in the loss of fluid containment. Another cause of free water occupying the transmission pipeline system is inadequate drying of the produced fluids. Pipelines are also hydro-tested with water before their commissions, and if not properly dried, water may remain in the installed pipeline section and result in hydrate formation. With today's operation of pipelines at increasingly higher pressures, even slight remnants of free water can be disastrous due to the consequences of hydrate formation. The likelihood of this occurring is especially high at pressure reduction stations where pressure reductions up to and exceeding 8 Mpa are a possibility. Because of the significant reduction in pressure, the accompanied large decrease in flowing gas temperature drastically increases the likelihood of hydrate formation. The presence of hydrates in transmission pipelines is unfortunately a real possibility and is often likely due to the mentioned reasons. In the interest of safer natural gas production and transmission, as well as more extensive knowledge regarding their characterisation and dissociation tendency, research into their prevention and physical properties is therefore highly beneficial.

2.4 Hydrates and the Environment

The influence of hydrates on the environment has been a difficult area of study, most of which focuses on the evolution of methane, a greenhouse gas, from its decomposing hydrate. One of the main challenges in assessing their impact is the continued uncertainty regarding the size of the global gas hydrate inventory and the quantity that is in danger of becoming destabilized. It has been estimated that $7x10^2$ to $1.27x10^4$ Gt of carbon is sequestered in oceanic gas hydrates (Dickens, 2011). In fact, the minimum global gas hydrate inventory is estimated to be ~$1.8x10^3$ Gt of carbon, which equates to ~$3\ x10^{15}$ m^3 of methane (Boswell & Collett, 2011). Current atmospheric methane levels are approximated to be ~1780 ppb (NOAA, 2015). If just 0.1% of the estimated global inventory is decomposed, methane concentrations in the atmosphere would increase to ~2900 ppb (IPCC, 2007). The stability of marine gas hydrates is therefore of interest for the well-being of the environment, particularly with climbing temperatures that increase the risk of hydrate decomposition.

2.4.1 Geological Locations

Methane hydrate deposits are known to occur in several different types of geological locations, all of which have different susceptibilities to hydrate decomposition. One of the rarer locales for hydrate deposition is onshore permafrosts, which account for less than 1% of the global hydrate inventory (Ruppel, 2011). Most onshore permafrost sediments are stable, even in warmer climates, as the majority are formed at depths in the hydrate stability zone. However, rare instances of shallow hydrates are known to exist at ~250 m within the permafrost and may be susceptible to destabilization in warmer climates. Chuvilin, et al. (1998) and others have suggested that hydrates may be present at very shallow depths of ~20 m as a result of regional ice cover formation which has trapped gas, some of which has formed hydrates. These shallow gas hydrates are particularly vulnerable to temperature increases.

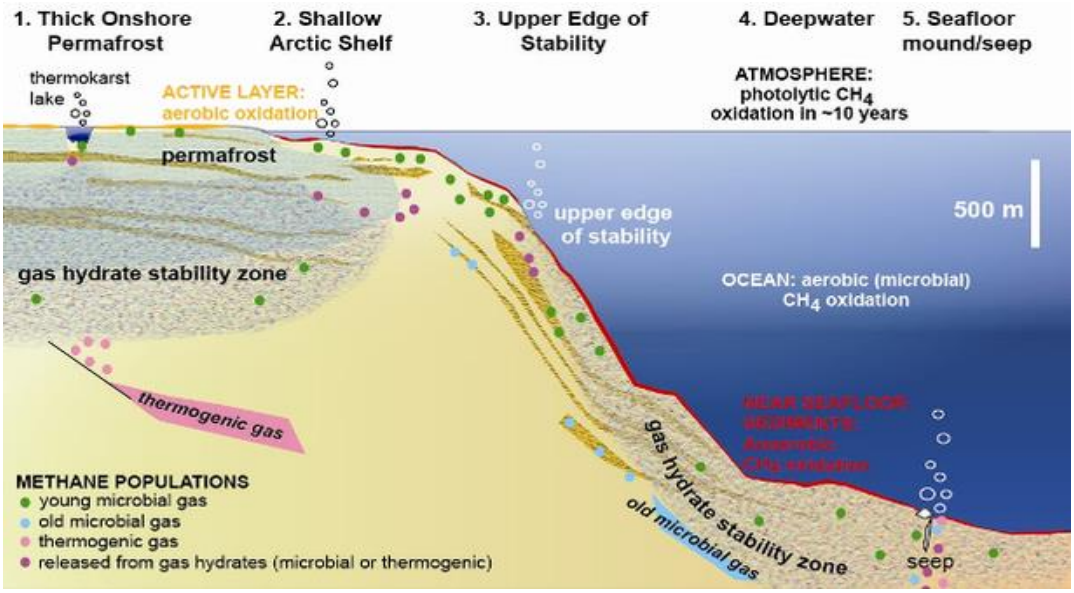

Figure 7 – Methane Hydrate Geological Locations (Ruppel, 2011)

Subsea permafrosts in shallow continental shelves of the Arctic Ocean make up a tiny fraction of natural gas hydrates (<0.25%), and have been present since Pleistocene times (12000-2.6 million years ago) (Ruppel, 2011). It has been estimated that some subsea permafrost hydrate has dissociated due to increased temperatures from this time period, leading to possible thawing of subsea permafrosts (Rachold, et al. 2007). Increasing pressures from higher sea levels act to counter the temperature increase, however, this pressure rise is marginal and not likely to ensure hydrate stability (Ruppel, 2011).

Deepwater gas hydrates constitute ~99% of the natural gas hydrate inventory, the majority of which is stable and not in danger of dissociating. Very high pressures and

freezing temperatures ensure that hydrates remain in the thermodynamically favourable zone, prevent instability. However, a small percentage (~3.5%) of deep-water hydrate exists at the upper bound of the hydrate stability zone in shallower (<500m) waters. The stability zone lies roughly in line with the seafloor, making upper continental slopes the most likely geographical location for a climate change to influence hydrate stability in these deposits (Ruppel, 2011). In the instance where methane evolves from its hydrate state, a large portion of methane gas bubbles will dissolve in the sea water or possibly oxidize, preventing the escape of methane into the atmosphere. In fact, dissolved oxygen and nitrogen almost entirely replace methane in liberated methane gas bubbles at depths greater than 90 meters (McGinnis, et al., 2006). McGinnis and co-workers (2006) note that this phenomenon occurs to a greater extent with depth, and calculates that less than 1% of the original methane gas in a bubble remains when it reaches the surface.

Gas hydrates have also been discovered in large mounds on the seabed and in shallow seafloor regions. They constitute only a trace amount of natural hydrates, but are capable of liberating methane gas very easily. Local fluctuations in water temperature can be triggered by the discharge of warm fluids from the seabed, naturally promoting methane evolution from the hydrate deposit (MacDonald, et al., 2005). During his tests, Macdonald, et al. (2005) noticed that water temperatures increased as much as 3 °C at the seafloor in the vicinity of the hydrate mound over a 20-day period. Such an increase can very easily change the thermodynamic stability of the hydrate deposit.

2.4.2 Global Warming and Methane Hydrates

Methane is a potent greenhouse gas, and has a greenhouse effect approximately 20 times more damaging than carbon dioxide. Methane gas is believed to originate from microbes within the seafloor that process organic matter (dead animals, algae) that has fallen from the sunlight zone of the ocean. At reasonable depths and cold temperatures, methane hydrates will inevitably synthesize and slowly grow with further microbial methane production over thousands of years. With large hydrate deposits around the globe, the long-term stability of methane hydrate deposits is of great concern because of the prospective effect that a large release of methane may have on global climate. Global warming not only involves increased atmospheric temperatures, but also warms the earth’s oceans, and could affect the stability of gas hydrates. Global warming and methane evolution from natural gas hydrates affect one another due to hydrate instability at elevated temperatures, resulting in a synergistic cycle that further adds to global climate change (Figure 8).

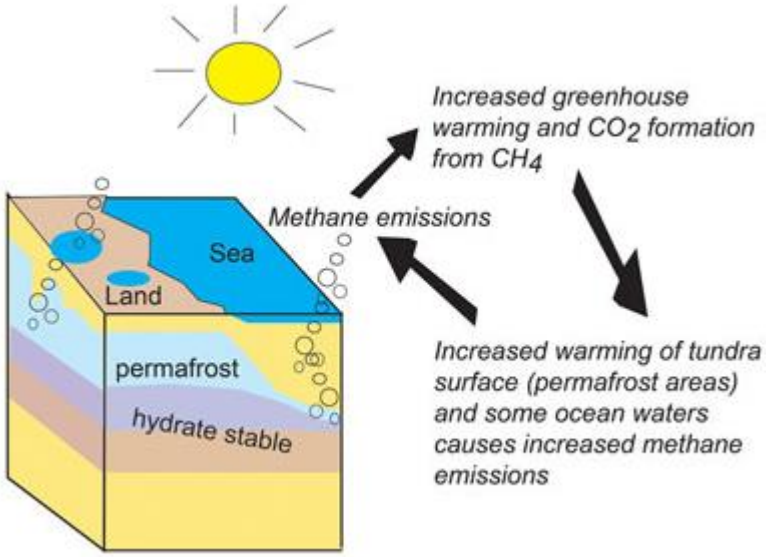

Figure 8 – Methane Hydrate Cycle (Ruppel & Noserale, 2012)

Atmospheric methane concentrations have risen over 150% since pre-industrial times, but are still substantially less (200 times) than carbon dioxide levels (IPCC, 2001). Lower methane concentrations are attributed to oxidative reactions which convert methane to carbon dioxide, a process lasting up to a decade (Ruppel, 2011). Any methane that reaches the atmosphere essentially adds to the amount of carbon dioxide, the primary greenhouse gas. Archer and co-workers have suggested that carbon dioxide is largely responsible for climate changes that result from dissociation of hydrate deposits because of methane oxidation and the excessive levels of longer-lived carbon dioxide in the atmosphere (Archer, et al. 2008). This furthers the need for attention with regard to the connection with preserved hydrates and climate change.

2.5 Gas Hydrate Crystal Structure

Clathrate hydrates of natural gas are defined as crystalline inclusion compounds composed of water and gas, which under the right conditions (low temperature, high pressure), will have the propensity to assume a crystallized state. Natural gas hydrates were first discovered by Hammerschmidt in 1934 in natural gas transmission lines, where he observed the collecting of solid matter that resembled snow. Prior to the identification of natural gas hydrates in pipelines, the plugging and hindrance of flow caused by this solid matter was attributed to the freezing of water caused by subzero ground temperatures (Hammerschmidt 1934). Experimentation with compressed natural gas and water vapour led to the finding that freezing occurred at temperatures higher than expected and that pressure was influential. Hammerschmidt discovered that the primary causes of hydrate formation in

transmission lines were the temperature, pressure and composition of the gas. These conclusions are still valid today and are the focus of extensive research in gas hydrate equilibrium and kinetics studies.

The water (host) forms hydrogen-bonded cavities which surround and enclathrate the gas (guest) molecule. Depending primarily on the size of the gas molecule and its ability to interact via van der Waal forces with the host, three different common gas hydrate structure types exist; structure I (sI), structure II (sII) and structure H (sH), shown in Figure 9 (Jensen, 2010). Type I hydrates are the most abundantly occurring hydrate structure in nature, with a preference to methane gas hydrates (Schicks, 2010). Two different forms of cavities are present in a sI unit cell, namely the dodecahedron denoted 5^{12} (twelve pentagonal faces) and the tetrakaidecahedron denoted $5^{12}6^2$ (twelve pentagonal and two hexagonal faces). Cavities of the sI hydrate are known to stabilize from smaller molecules such as CH_4, H_2S and CO_2 guests (Lederhos, et al., 1993). Complete occupancy is associated with a hydration number of 5.75, giving the general formula, G.5.75 H_2O for sI hydrate where G is the guest (Cady, 1983).

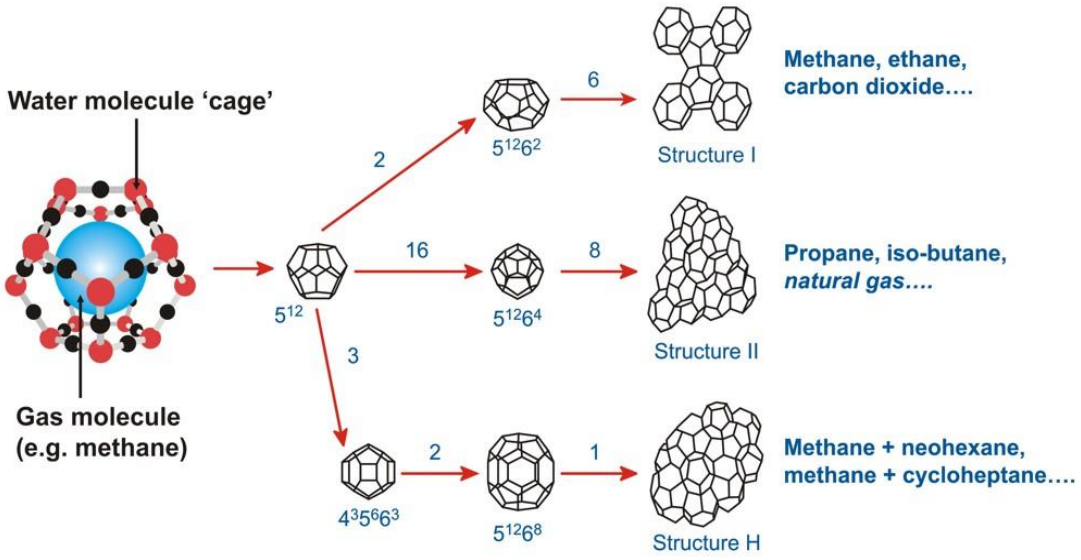

Figure 9 – Common Natural Gas Hydrate Structures (Jensen, 2010)

As the second most abundant gas hydrate, sII hydrates consist of moderately sized gas molecules. Two forms of cavities make up a sII unit cell; the dodecahedron 5^{12}, identical to that in sI hydrates, and the $5^{12}6^4$ hexakaidecahedron (twelve pentagonal and four hexagonal faces) (Mak & McMullan, 1965). Type II hydrate structures favour larger molecules such as propane and i-butane for occupancy on account of the larger $5^{12}6^4$ cavity (Sloan & Koh, 2008). When present, a smaller molecule (e.g. methane)

is also capable of contributing to the sII hydrate by filling the smaller cavities in sII hydrates in which the sII main hydrate former would normally not fit. For maximum occupancy, a hydration number of 17 is attributed to sII hydrates giving an empirical formula of G.17 H_2O (Cady, 1983).

Type H hydrates are the most recently discovered conventional hydrate structure (Ripmeester, et al., 1987). Unlike sI and sII hydrates, three different cavities exist in a sH unit cell – the common 5^{12} dodecahedron, an irregular $4^3 5^6 6^3$ dodecahedron (three square, six pentagonal and three hexagonal faces) and an irregular $5^6 6^8$ icosahedron (six pentagonal and eight hexagonal faces). On the contrary to sI and sII which can form in the presence of a single component, sH requires more than one component; a small component such as methane to occupy the smaller cavities and the structure-defining large molecule (e.g. 2-methylbutane, methylcyclopentane, cycloheptane) to occupy the larger cavities (Carrol, 2002). However, sH hydrates are uncommon with hydrates of natural gas due to the absence of (or very low compositions) heavy hydrocarbons in the gas phase.

A good indication of gas hydrate stability and the propensity for a particular gas-water system to form hydrates is provided by the size of the gas molecule relative to the size of the hydrate lattice cavity (Sloan & Koh, 2008). Knowledge of the relative sizes of hydrate guest constituents was important when predicting and describing the enthalpy of dissociation for the investigated gas hydrates, because it is also descriptive of hydrate stability and equilibria promotion. Thus, the gas molecule's size was used as an indicator for each species' role in a hydrocarbon gas mixture. Table 3 lists the molecule/cavity ratios for the guests encountered in the experimental research presented in the following chapters.

Table 3 – Gas Molecule/Cavity Size Ratio (Lederhos, et al., 1993)

	Structure I		Structure II	
H_2O molecules/unit cell	46		136	
Cavity Type	5^{12}	$5^{12}6^2$	5^{12}	$5^{12}6^4$
Cavity Coordination Number	20	24	20	28
Cavity Size (nm)	0.503	0.586	0.503	0.657
Cavities/unit cell	2	6	16	8
Lattice type	Cubic		Face-centered cubic	
Unit Cell Parameters (nm)	a = 1.2		a = 1.7	

Guest	Guest Size (nm)	Molecule/Cavity Size Ratio			
N_2	0.410	0.815	0.700	0.815	0.624
CH_4	0.436	0.867	0.744	0.867	0.664
CO_2	0.512	1.018	0.874	1.018	0.780
C_2H_6	0.550	1.094	0.939	1.094	0.838
C_3H_8	0.628	1.249	1.072	1.249	0.957
i-C_4H_{10}	0.650	1.292	1.110	1.292	0.990
n-C_4H_{10}	0.710	1.412	1.212	1.412	1.081

A consideration of the hydrate crystal structure was essential in providing an understanding of the relative stabilities of different hydrates throughout this research and subsequently describing this stability in the form of their enthalpy of dissociation. Because there are cavities in the crystal structure of gas hydrates, one guest may stabilize these cavities more than another species according to their molecular structure and size, even if they both fit into the same cavity. With reference to the research presented in the following chapters, the current literature on hydrate structure was helpful in rationalising why, say propane in methane, formed hydrates with water much more readily than n-butane in methane.

2.6 Physical Properties of Gas Hydrates

The physical properties of gas hydrates can be compared to ice in a number of ways because of their related crystal structures. Additionally, the water content is very high relative to the gas molecules in all common hydrate structure types; approximately 85% water and 15% gas given all lattice cavities are occupied, leading hydrates to have similar properties to those of ice (Sloan 1998). However, because of the slightly

different crystal structures of each hydrate structure type, their physical properties are expected to differ slightly. A summary of physical properties with data collected from Davidson (1983), Ripmeester et al. (1994) and Sloan (1998) are presented in Table 5.

Hydrate structures I and II have been studied extensively for their gas storage capabilities, and therefore their mechanical properties are of interest to researchers. However, there has been limited research into the mechanical properties of structure H hydrates. Structure H hydrates predominantly result from heavier natural gas components such as long/branched hydrocarbons and cyclic compounds which generally have low vapour pressures and favour the liquid state, even in low pressures. The idea behind gas storage as their hydrate as opposed to liquefaction by compression is the reduced energy requirements; a pre-determined mass of water is only required as opposed to expending energy into liquefying the gas in the form of LNG. This is mostly not necessary for heavier components as they generally have only small proportions of their content in the vapour phase. Given that a heavy hydrocarbon species will mostly exist in a liquid state, or only low pressures are required for the liquefaction of this species, it is more economical to store structure H forming components as liquids rather than as their hydrates.

Table 4 – Combustible Energy from Some Fuels

Source	Density (kg/m^3)	Energy Density (kJ/m^3)
Methane (gas at STP)	0.666	37,706
Methane (LNG)	420	21.2×10^6
Methane (hydrate)	910	6.2×10^6
Petrol	740	32.6×10^6
Diesel	780	37.1×10^6
Jet Fuel	780	33.9×10^6
Hydrogen (liquid)	70	8.5×10^6

In contrast, the storage of methane gas as its hydrate does have benefits. By converting methane gas to its hydrate form, the concentration of methane is increased substantially. Because of the increase in methane density, the energy density is also increased proportionally. As depicted in Table 4, Max et al. (2006) provided values where the increase in mass density and energy density can be deduced. In fact, methane as hydrate is so concentrated that the dissociation of a single cubic meter

of saturated hydrate results in approximately 164 cubic meters of methane gas (MHAC, 2002). Comparisons between fuel sources and their energy densities show that methane hydrate's energy density is low in comparison to other fuels; this is not so important because methane hydrate is not intended as a direct fuel source, but is an alternative method of storage. What is important is the relative increase in energy density. The energy density of methane as a hydrate is two orders of magnitude higher than its value as a gas at standard conditions. This makes methane hydrate an important energy resource, and it also implies that conversion to its hydrate is an effective means of storing methane gas.

Because of the proven reserves of methane hydrate and natural gas hydrate, it is important to understand their physical and chemical properties to efficiently extract the stored hydrocarbon gases. Another important reason for researching their physical properties is to be able to impose the necessary conditions to dissociate a hydrate plug or any small hydrate solids that may eventually grow and cause pipeline problems. For example, should a hydrate plug occupy a section of pipeline, applying a predetermined quantity of heat energy is a viable option. This amounts to the enthalpy of dissociation, which is reported as a function of composition in Chapters 4, 5 and 6 for various sI and sII hydrates of hydrocarbon gases. Using this information with the heat capacity for the formed hydrate type (Table 5), an approximation of the temperature increase necessary to dissociate the hydrate can be determined. This research used this approach in calculating the dissociating temperature differential.

Table 5 – Physical Properties of Gas Hydrates

Property	Ice	SI	SII	SH
Water molecules per cell	4	46	136	34
Lattice Parameters (273 K), nm	a=0.452 c=1.7	1.20	1.73	a=1.21 c=1.01
Dielectric Constant (273 K)	94	58	58	NA
Isothermal Young's Modulus (268 Pa) 10^9 Pa	9.5	8.4	8.2	NA
Poisson's Ratio	0.33	0.33	0.33	NA
Bulk Modulus (272 K)	8.8	5.6	NA	NA
Shear Modulus (272 K)	3.9	2.4	NA	NA
Compressional Velocity, m/s	3870.1	3778.0	3821.8	NA
Shear Velocity, m/s	1949.0	1963.6	2001.1	NA
Velocity Ratio	1.99	1.92	1.91	NA
Linear Thermal Expansion (200 K), K^{-1}	56 x 10^{-6}	77 x 10^{-6}	52 x 10^{-6}	NA
Adiabatic Bulk Compressibility (273 K), 10^{-11} Pa	12	14	14	NA
Heat Capacity, J kg^{-1} K^{-1}	1700 ± 200	2200	2200	NA
Thermal Conductivity (263 K), W m^{-1} K^{-1}	2.23	0.49 ± 0.02	0.51 ± 0.02	NA
Density, kg m^{-3}	916	912	940	NA

Almost all physical and thermal properties of hydrates are very similar in magnitude to those of ice; the one exception is thermal conductivity. Thermal conductivities for ice are markedly higher, approximately 4-5 times that of hydrate depending on the temperature. Interestingly, most crystalline structures exhibit a decrease in thermal conductivity with an increase in temperature. In fact, hydrate thermal conductivities are greater than 20 times that of ice at very low temperatures (Gabitto & Tsouris, 2010). This is rationalized by an increase in average distance between molecules, making them less efficient at transmitting heat energy. However, this is not consistent with clathrate hydrates – they experience increased thermal conductivities with

increasing temperatures, and have been measured to be in the range of 0.45-0.70 W/m.K for a corresponding temperature range of 265-280 K (English & Tse, 2010).

Interestingly, hydrates have been reported to exhibit glass-like behaviours. This was first reported by Ross et al. (1981), who studied the pressure-temperature dependence of thermal conductivity in hydrates (Ross, et al., 1981). This phenomenon was found to be prevalent at temperatures above 90 K (-183 °C), where thermal conductivities showed a more crystal-like temperature dependence below this point. Since the initial observation of this anomalous trend, researchers have sought to explain such behaviours. One of the most studied models is the "resonant scattering" model, which has been the subject of extensive research performed by Tse and co-workers. The resonant scattering model suggests that in the case of hydrates, there are "avoided crossings" of lattice phonons (a high frequency collective and quantized vibrational mode of a solid or liquid) with localized guest vibrations of identical symmetry which help dissipate heat (English & Tse, 2010). The reader is advised to consult Tse's work for a more detailed outlook.

2.7 Hydrate Formation

In terms of stability, gas molecules are required to be small enough to fit inside the water cavities but also be large enough to provide stability to the hydrate structure (Buffet, 2000). A guest molecule approximately 75% the size of the cavity is required to provide adequate structural stability of the resultant hydrate. If the molecule is over 100% the size of the cavity, the guest will not fit properly and the hydrate will not form. A similar situation arises if the guest size is significantly less than 75% of the cavity. In this case, the molecule is not large enough to supply adequate stability, therefore preventing formation from occurring (Christiansen & Sloan, 1994).

The structure type that forms is not solely dependent on the molecule/cavity ratio or stability in a particular cavity, but is also influenced by the fractional abundance of the favoured cavity. As pointed out by Sloan & Koh (2008), a small molecule like krypton provides little stability to the larger cavity of both sI and sII hydrates. Type II has the highest abundance of the smaller cavity (sII in this case) compared to sI, hence the sII hydrate forms (Christiansen & Sloan, 1994). The composition of the gas phase will also have some bearing on the hydrate structure type (Sloan & Koh, 2008). Composition has been shown experimentally to have an impact on the structure type. For example; only a very small amount of propane is necessary to induce a structure change from sI methane hydrate to sII hydrates of propane (Deaton & Frost, 1946). At low concentrations, much larger increases in equilibrium temperature are expected

when the system is exposed to an increase in propane concentration. Although the fractional abundance of propane's favoured cavity, $5^{12}6^4$, is less compared to the analogous $5^{12}6^2$ cavity in sI, the $5^{12}6^4$ is the only option due to sizing constraints which naturally overrides the greater abundance of $5^{12}6^2$ in sI and consequently forms sII hydrates. Conceptually, it can be understood that at very low concentrations, a greater proportion of $5^{12}6^4$ cavities are unoccupied and therefore are more available for filling. The availability diminishes with increased propane concentrations, therefore reducing the incremental elevation of the equilibrium temperature.

Another contributing factor is pressure (Sloan & Koh, 2008). The influence of pressure, however, has generally been related to the induced relative compositional changes when varied. Given there is an excess of water and the temperature and volume is fixed, composition changes will inevitably occur in the vapour, aqueous and hydrate phase. This is proportional to the controlled change in pressure (Jhaveri & Robinson, 1965). For example, in a 50:50 CH_4-C_2H_6 system at 277.6 K with excess water, sI hydrates will form at approximately 11 bar (Sloan & Koh, 2008). A much greater proportion of the larger $5^{12}6^2$ cavities (Table 3) in sI hydrates implies that the composition of the gas is enriched by methane due to ethane occupying the $5^{12}6^2$ cavities. With high methane gas composition and a change in pressure to 16 bar, sII hydrates will form (Sloan & Koh, 2008). Hence it is essentially the compositional changes brought about by pressure changes that influence structure type. This is one of the focuses of this thesis, which relates the partial pressure and composition of a sII former in the presence of methane, a sI former, to the hydrate structure type that results.

The basic thermodynamic conditions that favour the synthesis of gas hydrates are low temperatures and high pressures (Kvenvolden & McMenamin, 1980). Although similar to ice in many aspects, such as appearance and some physical and chemical properties, gas hydrates will form above 0 °C. Aside from favourable thermodynamic conditions, other requirements generally include the presence of free water, nucleation sites and an adequate amount of mixing and agitation (Makogon, 1997). While mixing and agitation are not fundamental requirements, they are essential in promoting further growth and crystallization of smaller hydrate nuclei which so often results in the plugging of pipelines. From Henry's Law of gas solubility, the amount of gas dissolved in water is proportional to that particular gas species' partial pressure (Henry, 1803). Henry's Law of gas solubility is expressed as,

$$P_a = x_{aq} K_H \qquad \text{Eq. 1}$$

K_H is Henry's volatility constant, P_a is the partial pressure and x_{aq} is the mole fraction of the gas dissolved in water. Henry's constant is defined as the ratio of a species in the aqueous phase mole fraction to its partial pressure at equilibrium. The constant is unique to each gas species, hence the molarity of the aqueous gas solution depends solely on its partial pressure. The influence of gas solubility and therefore pressure on hydrate formation has been investigated significantly, particularly in communications by Makogon (Makogon, et al. 1971; 1998; 1999; 2000). The partial pressure of various hydrate formers in the global gas composition is confirmed in Chapters 4, 5 and 6 to have a large influence on hydrate equilibrium. Experimentation has demonstrated that concentrating or diluting a particular hydrate former in the presence of methane and water shifted the hydrate equilibrium curve in accordence with said component's stabilising effects relative to methane. Henry's Law was an important concept to consider in this research.

2.7.1 Hydrate Formation Thermodynamics

A small subsection described in Chapter 4 focuses on the resultant change on the driving force for hydrate formation for methane in the presence of either nitrogen or carbon dioxide, relative to pure methane. While formation kinetics were not integral to this research, the use of chemical potential driving force aided in the understanding of how nitrogen and carbon dioxide can influence methane hydrate equilibria.

Assuming equilibrium between all the present phases in the system exists prior to hydrate formation, the following reaction of gas, G, and water, H_2O, to produce a hydrate, $G.nH_2O$, where n is the hydration number, must result in a lowering of the Gibbs free energy:

$$G_{(g)} + nH_2O_{(l)} \leftrightarrow G.nH_2O_{(s)} \qquad \text{Eq. 2}$$

Low temperatures are required for the transition from an aqueous phase to the hydrate phase because this results in the lowering of the free energy of the system, explained by Gibb's free energy (Gibbs, 1876):

$$\Delta G = \Delta H - T\Delta S \qquad \text{Eq. 3}$$

Gibb's free energy is used to determine whether a reaction is thermodynamically feasible. Provided there is no kinetic barrier, the reaction can only proceed if there is a lowering of the free energy and hence a negative overall Gibb's free energy value. The overall Gibbs free energy for a reaction is described simply as:

$$\Delta G^T = \Delta G^R - \Delta G^P \qquad \text{Eq. 4}$$

Here ΔG^T is the total Gibb's free energy of the reaction, ΔG^R is the free energy for the reactants and ΔG^P is the free energy of the products. When applied to a simple hydrate reaction with one gaseous component, the following relation is given:

$$\Delta G^H = \Delta G^W + \Delta G^G - \Delta G^H \qquad \text{Eq. 5}$$

Furthermore, the Gibb's free energy is an extensive variable, but it can also be expressed as a molar quantity, the partial molar Gibb's free energy,

$$\frac{\Delta G}{n} = \frac{\Delta G^W}{n_w} + \frac{\Delta G^G}{n_g} - \frac{\Delta G^H}{n_h} \qquad \text{Eq. 6}$$

It is equally represented by chemical potential, the intrinsic form of Gibb's free energy. The terms n_w, n_g and n_h refer to the moles of water, gas and hydrate respectively. The chemical potential driving force can be mathematically expressed as (Kaschiev & Firoozabadi, 2002b),

$$\Delta\mu^{driv} = \Delta\mu_g(T, P, x) + \Delta\mu_w(T, P, y) - \Delta\mu_h(P,T, z) \qquad \text{Eq. 7}$$

In the above equation, $\Delta\mu^{driv}$ is the overall driving force, $\Delta\mu_g$ is the chemical potential for the gas which is dependent on the system temperature, T, pressure, P, and mole fraction, x. The chemical potential for the aqueous phase, $\Delta\mu_w$, is dependent also on T, P and the mole fraction of dissolved gas, y. Similarly, the chemical potential for the hydrate phase, $\Delta\mu_h$, is a function of P, T and the composition of gas in the hydrate phase, z.

The chemical potential of water can be evaluated by considering its molar volume, ν_w, and the difference between its vapour pressure, P^{eq}, and the pressure, P, taken as the experimental or operating pressure:

$$\Delta\mu_w = \nu_w\left(P^{eq} - P\right) \qquad \text{Eq. 8}$$

For the vapour phase, the chemical potential of i is expressed in terms of its experimental fugacity, f_i, and the fugacity at equilibrium, f_i^{eq},

$$\Delta\mu_g = RT\sum x_i \ln\left(\frac{f_i^{eq}}{f_i}\right) \qquad \text{Eq. 9}$$

Symbols have their usual meanings, where R is the universal gas constant. Finally, the chemical potential describing the hydrate phase is given in terms of its molar volume, ν_h, and difference in pressure from the hydrate equilibrium pressure at

temperature T, except the signs are reversed due to the transformation from the water phase to the hydrate phase:

$$\Delta\mu_h = \nu_h\left(P - P^{eq}\right) \qquad \text{Eq. 10}$$

Combining Eq. 7-10 leads to the formation of the following expression for the driving force for the formation of multicomponent hydrates,

$$\Delta\mu^{driv} = \nu_w\left(P^{eq} - P\right) + RT\sum x_i \ln\left(\frac{f_i^{eq}}{f_i}\right) + \nu_h\left(P - P^{eq}\right) \qquad \text{Eq. 11}$$

The above equation describes the overall driving force for the formation of a hydrate phase given a system containing water and a single gaseous species (Sloan & Koh, 2008). As mentioned previously, the relationship expresses dependence on the pressure of the gas as well as its temperature and mole fraction (unity for a simple gaseous system).

Anklam and Firoozabadi (2004) computed the driving force for the synthesis of methane hydrate from supersaturated aqueous solutions. The hydrate driving force for other gases including ethane and propane and various mixtures with methane were also reported. Their work details the variation in chemical potential driving force with pressure at for an isothermal process and temperature under isobaric conditions and have been a reliable source in this thesis. Their illustrated computation using Eq. 11 are presented in Figure 10 for pure methane hydrate.

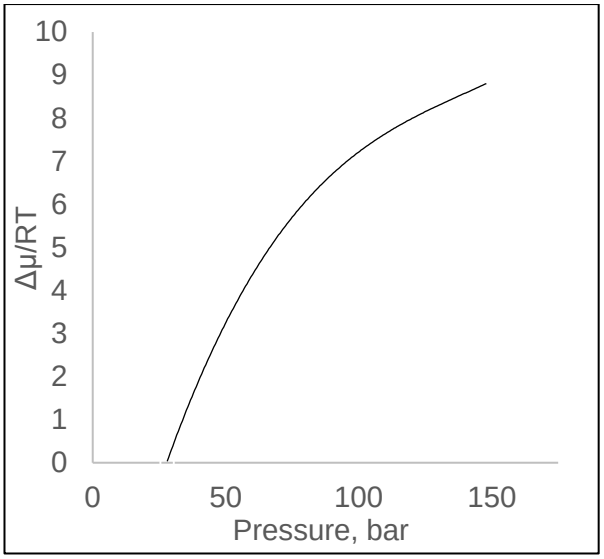

(a) Driving Force for Methane Hydrate as a Function of Pressure at 2 °C

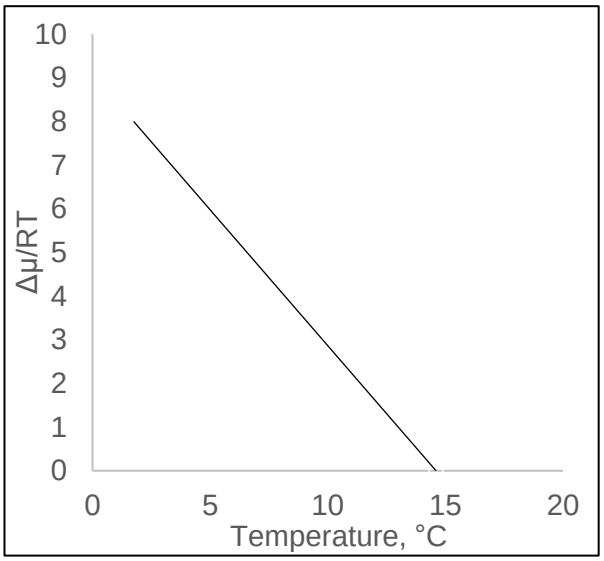

(b) Driving Force for Methane Hydrate as a Function of Temperature at 120 bar

Figure 10 – Methane Hydrate Formation Driving Force (Anklam & Firoozabadi, 2004)

The driving force is illustrated as a function of pressure and temperature respectively for pure methane. It can clearly be understood that the chemical potential driving force has a different mathematical relationship with pressure and temperature. The nature of these differing relationships is sourced from Eq. 11. The curvature of the pressure driving force in (a) is accounted for by the occurrence of the logarithmic fugacity term of the $\Delta\mu_g$ component (Eq. 9). In contrast, the dependence on temperature is linear. This also relates to the $\Delta\mu_g$ of Eq. 11, where it is clear that $\Delta\mu^{driv}$ depends linearly on temperature, hence a straight line is depicted in (b). In the case of both a temperature and pressure change, the overall change in chemical potential would equate to the sum of the chemical potential changes due to both temperature and pressure changes. Due to the non-linear dependence on pressure, the determination of the driving force for hydrate formation as part of this project's research was performed by

measuring the degree of sub-cooling required to induce nucleation under constant pressure conditions.

2.7.2 Hydrate Formation Mechanisms

Several experimental observations, as depicted in Chapters 4, 5 and 6, could not be explained without referring to the accepted mechanisms through which hydrate formation initiates and progresses. There are several individual but related processes that take place which must occur to form hydrate solids. Recognizing how the rate at which these processes occur can influence experimental observations in addition to becoming familiar with the general kinetics relations described previously was essential in determining influential factors associated with these observations.

The formation of nuclei is a fundamental process in hydrate formation and crystallization because nuclei are the macroscopic building blocks for the large hydrate solids which cause so many problems in gas processing and production. Hydrate nucleation is the general process where very small particles of hydrate grow and disperse throughout the system to achieve a critical size (Christiansen & Sloan, 1994). The process of nucleation is classed as a clustering phenomenon that occurs on a microscopic scale and involves the collection of many thousands of water and gas molecules and is extremely difficult to observe experimentally (Mullin, 2001).

There are two types of nucleation according to classical nucleation theory; heterogeneous nucleation and homogeneous nucleation, the latter of which is far less common in hydrate nucleation (Mullin, 2001). This relates to the practical impossibility of even the purest of solutions to be free from foreign particles, which are a requirement for heterogeneous nucleation. Filtration and other purifying techniques of solutions can reduce the presence of impurities and contaminants, but realistically, some will always remain where they can act as surfaces for heterogeneous nucleation (Mullin, 2001). Homogeneous nucleation is therefore often dominated by heterogeneous nucleation.

2.7.2.1 Homogeneous Nucleation

Homogeneous nucleation forms the basis of the classical nucleation theory founded by Volmer and Weber (1926). It states that nucleation arises when a parent phase is transitioned into a non-equilibrium metastable state, such as a super-cooled state (Kalikmanov, 2013). The metastable state is representative of a local minimum in free energy, ΔG. For the nucleation of hydrates, this is achieved experimentally by increasing the pressure beyond the equilibrium pressure, P^{eq}, or reducing the

temperature below the equilibrium temperature, T^{eq}. This causes an overall increase in $\Delta\mu^{driv}/RT$, making the formation of the new phase possible.

Homogeneous nucleation occurs when there are no impurities, favourable phase boundaries or surfaces present where the more favourable heterogeneous nucleation takes place. Thus, it relies on the collisions of phase transitioning molecules. Thousands of individual collisions occur throughout the volume of the parent phase, forming small individual clusters or embryos of the new hydrate phase (Sloan & Koh, 2008). Further collisions add to the small hydrate clusters where they increase in size, or radius, until a critical size is reached. A cluster of this status is termed as a critical nucleus; it corresponds to a size where spontaneous growth occurrs. Therefore, a critical nucleus has attained a size which gives it stability and the capability to sustain further growth.

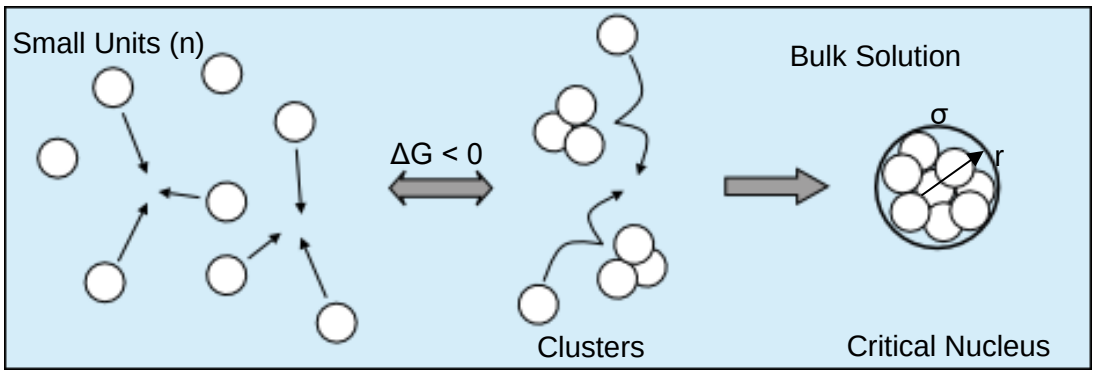

Figure 11 – Homogeneous Nucleation

The general homogeneous nucleation process for the formation of a critical nucleus is illustrated in Figure 11. Under favourable thermodynamic conditions, there is a gain in the free energy of the products allowing the phase transition to occur; i.e. $\Delta G < 0$. A collection of "n" small phase transitioning units collide randomly to overcome the kinetic barrier to form small clusters, which may revert to their individual constituents due to a lack of stability. Further additions of other units and clusters to the newly created clusters result in a larger and more stable cluster – a critical nucleus with specific surface energy between the hydrate and solution, σ.

2.7.2.2 Heterogeneous Nucleation

Heterogeneous nucleation is a first order phase transition where the formation of embryos of the new phase occurs from molecules adsorbing onto a surface (Kalikmanov, 2013). This adsorbing surface is usually any form of foreign particle or body existing in the parent phase. Examples include container walls, pipe walls and their irregularities, fluid interfaces, crevices, dirt and dust particles as well as the newly

forming nuclei. Because of the energy requirements in the creation of a new phase, hydrate nucleation and nucleation in general will occur at these surfaces because they are two-dimensional. This is in contrast to a three-dimensional surface such as the parent phase, or the water-gas aqueous solution in this context, which is free of two-dimensional surfaces.

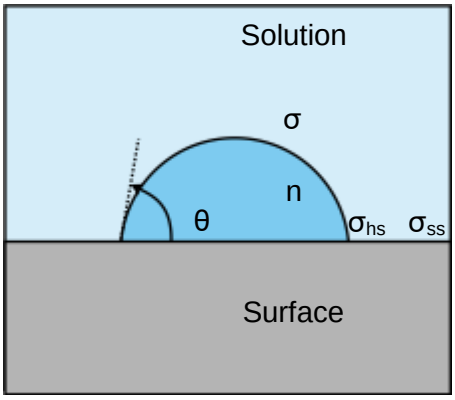

Figure 12 – Heterogeneous Nucleation

As with homogeneous nucleation, the energy required in the formation of the new hydrate phase is driven by the minimization of ΔG. However, when a surface is involved, ΔG is reduced per the angle of contact, θ, because only a partial spherical volume of the new phase is created compared to a complete sphere of hydrate in homogeneous nucleation. This is shown in Figure 12, which illustrates heterogeneously nucleated hydrate nuclei of n building blocks. Because of the presence of another medium, σ_{hs} and σ_{ss} represent the effective specific energies between the hydrate and foreign surface, and solution and surface respectively. The fraction, φ, is used to relate the contact angle and the free energy barrier for heterogeneous, ΔG', and homogeneous nucleation, ΔG, for the formation of a cluster with radius, r,

$$\Delta G = 4\pi\sigma r^2/3 \qquad \text{Eq. 12}$$

$$\Delta G' = \varphi \Delta G \qquad \text{Eq. 13}$$

$$\varphi = \frac{(2 + \cos\theta)(1 - \cos\theta)^2}{4} \qquad \text{Eq. 14}$$

It can be deduced that the free energy requirements are at a maximum when φ is unity, where the contact angle is at 180°. Any reduction in energy requirements is attributed to reducing this angle. A minimum angle of 0° corresponds to a complete minimization of the free energy for hydrate nucleation. This is clearly favourable, hence the high probability of nucleation occurring heterogeneously as opposed to homogeneously.

Understandably, the value of ΔG has an influence on the mass transfer rate of nucleation, J. The general formula for the rate of nucleation is of the following form:

$$J = K \exp\left(-\frac{\varphi \Delta G}{kT}\right) \qquad \text{Eq. 15}$$

K is a kinetic factor related to the frequency of building units adding to the growing nucleus and the concentration of available nucleating sites (Kaschiev & Firoozabadi, 2002b), k is the Boltzmann constant and T is the temperature. From the above expression, minimisation of the energy barrier, φΔG, and reduced temperatures equate to a high rate of nucleation. This relationship is common in all hydrate nucleation processes because of the greater change in chemical potential driving force that results.

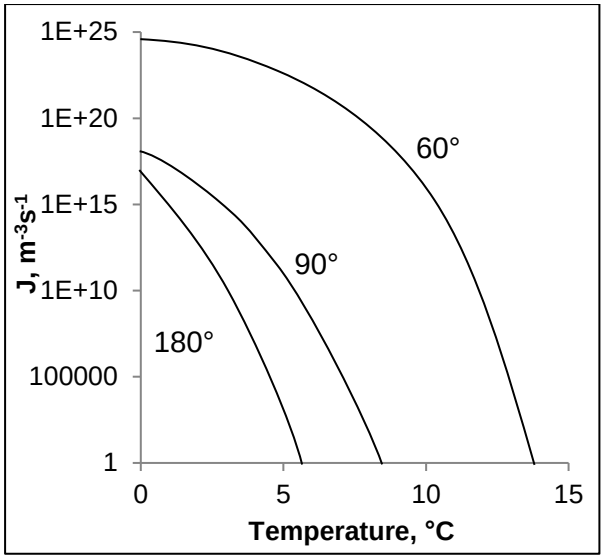

(a): P = 194 bar

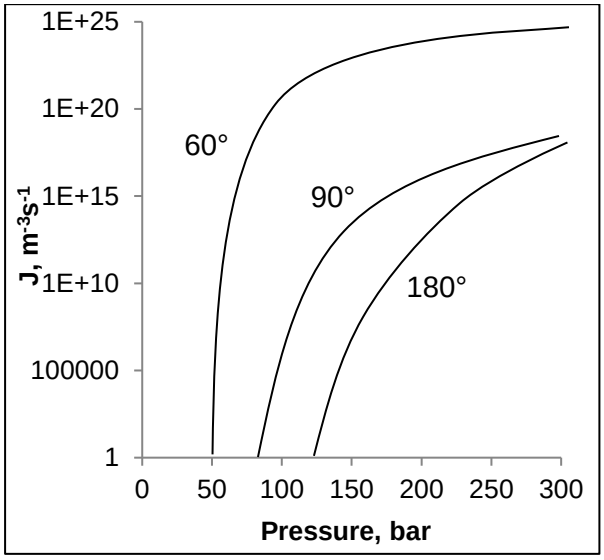

(b): T = 0 °C

Figure 13 – Temperature and Pressure Dependence of J (mod. from Kashciev & Firoozabadi, 2002)

In their review of hydrate nucleation, Kashciev and Firoozabadi (2002) determined values for the rate of mass transfer for various contact angles as functions of temperature and pressure. This included 180°, which corresponds to homogeneous nucleation. Profiles are illustrated in Figure 13 for temperature dependence (a) and pressure dependence (b) of the rate nucleation rate, J. Clearly, higher nucleation rates are calculated for smaller contact angles, where contact angles less than 180° correspond to heterogeneous nucleation. Heterogeneous rates are several orders of magnitude greater than homogeneous rates. For the heterogeneous 60° nucleation, there is a remarkable difference to 90°. This is expected due to the smaller free

energy requirements; φ is reduced and therefore the ΔG energy barrier is not as high. Given the expression for the rate of nucleation is expressed as a power function (Eq. 15), these large differences are understandable.

Similarly, lower temperatures are associated with higher nucleation rates. This relationship is not immediately obvious from Eq. 15 as T is the denominator in the negative power bracket; it would be expected that J would decrease with temperature. However, ΔG is also a function of temperature and dominates this effect. In contrast to temperature, an opposite trend is observed with pressure; increased pressures assure an increase in nucleation rate and this is also a direct result of reduced free energy.

Nucleation rates have noticeably greater sensitivities at lower pressures and higher pressures. This phenomenon is more pronounced with lower contact angles, or greater heterogeneous nucleation. Of note is the convergence of the 90° heterogeneous curves with the homogeneous (0°) curves. These conditions correspond to higher pressures and lower temperature, resulting in greater supersaturation and comparable nucleation rates (Kashchiev & Firoozabadi, 2002a).

2.7.3 Hydrate Cluster Formation Work

Overall, for the formation a hydrate cluster via homogeneous or heterogeneous mechanisms, the work, W, required to do so is represented by,

$$W = -n\Delta\mu + cV_h^{2/3}\sigma_{ef}n^{2/3} \qquad \text{Eq. 16}$$

The constant, c, is a numerical shape factor, where for simple spherical clusters,

$$c = (36\pi)^{1/3} \qquad \text{Eq. 17}$$

V_h refers to the volume of a hydrate unit cell – it has one gas molecule per n_w water molecules (n_w being the hydration number or theoretical stoichiometric amount of water molecules per gas molecule), and n is the number of building units. The effective surface energy, σ_{ef}, is dependent on whether homogeneous or heterogeneous nucleation is taking place. For homogeneous nucleation, $\sigma_{ef} = \sigma$, whereas for heterogeneous nucleation, $\sigma_{ef} < \sigma$, where σ is the specific surface energy of the hydrate/solution interface (Kashchiev & Firoozabadi, 2002a). Considering the case where $\sigma_{ef} < \sigma$, which is indicative of heterogeneous nucleation, the work required to form a cluster of n units is reduced. Therefore, from Eq. 12-17, heterogeneous hydrate nucleation is associated with less free energy requirements,

higher nucleation rates and less work for the formation of hydrate nuclei, making it the dominant process for initial hydrate formation.

2.7.4 Overall Picture of Hydrate Formation

The overall molecular mechanism for hydrate formation is currently still up for debate, although there are several plausible hypotheses on the matter. One of the more accepted approaches is the labile cluster nucleation theory proposed by Sloan and Fleyfel (1991). Sloan and Fleyfel theorized the formation of metastable or labile hydrate clusters upon the arrangement of gas molecules in water and is representative of primary nucleation in the induction period. Figure 14 illustrates this process (bold and light dashes are hydrogen bonds and van der Waals interactions respectively).

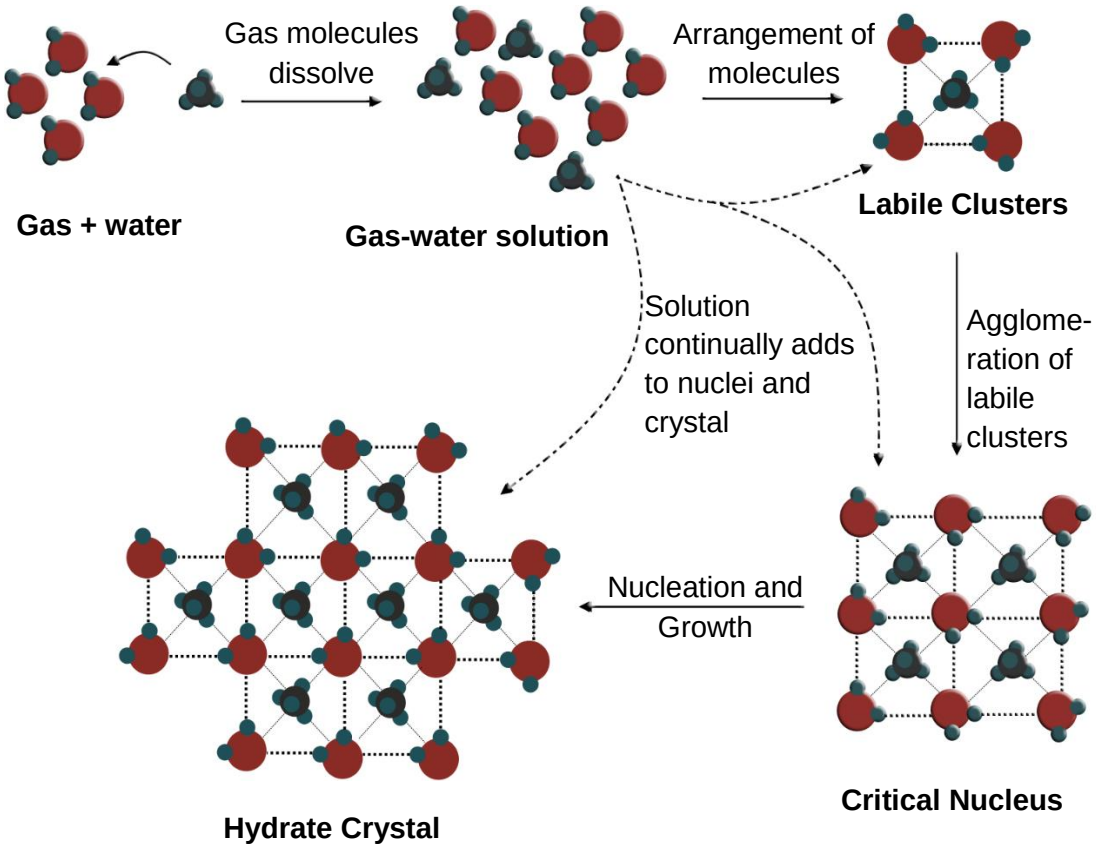

Figure 14 – Hydrate Formation Stages (mod. from Christiansen & Sloan, 1994)

When a hydrate-forming gas is introduced to free water, at that instant, they can be thought of as two separate phases. With time progression, an equilibrium will eventually establish. A small fraction of gas will dissolve in the water, where the exact amount depends on the solubility of the gas in water at the present conditions (Eq. 1) in addition to the quantities of both gas and water present in the system. Immediately following the dissolving of gas, labile clusters begin to form by the arranging of water

molecules about the adsorbed guest molecule. Depending on what gas has dissolved in the water, the coordination number of the labile cluster will vary, with smaller molecules typically having a lower coordination number (Sloan & Fleyfel, 1991). It is hypothesized that larger guest molecules may fluctuate between sI and sII, until vertice sharing causes the growth of sI hydrates. Alternatively, face sharing can dominate and result in the formation of sII units.

The labile clusters agglomerate via face sharing and/or vertice sharing after coming into immediate contact with one another, often by hydrophobic attraction to form larger and more stable structures – labile cluster agglomerates. Hydrophobic attraction refers to the attractive forces between the non-polar gas molecules captured as labile clusters, and when combined with mixing, aid with the formation of hydrates. Being relatively unstable, instead of agglomerating the labile clusters may degrade into smaller units, particularly if the concentration of clusters is low. In the case where clusters form larger agglomerates, they may attain a certain critical size. They are then labelled as stable nuclei, and are capable of accelerated growth to form large crystallized hydrate solids via the continued addition of hydrate units to the growing nuclei (Sloan & Fleyfel, 1991).

Another hydrate theory with credibility is that nucleation occurs on the vapour side at the phase interface via a heterogeneous nucleation process. This theory was proposed by Long (1994), and is conceptualised in Figure 15. This approach to the molecular mechanism of hydrate formation is also supported by Kvamme (1996).

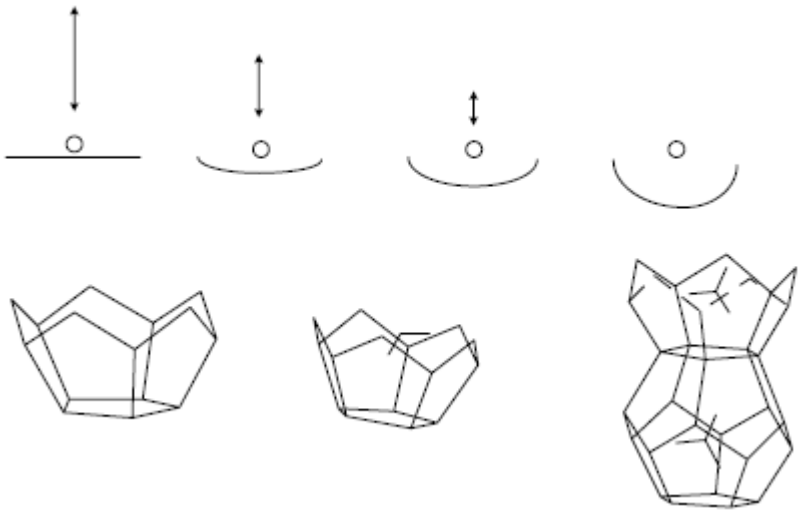

Figure 15 – Adsorption and Penetration of Solution-Gas Interface (Long, 1994)

Long's hypothesis says that gas molecules are adsorbed onto labile hydrate cavities at the solution-vapour interface via mass transfer. At standard pressure and temperature conditions, Long (1994) explains that the rate of penetration of a stagnant water-vapour interface is of the order of 10^{22} molecules/cm^2.s. The guest molecule migrates to a favourable location where it adsorbs onto the surface of the aqueous solution and then diffuses through the interface. During this process, water molecules will form fractional cages around the adsorbed guest molecule, which eventually go to completion to form a fully hydrated guest molecule. Other hydrated molecules cluster together to form labile clusters. The labile clusters grow into larger clusters and eventually critical nuclei, all of which occurrs on the vapour side of the water-solution interface. Colliding clusters join by vertice sharing and/or face sharing as with the agglomeration mechanism approach by Sloan and Fleyfel (1991). Growth may also occur according to further addition of water and gas molecules to the formed labile clusters and nuclei.

Long's hypothesis of interfacial clustering of hydrates does not necessarily mean that the transformation of small clusters to large hydrate solids is orderly. Many combinations of hydrogen-bonds are possible, some more stable than others, and may result in some clusters not growing as quickly or even reduce in size (Sloan & Koh, 2008). However, given that there are very large numbers of clusters, progression to larger clusters with more favourable hydrogen-bonding networks and orientations are certain.

2.7.5 Hydrate Formation Conditions

An understanding of the thermodynamic conditions that cause hydrate formation and how they differ from the dissociation conditions was of extreme importance. This understanding was applied regularly through this research program. The formation conditions of hydrates can be characterized thermodynamically by pressure and temperature conditions in the form of a phase diagram for a gas-water system. Not to be confused with the hydrate phase equilibrium/dissociation conditions, the formation conditions typically occur at lower temperatures where an unspecified amount of sub-cooling is necessary for the promotion of hydrate formation (Bai & Bai, 2005).

Figure 16 illustrates the formation and dissociation (or equilibrium) lines as characterized by pressure and temperature. The far right of the graph indicates that hydrates are unstable in this area, and are therefore not thermodynamically feasible for hydrate formation. This represents point A. Considering an isobaric process and following the cooling line, the potential for hydrates increases until it crosses the

dissociation line into the metastable region, an area between the formation and dissociation lines. Unless hydrates have already formed, it is unlikely that the formation of new hydrates from an aqueous phase will occur, although the possibility remains. Hydrates in this region are unstable due to insufficient sub-cooling, hence the low probability of formation. Hydrate formation will not occur readily, however, nucleation and growth may still take place in the metastable region (Sloan & Koh, 2008). Continued sub-cooling results in the crossing of the formation line into the stable hydrate zone, point B. Such a degree of sub-cooling generally results in favourable thermodynamic conditions for the formation of stable hydrates. In the hydrate-stable zone, there is a higher degree of supersaturation and driving force which ensures hydrate nucleation occurs more readily (Mullin & Jancic, 1979). Further cooling into this region results in more favourable conditions for hydrates and higher hydrate stability.

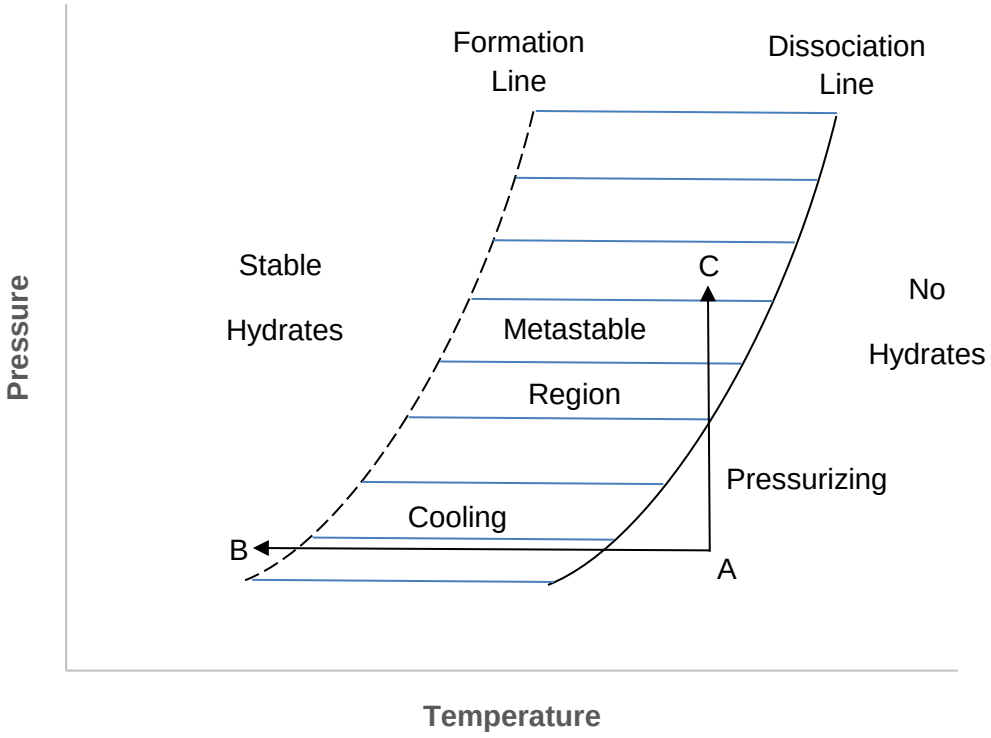

Figure 16 – Hydrate Metastability Region

The method of pressurization has a similar effect to sub-cooling. Considering an isothermal process, increasing the pressure along the pressure line from point A to C results in the entering of the metastable region, similar to the cooling line in an isobaric process. This results in the supersaturation of the aqueous. It can also be understood from Eq. 11 that an increase in pressure and fugacity is proportional to an increase in chemical potential driving force for hydrate nucleation. Although not pictured in Figure

16, further isothermal pressurization would be equivalent to a further increase in driving force where the thermodynamic conditions would be reflective of the stable hydrate zone.

However, the formation line is often not fixed even for a system fully characterized. No two experimental setups are the same and will therefore contain different amounts and types of nucleation sites, which are essential requirements for the formation of hydrate nuclei. The formation line is therefore not solely dependent on composition and thermodynamic conditions, whereas the dissociation line is (Tohidi, et al., 2000). Molecular movements can never be replicated exactly, as their movement depends on many factors including the degree of mixing, type of flow, agitation and Brownian diffusion. The metastable region can consequently vary, even with the same apparatus and equipment, making it difficult to predict.

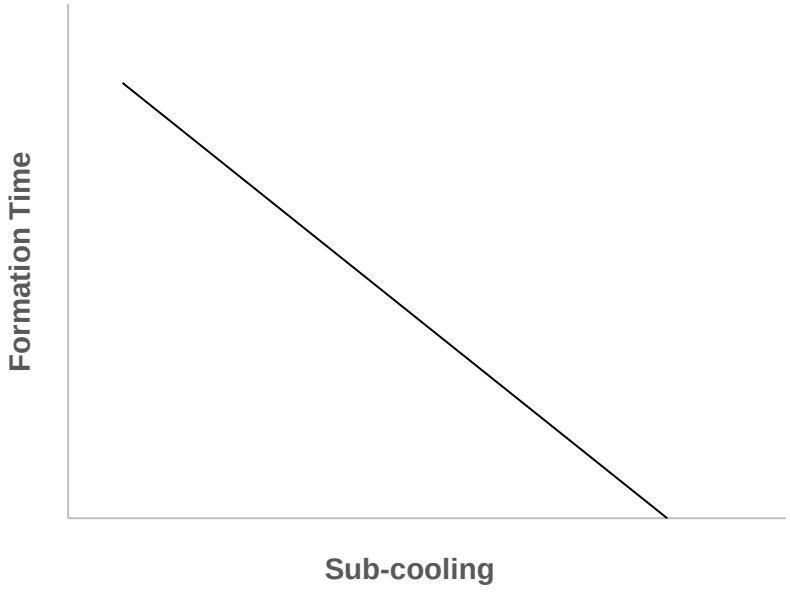

Figure 17 – Hydrate Formation Time Variation with Sub-cooling (Ellision & Gallagher, 2001)

Given a certain degree of sub-cooling, hydrates may not form for some time even though temperature and pressure conditions are to the left of the dissociation line. Although variable, the amount of sub-cooling required for hydrates to form is often only a few degrees. However, the time for hydrate formation to occur reduces with an increase in sub-cooling, as indicated in Figure 17 (Ellision & Gallagher, 2001).

Due to the many factors aside from pressure and temperature that affect the hydrate formation conditions, it has a somewhat random nature associated with it. Therefore, hydrate formation is classified as stochastic. This is opposed to deterministic, where

only thermodynamic properties are required to describe a set of equilibrium conditions (Sloan & Koh, 2008). For specific hydrate equilibrium conditions, only one temperature and pressure is therefore possible.

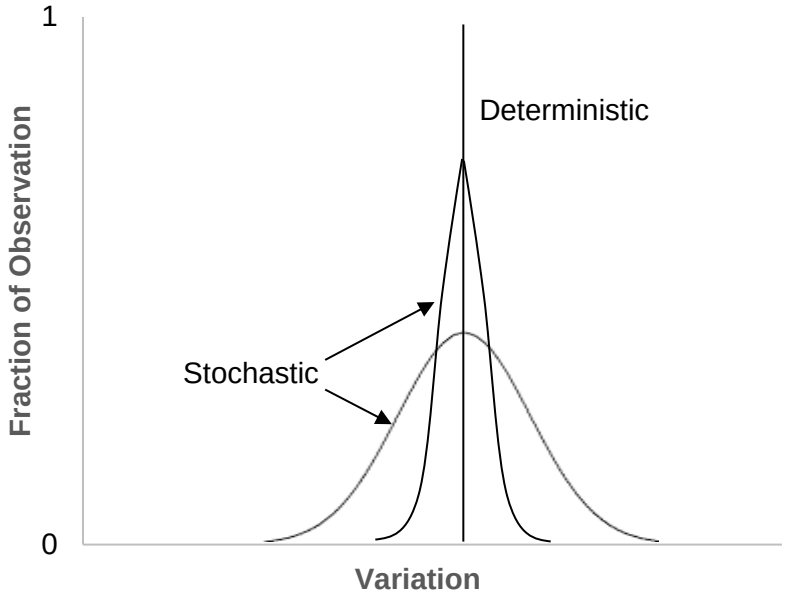

Figure 18 – Stochastic and Deterministic Properties (mod. from Rowley, 1994)

The probability of observation for a deterministic property is therefore unity, as illustrated in Figure 18, and is described by only one set of thermodynamic properties. Some properties are stochastic for certain processes, such as hydrate formation, and are dispersed over a range of possibilities. It is therefore not certain that one set of properties will be observed. Such properties are often normally distributed, but probabilities are not fixed and will vary with the amount of sub-cooling and chemical potential driving force. A greater amount of sub-cooling tends to reduce the distribution of possible thermodynamic conditions that bring about nucleation, and consequently result in less variation (Sloan & Koh, 2008).

2.7.6 Gas Solubility

The solubility of gases in water is one of the most important factors that influence the formation of gas hydrates and the results presented in this study. The more concentrated the aqueous solution is with gas molecules, the greater the chemical potential driving force is for hydrate nucleation and supersaturation. The solubilities and other solution properties at standard conditions (i.e. 25 °C and 101.3 kPa) of common natural gas components are presented in Table 6.

Table 6 – Solution Properties of Some Gases

Gas Species	Solubility[a], x_i ($\times 10^5$)	$-\Delta H_{sol}$[b] kJ/mol	$-\Delta S_{sol}$ kJ/mol
Methane	2.55	13.26	44.5
Ethane	3.40	16.99	57.0
Propane	2.72	21.17	71.0
i-Butane	1.66	25.87	86.8
n-Butane[c]	2.24	22.00	195
Nitrogen	1.18	10.46	35.1
Carbon Dioxide[c]	61.7	26.35	88.4

[a] Solubility data from Hayduk (1982;1986), Battino (1982), Clever and Young (1987;1988) and Crovetto (1991)

[b] Heat of Solution and entropy of solution data from Franks and Reid (1973)

[c] n-Butane, carbon dioxide and hydrogen sulfide data except solubility from Sloan (2008)

The solubility of hydrocarbon gases in water is not large because their opposite polarity to water. Even at higher pressures, where hydrate formation is possible, their solubilities are very small. This occurs because of the positive free energy, ΔG, associated with the dissolving of a nonpolar gas. From Eq. 3, $\Delta G = \Delta H - T\Delta S$ and from Table 6, the larger negative entropy of solution for each gas component will outweigh its heat of solution, meaning ΔG will be positive. The dissolving of natural gas components is therefore not thermodynamically favourable, giving rise to low solubilities.

Due to the unfavourable nature of these gases existing in a body of water, order and integrity of the system is retained by the forming of hydrates. This is evident by the large entropies of solution which correspond to the creation of cavities; it can be said that the solute has a structuring effect on the water molecules, to restore order (Sloan & Koh, 2008). The joining and agglomeration of the caged gas solute is said to occur due to the thermodynamic affinity towards lower entropies.

The solubility of gases during and after hydrate formation has been shown to change significantly. Gas hydrate solubilities were first performed by Makogon in 1971 with later studies in 1974 and onwards. The experiments of Makogon and co-workers presented interesting results, including sharp changes in the gas content of the water and hydrate phase after hydrate formation. Figure 19 details the change in solubilities

in the water phase prior to and after hydrate formation, and for the hydrate phase (Makogon, et al., 2000).

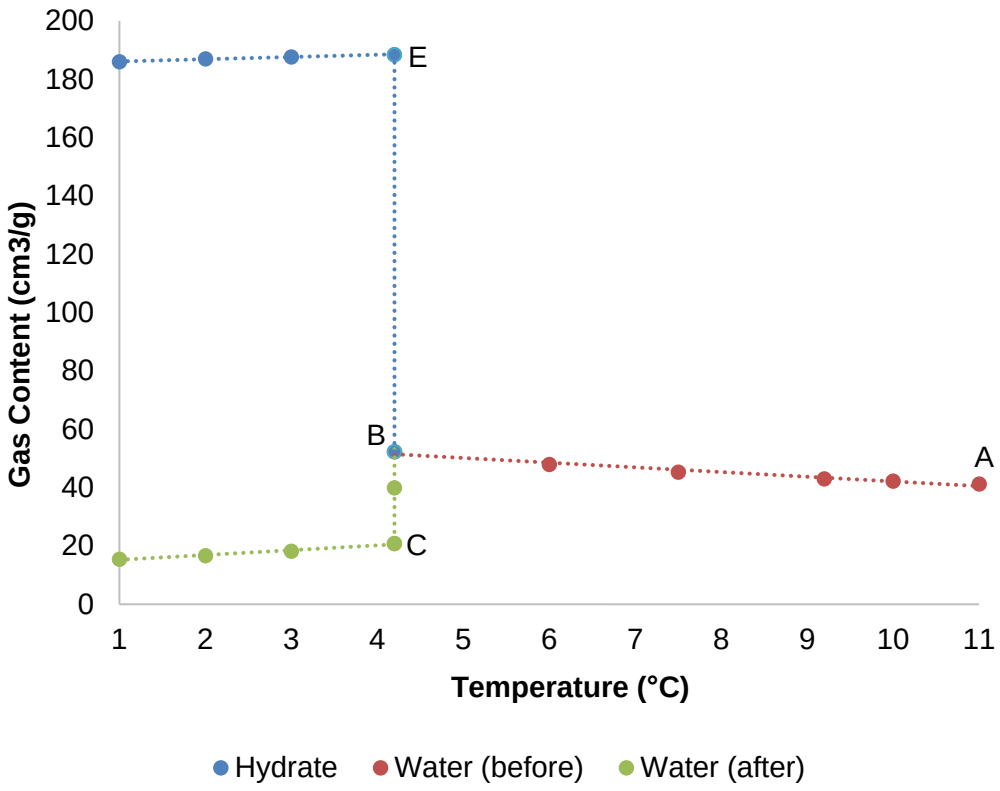

Figure 19 – Gas Solubility in Water (mod. from Makogon, et al., 2000)

The solubility of water before hydrate formation (Figure 19), represented by AB, was measured by maintaining the pressure and gradually reducing the temperature from A to B. An increase in solubility is observed throughout this period. At lower temperatures, gas molecules have less kinetic energy and are therefore less likely to escape the solution. Point B is the hydrate formation temperature and signifies a drastic increase in gas content of the hydrate phase, BC, coupled with a sharp decrease in water solubility, BE. Once at equilibrium and the hydrate phase is saturated, additional temperature reduction does not have any significant effect on the gas content in the hydrate or water phases. This information can then be used to calculate the volume of gas used in the formation of the hydrate. The difference between the gas content in water just before hydrates form (B) and after (C) their complete formation equates to the amount of gas consumed by the water as hydrate (Makogon, et al. 2000).

2.7.6.1 Natural Gas Solubility

The development of new technologies and resources in the recovery of natural gas from hydrate deposits depend largely on gas and reservoir water composition (Makogon, et al. 2004). The extent of natural gas saturation in reservoir water can therefore be of significant interest. Measurements of natural gas solubility in water have been performed by several researchers over the past 60 years, namely, Kobayashi and Katz (1953) and Namiot (1991). The solubility of natural gas during the metastable hydrate conditions as well as at equilibrium have been researched by Makogon et al. (1971; 1974).

The solubility of natural gas in water can be approximated with reasonable accuracy both before hydrate formation under hydrate forming conditions, i.e. the two-phase water (L_w) and vapour (V) system L_w–V, and after, where a three-phase water, vapour and hydrate (H) equilibrium (L_w–V–H) exists. This is achieved by modelling empirical parameters in the evaluation of the Henry constant, thus allowing the solubility of the natural gas to be determined at a specified pressure. The Henry constant for natural gas, H_{NG}, is evaluated as follows (Makogon, et al. 2000):

$$H_{NG} = (aP + b)T + cP + d \qquad \text{Eq. 18}$$

The empirical parameters are designated a, b, c and d and have been experimentally determined by Makogon (Table 7). From Henry's Law,

$$x_{NG} = P/H_{NG} \qquad \text{Eq. 19}$$

Where x_{NG} is the solubility of natural gas at a specified pressure, P. Substitution of Eq. 18 into Eq. 19 yields,

$$x_{NG} = \frac{P}{(aP + b)T + cP + d} \qquad \text{Eq. 20}$$

The above expression is used in the calculation of the gas quantity in solution (cm^3/g) at certain pressure (MPa) and temperature (°C) conditions.

Table 7 – Henry Constant Empirical Parameters (Makogon, et al. 2000)				
Equilibrium	**a**	**b**	**c**	**d**
L_w–V	0.0029	0.0296	0.0692	0.720
L_w–V–H	-0.0013	-0.0628	0.2058	1.942

Using the empirical constants provided in Table 7, the change in gas solubility with various equilibrium pressures can be observed.

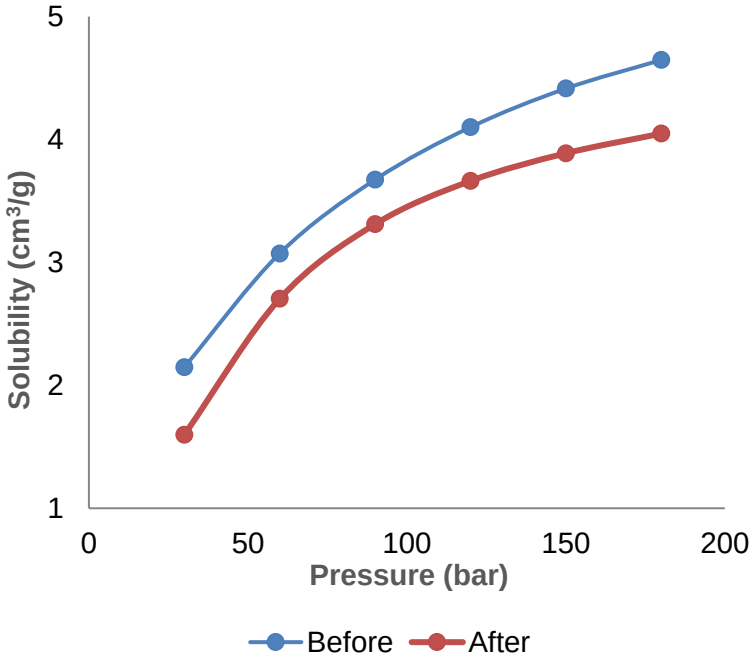

Figure 20 – Gas Solubility Before and After Hydrate Formation

Application of Eq. 20 with hydrate equilibrium pressure and temperature data is illustrated in Figure 20. The solubilities were evaluated at predetermined pressures and their corresponding equilibrium temperatures. The computed solubilities decrease after hydrate formation throughout the entire pressure range, and are consistent with Figure 19.

According to Henry's law, the solubility of a gas species in water is proportional to its pressure and its Henry constant. The constant itself is proportional to temperature, meaning that gas solubility is inversely proportional to changes in temperature. At low pressures, the effect of pressure on solubility is more significant than at high pressures. An increase in pressure results in a higher associated equilibrium temperature, and therefore a greater negative temperature weighting on solubility occurs.

Table 8 – Modelled Gas Composition (mol%)
(Makogon, et al. 2000)

CH_4	C_2H_6	C_3H_8	i-C_4H_{10}	n-C_4H_{10}	N_2	CO_2	i-C_5H_{12}
87.2	7.6	3.1	0.5	0.8	0.4	0.1	0.3

One aspect the modified Henry constant doesn't account for is gas composition. The natural gas mixture (Table 8) used to provide experimental data for the modification of the Henry constant was representative of a typical natural gas. However, there is expected to be inaccuracies when the modified Henry constant is applied to a system composing of different gas component proportions. This is because the empirical parameters are a function of gas composition and will vary to an extent that is dependable on how different the gas composition is to the one described in Table 8 (Makogon, et al. 2000). The gas composition is also a function of pressure when a closed system is considered, particularly when less volatile components are present. At higher pressures, the less volatile gas species with low vapour pressures will condense out of the vapour phase, therefore changing the relative compositions of all species in the vapour phase. This change in composition means that the current vapour phase may not be accurately representative of the original composition. Inaccuracies will consequently be a product of estimating natural gas solubilities at high pressures or any thermodynamic conditions that breach the dew point for that matter.

2.8 Hydrate Dissociation

Unlike the hydrate formation point, the dissociation point is governed by deterministic temperature and pressure conditions. The dissociation conditions do not depend on the rate of cooling, degree of sub-cooling, water history or the presence of foreign materials, but is defined as a fixed thermodynamic equilibrium point and is repeatable (Tohidi, et al., 2000). The dissociation conditions are therefore synonymous with the hydrate equilibrium point and can be used to establish hydrate phase equilibria.

Hydrate dissociation is an endothermic process which involves breaking of the hydrogen bonds between the network of water molecules and the van der Waals attractive forces between the guest molecule and the surrounding water host molecules. Dissociation results in the hydrate decomposing into water and gas, although labile hydrates not visible to the naked eye may remain in solution (Christiansen & Sloan, 1994). These labile hydrates are thought to be responsible for

the “memory effect”, where experiments have shown that the remnants of hydrate dissociation can promote the formation conditions (Wu & Zhang, 2010). The high concentration of these labile clusters act as nucleation sites which would otherwise require a higher chemical potential driving force for their formation. Hence, the formation of hydrates may occur in the metastable region of Figure 16 due to a source of extra mass transfer sites which alleviate the formation of initial labile nuclei.

2.8.1 Thermal Stimulation

The dissociation of a hydrate can primarily occur via three different methods; thermal stimulation, depressurization or the introduction of some form of thermodynamic inhibitor. The thermal stimulation and depressurization methods are opposite to that of forming hydrates. Thermal stimulation is essentially the reverse of cooling, and shifts the thermodynamic conditions into the “hydrate-free” zone. This method is used in the experimental work associated with this thesis. It requires a heat source to elevate the temperature of the system, leading to the freeing of gas molecules from the hydrate state. In an experimental environment, heat can easily be applied with any form of heating, but this is hardly feasible for *in situ* hydrates. Heat is often supplied by injecting a heated warm fluid, such as water or steam, into the reservoir. Heat can be supplied electrically, or alternatively it can be heated by adjacent oil and gas recovery operations (Giarvarini & Hester, 2011).

Methane hydrates make up the majority of hydrates in sediments – they usually dissociate at temperatures less than 20 °C at lower pressures as displayed in Figure 21. Therefore, the injection of warm water will dissociate the hydrate given the production of natural gas has reduced the operating pressure (Giarvarini & Hester, 2011).

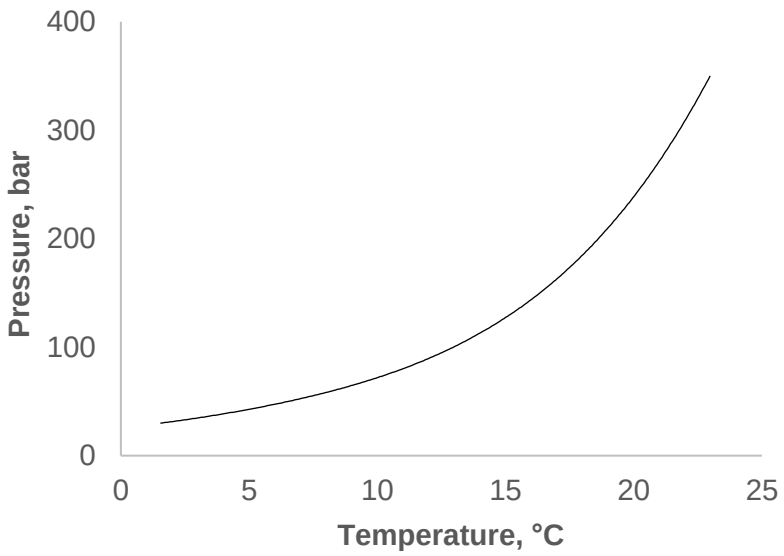

Figure 21 – Methane Hydrate Equilibria (PVTsim)

2.8.2 Depressurization

Depressurization has an identical outcome, and promotes the dissociation of the hydrate. It is by far the easiest and simplest method to dissociate hydrates because it does not involve energy expenditure. It is a relatively cheap method in recovering methane gas from hydrate deposits since depressurization is the conventional method of recovering natural gas from a reservoir. A lowering of the reservoir pressure will cause the eventual dissociation of hydrate and a gradual supply of methane. The current technologies are therefore applicable in dissociating methane hydrate reserves, making it the preferred dissociation technique in methane recovery from hydrate-bearing sediments (Giarvarini & Hester, 2011).

2.8.3 Modes of Dissociation

Due to hydrates commonly being formed in pipelines and in most experimental setups as cylindrical plugs due to their physical dimensions, hydrate dissociation has been commonly observed to occur from a combination of radial and axial perspective (Figure 22). Given the surface area available for heat transfer is often, greater longitudinally, radial dissociation is the dominant mode of dissociation in pipelines and setups that use a pressure-volume-temperature (PVT) reactor cell. Realistically, dissociation occurs axially as well since the ends of the cylindrical plug are exposed to the heat transfer medium. Therefore, hydrate dissociation is the result of a combination of both axial and radial effects.

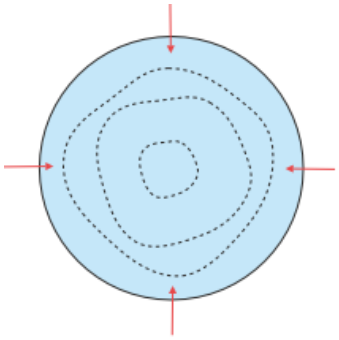

(a) Radial Dissociation

(b) Axial Dissociation

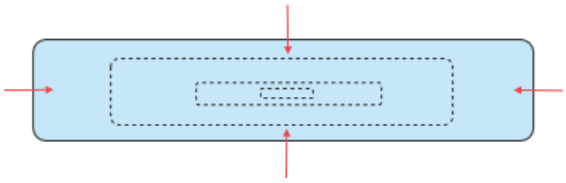

(c) Radial and Axial Dissociation

Figure 22 – Modes of Hydrate Dissociation

The generally accepted understanding is that the hydrate plug, which is situated in the center of a horizontal pipe, is surrounded by an immobile water phase. The water phase acts as an efficient heat conductor, particularly with water's relatively high specific heat capacity. Being surrounded by heat-conducting water, heat is effectively administered to the dissociating hydrate, leading to complete dissociation. Since heat is being removed from the water by the hydrate during dissociation, the temperature will decrease at the water-hydrate interface. Consequently, a temperature profile is the result which manifests throughout the hydrate radially with heat being conducted from the center of the hydrate plug to the interface (Sloan & Koh, 2008).

Experiments on hydrate plug dissociation were performed by Davies et al. (2006), who showed that hydrate dissociation is heat-transfer limited and that mass transfer and intrinsic dissolution kinetics are fast-acting and do not hinder dissociation rate (Davies, et al., 2006). One-dimensional heat transfer models were formulated to describe dissociation rates for axial and radial dissociation, which accurately predicted the radial dissociation rate is far greater than the axial dissociation rate, the extent of which depends on the radius/length ratio.

The control of hydrate dissociation by heat-transfer has been investigated by several works, many of which confirm the high dependence of the rate of dissociation on heat transfer (Løken, et al., 1999); (Gupta, et al., 2004). Evidence in the form of x-ray computed tomography (CT), which are able to capture density mappings of the dissociating hydrate, validate the radial hydrate dissociation model (Gupta, 2007).

Emergence of zero density regions about the length of the plug occurred, indicating a reducing plug diameter. This confirmed the extent of which radial dissociation manifests over axial dissociation in a typical cylindrical hydrate plug.

Chapter 3

3. General Experimental Methods

Clean Gas Technology Australia (CGTA) is a research facility in association with Curtin University at the Bentley campus in Perth, Australia, as part of the Technology Park complex. Depicted in Figure 23, CGTA was founded in 1999 as the Woodside Research Facility, and is considered one of the great success stories in the Australian oil and gas research industry. The facility is operated by the School of Chemical and Petroleum Engineering and is actively involved in many research areas. These areas concern gas hydrate technology, corrosion in the oil and gas industry, carbon capture, modelling of hydrocarbon processing conditions, dehydration with application to sub-sea conditions, two-phase fluid behaviour, particle formation/deposition studies within natural gas lines and low temperature separations processes among others. The CGTA research center is home to specialized laboratories including corrosion chemistry labs, a sapphire cell hydrate reactor pilot plant, a fuels and energy lab and a monoethylene glycol (MEG) regeneration pilot plant.

Figure 23 – Clean Gas Technology Australia (CGTA) Research Center

3.1 PVT Cell Applications

The centrepiece for the research work presented in this thesis is the sapphire cell hydrate reactor pilot plant, constructed in 2002. The sapphire cell is a pressure-volume-temperature (PVT) cell reactor vessel and specialises in analysing the

behaviour of oil and gas fluids when exposed to different thermodynamic conditions. The PVT cell is based on a through-window cell and offers complete visibility of the fluid sample allowing for clear observation of fluid phase behaviours and properties. They are commonly employed for characterising reservoir fluids; swelling tests, volatile oil studies and gas condensate studies are examples of the potential operations a PVT cell can perform.

3.1.1 Bubble-point Determination

Hydrocarbon composition, density, viscosity and compressibility all change with pressure and temperature, all of which are essential knowledge when determining the fate of hydrocarbon gases that evolve from the reservoir fluid as it travels to the surface. Bubble-point determination via flash liberation of a fluid sample is a standard procedure that can be indicative of the mentioned properties, and is crucial in understanding how hydrocarbons behave in the reservoir and the possible drive mechanism (Danesh, 1998). For example, if the reservoir pressure is initially at the bubble-point, then it is expected that a gas cap likely exists that will expand, aiding the recovery of fluids considerably. Starting at a pressure above the bubble-point, the flash liberation test simply involves isothermally decreasing the pressure in increments by removing mercury from the cell. The corresponding change in hydrocarbon volume is plotted against pressure (Figure 24).

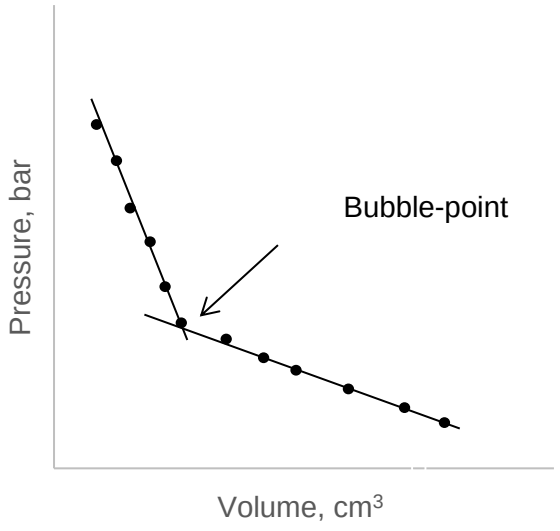

Figure 24 – Bubble-point Determination

Because only oil is initially present, the initial pressure-volume relationship is negatively steep. As mercury is removed from the cell, the pressure decreases to a point where the liquid becomes saturated and gaseous hydrocarbons come out of solution, i.e. the bubble-point. Any further volume increases result in small cell

pressure declines, resulting in a drastically reduced slope. The reduced slope is clearly observable (Figure 24), and represents the bubble-point.

3.1.2 Reservoir to Surface Volumes

In addition to bubble-point testing, a PVT cell operation that relates surface volumes to reservoir volumes is an equally important endeavour. The oil formation volume factor, B_o, gas formation volume factor, B_g, and the solution gas-oil ratio, R_s, are all parameters that describe the volume change as the fluid travels from the reservoir to the surface and help determine the amount of hydrocarbons in the reservoir (Pederson, et al., 2015). The formation volume factors and the solution gas-oil ratio are all functions of reservoir pressure, and can be evaluated by reproducing the pressure changes that occur during the production of the fluid. To simulate these pressure changes, differential liberations are performed to simulate flow in the reservoir, and flow between the well and the separator are best represented by multiple flash liberations or separations (Freyss, et al., 1989).

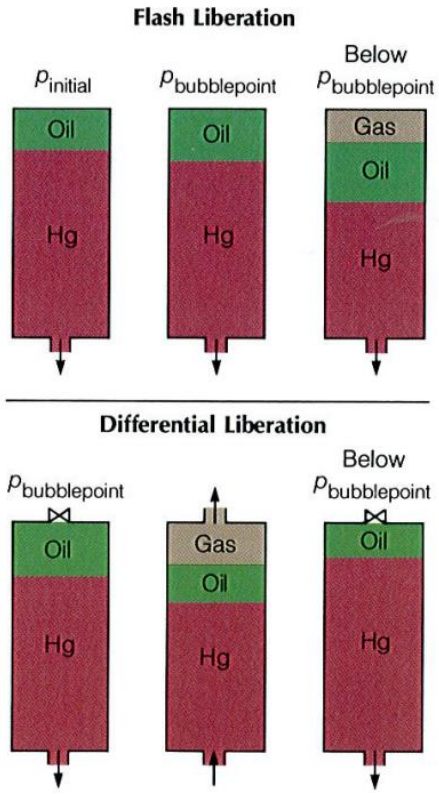

Figure 25 – Flash and Differential Liberation (Freyss, et al., 1989)

The experimental PVT setup for differential liberation is similar to the flash separation procedure used in bubble-point tests, except the starting pressure is the bubble-point pressure. The liberated gas after each pressure reduction (or mercury removal) is collected and removed from the PVT cell, prompting the isobaric injection of mercury

(Figure 25). The decrease in oil volume, volume of liberated gas and volume of gas at standard conditions are measured for each stage. Pressure is decremented until all gas has been liberated, resulting in residual oil at atmospheric pressure and reservoir temperature. Finally, the volume of the residual oil is measured at standard temperature.

$$B_o = \frac{V_o}{V_r\varphi(1-S_w)} \quad \text{Eq. 21}$$

$$B_g = \frac{V_g}{V_r\varphi(1-S_w)} \quad \text{Eq. 22}$$

$$R_s = \frac{B_o V_{g,stp}}{V_r\varphi(1-S_w)} \quad \text{Eq. 23}$$

The number of separation stages and appropriate operating pressure for the surface separator are estimated using a series of flash separation tests performed on the fluid sample (Danesh, 1998). A small-scale separation system is used in this instance, where separation pressures and temperatures vary between subsequent separations (Freyss, et al., 1989). The volumes of the produced gas and remaining liquid after each flash stage are measured. The measured volume and volume changes of the respective liberated gas and residual oil from differential liberation and flash liberation experiments are subsequently used in establishing B_o, B_g and R_s. The above expressions detail their evaluation, where V_o is the volume of oil in place, V_g is the volume of gas in place, $V_{g,stp}$ is the volume of gas at standard conditions, V_r is the reservoir volume, φ is porosity and S_w is water saturation.

3.1.3 Hydrate Formation and Equilibrium Conditions

Hydrate formation in oil and natural gas systems is of great concern in flow assurance of the produced hydrocarbons. The temperature and pressure conditions that a reservoir fluid will form hydrates or dissociate at indicates what operating conditions are viable for piping and equipment. Should hydrate formation be detected in a processing system, the quantity and concentration of inhibitor or the extent of pressure reduction are all critical information in solving hydrate flow assurance issues. A PVT cell has the capability of evaluating hydrates at a range of fluid and phase conditions, and assessing the effectiveness of inhibitors.

There are three different modes that the operation of the cell for hydrate purposes may proceed in – isothermal, isobaric and isochoric. In the isothermal process, starting at a pressure above the hydrate formation point, the formation of hydrates ensues upon mixing of the two phases. Hydrates are almost always first observed at

the solution-gas interface (Mork, 2002), because of the less energy required for heterogeneous nucleation, which commonly transpires at phase interfaces (Kashchiev & Firoozabadi, 2002a). The system pressure is controlled by an external source, such as a piston pump, for the addition or withdrawal of gas. Pressure in the cell is reduced in decrements after the formation of the hydrate is complete, where the equilibrium pressure corresponds to the observation of hydrate degradation.

An isobaric hydrate test involves maintaining the pressure, usually by an associated automated pump which contains the source of gas. The temperature of the fluid is gradually decremented until hydrate formation is visually detected. After the hydrate has developed, the temperature of the system is increased slowly at constant pressure until the hydrate solid has completely dissociated (Sloan & Koh, 2008). Similar to the isothermal process, the equilibrium point, or temperature in this operation, is representative of the point where degradation of the synthesized hydrate begins (Tohidi, et al., 2000).

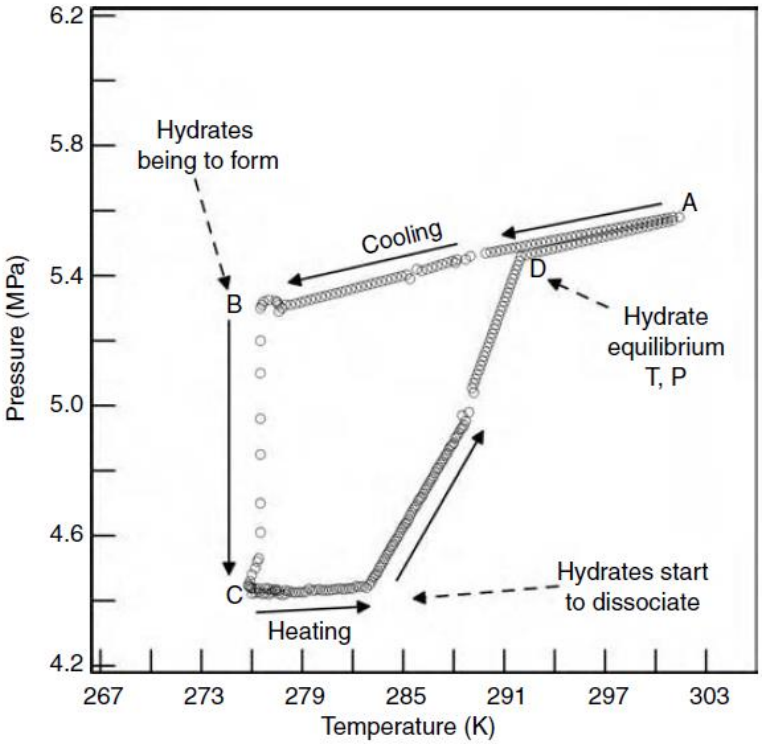

Figure 26 – Isochoric Formation and Equilibrium Path (Sloan & Koh, 2008)

The isochoric hydrate operation differs from the isobaric and isothermal procedures in the sense that no gas or liquid is supplied or removed in the maintenance of pressure, nor is the equilibrium point determined by visual observation. Instead, a closed system exists, where temperature is the controlled parameter and pressure is allowed to change. Figure 26 illustrates the thermodynamic route taken during the

isochoric analysis of a hydrate-forming system. Starting in the vapour-liquid region (A), the fluids are cooled to the hydrate formation temperature (B), which is accompanied by a temperature-induced pressure reduction. The formation of hydrates consumes gas molecules, ultimately reducing the pressure considerably (C). Given complete formation of the hydrate phase, the temperature is increased, causing dissociation of the hydrate. The intersection of the cooling line and the dissociation line (D) on a pressure-temperature plot is indicative of the hydrate equilibrium point (Sloan & Koh, 2008).

3.2 PVT Sapphire Cell Setup

Manufactured by Sanchez Technologies, the PVT sapphire cell system was used to generate hydrate experimental data in this study. The apparatus has largely remained unchanged, except for a positive displacement pump that was introduced for better pressurization procedures and control. Additionally, a manifold was installed, allowing multiple gas sample canister connections and greater quantities of gas into the flow loop at one time. The apparatus in its entirety constitutes the sapphire cell unit, the air bath for which it is contained in, the positive displacement pump, a vacuum pump, pneumatic gas booster pump, chiller, electrical heating system, manual ball valves, two recording cameras mounted against the viewing window, a stainless steel magnetic actuator, various thermocouples and pressure monitoring equipment, digital displays and a computer with software capable of displaying temperature and pressure readings relayed from each instrument. All gas supply and transport lines are ¼ inch (6.4 mm) stainless steel tubing, and are supplied by Swagelok Western Australia, in addition to all associated fittings and valves.

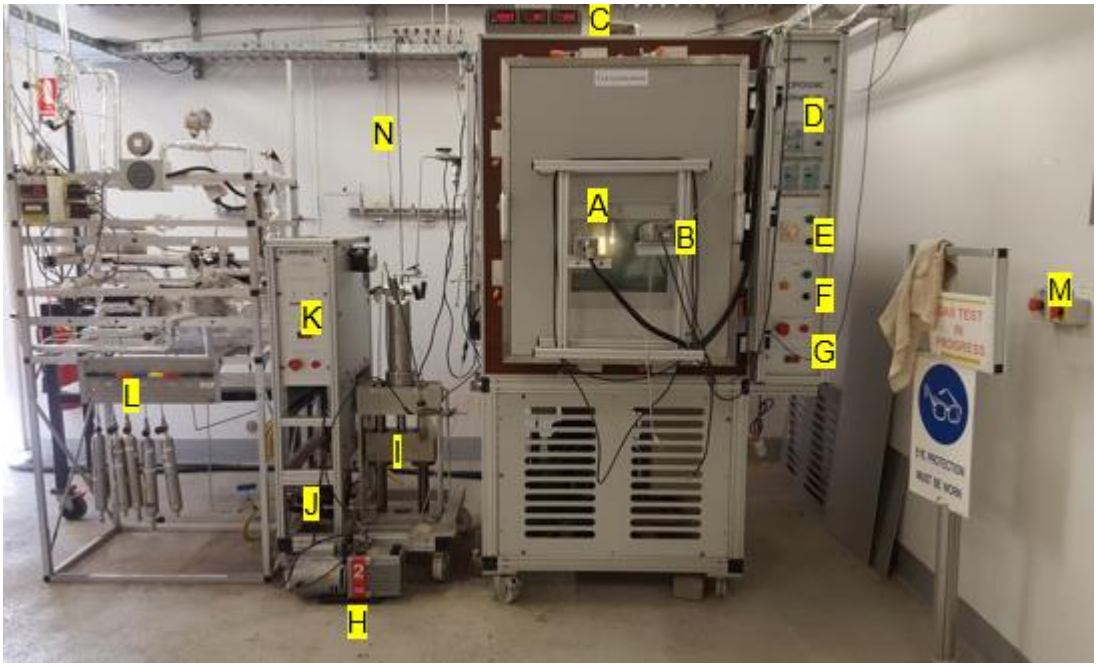

Figure 27 – PVT Sapphire Cell Apparatus

The primary components and safety accessories of the sapphire cell pilot plant are identified and labelled in Figure 27:

A. High pressure PVT sapphire cell and viewing window
B. Mounted Panasonic video cameras
C. Overhead digital output (pressure and actuator displays)
D. Temperature measurements for the gas and liquid phases
E. Control dials for magnetic stirrer rotational velocity and air bath circulating fan
F. Heating and cooling switches
G. Emergency shut-down of apparatus button
H. Vacuum pump
I. Positive displacement pump
J. Pneumatic gas booster pump
K. Positive displacement pump power switch and emergency stopping button
L. Gas injection manifold
M. Emergency button for shut-down of entire laboratory
N. Venting line

An important and heavily relied upon aspect of the CGTA sapphire cell apparatus is the visibility of all fluids, phases, phase changes and any other physical phenomena in PVT studies. The viewing window, A, is the essential centerpiece of the setup that allows a clear vision of the fluid content in the high pressure cell. Also designated A, the cell is submersed in a climatic air-bath with a circulating fan for effective

temperature control of the cell's fluids. The cell is constituted of a tube of thick sapphire glass and is mounted between two stainless steel flanges, which accommodate the fluid inlet/outlet steel tubing and the magnetic stirrer. These features, in addition to clamping of the air-bath door, ensure the safe and low risk containment of the working fluid system. Mounted video cameras, B, add clarity and visual observation capabilities to the apparatus, and are extremely useful in hydrate formation and equilibrium experiments because of the reliance on visual changes and cues. Video monitoring and recording of the cell throughout the experimental procedure enables re-examination of important events and processes that in real-time may be difficult to detect. For example: hydrate dissociation is often subtle, and rarely spontaneously (macroscopically) occurs. Revisiting footage of the experiment can substantially aid in narrowing down the range where hydrate dissociation is believed to occur initially.

For safety and experimental purposes, monitoring of all parameters in a hydrate experiment is essential. A digital overhead display, C, detailing cell pressures and temperature indicators for liquid and gas phases, D, provide a means for quick readings. Alternatively, pressure and temperature readings are provided by software packages (not pictured), where control set points are also specified. Heating and cooling rates may also be specified as opposed to a temperature, both of which can be activated/deactivated with their control panel, F. Additionally, the heating/cooling rate may be manually controlled by a switch and dial, E, which alters the velocity of rotation for the air-circulating fan in the air-bath.

The positive displacement pump, I, is the primary mechanism through which pressure is controlled in the system, and is responsible for a large proportion of the pressurization process when higher pressures are desired. When required, the pneumatic gas booster pump, J, is operated in conjunction with the positive displacement pump, in an effort to further pressurize the PVT cell. Gas is introduced into the flow loop by connecting pressurized gas canisters to the manifold, L, and releasing their contents. Naturally, a relatively large proportion of the original content of the gas canisters will not enter the system, which is needed for higher pressure experiments. The gas booster pump effectively extracts the remaining gas in the canisters, boosting the overall pressure in the system. In the instance of removing gases from the flow loop, or various compartments of the setup, flow is directed to the vent line, N, where gas is safely released into the atmosphere. Residual gas and air will always remain after venting, and is where the vacuum pump, H, serves its purpose. For experimental accuracy and reproducible data, all remnants of fluids that

inhabited the system in any previous use of the sapphire cell flow loop are required to be vented. The vacuum pump is particularly applicable for this service.

The safety and well-being of all laboratory personnel, equipment, instruments and the facility in general are of utmost conern, and for that reason, it is essential that potentially dangerous components are equipped with emergency stopping capabilities. The displacement pump and PVT cell are both fitted with emergency shutdown buttons, as depicted by K and G respectively. As a further measure, the emergency power switch, M, is installed in the event where power to all laboratory components must be immediately discontinued, such as a fire. Methane and carbon dioxide analyzer alarms (not pictured) supplied by Gas Alarm Systems are also installed in the hydrate laboratory. High concentrations of methane and/or carbon dioxide in the lab environment are hazardous, as methane is combustible and above-normal carbon dioxide concentrations promote asphyxiation. The implemented gas alarms are an effective preventative measure for the mentioned hazards.

3.2.1 Equipment and Instrumentation

The PVT cell flow loop at the CGTA hydrate laboratory was the primary apparatus used for experimental work and procedures. Notable operational equipment implemented in this study are the sapphire cell unit, positive displacement pump, pneumatic vacuum pump and two video recording cameras (with live feed directed to the controlling PC). The gas booster pump was also available for use when higher pressures were required, or when the gas cylinder pressure was low. A schematic for the plant is depicted in Figure 28.

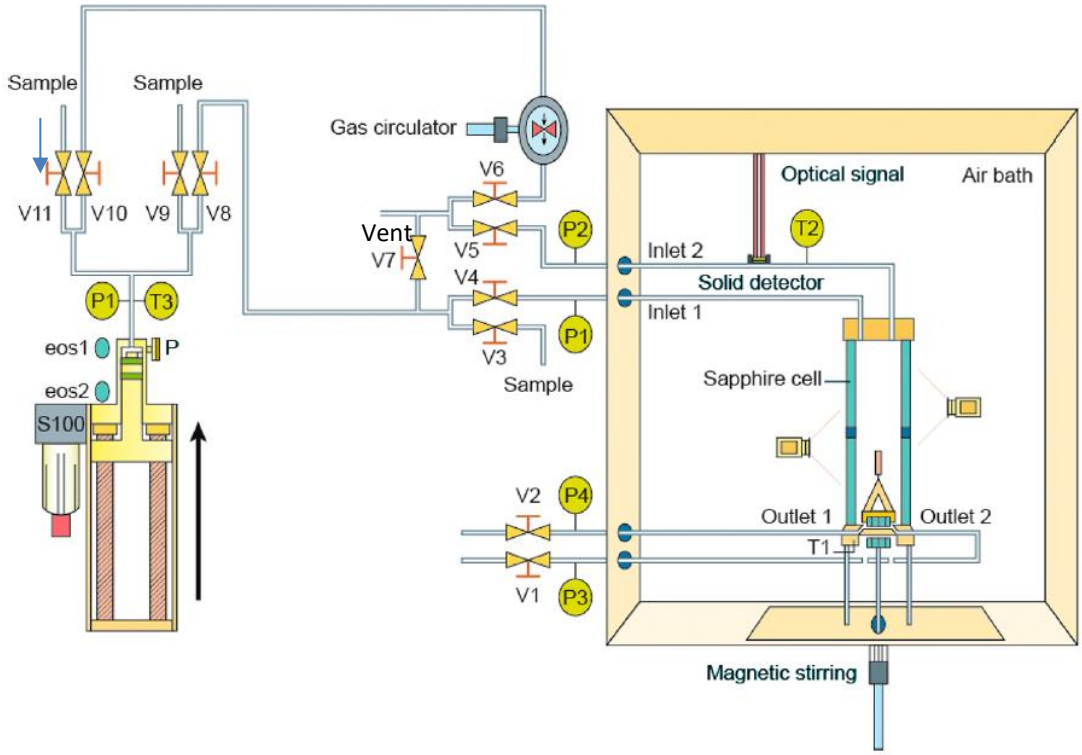

Figure 28 – PVT Cell Flow Loop (Obanijesu, et al., 2014)

The sapphire cell unit was modified by screwing thermocouple probes, T1 and T2 (±0.075 °C), onto the top and bottom stainless steel flanges connected to the cell, such that they are exposed to the gas and liquid phases respectively for temperature readings of both phases. Pressure transmitters P1 and P2 (±0.25 bar) were supplied by Hinco Instruments Pty Ltd and used for pressure readings where readings for P1 are directed to an overhead digital display and P2 readings relayed to the PC. For composition analysis of prepared gas mixtures, an MSR Electronics methane and carbon dioxide analyse was available. This was useful for the Chapter 5 and Chapter 6 experiments, since bi-component gas mixtures were prepared. It was necessary to only use the methane analyser, although the carbon dioxide analyser was used for additional confirmation of methane-carbon dioxide compositions. Numerous sample points throughout the process allow for compositional analysis of the gas mixture at the piston pump and the sapphire cell. On some occasions, the gas composition differed slightly between both locations, and was determined to be caused by inadequate mixing. This problem was resolved by leaving the system to settle and equilibrate, so that the composition in the cell matched the upstream composition.

3.2.2 Application of Apparatus

The pressurization of the prepared gas mixture is performed using the positive displacement pump (Figure 28) and is maintained with specialised software that

controls the position of the piston. Pressure is controlled with a Baldor motion PID controller which responds accordingly to Mint Workbench (software used for inputting pressure set points and monitoring). The thermocouple installed at the base of the sapphire cell (T1) is designated as the control thermocouple, as it transmits the temperature of the liquid phase and is reflective of the temperature that the hydrate phase will form/dissociate at. If the temperature of the liquid phase is considerably higher or lower than the vapour phase, a temperature differential will exist and not reflect the phase transformation conditions, especially considering that heat transfer is the controlling factor in hydrate phase changes (Davies, et al., 2006). As a countermeasure, heating and cooling rates were performed in small increments, thereby reducing temperature differences between the liquid and gas phases. Temperature control is provided by FALCON software, and permits the input of the desired liquid phase temperature which is maintained with the PID controller packaged with FALCON software. Cooling of the fluids is supplied by a chiller using cooling water set at 3.0 °C, and the electrical heater installed in the air bath provides heating.

Figure 29 – Insufficient Agitation of Liquid Surface

Mixing and agitation of the liquid phase is essential in the promotion of hydrate formation because it facilitates nucleation and aggregation and enhances gas dissolution. This is partly the reason for the formation of large hydrate plugs in transmission pipelines. These conditions are of course desirable from an experimental perspective. This exemplifies the purpose of the magnetic stirrer, which is maintained at approximately 120 RPM during the experimental procedures. Figure 29 illustrates the result of a failed hydrate experiment due to the inability of the stirrer to sufficiently agitate the surface of the liquid phase. An excessive quantity of Milli-Q distilled water was mistakenly added to the PVT cell such that during operation, the water level exceeded the top of the stirrer. The resulting hydrate formation formed a

sheet over the liquid phase which the stirrer could not disrupt. This hydrate sheet effectively acted as a barrier between the gas and liquid and prevented the growth of the hydrate phase substantially. The hydrate was left for several hours upon which no bulk hydrate growth took place. A similar experience was noted by Dicharry, et al. (2013). Water amounting to 5.0 mL is optimal in that the water level lies just below the top of the actuator, enabling it to agitate the surface of the liquid phase.

In the event of cleaning the internals by purging of the plant or the disposing of gas, an additional line is connected to the sapphire cell unit where gas is safely directed to a rooftop outlet and released. Gas may also be preserved and stored temporarily by isolating the gas in the piston pump for a future operation rather than wasting it in the venting/purging process.

3.2.3 Apparatus Operating Method

For the determination of the hydrate formation and dissociation conditions, the temperature-search method at constant pressure, i.e. the isobaric process (section 3.1.3), was employed. This involved stimulating the fluid mixture in the form of cooling and heating to promote formation and dissociation of the hydrate phase respectively whilst controlling the pressure. The way temperature control of the fluid contents proceeds can potentially influence the observed formation and dissociation temperature. Tohidi and co-workers proved this phenomenon, and concluded that more accurate and reproducible measurements are provided when the system is allowed to thermally equilibrate (Tohidi, et al., 2000). Being a heat-transfer driven process (particularly dissociation), heating and cooling is therefore applied cautiously.

3.2.4 Gas Mixture Preparation

Preparation of the experimental gas mixtures were performed gravimetrically using 500 ml stainless steel gas canisters. Initially, the sample canisters were vacuumed and then weighed using a Shimadzu balance (±0.0005g). All gases were purchased from BOC Australia and of high purity (99.99% to 99.995%). After collecting gas samples, the canisters are weighed again and the quantity of gas and composition when mixed was determined by,

$$n_i = \frac{\Delta m_i}{M_i} \qquad \text{Eq. 24}$$

$$x_i = \frac{n_i}{n_t} \qquad \text{Eq. 25}$$

Mass and moles of gas i are designated n_i and Δm_i respectively, M_i is component i's molecular weight and x_i is its composition. For Chapter 4 and 6 experimental

procedures, the diluting gas enters the system first to ensure the contents are released into the pump as it is at a far lower pressure in the canister, followed by the methane. Its composition was confirmed with the methane and/or carbon dioxide gas analyser.

3.2.5 Experimental Procedure

Before the commencement of any experimental procedures, the plant was purged with nitrogen to remove any foreign species that may have the capacity to influence experimental results. Milli-Q distilled water (5.0 mL) was syringed into the sapphire cell unit through a capped inlet on the steel flange connected to the top of the cell chamber. The nitrogen occupying the internals was vacuumed with the pneumatic vacuum pump, followed by the pressurization of the prepared gas mixture in the piston pump. After allowing the system to equilibrate, the gas composition was analysed at sample points located at the pump and the PVT cell (Figure 28). Once the desired pressure was achieved, cooling of the fluids in the reactor was initiated. Software packages capable of providing estimates for the hydrate equilibrium/dissociation temperature were consulted prior to the experimental procedure. Hydrate formation temperatures were determined based on previously observed sub-cooling requirements for hydrate formation. A reasonable estimate of the formation temperature, T_f, was calculated by a straight-forward calculation,

$$T_f = T_{eq} - \Delta T_{sub} \qquad \text{Eq. 26}$$

The sub-cooling required for hydrate formation, ΔT_{sub}, which is usually 2-4 °C less than the equilibrium temperature, was simply subtracted from the equilibrium temperature, T_{eq}, approximated using hydrate utilities implemented in PVTsim and HYSYS. The cooling rate was reduced to approximately 1.0 °C per hour when the temperature of the liquid phase approached the predicted T_{eq} until hydrate formation was visually confirmed. At this point, cooling was discontinued and the temperature was maintained. The required degree of sub-cooling had already been achieved so no further cooling was necessary. Growth and crystallization of the hydrate phase was allowed to take place until blockage of the sapphire cell ultimately followed. Heating of the hydrate solid was performed at a rate of 1.0 °C per hour also, to procure a reliable hydrate dissociation temperature. The hydrate mixture was further heated, thus dissociating the hydrate solids completely. Finally, the PVT cell was depressurized and the liquid phase drained from a capped outlet on the bottom flange of the cell. All liquid remnants were flushed out with water multiple times and cleaned for future procedures.

Chapter 4

4. Hydrates of Nitrogen and Carbon Dioxide with Methane

An experimental correlation that describes and predicts hydrate equilibrium conditions of gas systems containing the studied gas species is developed with experimental data composing of methane-carbon dioxide and methane-nitrogen gas with water. Hydrate equilibrium data and illustrations are provided to aid in the development of empirical equations describing such data. It is also demonstrated that modelling and simulation software cannot always be relied upon when seeking hydrate equilibrium figures for a gas-water system. The importance of considering alternative methods for the generation of hydrate equilibria is outlined by discussing observed inconsistencies with modelling software hydrate predictions that were encountered during this research. Specifically, predictions of nitrogen in methane gas hydrate equilibria are noted. In these instances, it is beneficial to have access to another source, one which is underlined by an experimental approach as opposed to a theoretical approach. The remainder of this sub-section respectively introduces carbon dioxide and nitrogen as a hydrate promotor and inhibitor with respect to methane hydrates and the outcomes in terms of their hydrate capabilities and influences relative to methane that arise when they are mixed. Summaries of data acquired from various literature sources pertaining to simple methane, carbon dioxide and nitrogen gas hydrates are also presented for perspective.

4.1 Carbon Dioxide as a Hydrate Promotor

Promotion (and inhibition for that matter) of the hydrate equilibria is relative to an initial starting system. In the context of a two-phase pure methane gas and water system, many chemical species can promote hydrate formation. These species can exist in the liquid phase and dissolve in the water, or they can mix with the methane in the gas phase, creating a gas mixture with a greater propensity towards forming a hydrate phase at a given temperature at constant pressure conditions. One example is carbon dioxide: by itself in the presence of water, carbon dioxide hydrate will synthesize at greater temperatures than methane, particularly at lower pressures.

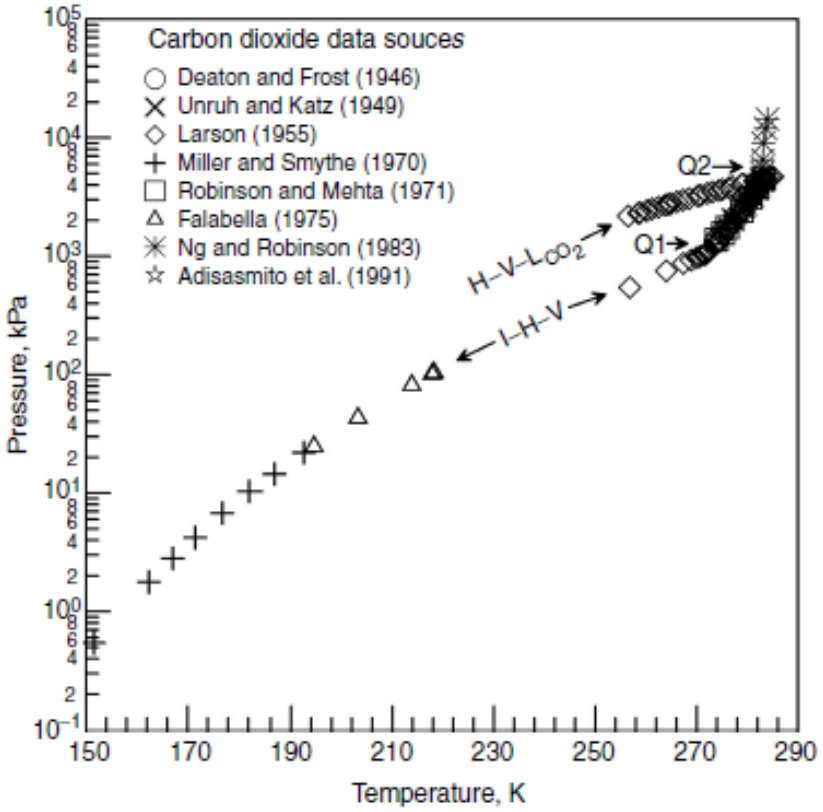

Figure 30 – Carbon Dioxide Hydrate Data (Sloan & Koh, 2008)[*]

[*]Data Sources: (Deaton & Frost, 1946), (Unruh & Katz, 1949); (Larson, 1955); (Miller & Smythe, 1970); (Robinson & Mehta, 1971); (Falabella, 1975); (Ng & Robinson, 1983); (Adisasmito, et al., 1991).

Over the past sixty years, carbon dioxide hydrate equilibrium data has demonstrated that the pressure-temperature relationship changes drastically after reaching either of the quadruple points (Q_1 and Q_2 in Figure 30). This relates to the phase behaviour of carbon dioxide. The proximity of the gas-liquid phase boundary with the hydrate equilibrium line means that as the pressure increases, carbon dioxide will condense. From the pressure-temperature phase diagram for carbon dioxide (Figure 31), the similar hydrating and condensing conditions for carbon dioxide are apparent. Expectedly, the intersection of the saturation line with the hydrate equilibrium line coincides with Q_2, leading to a change in the slope of the hydrate line as it moves into the liquid carbon dioxide region.

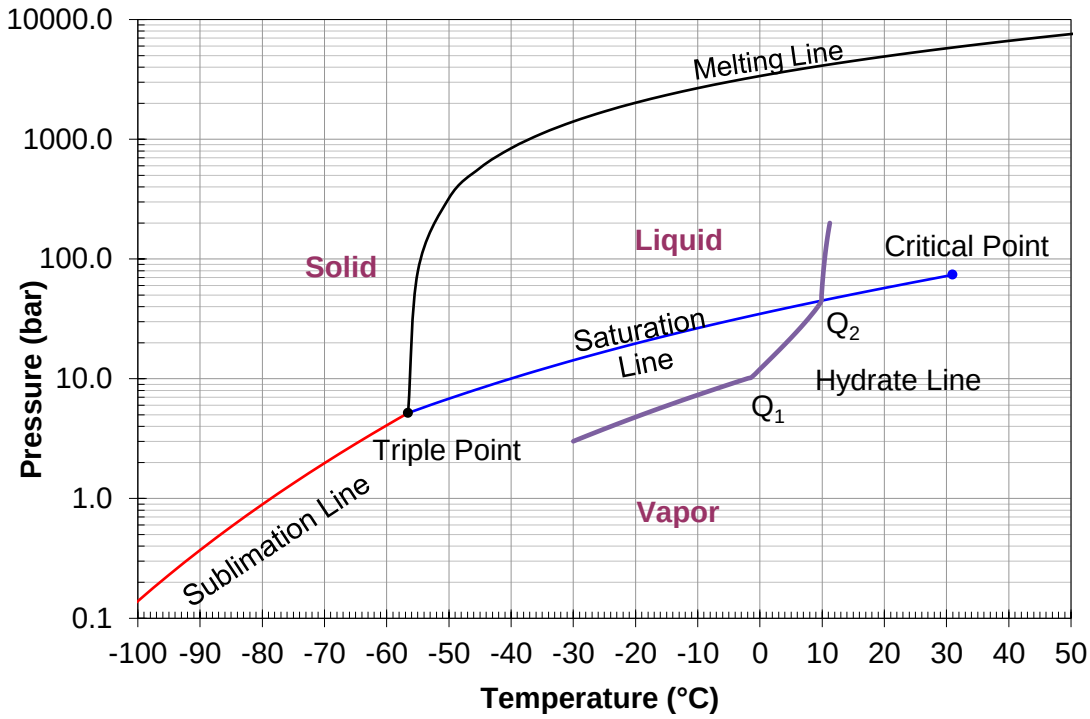

Figure 31 – Carbon Dioxide Phase Diagram (ChemicaLogic, 1999)

Q_2 occurs at 45 bar, 9.8 °C (Sloan & Koh, 2008). Steepness of the hydrate equilibrium line increases because of liquefaction. Comparatively, methane only has a single quadruple point occurring at 25.63 bar, -0.25 °C (Sloan & Koh, 2008), meaning there is no coexistence of a liquid methane and hydrate phase as with carbon dioxide hydrates (see Figure 32). The slope of its semi-log hydrate curve is relatively constant and less steep than carbon dioxide's beyond carbon dioxide's Q_2 conditions. Methane hydrates still exist in a three-phase L_w-H-V system at such conditions.

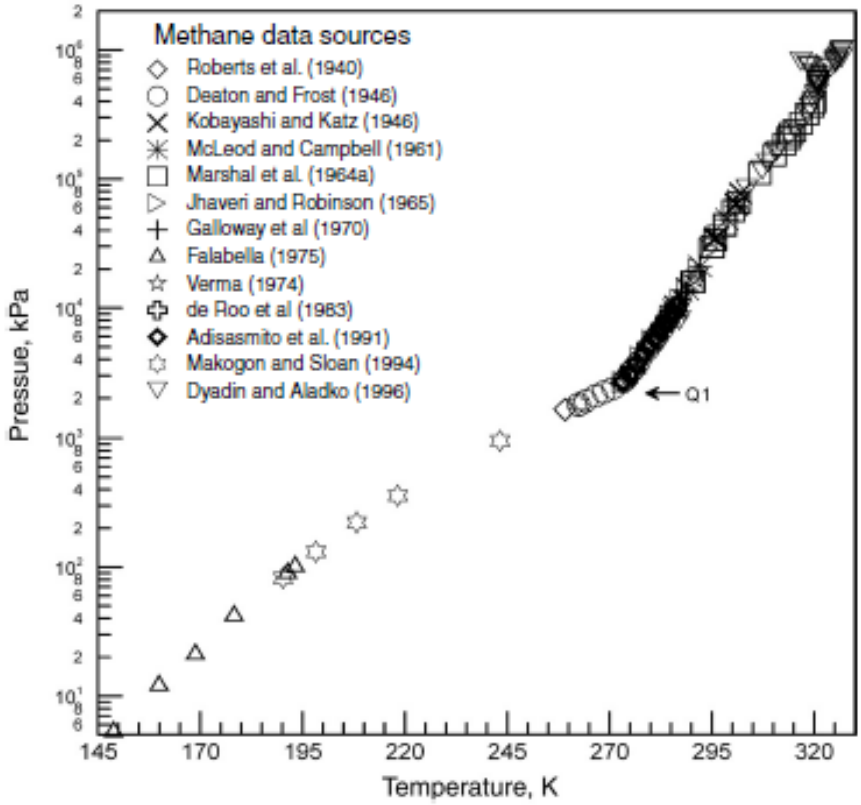

Figure 32 – Methane Hydrate Data (Sloan & Koh, 2008)[*]

[*]Data Sources: (Roberts, et al., 1940); (Deaton & Frost, 1946); (Kobayashi & Katz, 1949); (Mcleod & Campbell, 1961); (Marshall, et al., 1964); (Jhaveri & Robinson, 1965); (Galloway, et al., 1970); ; (Falabella, 1975); (Verma, 1974); (de Roo, et al., 1983); (Adisasmito, et al., 1991); (Mehta & Sloan, 1994); (Dyadin & Aladko, 1996).

The methane and carbon dioxide hydrate equilibrium curves ultimately intersect, which arises at 71 bar, 9.9 °C (Figure 33), after plotting the compiled experimental data from the previous illustrations. Beyond this point, pure methane will form its hydrate at higher temperatures for a given pressure. Because of the described phase phenomenon, the phase behaviour of methane-carbon dioxide gas mixtures should be consulted when considering their hydrate equilibrium conditions. The experimental work performed in this chapter uses carbon dioxide compositions of <20 mol% in methane, and according to PVTsim, the cricondentherm is -52 °C. The cricondentherm decreases as the carbon dioxide composition approaches 0 mol%. All three-phase L_w-H-V equilibrium temperatures that are encountered in this section's experimental research are above 0 °C, confirming that no gas condensation occurs and thus, the gas composition does not change with heating/cooling.

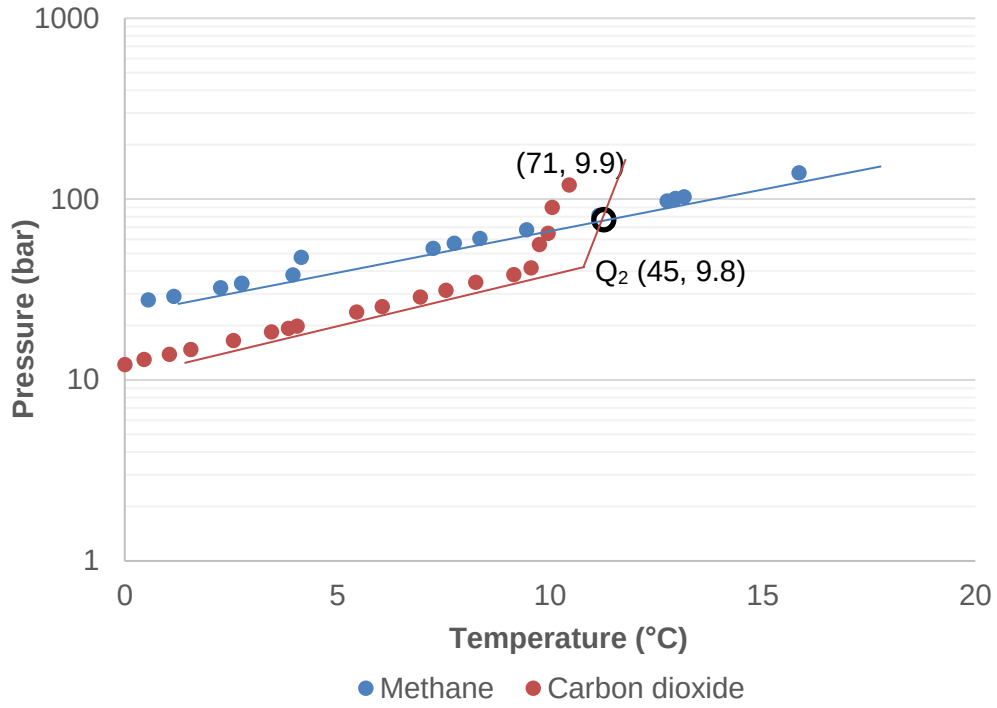

Figure 33 – Methane and Carbon Dioxide Hydrate Equilibrium Lines

Carbon dioxide hydrates in comparison are considerably more vulnerable to becoming hydrated in a water-containing environment than nitrogen. Much lower pressures can result in the formation of carbon dioxide hydrates as first discovered by Deaton and Frost (1946). At a temperature of 0 °C, a pressure of approximately 12 bar can initiate formation of a hydrate phase (Deaton & Frost, 1946) – an order of magnitude lower than nitrogen. This reflects their opposing roles when coupled with methane in hydrate forming conditions.

The carbon dioxide molecule is too large to inhabit small 5^{12} cavities, instead preferring the $5^{12}6^2$ cage of sI hydrates because it more closely matching the cavity radius (Lederhos, et al., 1993). The role of carbon dioxide in a methane mixture is to occupy these larger cavities, which is only stabilized by methane to a small extent. A greater concentration of occupied $5^{12}6^2$ sites stabilizes the hydrate and raises the equilibrium temperature. This promotion is studied by establishing hydrate equilibria for various carbon dioxide compositions in methane and determining their heats of dissociation. The differing heat of dissociation values reflects the difference in equilibrium conditions by inferring changes in stability. Hydrates with higher dissociation enthalpies require more energy to dissociate and are therefore more stabilized.

4.2 Nitrogen as a Hydrate Inhibitor

The hydrate equilibria for nitrogen is a recognized concept in the field of gas hydrates. Nitrogen is known to form hydrates at relatively extreme conditions compared to most light to intermediate hydrocarbon gases. Early studies have demonstrated that pure nitrogen three-phase hydrate equilibria (water-vapour-hydrate) extends far upwards of 1000 bar and a pressure greater than 150 bar is necessary for hydrates to form at 0 °C (van Cleef & Diepen, 1960). A compilation of literature data for simple nitrogen hydrate equilibria in Figure 34 illustrates the relatively extreme thermodynamic conditions necessary for a stable nitrogen hydrate phase to exist.

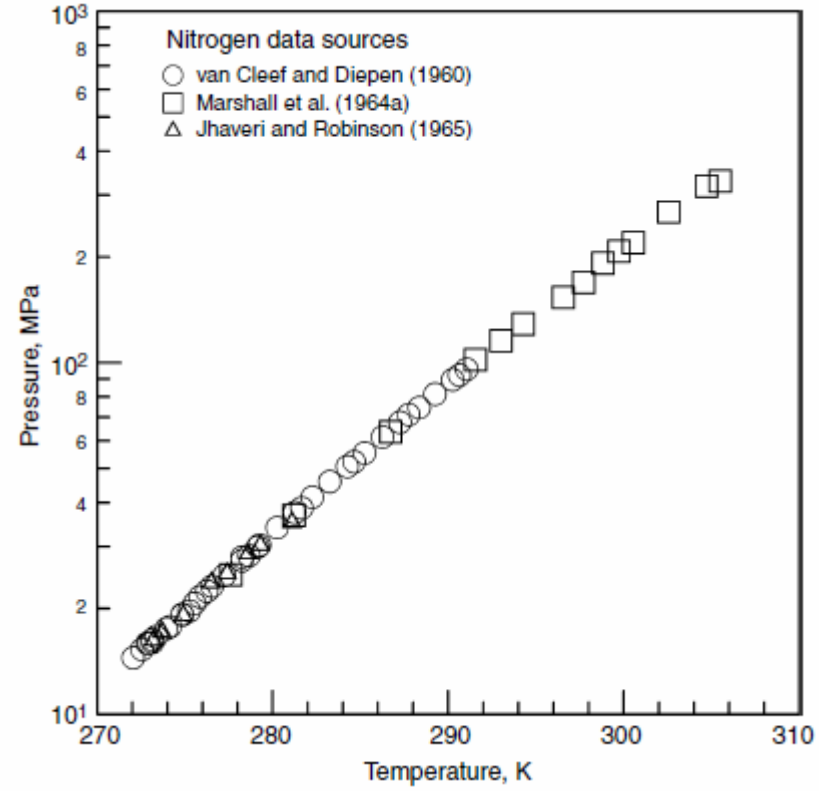

Figure 34 – Nitrogen Hydrate Data (Sloan & Koh, 2008)*

*Data Sources: (van Cleef & Diepen, 1960); (Marshal, et al., 1964); (Jhaveri & Robinson, 1965)

Given the high pressure demands for nitrogen hydrate formation, it can be introduced to another hydrate-forming gas with more lenient thermodynamic requirements as a hydrate preventative measure by behaving as a diluent. Hydrate equilibria of methane and its behaviour with nitrogen addition are examined in this chapter to observe and quantify the concentration of nitrogen in methane that affords a significant depression in the hydrate equilibrium conditions. Stability of the hydrates are also investigated using the Clausius-Clapeyron relationship in providing the heat of dissociation. The heat of dissociation is known to correlate with hydrate stability and its phase equilibria,

where changes in the hydrate equilibrium conditions due to the presence of another component are perceived by changes in the heat of dissociation.

The more intense thermodynamic conditions necessary for a stable nitrogen hydrate phase is implied by the use of MPa units in Figure 34, compared to kPa in the carbon dioxide and methane simple hydrate equilibria plots (Figure 30 and Figure 32 respectively). For example, at a temperature of 0.0 °C, the required pressure for methane to form hydrates with water is approximately 25-30 bar; for nitrogen at the same temperature, 160-165 bar. A graphical comparison is made between both hydrate equilibrium lines in Figure 35 (using literature data presented in Figure 34).

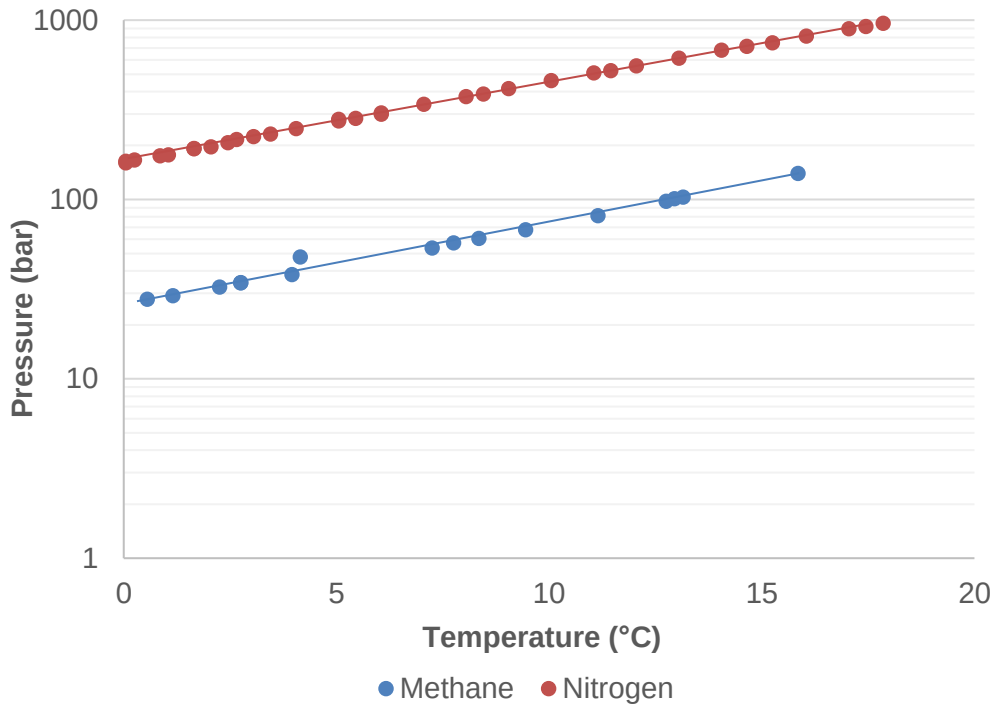

Figure 35 – Methane and Nitrogen Hydrate Equilibrium Lines

Given that simple nitrogen hydrates require far more excessive pressures, adding nitrogen to methane will depress the thermodynamic conditions of methane by reducing methane's partial pressure. Essentially, nitrogen is diluting methane, suppressing the thermodynamic conditions that favour hydrates. The effect of dilution increases as the concentration of nitrogen in methane increases, given that the partial pressure of nitrogen does not exceed its hydrate equilibrium pressure, else nitrogen hydrates may synthesize.

Nitrogen concentrations tested in this chapter are <25.0 mol% in methane. The cricondentherm of such a mixture is approximately -93 °C (PVTsim); such a low cricondentherm is the product of nitrogen's very low boiling point of -196 °C. The

methane-nitrogen cricondentherm decreases with an increasing nitrogen composition, and confirms that no gas liquefaction occurs in the region of experimentation (>0 °C). Confirmation of the phase behaviour of experimental methane-nitrogen mixtures is essential because the composition of the gas should ideally not change so that the exact gas concentrations are known throughout an experiment. Because of the extremely low solubility of nitrogen and methane in water, the composition can accurately be assumed to be equal to the initial global gas composition throughout an experimental process.

Reasoning behind nitrogen's difficulty in forming a stable hydrate phase at less extreme thermodynamic conditions was revealed through the implementation of x-ray diffraction. These studies revealed that nitrogen is a sII hydrate former and occupies the small 5^{12} cavities (Davidson, et al., 1986). With quite a small radius relative to the cavity size, it is understandable why high pressures are needed. Ideally, the molecular radius of a hydrate former should lie between 75-100% the size of the hydrate lattice cavity (Sloan & Koh, 2008). Nitrogen lies at the lower end of this range at 81% for the 5^{12} cavities. It is also a diatomic molecule with no net polarity, discouraging any significant polar interactions with the water cage molecules. Nitrogen would also be equally stable in the nearly identical sI 5^{12} cavity as the sII 5^{12} cavity is only very slightly larger, but there are far more small cavities in sII hydrates making sII a more favourable arrangement (Sloan & Koh, 2008). With sII small cavity fillings, a greater concentration of occupied cavities is permitted and therefore greater overall lattice stability.

4.3 Experimental Observations

The physical observations for hydrates of methane diluted with either nitrogen or carbon dioxide were identical to one another, with no distinguishing macroscopic features. Sub-cooling of approximately 2-4 °C below the dissociation temperature was sufficient to initiate the hydrate formation process. For experimental continuity, a fixed mixing velocity of 120 RPM was applied across all thermodynamic conditions tested, promoting hydrate agglomeration and growth. Prior to observable hydrates masses, there is a short period where the solution appears slightly opaque, corresponding with the induction period where very small hydrate particles are present (Sloan & Koh, 2008). The induction period is defined as the time required for the first macroscopically observable hydrate mass to form once the pressure and temperature conditions are in the hydrate stability zone. This period predominantly consists of hydrate nucleation (not observable), but also involves a small amount of

growth to the point where hydrates are first visible (Sloan & Koh, 2008). This is pictured in Figure 36 (a), where the presence of a hydrate phase was detected at the solution-gas interface. Mori (1998) performed studies on hydrate films, and also made note of hydrate solids becoming visually detectable at the phase interface before hydrates in the body of the solution is observable.

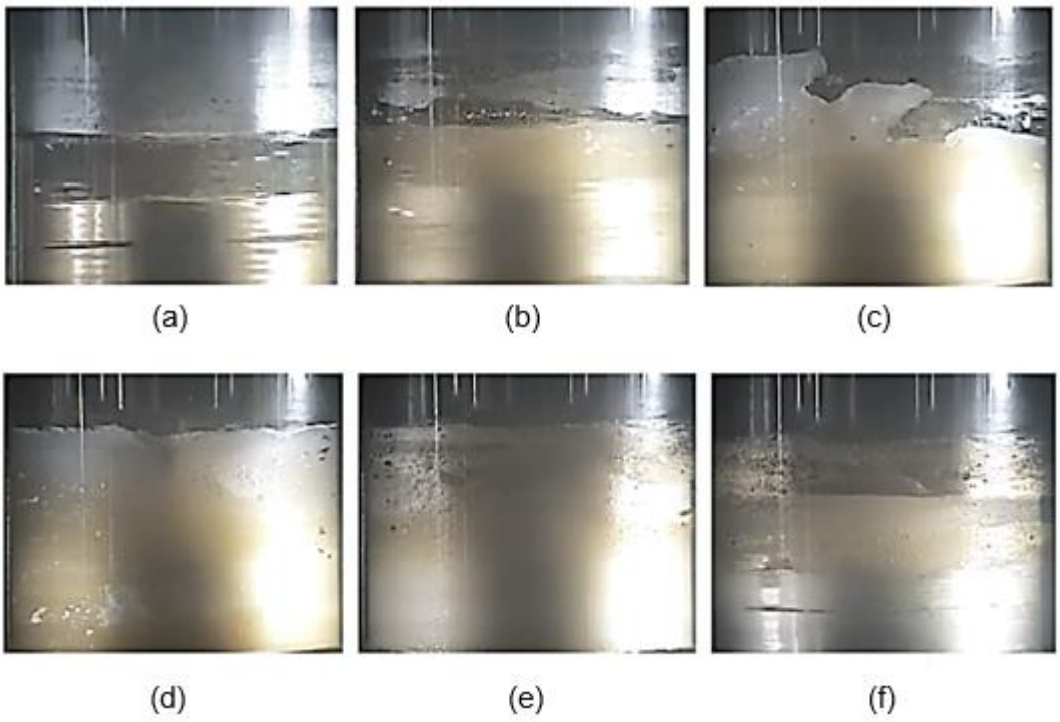

Figure 36 – Experimental Observations (Smith, et al., 2015)

After progressing further, growth of the hydrate phase transformed the mixture into a more solid-concentrated state (b), and resembled very icy water. The hydrate slurry was still able to flow freely, as the magnetic stirrer was able to easily maintain its RPM without any noticeable resistance. It was evident that this initial formation period occurred rapidly at first, but decreased over time. With time, the hydrate lattice is being concentrated with gas molecules, leading to a lower concentration of water molecules and therefore a less negative Gibbs free energy value (ΔG). From Eq. 15, the hydrate growth rate decreases exponentially with higher ΔG values, explaining this phenomenon.

Parts of the hydrate slurry transitioned into larger masses with further growth and were forced up against glass in a nearly immobile state (c). This usually had little effect on the flowing capability of the remaining hydrate slurry, as evidenced by the continuous rotation of the actuator. However, resistance to flow occurred with further addition to the crystal mass, causing the stirrer to stutter and drastically slow down at

times as a consequence of the small quantity of liquid remaining. A more pronounced resistance to flow resulted with additional development of the larger hydrate solids, and occurred on a more frequent basis. In time, the hydrate phase developed into a single crystal mass and completely consumed the liquid phase in the process (d). Because of the absence of a liquid medium, the magnetic stirrer was rendered completely immobile, and was unable to move the large continuous hydrate. Thermally stimulating the hydrate to the dissociation point resulted in the subtle degradation of the structure (e). The initial indications of dissociation can be difficult to identify, particularly with a low heating rate, but can be detected by the formation of small cavities on the outside of the hydrate and small amounts of liquid formation. Under continued thermal stimulation, the hydrate mass degrades to a point where it is no longer continuous, and becomes fragmented. Hydrate solids were continually reducing in size, causing the collection of a liquid phase at the base of the cell, thereby freeing the actuator and allowing rotation. The actuator initially struggled due to the presence of large dissociating hydrate, but quickly rotated more fluently as the solid masses reduced in size, inferring reasonable flowing conditions. Throughout the course of dissociation, it was immediately apparent that liquid formation was prominent on the outside surface of the cylindrical hydrate before it fragmented. It can be concluded that radial dissociation was therefore the primary mode of dissociation.

After significant reformation of the liquid phase and liberation of hydrated gas, the dissociated hydrates were reduced to small, macroscopic particles (f). Small quantities of dirt were commonly deposited on the edge of the cell, adhered to the glass. This was attributed to dislodged corrosion products, and prompted regular cleaning and maintenance of the PVT cell at Future Engineering workshop. At this point, the mixture, now in a comparable state to (b), was flowing without any perceived hindrance of the mixer caused by the smaller hydrates. Continued heating eventually dissociated all macroscopic hydrate solids to a point where no hydrate phase was visible and both liquid and gas phases were completely reformed.

4.4 Results and Discussion

4.4.1 Equilibrium Results

Nitrogen and carbon dioxide are very common impurities in many natural gas reservoirs, and are of no particular use as they do not add to the calorific value of the recovered natural gas. Carbon dioxide is especially non-desirable because of its ability to dissolve in water-containing fluids, thus creating a corrosive environment. Freezing of carbon dioxide in pipelines can also occur, causing blockages. Its early

removal is clearly paramount to further downstream processes. The presence of a water-containing fluid can also be unwelcome because of its capacity to form hydrates with the flowing natural gas. It is therefore vital to understand the hydrate phase behaviour of carbon dioxide and nitrogen to comprehend their role in natural gas hydrates.

4.4.1.1 Methane

As a starting point, it is necessary to determine the hydrate equilibrium curve for pure methane gas since it is the shift of the equilibrium line relative to methane that is of interest in the proceeding sections. The hydrate equilibria for pure methane has been studied greatly and thoroughly established, however, the shifts of the equilibrium line should be relative to measurements taken from the apparatus used for all subsequent hydrate experiments for continuity and quality assurance purposes. Hydrate equilibrium measurements for methane using the CGTA sapphire cell apparatus is presented in Figure 37. For comparative purposes, methane hydrate measurements from various literature sources are also included (Gayet, et al., 2005); (Pahlavanzadeh, et al., 2012); (Zare, et al., 2013); (Keshavarz, et al., 2013).

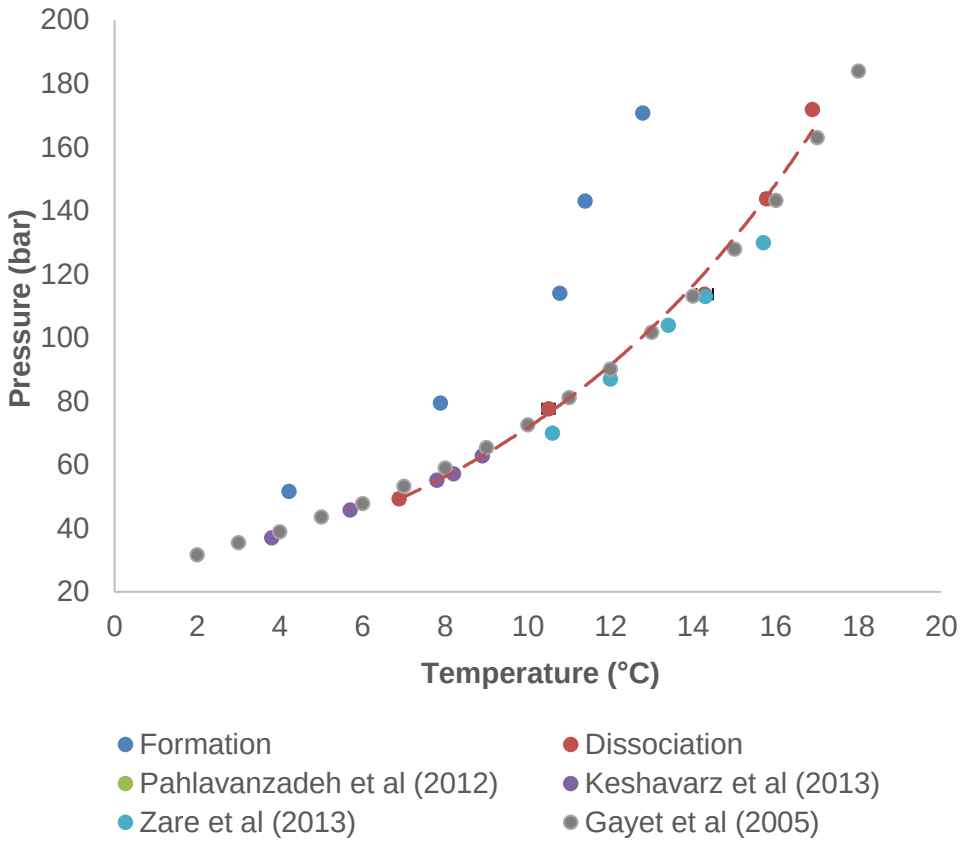

Figure 37 – Methane Hydrate Equilibria (Smith, et al., 2015)

Using the isobaric temperature-search method, several pressure-temperature points describing methane hydrate formation and dissociation/equilibrium were acquired and are fitted by the red dashed curve. Each experimental data point represents the average of duplicate measurements. The collected dissociation measurements are very consistent with experimental work performed by the listed researchers giving confidence in this work's methane hydrate line as a reliable reference point. As such, it is reproduced in all proceeding chapters that include pressure-temperature hydrate equilibria profiles for perspective on the extent the studied gas mixtures deviate from this equilibrium line. All results are complemented by a combined expanded uncertainty (95%, k = 2). An uncertainty of ±1.36% was calculated (see Appendix A for the calculation procedure) for the instruments used. The collective effects of pressure and temperature transmission, temperature sensitivity, stability and calibration uncertainty were considered. Importantly, the uncertainty for the equilibrium temperature is described by the thermocouple's uncertainty (±0.075 °C) and scatter, which are combined by a root-mean-square (RMS) average. Combined with scatter, each data point varied slightly as dictated by their corresponding error bar.

An important note with the methane hydrate profile is the formation points, which are not only noticeably inconsistent with the dissociation conditions, but also do not appear to correlate to the same extent. Lower temperatures than the dissociation/equilibrium temperature are of course required to provide the necessary sub-cooling that creates a driving force for hydrate crystallisation (Kaschiev & Firoozabadi, 2002b). As mentioned previously, there are more factors that contribute to the degree of sub-cooling that induces formation (mixing rate, nucleation sites etc.) than the two pressure-temperature parameters for dissociation. Consequently, the replication of the formation inducing conditions is difficult and can become apparent in the form of less correlation and more variation about the fitted curve.

Table 9 – Methane at 100 bar (Smith, et al., 2015)

	TEST						
	1	2	3	4	Average	St. Dev	C.I. (95%)
T_f (°C)	10.6	10.4	9.9	10.2	10.3	0.30	± 0.477
T_{eq} (°C)	13.0	13.2	13.0	12.9	13.0	0.13	± 0.207

A test was conducted to deliver a numerical interpretation of the variation of the formation and equilibrium points. For this experiment, methane was added to the sapphire cell with 5.0 mL of Milli-Q distilled water and pressurised to 100 bar. The formation and dissociation point was subsequently measured on n occasions (4) using the isobaric method with the operating pressure maintained at 100 bar. After each run, the sapphire cell was drained and flushed with Milli-Q water and another 5.0 mL injected for the following run. The results were averaged and the standard deviation was calculated with the following common statistical formula with n-1 degrees of freedom,

$$s = \sqrt{\frac{\sum_i (T_i - T_{ave})}{n - 1}} \qquad \text{Eq. 27}$$

In the above equation, T_i is the individual temperature measurement for the formation or equilibrium point at 100 bar, T_{ave} is the average T_f or T_{eq} and s is the standard deviation. The confidence interval (C.I.) at the 95% level was subsequently calculated using,

$$C.I. = t_{n-1} \frac{s}{\sqrt{n}} \qquad \text{Eq. 28}$$

At the 95% confidence level, the t-statistic at n-1 degrees of freedom, t_{n-1}, is 3.182. After applying Eq. 28, the formation and equilibrium temperatures are represented as T_f = 10.3 °C ± 0.5 °C and T_{eq} = 13.0 °C ± 0.2 °C respectively after rounding. It can be concluded that there is far less confidence and precision in the T_f measurements compared to T_{eq} at the 95% confidence level. There is a larger range for where the true value may lie for the set of hydrate formation measurements compared to the hydrate equilibrium data. This is in support of Figure 37 which qualitatively depicts more scatter and variation in the hydrate formation points than the equilibrium data points.

4.4.1.2 Methane-Nitrogen

The hydrate phase behaviour of pure nitrogen has been well established, and has been shown to form at far higher pressures compared to pure methane (Deaton & Frost, 1946); (Adisasmito, et al., 1991). With far higher operating pressures required for the formation of its hydrate, nitrogen can favourably shift the equilibrium curve of methane to the left when introduced. A lower temperature is essentially required to induce hydrate formation if a specified quantity of nitrogen is present with methane, where further reductions in temperature occur with higher nitrogen compositions. The

three-phase gas-water-hydrate equilibria for nitrogen compositions ranging from 1.0-25.0 mol% with methane were measured, with their profiles illustrated in Figure 38.

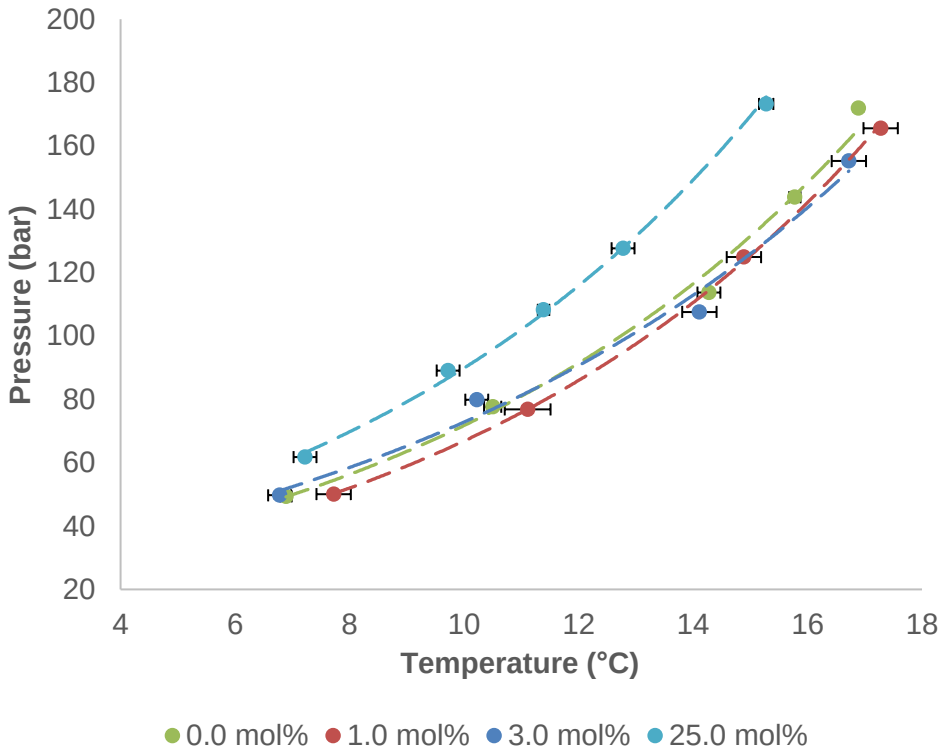

Figure 38 – Methane-Nitrogen Hydrate Equilibria (Smith, et al., 2015)

One of the most prominent features of the methane-nitrogen equilibrium profile is the significant overlap observed with low nitrogen compositions. There was no definitive reduction in T_{eq}, although theoretically, a reduction in methane partial pressure via nitrogen dilution would correspond to a lower T_{eq} value (Sloan & Koh, 2008). The cause of no experimental reduction in T_{eq} is attributed to the very low nitrogen composition, where the margin for error is very low to produce measurements that are distinct from one another. The thermocouple's uncertainty of 1.21% is reasonable but combined with scatter, is not low enough to be able to distinguish between overlapping lines.

In contrast, the addition of 25.0 mol% nitrogen results in a considerable depression of the hydrate equilibrium conditions. The hydrate equilibrium pressure for pure nitrogen exceeds 250 bar at 6.0 °C (Mohammadi, et al., 2003) – these conditions are outside the experimental pressures and temperatures encountered throughout this research. This characteristic effectively dictates that nitrogen is hydrate-inert throughout the range of pressures tested. Therefore, it can be understood that nitrogen acts as a diluent by decreasing the composition of methane, consequently

giving a lower T_{eq} value. Nitrogen is a relatively small molecule, having a molecule/cavity size ratio of 0.81 for the smaller 5^{12} cavities in sI and sII hydrates, compared to methane with a ratio of 0.87 (Lederhos, et al., 1993). Furthermore, nitrogen is less soluble in water than methane with mole fractions of $1.2x10^{-5}$ and $2.6x10^{-5}$ respectively at standard conditions (Green & Perry, 2008). The solubility and relative size of the gas is one of the primary characteristics to consider when assessing its hydrate-forming possibilities. Clearly methane is a superior hydrate former given that it is a better fit for the cavity and is more capable of entering solution. Also, when the nitrogen composition is elevated, the quantity of methane dissolved in the liquid phase is also reduced because its partial pressure is lower (Zarenezhad, et al., 2015). As stated in Henry's Law, the mole fraction of a gas in water is directly proportional to its partial pressure,

$$x_i = P_i/K_H \qquad \text{Eq. 29}$$

Ultimately, the mole fraction of the gas dissolved in water, x_i, will influence the chemical potential driving force, $\Delta\mu^{driv}$, for the formation of the hydrate phase (Eq. 11),

$$\Delta\mu^{driv} = v_w(P^{eq} - P) + RT\sum x_i \ln\left(\frac{f_i^{eq}}{f_i}\right) + v_h(P - P^{eq})$$

According to the above equation, $RT\sum x_i \ln\left(\frac{f_i^{eq}}{f_i}\right)$ will decrease in magnitude for the case of methane-nitrogen mixtures because increasing the nitrogen content implies a subsequent reduction in methane's x_i. The overall driving force for hydrate formation is therefore lower at a specified degree of sub-cooling for a nitrogen diluted methane mixture compared to the case of pure methane gas.

4.4.1.3 Methane-Carbon Dioxide

Hydrate phase equilibria for carbon dioxide has also been investigated quite extensively. Pure carbon dioxide is known to form hydrates at higher temperatures than pure methane throughout the pressure region of 0-70 bar (Adisasmito, et al., 1991). Above 70 bar, liquefaction of the carbon dioxide becomes a prominent factor and hampers its ability to form hydrates. However, small compositions in methane at pressures higher than 70 bar do not cause significant liquefaction, and are therefore able to participate in the formation of the hydrate phase. To observe the extent of carbon dioxide's participation, several gas mixtures with methane were examined, ranging from 7.0-19.0 mol% carbon dioxide. Their hydrate equilibrium profiles are portrayed in Figure 39.

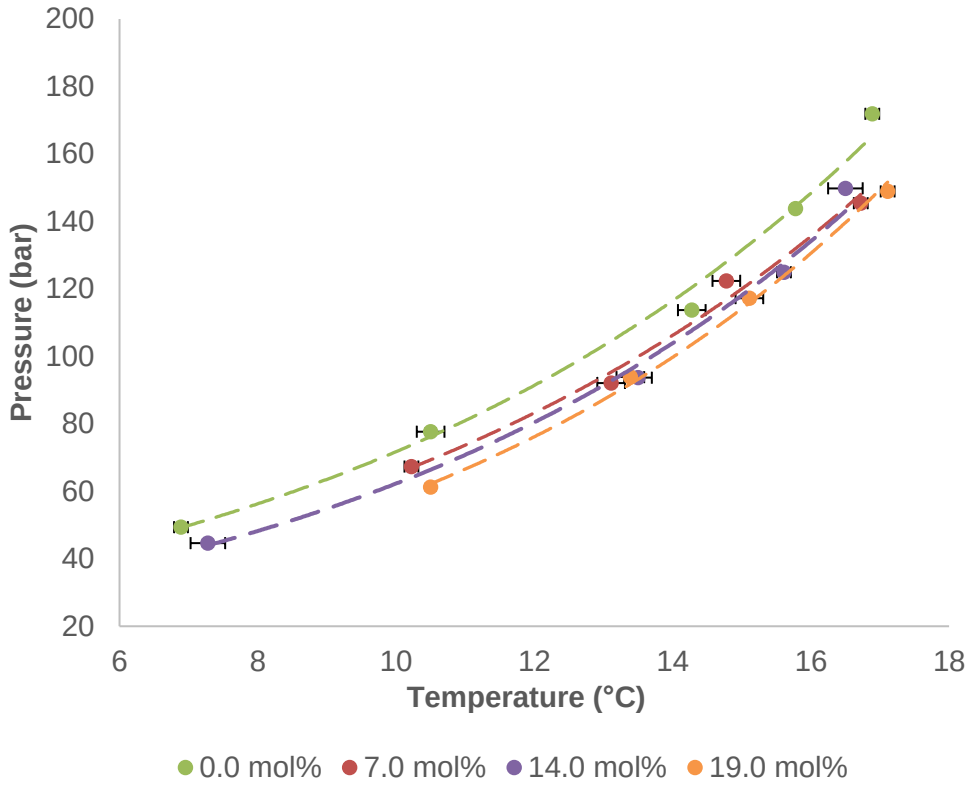

Figure 39 – Methane-Carbon Dioxide Hydrate Equilibria (Smith, et al., 2015)

Contrary to nitrogen, carbon-dioxide had a hydrate promoting effect in the presence of methane. There is a clear and gradual increase in the hydrate equilibrium conditions upon the introduction of higher quantities of carbon dioxide, which is not unexpected given pure carbon dioxide's elevated hydrate thermodynamic conditions compared to methane. With 7.0 mol% carbon-dioxide, T_{eq} was promoted by about 1 °C across the analysed pressure range. At 19.0 mol%, the hydrate phase conditions are promoted further, equating to roughly a 2 °C increase from pure methane hydrate conditions. This implied increase in the stability of the hydrate lattice is accounted for by carbon dioxide's higher solubility in water and greater molecular size relative to its designated lattice cavity.

The water solubility of carbon dioxide is far greater than methane – the two oxygens of carbon dioxide are hydrogen bond acceptor sites, allowing for strong polar interactions with water molecules. The mole fraction of carbon dioxide in water is 7.1×10^{-4} at standard conditions, which is more than 10 times greater than methane (Green & Perry, 2008). Understandably, the presence of carbon dioxide will ensure a high susceptibility to hydrate formation. Being a small molecule, pure methane hydrates are sI type where the majority of methane molecules occupy the small 5^{12} dodecahedron cavity and not necessarily all the larger $5^{12}6^2$ cavities (Anderson 2003). Some cavitites are therefore left unoccupied, and have the capacity to be stabilized

by carbon dioxide molecules. Carbon dioxide is the preferred occupant of this cavity over methane due to its greater size, resulting in a more favourable molecule/cavity size ratio of 0.87 compared to 0.74 (Lederhos, et al., 1993). Occupation of the larger cavity adds stability to the hydrate lattice, and therefore requires a greater amount of energy to dissociate. This is reflective of the increase in T_{eq} relative to methane hydrate equilibria (Herri, et al., 2011).

A similar logic to methane-nitrogen hydrate equilibria with regard to the driving force for hydrate formation can be applied here as well. In this instance with the methane-carbon dioxide system, both components contribute to the hydrate structure. Therefore, the $RT\sum x_i \ln\left(\frac{f_i^{eq}}{f_i}\right)$ solubility term is expected to be greater in comparison to pure methane, because of a higher overall concentration of hydrate-forming molecules in solution. At a certain level of sub-cooling, the hydrate phase driving force for carbon dioxide diluted methane is consequently higher than that of methane.

4.4.2 Experimental Correlation

The acquired experimental measurements were used in the modelling of an empirically derived relationship between equilibrium pressure, equilibrium temperature and the concentration of the diluting gas. Each equilibrium curve is represented by an exponential function since there was a greater pressure-temperature correlation between the extremities of the tested pressure ranges. This was true for all equilibria describing methane-nitrogen/carbon dioxide hydrates. Other fitting functions were also considered, particularly the polynomial function which regularly offered similar correlation coefficients, however, the pressure-temperature relationship for the presented experimental data follows a predictable, consistent and set path, one that a polynomial function (orders greater than 2) may not offer. For the pressure range considered, the line fitting the experimental data is of the form (b and d are constants),

$$P_{eq} = f(T_{eq}) = d\exp(bT_{eq}) \qquad \text{Eq. 30}$$

or in terms of T_{eq},

$$T_{eq} = f(P_{eq}) = \frac{\ln(P_{eq}/d)}{b} \qquad \text{Eq. 31}$$

Any shift of the equilibrium curve will naturally occur about the x-axis, i.e. from one temperature to another at a certain pressure. This shift about the x-axis is relative to the methane line. The extent of the shift at any pressure will be proportional to the

composition of nitrogen or carbon dioxide in the gas mixture. Throughout the entirety of the y-axis (pressure), the average deviation can be quantified by finding the areas for the methane-nitrogen/carbon dioxide lines and relating them to the area associated with the pure methane curve. Areas for the gas mixtures with the highest concentration of nitrogen (25.0 mol%) and carbon dioxide (19.0 mol%) can be found and represent the largest shift relative to the methane reference line out of all gas mixtures. Therefore, the lowest area corresponds to the nitrogen and greatest to carbon dioxide.

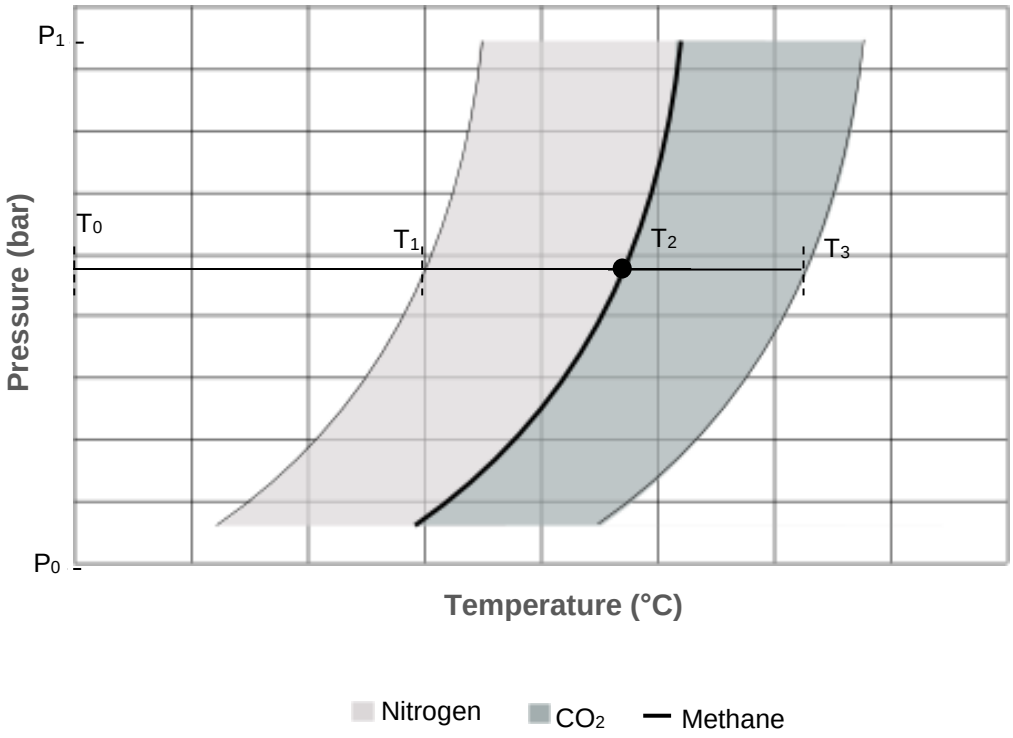

Figure 40 – Impact of Nitrogen and Carbon Dioxide (Smith, et al., 2015)

The above illustration aids with the formulation of the experimental model that predicts hydrate equilibrium conditions for methane-nitrogen/carbon dioxide systems when water is present. All possible hydrate equilibrium points for any methane-nitrogen gas ranging from 0.0-25.0 mol% nitrogen is represented by the lighter shading and the darker shading represents all equilibrium points for methane-carbon dioxide gases that constitute 0.0-19.0 mol% carbon dioxide. Integrations are performed about the P_0-P_1 region in each case where T_0-T_1 is the region corresponding to the minimum area (25.0 mol% nitrogen), T_0-T_2 is the region for methane and T_0-T_3 will give the maximum area (19.0 mol% carbon dioxide). The corresponding areas are represented by,

$$A_{N2} = \int_{P_0}^{P_1} T_1(P_{eq})dP \quad \text{Eq. 32}$$

$$A_{C1} = \int_{P_0}^{P_1} T_2(P_{eq})dP \quad \text{Eq. 33}$$

$$A_{CO2} = \int_{P_0}^{P_1} T_3(P_{eq})dP \quad \text{Eq. 34}$$

The preceding definite integrals portray the area, A, for nitrogen, methane and carbon dioxide respectively. For $A_{N2,}$ a smaller value corresponds to a higher nitrogen concentration whereas a higher A_{CO2} value implies greater carbon dioxide compositions. With this simple relationship, and using the experimental equilibrium measurements for the highest nitrogen and carbon dioxide content in methane mixtures, the hydrate equilibrium point for a gas composition that doesn't exceed this maximum content can be interpolated. For a methane-nitrogen gas system with a nitrogen composition of x_{N2} and at a pressure P_{eq}, T_{eq} is interpolated by,

$$T_{eq}(P_{eq},x_{N2}) = T_2(P_{eq}) + \frac{\ln(P_{eq}/d_{N2})}{b_{N2}} \frac{x_{N2}c_{N2}}{x_{N2,ref}} \quad \text{Eq. 35}$$

The first term is simply T_{eq} for methane at the specified pressure and the second term describes the deviation from this temperature due to the dilution of nitrogen by expressing it as a fraction of the maximum diluting effect. The c component depicts the fractional change brought about by the added component with respect to methane for the equilibria describing the highest concentration of nitrogen or carbon dioxide. It is a constant and is calculated using,

$$c_i = \left(\frac{A_i}{A_{C1}} - \frac{A_{C1}}{A_{C1}}\right) \quad \text{Eq. 36}$$

It should be noted that c_i is unity for methane since the methane hydrate equilibria is essentially a reference point. A nearly identical equation is formulated for the carbon dioxide component,

$$T_{eq}(P_{eq},x_{CO2}) = T_2(P_{eq}) + \frac{\ln(P_{eq}/d_{CO2})}{b_{CO2}} \frac{x_{CO2}c_{CO2}}{x_{CO2,ref}} \quad \text{Eq. 37}$$

Each term is identical to the nitrogen equation except the second term calculates the added effect of carbon dioxide. An overall equation encompassing the opposing effects of nitrogen and carbon dioxide may be detailed by including both terms on the far-right side of the previous equations:

$$T_{eq}(P_{eq},x_{N2},x_{CO2}) = T_2(P_{eq}) + \frac{\ln(P_{eq}/d_{N2})}{b_{N2}} \frac{x_{N2}c_{N2}}{x_{N2,ref}} + \frac{\ln(P_{eq}/d_{CO2})}{b_{CO2}} \frac{x_{CO2}c_{CO2}}{x_{CO2,ref}} \quad \text{Eq. 38}$$

The c_i, $x_{i,ref}$ and b_i constants can be combined to produce a collective constant, a_i. This simplification yields,

$$T_{eq}(P_{eq},x_{N2},x_{CO2}) = T_2(P_{eq}) + x_{N2}a_{N2}\ln(P_{eq}/d_{N2}) + x_{CO2}a_{CO2}\ln(P_{eq}/d_{CO2}) \quad \text{Eq. 39}$$

All a_i and d_i constants are listed for methane, carbon dioxide and nitrogen in Table 10. Note the positive a_i for carbon dioxide and the negative for nitrogen. This is indicative of the promoting and suppressing effects of carbon dioxide and nitrogen respectively.

Table 10 – Collective Empirical Terms (Smith, et al., 2015)

Component	a_i	d_i
Methane	8.264	21.31
Carbon-dioxide	4.573	15.12
Nitrogen	-5.058	25.24

4.4.2.1 Application of Correlation

The experimental correlation founded in this chapter was applied to several hydrate equilibrium measurements in literature. For methane-nitrogen gases, equilibria for compositions of 11 mol% nitrogen and 27 mol% (Mei, et al., 1996); (Jhaveri & Robinson, 1965) were acquired and are presented in Figure 41 alongside the calculated pressure-temperature points using the experimental parameters in Table 10 and the derived correlation for nitrogen. Also, hydrate equilibrium predictions using utilities in simulation software Aspen HYSYS and Calsep PVTsim, are illustrated. The predictions are based on the Peng-Robinson (PR) and Soave-Redlich-Kwong (SRK) equation of state (EoS) which produced different results (discussed in Chapter 7).

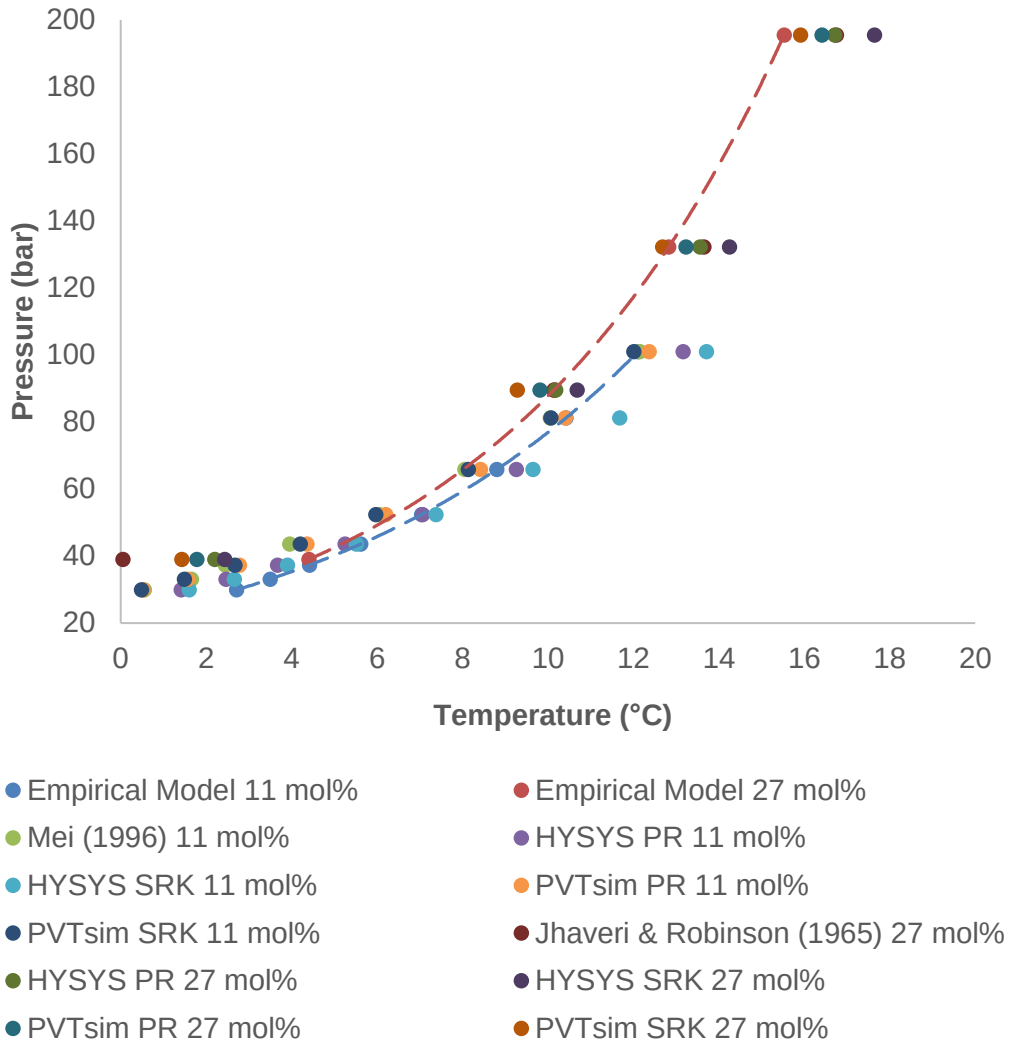

Figure 41 – Methane-Nitrogen Equilibrium Predictions (Smith, et al., 2015)

The red and blue dashed lines represent the fitted curves for 27 mol% and 11 mol% nitrogen respectively. Aside from the extremes about the y-axis (pressure), this study's results generally agree with Mei (1996) and Jhaveri and Robinson (1965). There is also reasonable agreement with the predictions offered by HYSYS and PVTsim, although HYSYS seems to overshoot quite regularly for methane-nitrogen systems. To confirm this as a possibility, the 11 mol% nitrogen gas was examined using the HYSYS hydrate utility which predicts an equilibrium temperature of 13.05 °C with the PR EoS at 100 bar. For the exact same conditions, 100 mol% methane is predicted to be 12.70°C. The pure methane temperature should be unquestionably higher, not lower. A similar occurrence with the SRK EoS was noticed. With these predictions, HYSYS's model indicates that no suppression by nitrogen dilution will occur at 11 mol%, which is not realistic.

The methane-carbon dioxide correlation was also applied to methane-carbon dioxide equilibria available in literature and compared. Specifically, equilibrium points for carbon dioxide concentrations of 8 mol% and 40 mol% were acquired (Adisasmito, et al., 1991). Similarly, predictions corresponding to these gas compositions were acquired from HYSYS and PVTsim using the same EoS. They are portrayed in Figure 42 alongside the literature values and software predictions using the PR and SRK EoS.

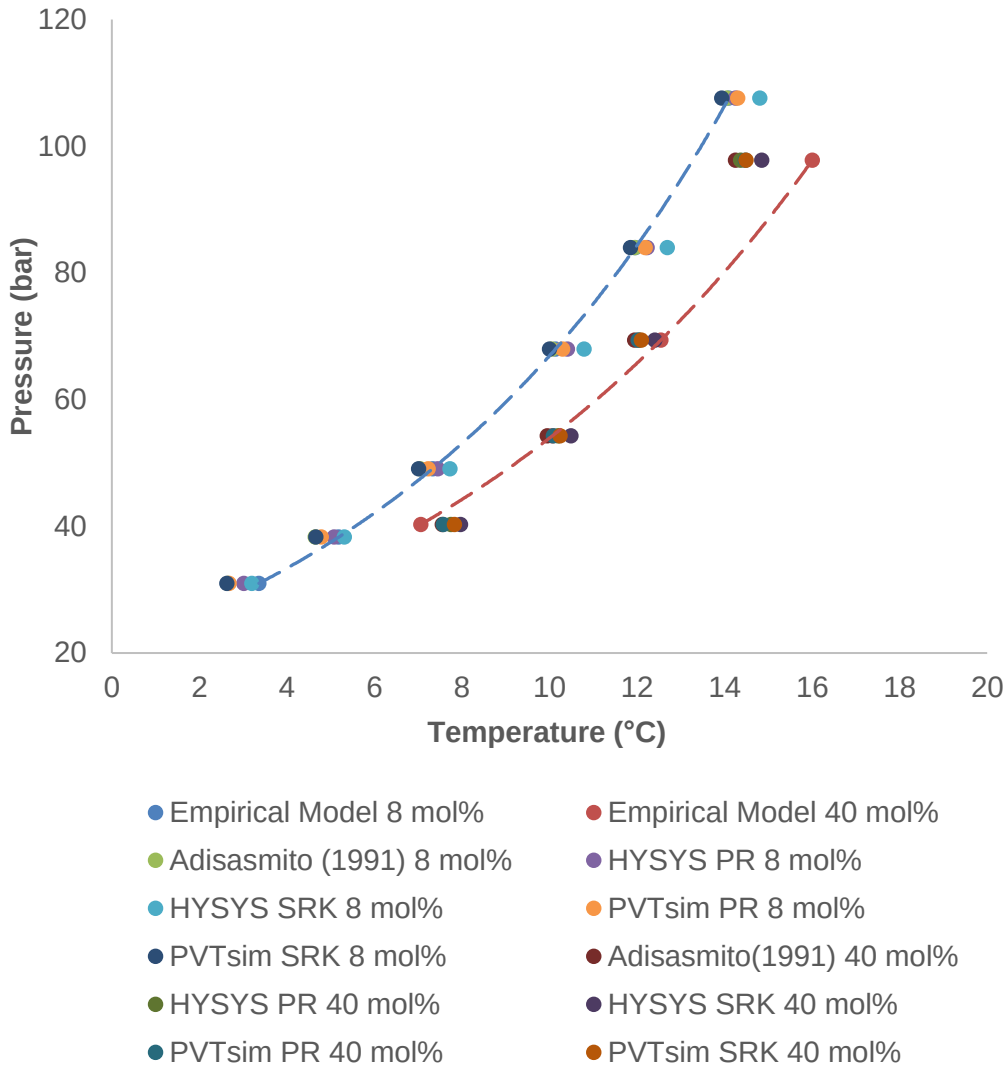

Figure 42 – Methane-Carbon Dioxide Equilibrium Predictions (Smith, et al., 2015)

For the above figure, a blue and red dashed line describe the best fitted relationships for the correlation's predictions of 8 mol% and 40 mol% carbon dioxide respectively. There is agreement between this work's methane-carbon dioxide's equilibrium predictions and those in literature to a great extent, but observably becomes less reliable at the pressure extremities and beyond. This stems from the averaging of the

deviations of the experimental equilibrium points to that of methane over the entire pressure range, and therefore greater accuracy is to be expected about the middle of the curves rather than at each end.

There is very good agreement of the correlation with 8 mol% carbon dioxide equilibria acquired from Adisasmito, et al. (1991) as well as values from simulation programs. The provided 8 mol% measurements by Adisasmito mostly occupy the middle of the experimented pressure range (40-180 bar), therefore, from a statistical perspective, less error is associated about the centre of the range. This is seemingly the case for the predicted 8 mol% carbon dioxide conditions sourced from the correlation.

The empirical correlation was also applied outside the maximum carbon dioxide composition from which it was modelled from to determine its applicability towards extrapolating equilibrium conditions. Data sourced from Adisasmito, et al. (1991) was also used in comparing equilibrium predictions. They tested for hydrates using a 40 mol% carbon dioxide in methane gas mixture (data is illustrated in Figure 42). Our correlation exhibits consistency at lower pressures with Adisasmito's results as well as the utilised simulation programs, but appears to stray at approximately the 60-80 bar mark. This is a consequence of working outside the modelled composition range and the assumed linear sensitivity of carbon dioxide concentration with equilibrium temperature at a certain pressure. It is therefore recommended that the correlation be applied to carbon dioxide compositions ≤19.0 mol% for more reliable hydrate equilibrium predictions.

4.4.3 Heat of Dissociation

The heat required to induce the dissociation of a hydrate is of great interest to flow assurance experts because it provides important information on how much energy will be required. The heat of dissociation, ΔH_d, can be measured using calorimetry, similar to the works of Handa and co-workers (1984;1986a;1986b), or using the Clapeyron equation, which is derived from $\Delta G = \Delta H - T\Delta S$:

$$\frac{dP}{dT} = \frac{\Delta H_d}{T\Delta V} \qquad \text{Eq. 40}$$

Given that the density of hydrate is approximately the same as water, then $\Delta V \approx V_g$ (Mcleod & Campbell, 1961). Using the gas equation, a formulation for V_g is,

$$V_g = \frac{ZRT}{P} \qquad \text{Eq. 41}$$

Symbols have their usual meaning; in particular, Z is compressibility and R is the universal gas constant. Substitution of V_g into the Clapeyron equation for ΔV yields,

$$\frac{d\ln P}{d(1/T)} = \frac{\Delta H_d}{ZR} \qquad \text{Eq. 42}$$

This is known as the Clausius-Clapeyron equation, and is applied to hydrate equilibrium data for the evaluation of ΔH_d. The general process entails constructing a semi-logarithmic plot of lnP against 1/T. The slope of the line fitting the data is representative of the structure type of the formed hydrate, i.e. the cavity size occupied by the guest molecules, and not so much on the actual gas species (Sloan & Fleyfel, 1992). It is generally understood that slopes are relatively constant (±10 %) for all sI and sII hydrates, no matter what sI or sII guest is occupying the hydrate cavities. Each structure type is classified by the numerical value of the slope computed; sI range from approximately -7000 to -12000, and sII from -14000+ (Sloan & Fleyfel, 1994). Using the calculated slopes, ΔH_d can then be evaluated, where its magnitude is dependant primarily on slope, and therefore structure type.

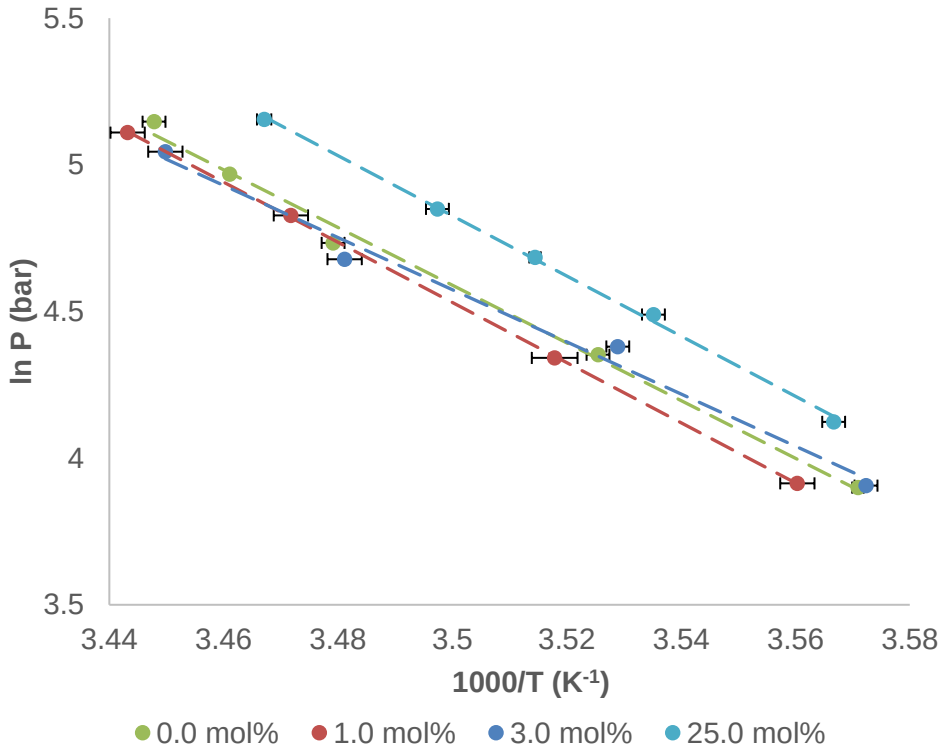

Figure 43 – Clausius-Clapeyron Plots for Methane-Nitrogen (Smith, et al., 2015)

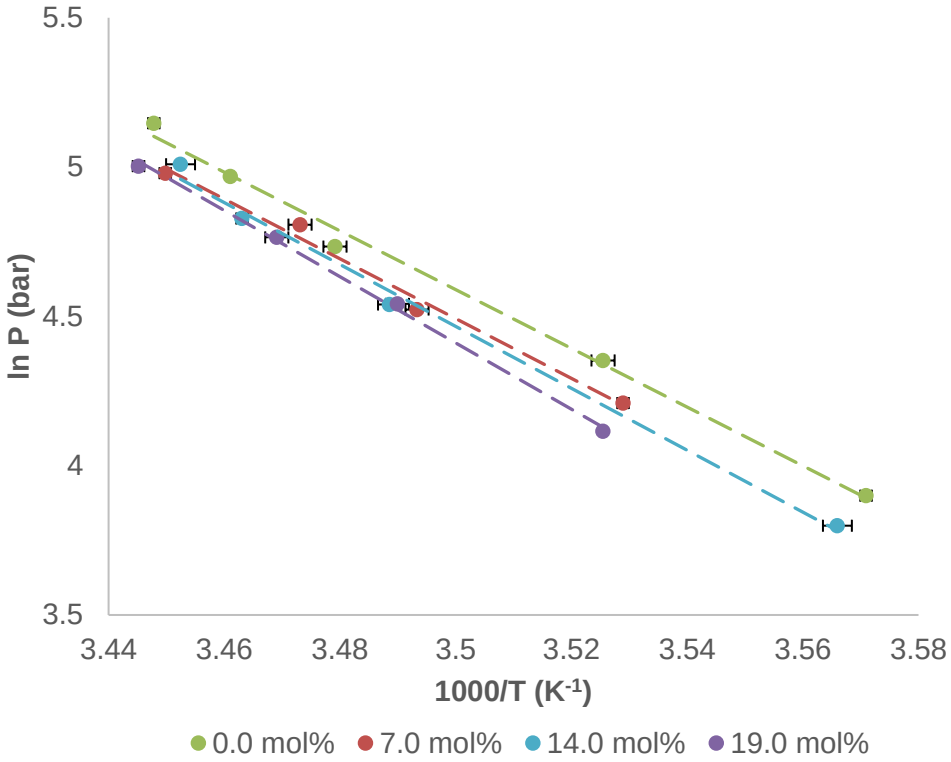

Figure 44 – Clausius-Clapeyron Plots for Methane-Carbon Dioxide (Smith, et al., 2015)

Clausius-Clapeyron lines for nitrogen and carbon dioxide diluted methane are illustrated in Figure 43 and Figure 44 respectively. A common observation between both cases is that the slopes for all compositions are relatively constant. The only variation with composition is the vertical position of the trend-line attributed by the shift in hydrate equilibrium conditions due to the nitrogen/carbon dioxide component in each mixture. Therefore, the addition of nitrogen/carbon dioxide does not cause a structure change of the hydrate lattice. Methane and carbon dioxide are sI guests, so a structure change would not be expected. This is not unheard-of, however. For example, pure methane and ethane form sI hydrates, but in the presence of each other with methane concentrations between approximately 67-99%, sII hydrates are preferred (Sloan & Koh, 2008). To better compare Clausius-Clapeyron parameters, Table 11 and Table 12 summarize the numerical calculation of slopes and the corresponding ΔH_d value.

Table 11 – N_2 in CH_4 Clausius-Clapeyron Slopes

Gas	$\frac{-d\ln(P)}{d(1/T)}$, K	ΔH_d, kJ/mol	Structure Type
CH_4	8650	60.0 ± 0.6	I
1.0 mol%	10252	66.9 ± 1.7	I
3.0 mol%	8888	58.5 ± 1.1	I
25.0 mol%	10253	72.3 ± 0.6	I

Table 12 – CO_2 in CH_4 Clausius-Clapeyron Slopes

Gas	$\frac{-d\ln(P)}{d(1/T)}$, K	ΔH_d, kJ/mol	Structure Type
CH_4	9704	60.0 ± 0.6	I
7.0 mol%	10010	64.0 ± 0.5	I
14.0 mol%	10365	64.7 ± 0.7	I
19.0 mol%	11091	68.1 ± 0.4	I

As demonstrated in the above tables, the calculated slope values are consistent with the illustrated Clausius-Clapeyron plots. They show little variation, and are all within the designated slope range for sI hydrates. In the case of nitrogen mixture slopes, there appears to be no definitive trend with composition. As mentioned previously, nitrogen will not contribute to cavity occupation since its pure hydrate phase equilibria is outside the range of the tested conditions – only methane contributes to the hydrate phase, so ultimately there should be no change in slope with the addition of nitrogen. The variation observed is expected to lie within experimental error. In the instance of carbon dioxide, there does seem to be a general increase in steepness with higher concentrations, which may not be coincidental. This is because carbon dioxide contributes to the hydrate phase by stabilizing the $5^{12}6^2$ cavities in the sI lattice (Giavarini, et al., 2007); (Adisasmito, et al., 1991). At greater concentrations, carbon dioxide will occupy the hydrate lattice to a greater extent and exhibit a higher fractional occupancy of hydrate cavities. From the fundamental statistical thermodynamic theory by van der Waals and Platteeuw (1959) which is the foundation for most theoretical hydrate equilibrium models, the occupancy of a cavity is given by the Langmuir expression,

$$\theta_{ij} = \frac{C_{ij} f_i}{1 + \sum_i C_{ij} f_i} \qquad \text{Eq. 43}$$

θ_{ij} represents the fractional occupancy of guest i in cavity j. It is a function of its Langmuir constant (C_{ij}), fugacity (f_i) and all Langmuir constants and fugacitites of every other guest capable of occupying cavity j. The Langmuir constant is specific for each guest/cavity combination and is a representation of the strength of van der Waals and/or hydrogen bonding interactions between the guest molecule and the water molecules that are arranged to form cavity j (Shin, et al., 2009). In relation to methane-carbon dioxide mixtures, the occupancy of the large cavity of sI for carbon dioxide will increase with its fugacity and therefore composition. This supposed increased occupancy is a valid explanation for the observed general increase in slope.

Because ΔH_d is calculated directly from the slope of the Clausius-Clapeyron equation, any associated trends with the slope and composition are expected to be passed on to ΔH_d. At a molecular level, ΔH_d is a function of the strength of interactions between the hydrogen bonds of the hydrate crystal, which may be stabilized by the occupation of cavities by a guest (Sloan & Koh, 2008). Similar to their slopes, the ΔH_d values for nitrogen mixtures show no trend with composition, and vary up to a maximum of about 20%.

All ΔH_d were evaluated at 15.0 °C at the corresponding P_{eq}. Interestingly, the 25.0 mol% nitrogen gas was calculated to exhibit the highest ΔH_d. This is unusual, because the concentration of methane is far lower than other tested nitrogen mixtures. In this instance, it is important to consider occupancy and hydration numbers, which are known to be functions of pressure (Anderson, 2003). This is evident theoretically by the Langmuir expression; an increase in overall pressure will result in slightly higher occupancy, and greater stability. It can also be understood in terms of gas solubility, which increases with pressure. Importantly, with 25.0 mol% nitrogen, the equilibrium pressure to achieve a T_{eq} of 15.0 °C is higher and therefore implies higher occupancy and stability of the hydrate despite the nitrogen composition is higher, and methane composition being lower. It seems the increase in methane's occupancy brought about by its higher partial pressure (therefore fugacity) relative to the 1.0 and 3.0 mol% mixtures may compensate for its higher nitrogen dilution. This is understandable from the Clausius-Clapeyron equation, which shows that ΔH_d is proportional to the volume of gas (Eq. 41) and therefore pressure, which in turn is proportional to occupancy (Eq. 43). The gas compressibility change can also be

apparent in ΔH_d (Sabil, et al., 2010). Kang, et al., (2000) calculated the ΔH_d for pure nitrogen (sII former when pure) to be about 66 kJ/mol at a pressure of 10 bar at 0.5 °C. Because nitrogen was not expected to participate in the hydrate lattice in this study, this value cannot be compared, and was included for the reader's reference.

Enthalpy values for the carbon dioxide mixtures demonstrated an increasing trend, and to a reasonable engineering approximation, they should remain relatively constant (Sloan & Fleyfel, 1992). Theoretically and conceptually, it makes sense that an increase in carbon dioxide concentration/fugacity will stabilize the hydrate lattice by occupying more lattice cavities, thus elevating ΔH_d. Additionally, Z did not differ by the same degree as the nitrogen mixtures, thereby minimizing the effect of compressibility changes amongst different concentrations at the same temperature. Pressures corresponding to T_{eq} of 15.0 °C are lower for methane-carbon dioxide hydrates than methane-nitrogen, meaning fugacities are also lower. Hence, occupancies and stabilities are also predicted to be lower; this explains the slightly lower ΔH_d values for methane-carbon dioxide hydrates. This is supported by experimental work performed by Sabil, et al. (2010), who calculated enthalpies for carbon dioxide hydrates at several thermodynamic equilibrium conditions. Therefore, ΔH_d can be a strong function of the respective thermodynamic conditions. Overall, it is with confidence that the increase in enthalpy with carbon dioxide composition is ultimately attributable to increased stability of the hydrate lattice as opposed to biased experimental error, despite the counteracting effect of decreased compressibility.

4.4.4 Chemical Potential Driving Force

Since there was insufficient time and experimental measurements to perform a complete analysis on the kinetics of hydrate formation for the various tested gas mixtures, this section is limited to chemical potential driving force calculations. The calculated data is inconclusive, but does confirm there is a dependence on the required sub-cooling necessary to induce hydrate formation.

The chemical potential for hydrate nucleation is given by the expression derived in Chapter 2 (Eq. 11),

$$\Delta\mu^{driv} = \nu_w\left(P^{eq} - P\right) + RT\sum x_i \ln\left(\frac{f_i^{eq}}{f_i}\right) + \nu_h\left(P - P^{eq}\right)$$

This formulation is used for an isothermal regime, whereas experiments in this study were performed under isobaric conditions. Using the gas equation, pressure (P) of 1 mole of gas may be expressed as,

$$P = \frac{RTZ}{v_g} \qquad \text{Eq. 44}$$

Substituting this expression into the chemical potential equation, equating fugacity to pressure and the fugacity coefficient (φ_i), then simplifying results in the following:

$$\Delta\mu^{driv} = \frac{R(v_w - v_h)}{v_g}(T_{eq}Z_{eq} - TZ) + RT\sum x_i \ln\left(\frac{\varphi_i^{eq}T_{eq}Z_{eq}}{\varphi_i TZ}\right) \qquad \text{Eq. 45}$$

The resulting equation relates the driving force to the formation temperature, T, and the equilibrium temperature, T_{eq}. The fugacities for each component at experimental conditions, f_i, and at equilibrium, f_i^{eq}, were evaluated using the SRK EoS. The remaining symbols have their usual meaning; R is the universal gas constant, v_g is the volume of gas in the cell (55 cm^3), Z is the compressibility at formation conditions and Z_{eq} is the gas compressibility at hydrate equilibrium. However, an additional term is necessary to account for the entropic driving force, since free energy is also dependent on the entropy increase of the universe. The change in entropy for the phase change from water to hydrate, ΔS_d, can be accurately estimated using an expression Kaschiev & Firoozabadi (2002b) used in their driving force calculations for an isobaric regime,

$$\Delta\mu^{driv} = \Delta S_d(T_{eq} - T) \qquad \text{Eq. 46}$$

This formula is a simplified form of a Taylor series expansion and assumes there is negligible water mass transfer from the aqueous to the vapour phase at temperature T to T_{eq} and that the amount of gas molecules occupying cavities does not change between these temperatures. Because pressure is constant, ΔH_d can be used to quantify ΔS_d using the simple thermodynamic relation derived from Gibbs free energy,

$$\Delta S_d = \Delta H_d / T_{eq} \qquad \text{Eq. 47}$$

Adding this equation to the previous derivation yields an expression for the overall driving force,

$$\Delta\mu^{driv} = \frac{\Delta H_d}{T_{eq}}(T_{eq} - T) + \frac{R(v_w - v_h)}{v_g}(T_{eq}Z_{eq} - TZ) + RT\sum x_i \ln\left(\frac{\varphi_i^{eq}T_{eq}Z_{eq}}{\varphi_i TZ}\right) \qquad \text{Eq. 48}$$

Results were calculated for a T_{eq} of 15.0 °C and the corresponding P_{eq} for pure methane, 25.0 mol% nitrogen and 19.0 mol% carbon dioxide with the dissociation enthalpies reported in this chapter. Numerical values for ΔS_d and the resultant driving forces are listed in Table 13.

Table 13 – Hydrate Nucleation Chemical Potential at 15.0 °C

Gas	P_{eq}, bar	ΔS_d, J/mol.K	$\Delta S_d/P_{eq}$, J/mol.bar.K
Methane	130.4	208.2	1.60
25.0 mol% N_2	169.5	250.9	1.48
19.0 mol% CO_2	114.1	236.3	2.07

The driving force for hydrate nucleation is a representation of the change in free energy required for hydrate nucleation to occur (Sloan & Koh, 2008). For this study, the volume of gas in the sapphire cell was far greater than the molar volume of water (55 cm^3 to 5 cm^3). Also, the difference in molar volume between water in the liquid and hydrate state, $v_w - v_h$, is very small; 0.044 nm^3/cell or 0.576 cm^3/mol (Kaschiev & Firoozabadi, 2002b). Collectively, these factors effectively rendered the second term of the expression insignificant. The entropy driving force was the dominating term for all scenarios and accounted for more than 90% of the total magnitude. Therefore, it can be assumed that $\Delta\mu^{driv}$ is primarily dependent on (T_{eq} - T) and ΔH_d (or latent heat). ΔH_d is also relatively constant and does not vary considerably with guest species or pressure and temperature (Sloan & Fleyfel, 1992). A reasonable engineering approximation for $\Delta\mu^{driv}$ is therefore given as,

$$\Delta\mu^{driv} = \frac{\Delta H_d}{T_{eq}}(T_{eq} - T) \qquad \text{Eq. 49}$$

All calculations and results in Table 13 are specific to an equilibrium temperature of 15.0 °C, and would be expected to change accordingly with the pressure dependence exhibited by free energy. When pressure is maintained, and thus, in terms of sub-cooling (T_{eq} – T), it is reasonable to expect that for a gas-water mixture that contains only hydrate formers, nucleation will be more likely to initiate at a temperature closer to T_{eq} than a system constituting hydrate-inert species. To approximate the influence of pressure, $\Delta\mu^{driv}$ was divided by P_{eq}. Furthermore, the addition of an effective hydrate contributor, such as carbon dioxide (filling the majority of sI $5^{12}6^2$ cages), should have a similar effect. Its propensity to enter solution enables an increased probability of hydrate crystals to form and stabilize, where the high solution concentration can quickly add to microscopic clusters due to the high availability.

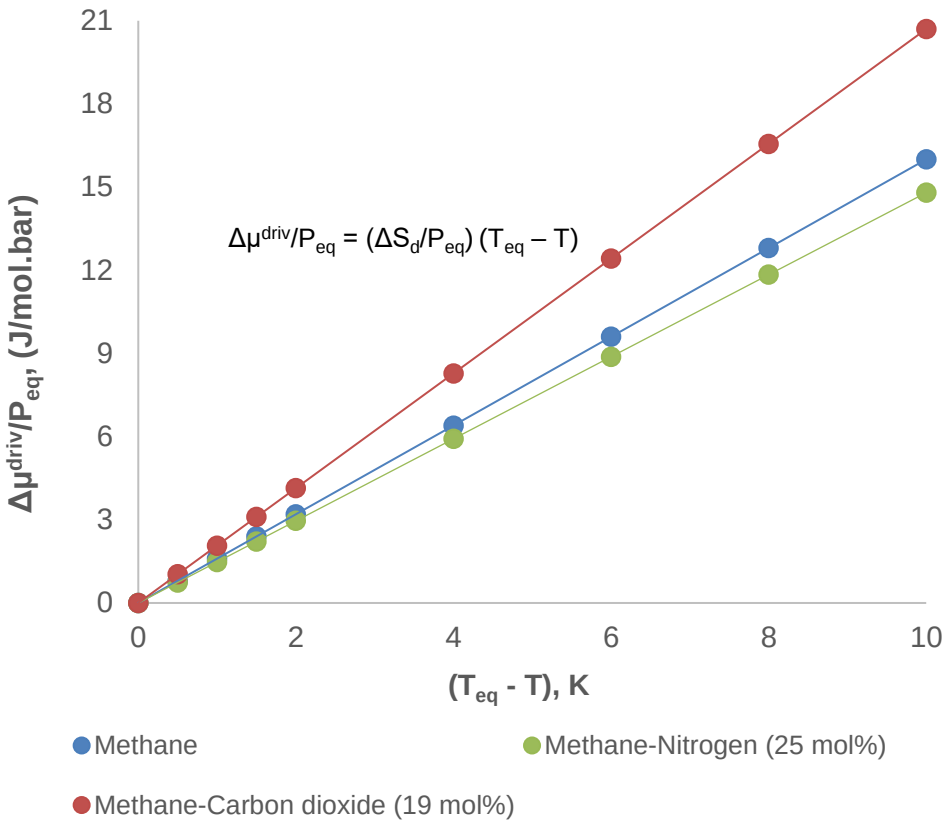

Figure 45 – Chemical Potential Driving Force at 15.0 °C

Under the experimental sub-cooling conditions that brought about the observed hydrate formation, the driving force values are not associated with the same trend discussed in previous paragraphs. These values simply correspond to the driving force for hydrate formation at the point nucleation is observed, and are coupled with different sub-cooling requirements, hence different driving forces. They are not the same because of the uncertainty attributed to the initial nucleation process, the different species present in each hydrate testing scenario, the different temperature conditions (Kaschiev & Firoozabadi, 2002b); (Anklam & Firoozabadi, 2004) and unavoidable irregularities between each hydrate experiment that manifest despite maintaining all contributing factors. A better measure of comparison is represented by Figure 45, which demonstrates the driving force as a function of sub-cooling only, according to Eq. 49.

From Figure 45, the significance of sub-cooling between the gas-water systems of interest becomes apparent at approximately 3-4 °C of sub-cooling. The carbon dioxide gas mixture extends to higher $\Delta\mu^{driv}$ at a given (T_{eq} - T) which is to be expected of a system with a higher entropic driving force towards the hydrate phase. The illustration, constructed using Eq. 49 provides a slightly different $\Delta\mu^{driv}$ than Eq. 48. Pressure-volume contributions, i.e. work, and compressibility changes between the

equilibrium and operating pressure-temperature conditions, appear to have only minute effects on $\Delta\mu^{driv}$. It is this minor difference and the simplicity of Eq. 49 that make it a useful and easy approximation. However, this would not be the case in systems that are more compressible and/or more sensitive to molar volume changes between the liquid and hydrate phases.

It should be noted that using the driving force necessary to induce hydrate nucleation based on the experimentally observed (T_{eq} - T) sub-cooling is not particularly useful. For confirmation of the varying nucleation driving force between each hydrate system, these values cannot be compared. This data simply informs the change in chemical potential at the formation point. By presenting $\Delta\mu^{driv}$ in form of J/mol.bar.K, viable comparisons can be made because each gas-water system is quantified per unit temperature and per unit pressure. By calculating $\Delta\mu^{driv}$ with the mentioned units (i.e. dividing by P_{eq}), a better perspective on each system's driving force is achieved because it is simplified and a more interpretable parameter.

Compared to pure methane, the 25.0 mol% nitrogen mixture requires a higher degree of sub-cooling. For example, using the values from Table 13, it can be deduced that to achieve a $\Delta\mu^{driv}$ of 10.0 J/mol.bar, a pure methane system only requires 6.25 °C of sub-cooling whereas a 25.0 mol% nitrogen system requires 6.76 °C. This further implies the driving force for nucleation is dependent on the species and their partial pressure or fugacity of the hydrate forming species (Anklam & Firoozabadi, 2004); (Abay & Svartaas, 2011). The partial pressure in the 25.0 mol% nitrogen mixture for methane is lower, and therefore the system requires greater cooling below the equilibrium temperature to achieve the same $\Delta\mu^{driv}$ as pure methane hydrates. Hence, by introducing nitrogen to methane, hydrate nuclei will not nucleate as easily and therefore can reduce the likelihood of methane hydrate nucleation.

Regarding 19.0 mol% carbon dioxide gas, the sub-cooling and necessary driving force is less. For the 19.0 mol% carbon dioxide system, 4.83 °C is required to produce a $\Delta\mu^{driv}$ of 10.0 J/mol.bar. Carbon dioxide is an established hydrate promoter in the presence of methane, allowing hydrate nucleation to occur more readily and at smaller levels of sub-cooling. This is provided all other nucleation factors such as mixing are consistent. Carbon dioxide's high water solubility means a higher population of carbon dioxide molecules in solution relative to methane (if their partial pressures are equal), and therefore a higher probability

of methane, carbon dioxide and water molecules arranging into a crystallized phase.

While the relative ease at which hydrates will form below T_{eq} is an undesirable phenomenon with respect to flow assurance, this feature of carbon dioxide hydrate nucleation can be beneficial for the preservation and storage of carbon dioxide in the form of hydrate (Giavarini, et al., 2007). For example, Giarvarini, et al. (2007) determined that temperature was more of a controlling factor in the stability of its hydrate rather than pressure and found that -2 °C at atmospheric pressure was sufficient for the hydrate to remain stable. This was relative to methane, where it was determined that pressure was the dominant parameter in terms of its stability. The stability of hydrates and their prolonging under atmospheric to low pressures has shown to be an attractive area of study because of the reported financial savings regarding gas compression and transportation.

A total cost reduction of 24% for transportation via hydrate compared to an equivalent LNG chain has been reported with the hydrate stored under atmospheric conditions at -15 °C (Gudmundsson & Borrehaug, 1996). Gudmunsson (1996) also demonstrated that at atmospheric conditions, natural gas hydrates did not decompose when stored at temperatures from -15 to -5 °C. One of the main issues pertaining to gas storage and transportation in the form of hydrate is the slow formation rates often observed in industrial applications (Sun, et al., 2004). This is a prime example of how hydrate kinetics can be applied and why further study, particularly in combination with hydrate inhibitors and promotors, is necessary to realise the potential of natural gas storage and transportation as hydrate.

4.5 Conclusion

The hydrate equilibria for methane-nitrogen and methane-carbon dioxide gas mixtures ranging from 0.0-25.0 mol% and 0.0-19.0 mol% were the main point of focus in this chapter. Depression and promotion of the methane hydrate equilibrium curve brought about by introducing different concentrations of nitrogen or carbon dioxide respectively was discussed and it was concluded that for a specified pressure, the methane curve could be depressed or promoted by several degrees with 25.0 mol% nitrogen and 19.0 mol% carbon dioxide. Although results were inconclusive for 1.0 and 3.0 mol% nitrogen gas mixtures, it was clear that with higher concentrations of nitrogen there was greater equilibrium suppression. This occurrence was attributed

to nitrogen's inability to contribute to the hydrate phase at the tested pressures, essentially diluting the methane hydrate former and reducing its partial pressure. It was also found that nitrogen did not significantly change the driving force for hydrate nucleation, and did so only by reducing methane's partial pressure. Contrarily, increasing the carbon dioxide concentration in methane also reduced methane's partial pressure, but the hydrate equilibria was promoted incrementally because carbon dioxide constitute the large cages of the hydrate phase, therefore providing stability to the crystal structure. Promotion of the equilibrium curve was also supported by a reduced amount of sub-cooling required to initiate nucleation, implying hydrate formation occurs more readily with the inclusion of carbon dioxide rather than nitrogen.

Nitrogen's suppression of methane hydrate equilibria was not evident from the calculated enthalpies, which more-or-less are known to be relatively constant for the same hydrate structure regardless of the hydrated guest species. The increased ΔH_d for 25.0 mol% nitrogen was unexpected, but investigation into the higher pressure for which it was evaluated at as well as the gas compressibility of the mixture led to the conclusion that the increased ΔH_d relative to methane was a result of the increased methane partial pressure relative to the other mixtures. When carbon dioxide is added to methane, its hydrates evidently became increasingly more stable and was demonstrated by a gradual increase in ΔH_d with higher carbon dioxide concentrations. A more consistent trend of additive concentration with ΔH_d was apparent and credited to the increasing composition of carbon dioxide in the hydrate phase and only small changes in gas compressibility.

The experimental measurements were incorporated into an empirical correlation by setting the methane equilibrium point as a reference point and averaging the deviation produced by the respective methane-nitrogen/carbon dioxide gas mixture that have the highest concentration. An equilibrium point can be determined for a specified nitrogen or carbon dioxide concentration by an interpolation procedure. Empirical constants were derived and their application with the correlation proved to predict equilibrium temperatures that were consistent with other experimental works in literature. Unsurprisingly, it was discovered that the correlation did not provide temperatures that agreed with literature when applied outside its modelled composition range. Simulation software, HYSYS and PVTsim, displayed consistency with the correlation. However, some equilibrium points predicted by these programs were not consistent with some of their own computations of hydrate equilibria, the correlation's values or those in literature. While these simulation programs generally

provide reliable PVT data, the occasional inconsistency or contradiction that can sometimes be encountered outlines the importance of not solely relying on such models. The specific example outlined in this chapter regarding 11 mol% nitrogen in methane was evidence of such an encounter, where it would be beneficial to consult another hydrate modelling program or some form of empirical correlation for confirmation and as a precautionary measure.

Chapter 5

5. Helium Substitution of Hydrocarbons in Natural Gas

Knowledge of the equilibrium conditions for a hydrate system is one of many important hydrate-related factors to scientists and engineers involved with flow assurance in oil and gas recovery and processing. This information enables the appropriate precautions and measures to be taken to ensure that hydrate formation will not be an issue in the acquisition and processing of natural gas. Equally important is an understanding of how the hydrate equilibria for the parent natural gas changes throughout its processing lifetime, as it undergoes many stages of refinement by separating procedures. To avoid moving into the hydrate stability region, such changes can have an impact on the operating requirements of processing lines, equipment, separators, columns and other equipment where gas is in contact with an aqueous phase. The effect of separating natural gas components on the hydrate equilibrium conditions of a natural gas is explored in this chapter, where conclusions are made concerning which hydrocarbon separations would be beneficial for depressing the equilibrium curve. Typical natural gas constituents including ethane, propane, i-butane, n-butane, i-pentane and n-pentane are investigated.

In this study, a novel and alternative experimental approach to the identification of the roles of common hydrocarbons in a produced natural gas concerning their hydrates is introduced. This approach is demonstrated by acquiring several natural gas samples, all of which are identical apart from the absence of a different hydrocarbon for each sample. Establishing their hydrate equilibria would permit comparisons to be made regarding their contribution to the stabilisation of the hydrate phase. A natural gas that constitutes all the individual hydrocarbons not present in the previously mentioned natural gases is necessary as a reference point so that deviations in hydrate equilibria may be quantified. To compare hydrate equilibria justifiably, all the components common amongst each natural gas sample must be equal. Removing a component from a gas mixture would understandably change the relative quantities of all species, which would result in non-viable comparisons. To maintain relative compositions, the removed hydrocarbon may be equally substituted with a hydrate-inert gas. This ensures that gas compositions are consistent amongst all natural gas samples (except the removed component), and that the inert gas does not affect the hydrate equilibria in any way. The experimental approach introduced is unique in the

sense that this hydrate analysis focuses on the removal of a component, rather than its addition, and then analysing the change in equilibrium conditions.

Helium is a highly hydrate-inert gas, and is known to be completely inert throughout the range of pressure conditions imposed as part of this study's experimentation (Belosludov, et al., 2011;2014). Helium also does not form conventional (sI, sII, sH) hydrate structures, although molecular dynamic simulations predict that sII hydrates may be possible at pressures greater than 1000 bar (Belosludov, et al., 2011), which is far greater than the experimented operating pressures and of natural gas transmission lines for that matter. Such characteristics make helium an ideal substitute for the removed hydrocarbons in the assurance of consistent compositions of unchanged gas species.

5.1 Methodology

5.1.1 Equipment and Instrumentation

The equipment involved in this study was largely the same as the previous section. The PVT sapphire cell flow loop at the CGTA hydrate laboratory was the apparatus used for performing the hydrate experiments. The only modification made to the system was that of the compressor. A new compressor universal to the entire facility, was installed, replacing the older compressor, and provided far better recovery of residual gas in the gas sample canisters when applied to the booster pump after unloading gas into the flow loop. The gas booster pump was the only addition to the equipment used, since the natural gas cylinders acquired for the natural gas hydrate experiments were extremely low in pressure, making it difficult to extract gas. Also, the gas phase thermocouple probe (T2 in Figure 28) was replaced with an identical unit, because the wiring becoming detached. Overall, the composition analysers, piston pump, vacuum pump, video recorders, chiller and all other important accessories have remained unchanged.

5.1.2 Apparatus Operating Method

In determining the hydrate formation and equilibrium temperatures for the natural gas mixtures, the isobaric process (section 3.1.3) was the most fitting. The pressure was simply maintained using the piston pump and its associated software, and the temperature of the PVT cell slowly decreased or increased when measuring the formation and equilibrium temperature respectively. Heating and cooling was applied vigilantly to once again avoid overshooting and potentially obtain temperatures that were not accurately reflective of the point where a phase transition was first observable. This allowed all transport phenomena to occur at a relatively gradual rate.

5.1.3 Experimental Procedure

The experimental procedure for this study was almost identical to the procedure for analysing methane-nitrogen/carbon dioxide hydrates. The only exception was the manner of pressurisation, which involved the gas booster pump in addition to the piston pump. The procedure is summarised below:

1. The entire flow loop was purged with nitrogen, flushing out foreign particles
2. Milli-Q distilled water (5.0 mL) was injected into the PVT cell unit via a capped inlet
3. The system was vacuumed with the vacuum pump, including the cell
4. Pressurised steel gas sample canisters (500 mL) were unloaded at the manifold and directed to the piston pump
5. Using the gas booster pump, the residual gas in the canisters was extracted
6. Steps 4 and 5 were repeated until the gas in the piston pump was of sufficient pressure
7. Gas was allowed to enter the cell, and left to equilibrate
8. The sapphire cell was cooled in small decrements until hydrate formation was observed
9. After a complete phase transformation, the temperature was increased in small increments to the point where the hydrate began to degrade
10. The hydrate was allowed to completely dissociate
11. All gas was vented and the cell drained and thoroughly cleaned

5.1.4 Gas Mixtures

The natural gas mixtures were not prepared in the same manner as the methane-nitrogen/carbon dioxide gases because of the lack of instrumentation necessary to prepare almost identical gas mixtures. Maintaining the concentration of all but one component was a fundamental requirement for this study, because it was the only method which would permit an accurate comparison of hydrate equilibria for each modified natural gas. For this purpose, the source of natural gas was supplied and prepared by BOC Australia. The composition of the natural gas was decided based on typical compositions from methane down to the pentanes including a carbon dioxide impurity. Starting at ethane, each subsequent hydrocarbon was substituted with helium, and resulted in the requirement of 5 natural gas mixtures (Table 14).

Table 14 – Gas Mixture Compositions (mol%)

	M0	M1	M2	M3	M4
Methane	79.1	79.1	79.1	79.1	79.1
Ethane	7.0	-	7.0	7.0	7.0
Propane	3.0	3.0	-	3	3.0
i-Butane	2.5	2.5	2.5	-	2.5
n-Butane	2.5	2.5	2.5	-	2.5
i-Pentane	1.7	1.7	1.7	1.7	-
n-Pentane	1.7	1.7	1.7	1.7	-
CO_2	2.5	2.5	2.5	2.5	2.5
Helium	-	7.0	3.0	5.0	3.4

All natural gas mixtures were alpha grade. Unfortunately, the process of pressurizing the system was notably tedious and time-consuming because the very low pressures of the supplied natural gas cylinders. All gas cylinders were in the ranges of 6-7 bar because of the relatively high concentrations of the heavier butanes and pentanes, otherwise, condensation would occur. The only exception was M4, which was supplied with a cylinder pressure of approximately 20 bar. The consequence of such low pressures meant many of the 500 mL gas sample canisters had to be filled and refilled several times to achieve the required pressures. Without the gas booster pump, this work would not be possible since workable pressures would not be achievable.

5.2 Experimental Observations

As with most hydrate experiments, there are several distinct phase transitions that occur as a result of changing the thermodynamic conditions of the fluids. In this study on the hydrates of natural gas with helium substitution, similar observations to the methane-nitrogen/carbon dioxide hydrate studies were made except for some key elements primarily associated with the physical appearance of the synthesized hydrate. Amongst natural gas mixtures M0 through to M4, hydrate observations were generally identical to one another.

(a) (b) (c)

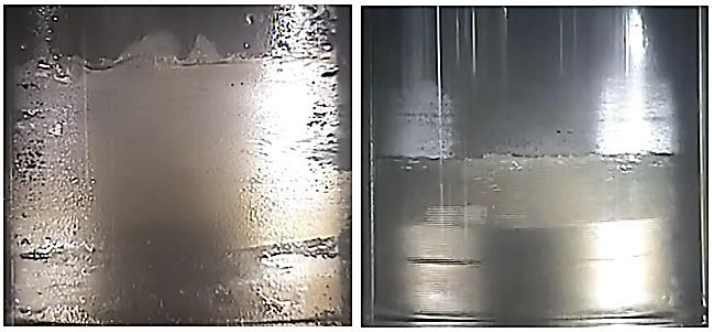

(d) (e)

Figure 46 – Experimental Observations (Smith, et al., 2015)

The general principle of hydrate formation observed with the sI hydrates in the previous chapter applies with the hydrates of natural gas, even though these hydrates are sII (confirmed in section 5.3.2). That is, hydrate nucleation was initially observed at the water-gas interface resulting in small, easily flowing hydrate crystals shown in Figure 46 (a) after sufficient cooling. Hydrate nucleation initialises at the phase interface because nucleation is heterogeneous, and therefore a full spherical volume of hydrate crystal need not occur because of the lower energy requirements (see Figure 12); (Kashchiev & Firoozabadi, 2002a).

With further hydrate development, thousands of small hydrate crystals began to concentrate the aqueous phase, and had the appearance of very white specks (b). This is in contrast to the initial hydrates (a), where there was little structure, and appeared more ‘flaky’. The hydrate kinetics also exhibited similar trends to the previous study. The rate of hydrate formation reduced significantly over time. As previously mentioned, the driving force for hydrate formation will change dynamically, where a greater concentration of the hydrate phase existing in the system will reduce the chemical potential driving force. A reduced Gibbs free energy is synonymous with a reduced driving force, and as stated by Kashchiev and Firoozabadi (2002), relates to the rate of hydrate nucleation (Eq. 15):

$$J = K \exp\left(-\frac{\varphi \Delta G}{kT}\right)$$

One can see that as the free energy driving force decreases in absolute magnitude, the rate of hydrate formation will reduce exponentially. The kinetics of hydrate formation and dissociation is not focused on in this thesis – this is simply a brief explanation that aims to explain the observed experimental phenomenon. For a better understanding of hydrate nucleation kinetics, the reader is referred to the works of Kashchiev and Firoozabadi (2002a;2002b) and Anklam and Firoozabadi (2004).

The completely crystallized structure of the natural gas hydrate (c) was one of the primary differences in observations compared to the methane-nitrogen/carbon dioxide hydrate. Hydrate in this case appeared to be more defined and the shape of the complete solid was sharper and appeared more 'solid' and harder. In comparison, the hydrate solid observed in the previous study did not exhibit these physical characteristics to the same extent, and could even be described as softer to the naked eye. These observations may be explained by the different hydrate structure types, where sII hydrates are dominant with all natural gas mixtures in these experiments. Limited studies focusing on the exact difference between the physical appearances of various types of hydrate are available, as all hydrates seem to be grouped together as ice-like in appearance. Consequently, the proposed reasons for differences in appearance are solely speculation.

Dissociation of the formed hydrate mass proceeded as expected, based on previous experimental procedures. First indications of hydrate dissociation were identified by the formation of a wet film on the outside of the cylindrical plug, as well as the emergence of small cavities (d). With continued heating and degradation of the hydrate, these cavities grew to the extent where the hydrate mass was no longer continuous, while simultaneously, water was pooling at the base of the cell. This enabled the mixture to flow once again, until eventually the hydrate degraded to the point where the aqueous phase dominated, and only remnants of the hydrate phase existed as tiny solids (e). These solids eventually dissociated completely, and the transparency of the water returned.

5.3 Results and Discussion

5.3.1 Equilibrium Results

The study of natural gas hydrate phase equilibria was prompted by the discovery of their impact on natural gas transmission lines by Hammerschmidt in 1934. The next two decades involved copious research pertaining to establishing the equilibria of

natural gas hydrates, one of such studies being conducted by Wilcox, et al. (1941) who tested multiple natural gas mixtures containing methane up to the pentanes (including carbon dioxide and nitrogen impurities). Deaton and Frost (1946) were also amongst the first to provide experimental measurements of natural gas hydrate equilibria. Their work was comprehensive, covering more than 10 natural gas variants comprising methane up to the butanes, including nitrogen, carbon dioxide and in one case hydrogen sulphide. Additionally, Adisasmito and Sloan (1992) investigated numerous natural gas mixtures as well as the effect of altering the carbon dioxide concentration.

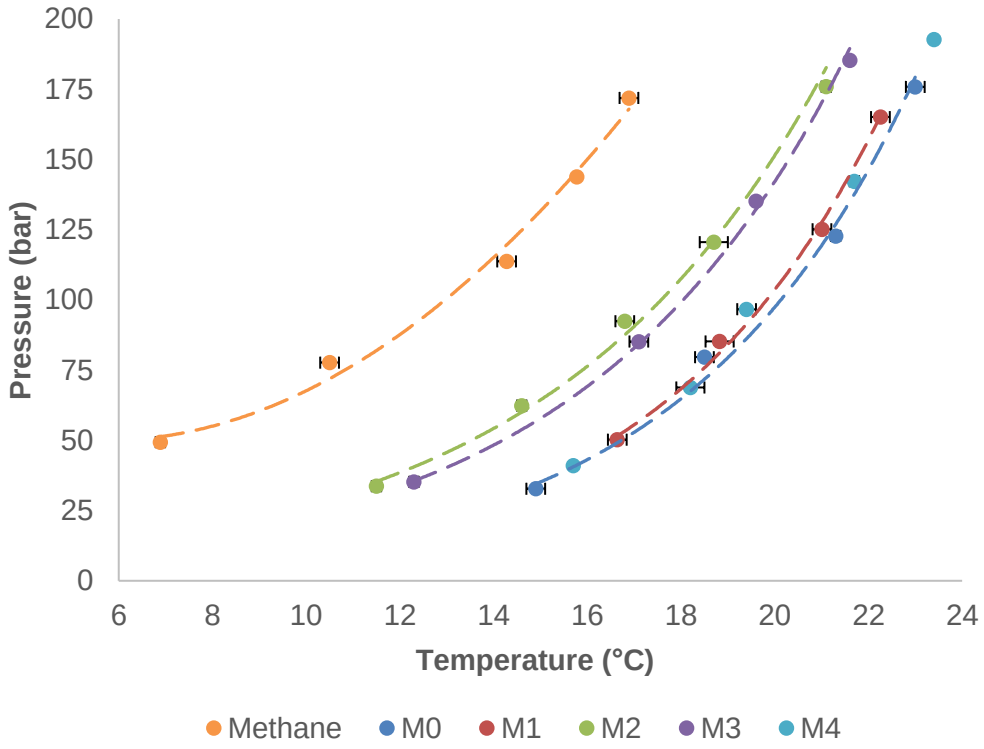

Figure 47 – Hydrate Equilibrium Conditions for Helium-Substituted Natural Gas (Smith, et al., 2016)

As shown in Figure 47, a common trait attributed to all the reported natural gas equilibria is that the equilibrium temperature is considerably greater than methane at a given pressure. This phenomenon is credited to sII-forming species present in the natural gas, such as propane, which can provide extra stability to the hydrate structure than a sI former like methane (Kini, et al., 2004). Another prominent sII hydrate species is i-butane, which is also a relatively common component in natural gas. Propane and i-butane are examples of gas species that will not readily form hydrates on their own; they instead require a 'help gas', so that the 5^{12} cavity is stabilized (Sloan & Koh, 2008). Methane is an ideal help gas because of its well-established ability to

occupy this small cavity in both sI and sII hydrates. It is the dominant species in natural gas, and given that sII gas components are common in natural gas, hydrates of natural gas are primarily type II structures (Kini, et al., 2004). The produced hydrate equilibria in this section aims to provide insight pertaining to the competitiveness of hydrate-forming hydrocarbons in natural gas, by comparing the produced equilibria of helium-substituted natural gases. Figure 47 summarizes the equilibria for all the examined natural gases and includes the confidence interval with duplicate measurements. The pure methane profile is also included to illustrate the substantial difference that larger hydrocarbons can have on hydrate equilibria.

The substitution of some natural gas hydrocarbons with helium clearly result in varying degrees of hydrate stabilization changes as indicated by reductions in T_{eq} at a given pressure. A rough estimation of the stability provided by a particular guest molecule is its molecule/cavity size ratio, which ideally should range between 0.75-1.00 for a guest to be able to occupy a hydrate cavity (Ripmeester, et al., 1987); (Christiansen & Sloan, 1994). Different gas species will also experience varying degrees of van der Waal interactions with the water molecules in a hydrate unit cell as well as in solution, which understandably will also contribute to a hydrate-former's ability to stabilize a hydrate structure. A guest's size, shape and molecular make-up are therefore the primary aspects to consider when analysing shifts in hydrate equilibria, which in this instance is relative to the reference M0 natural gas.

The substitution of ethane had a very minor impact on the natural gas hydrate equilibria, as depicted in Figure 47 by the M1 gas. A slight reduction in T_{eq} occurs, which may result from the fact that ethane was contributing to the hydrate phase (therefore its removal provides destabilisation and a reduction in T_{eq}) or it was in fact not contributing, but rather diluting other hydrate-formers. As a simple hydrate, pure ethane is individually classified as sI (Sloan & Koh, 2008). Binary hydrates of methane and ethane are also known to be type I, however it has been shown that a transition to sII hydrates may arise under certain pressures and/or compositions (Subramanian, et al., 2000). Subramanian and co-workers indicated using Raman and NMR spectroscopy that a transition from sI to sII will take place when the methane component is reduced to ~75%. The ethane content in M0 is only 7.0 mol%, so it is highly unlikely that ethane occupied any sII cages. As a sI hydrate, ethane occupies the larger $5^{12}6^2$ lattice cavity (Subramanian, et al., 2000). Assuming that the studied natural gases form sII hydrates (confirmed in section 5.3.2), it can be deduced that there are no suitable sites in the hydrate lattice that ethane can comfortably situate.

This explains the minimal shift in the equilibrium line for the substitution of ethane with helium.

The case for M4 is similar to that of M1 in that only a very minute change in the equilibrium profile occurs relative to M0. This natural gas mixture involved the substitution of both n-pentane and i-pentane, which were primarily responsible for low cylinder pressures. One major source for the small shift in equilibria is that n-pentane is not capable of forming any type of hydrate (Mehta & Sloan, 1996), and consequently acts as a diluent to the sII guests in the natural gas. This is presumably because of its excessive length and lack of bulk which may aid in interactions with the caging water molecules. On the contrary, i-pentane can form sH hydrates with the help of methane, and occupies the large $5^{12}6^8$ cage (Østergaard, et al., 2001). The type of hydrate a gas mixture will form is usually determined by the largest component capable of contributing to the hydrate structure (Sloan, 1998). The largest hydrate-forming molecule is i-pentane, and evidently, the 1.7 mol% of i-pentane was not sufficient to favour a sH hydrate lattice over sII. Thus, the role of the pentanes in M0 is thought to be similar to ethane as a diluent, and is essentially hydrate-inert within the working conditions.

With the substitution of propane, represented by M2, a considerable reduction in the hydrate equilibrium conditions is observed. On average, this amounted to approximately a 2.0 °C decrease in T_{eq} from the 30-200 bar range, and indicates that propane provides substantial stability to the M0 hydrate phase. As mentioned earlier, propane requires the assistance of a small guest molecule to fill the 5^{12} cavities of the sII hydrate lattice for the hydrate to form, as propane itself is too large (Engel & Macko, 2013). This is clearly provided by methane, having a composition of 79.1 mol% in all instances. The hydrate stability provided by propane can be estimated based on its molecule/cavity size ratio, which stands at 0.957 (Lederhos, et al., 1993). A value of 0.957 is very close to 1.00, and implies that the van der Waals radius of propane is in close proximity to the water molecules, where van der Waals attractions ensure a strong accommodation. A sII hydrate unit cell also consists of far more water molecules compared to sI (136 to 46), thus permitting a greater surface area for molecular interactions between the guest and host molecules. Because of the removal of propane, a very hydrate-stabilizing component, the hydrate equilibrium profile for M2 shifts to the left which would be a favourable outcome in terms of hydrate flow assurance. However, a sizeable margin still exists between the equilibria

for methane and M2. This remaining stabilization is provided by the butane content of the natural gas.

The substitution of the butane components with helium provides a similar effect on depressing the equilibrium profile to that of propane. Similar to propane, the butanes also require a help gas (methane) to occupy the small cavity in the formation of their sII hydrates. Out of n-butane and i-butane, the occupation of the sII $5^{12}6^4$ cavity by n-butane has been established as being the least stable by a considerable margin. The formation of n-butane hydrate is not overly favourable, and it has been shown that a transition zone exists between approximately 10.0-13.8 bar where n-butane behaves as a non-former (Ng & Robinson, 1976a). Instability of n-butane hydrates is also evidenced by its unfavourable molecule/cavity size ratio of 1.081 for the large sII cavity, which may distort the lattice due to its excessive size. In contrast, i-butane exhibits a ratio of 0.990, and therefore likely does not strain the hydrate structure, but in fact can experience strong intermolecular forces with water molecules because of their proximity. The i-butane therefore contributes to the hydrate stability more extensively than n-butane, and propane for that matter considering the i-butane is 2.0 mol% and propane is 3.0 mol%, considering the replacement of both components individually yields similar degrees of equilibrium depression. It can be concluded that propane and i-butane were the primary contributors to the hydrate phase and stability as well as methane, which fills the smaller cavity that propane and i-butane are too large to occupy.

5.3.2 Heat of Dissociation

An identical process for the heat of dissociation (ΔH_d) evaluation for methane-nitrogen/carbon dioxide is implemented for natural gas hydrates. For a system containing water and a gas, the corresponding hydrate's ΔH_d may be resolved with the Clausius-Clapeyron equation (Eq. 42),

$$\frac{d\ln(P)}{d(1/T)} = \frac{\Delta H_d}{ZR}$$

The slope of the equation's linearly fitted line is used to calculate ΔH_d, and is an alternative to direct measurement using calorimetry. Clausius-Clapeyron plots for each natural gas variant are illustrated in Figure 48. Some trend-lines have been omitted for improved clarity.

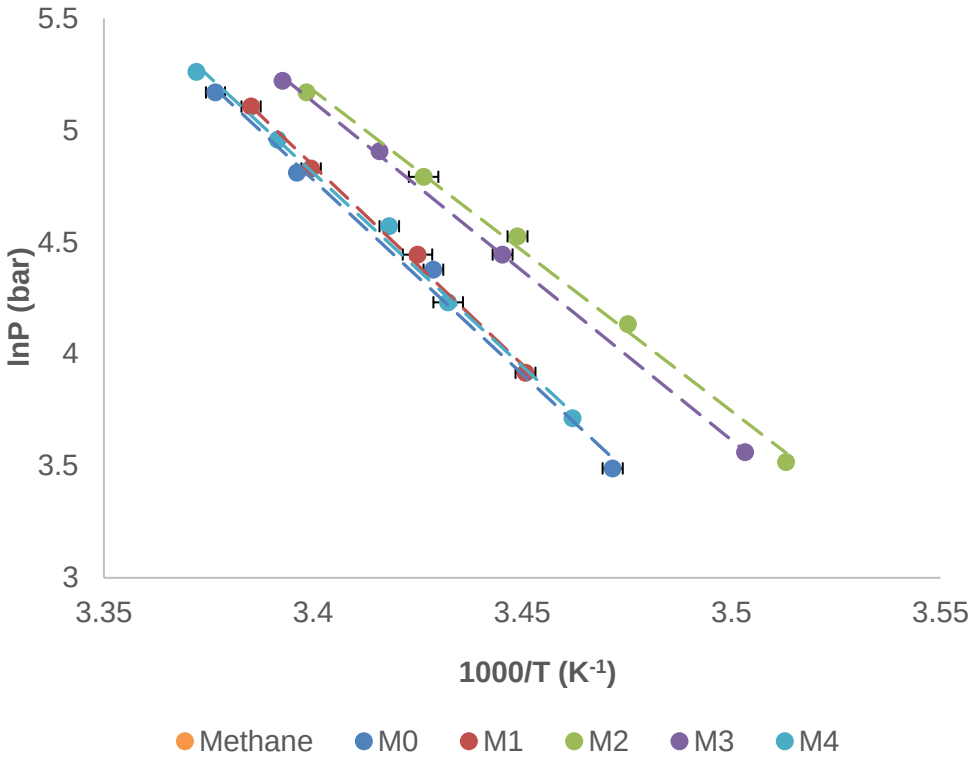

Figure 48 – Clausius-Clapeyron Plots for Natural Gas (Smith, et al., 2016)

One of the more notable characteristics is the difference in slopes of the collective natural gases compared to pure methane hydrates. Also, at a glance, the slopes of the natural gas hydrates are relatively similar in steepness. The positions of the trend-lines are another noteworthy observation; however, this is more important in analysing hydrate equilibrium profiles, not in Clausius-Clapeyron plots which still technically depict equilibria, but also includes the extra element of inferring structure type. This observable difference in slope between methane and natural gas is believed to be a consequence of the hydrate structure type. As mentioned by Sloan and Fleyfel (1992), the slope of the Clausius-Clapeyron equation is related to the guest size, and therefore the type of hydrate. Because propane and/or i-butane are present in the tested mixtures, sII hydrates are highly favoured and is the reason most natural gases form type II hydrates (Sloan & Koh, 2008). The calculated slopes and corresponding ΔH_d for gases M0-M4 including methane are summarised in Table 15.

Table 15 – Natural Gas Hydrate Dissociation Enthalpies

Gas	$\frac{-d\ln(P)}{d(1/T)}$, K	ΔH_d, kJ/mol	Structure Type
Methane	8650	60.0 ± 0.6	I
M0	17372	120.7 ± 0.4	II
M1	17798	127.9 ± 1.5	II
M2	14334	91.5 ± 0.4	II
M3	15118	99.9 ± 0.8	II
M4	17935	124.7 ± 1.1	II

Table 16 – Literature Dissociation Enthalpies*

Gas	$\frac{-d\ln(P)}{d(1/T)}$, K	ΔH_d kJ/mol	Structure Type
Methane	8100	56.9	I
Ethane	9000	71.1	I
Propane	15400	126.0	II
i-Butane	15800	130.4	II
i-Pentane	9333	72.2	H

*Data source: Sloan & Fleyfel (1994)

The substitution of some natural gas constituents with helium understandably have different effects relative to the M0 reference natural gas because of the different roles associated with each component regarding hydrate stabilisation. This is evidently true from the changing magnitude of the calculated slopes between each gas mixture. Different slopes imply different hydrate lattice stabilities which relates to the fact that different guests offer varying degrees of stability.

Methane's slope was previously calculated to be -8650, and is consistent with a sI hydrate former (Sloan & Fleyfel, 1994); (Juan, et al., 2015). In contrast, the natural gases all exhibited slopes well above the sI methane hydrate which is typical

behaviour for sII hydrates. In the previous section, it was concluded that ethane and the pentanes were diluting the propane and i-butane as the primary sII formers because:

- The removal of propane and the butanes resulted in significant declines in T_{eq}
- Ethane is a sI former and is too small to occupy the large sII cavity (therefore does not contribute to the hydrate structure)
- n-Pentane is not known to form hydrates and i-pentane's abundance is too low to favour the sH lattice.

The determined Clausius-Clapeyron equation slopes confirm these points. For point 1, M2 and M3 are the natural gases with propane and the butanes substituted with helium. Their corresponding slopes of -14334 and -15118 are notably less in magnitude than the reference M0 natural gas, -17372, which includes both these constituents. With such a decline in slope, both propane and i-butane can ultimately be confirmed to occupy the large sII cage, thus providing the greatest stability to the hydrate phase. Regarding point 2, the substitution of ethane prompted a minor increase in slope which may lie within experimental error, since logically, a minor increase should not occur because helium, a non-former, is substituting ethane which can also be considered a non-former in this instance. No change in the relative concentrations of the established hydrate-formers occurs, so a similar slope would be expected, and is indeed the case. A similar logic applies to point 3. A relatively marginal increase in slope from the M0 reference gas also likely lies within experimental uncertainty, since n-pentane and i-pentane are also not contributing to the structure and therefore behave identically (or very nearly) to their corresponding helium-replaced gas mixture. This is consistent with the small deviation in slope observed for the M4 mixture.

The heat of dissociation for a hydrate is defined as the required change in enthalpy that dissociates the hydrate phase to a liquid and vapour state (Sloan & Koh, 2008). Because the Clausius-Clapeyron slopes are pivotal in the process of calculating enthalpy changes and exhibit a proportionality, ΔH_d for the natural gases subsequently have similar trends to their conforming slope values. The ΔH_d for the reference M0 natural gas is markedly greater than the simple methane sI hydrates, and is indicative of the lattice stabilisation capabilities of propane and i-butane.

Likewise, mixtures M1 and M4 are the only other natural gases that include both propane and i-butane, and within experimental uncertainty, both mixtures have relatively similar ΔH_d values to M0. Ideally, their enthalpy changes should essentially be identical for the same reason their slopes should be. Besides experimental error, different P_{eq} values at the evaluated temperature of 15.0 °C between the measured natural gases will contribute to variation in ΔH_d. Regarding M1, its composition differs the most from all other mixtures with a replacement of 7.0 mol% with helium. A larger change in Z, and therefore influence of compressibility on ΔH_d, is attributed to M1. This was investigated by computing Z at the evaluating conditions (15.0 °C, P_{eq}): 0.8258, 0.8529, 0.7670, 0.7951 and 0.8677 were obtained using the PR EoS for M0, M1, M2, M3 and M4 respectively. Except for M2 and M3, the compressibility values for the gas mixtures do not differ substantially, particularly M1 and M4. Variation in Z occurs due to different P_{eq} for each mixture at 15.0 °C and each mixture's composition. Relative to M0, enthalpies are classified as vastly reduced – M2 and M3, or relatively unchanged – M1 and M4. These groupings are consistent with the propensities to promote hydrate equilibria (relative to pure methane) for the substituted species.

5.3.3 Uncertainty

The total uncertainty covers pressure and temperature readings, consumables as well some minor error sources. With reference to the ISO Guide to the Expression of Uncertainty in Measurement (GUM) (ISO, 2008), the overall uncertainty was calculated per its guidelines. The calculation procedure is given below for the pressure reading uncertainty.

Sources (i) to be accounted for: transmitter uncertainty (±0.5%), stability (±0.1%), temperature effect (±1%), calibration uncertainty (±0.5%).

At the 95% confidence level, the divisor (k_i) is 2 and the degrees of freedom (v_i) is $20^2/2 = 200$, as there is a 1/20 chance that the chosen uncertainty range is an underestimate. The procedure for evaluating the uncertainty associated with the pressure reading is as follows:

- Determine the standard uncertainty (u_i) from the expanded uncertainty (a_i) and k_i, with $u_i = a_i/k_i$
- Find the sensitivity (c_i) weighted standard uncertainty, $u_i c_i$
- Evaluate $(u_i \times c_i)^2$
- Calculate $(u_i \times c_i)^4/v_i$

- The combined uncertainty (u_c) is provided by $u_c = \text{sqrt} \sum_i (u_i c_i)^2$
- Using the result in step 4, the effective degrees of freedom (v_{eff}) is calculated as $\sum_i (u_i c_i)^2 / \sum_i (u_i c_i)^4 / v_i$
- The coverage factor (k), is determined from the students' t-distribution according to v_{eff}
- Expanded uncertainty at the 95% confidence limit (U_{95}) is calculated using $U_{95} = u_c k$

Instrumental and consumables uncertainty was dominated by pressure readings, with a propagated error amounting to ±1.36% across all instruments. See Appendix A for a more detailed breakdown of the quantitative aspect of the uncertainty evaluation. Like Chapter 4, the temperature uncertainty is a combination of instrumental uncertainty and scatter and are represented by error bars.

5.4 Experimental Correlation

5.4.1 Derivation

Experimental natural gas hydrate equilibria acquired in this study were used in the construction of an experimental correlation that estimates the hydrate equilibrium conditions for similar natural gases. The correlation can determine the dissociation temperature at a specified pressure given the global composition of the natural gas and that liquid water is present. This equation assigns empirical factors to the gas components that constitute the natural gases used for experimentation in this section. Methane, ethane, propane, i-butane, n-butane, i-pentane, n-pentane, carbon dioxide and nitrogen are included in the correlation, where the results for the methane-nitrogen/carbon dioxide equilibria in Chapter 4 are used in the determination of their empirical constants. Consequently, the model is solely dependent on gas composition, temperature and pressure.

The hydrate equilibria for the reference M0 natural gas is representative of the benchmark, or upper bound, where decreases in the composition of component i, x_i, relative to its composition in M0, $x_{ref,i}$, relate to the perceived reduction in T_{eq} from the experimentally established equilibria. A gas with a decrease in x_i reflects the helium-substituted natural gases, where the decrease is its elimination. Its hydrate equilibria are known experimentally in addition to M0, allowing the deficit in T_{eq} to be quantified by an analytical comparison with the reference, or upper bound, $T_{eq,ref}$.

Since the empirical parameters are determined based on the relative change in equilibrium temperature for component i, $\Delta T_{eq,i}$, such a deviation corresponds to a

certain change in mole fraction, Δx_i. The value for $\Delta T_{eq,i}$ can be calculated to a reasonable engineering approximation by interpolation of the experimental natural gas hydrate equilibria measurements. Because the helium replaces component i entirely, the lower bound in developing the experimental parameters is the equilibrium temperature when $x_i=0$, and is designated as $T_{eq,i0}$. The change in temperature from the upper bound to the lower bound (from $T_{eq,ref}$ to $T_{eq,i0}$) is depicted as $\Delta T_{eq,i0}$ for a particular Δx, and formulated as:

$$\Delta T_{eq,i0} = T_{eq,ref} - T_{eq,i0} \quad \text{Eq. 50}$$

In the equation above, the relative change in equilibrium temperature associated with the helium-substitution of a single component, i, with the reference M0 natural gas is expressed. For more than one alteration of a component's composition, the overall ΔT_{eq} would equate to the total of all changes in equilibrium temperature for each corresponding species and their corresponding Δx_i. Because these deviations are relative to T_{eq} for M0, the new equilibrium temperature is determined by the adding $T_{eq,ref}$. This is essentially an interpolation procedure, and therefore the concentrations of all gas species must be such that $0 < x_i < x_{i,ref}$ and the pressure not exceed 200 bar. For a natural gas that has several relative component composition changes, the proceeding relationship is used to determine the resultant T_{eq} brought about by each Δx_i,

$$T_{eq}(P_{eq}, x_i \ldots x_n) = T_{eq,ref}(P_{eq}) + \sum_{i=1}^{n} \Delta T_{eq,i}(P_{eq}, x_i) \quad \text{Eq. 51}$$

Where $\Delta T_{eq,i}$ is expressed as,

$$\Delta T_{eq,i}(P_{eq}, x_i) = \frac{x_i}{x_{i,ref}} \Delta T_{eq,i0}(P_{eq}) \quad \text{Eq. 52}$$

This equation may be substituted into the previous expression for evaluating T_{eq}, providing the following relationship:

$$T_{eq}(P_{eq}, x_i \ldots x_n) = T_{eq,ref}(P_{eq}) + \sum_{i=1}^{n} \frac{x_i}{x_{i,ref}} \Delta T_{eq,i0}(P_{eq}) \quad \text{Eq. 53}$$

In the representation of the experimental hydrate equilibria, a best-fitted exponential function was used to describe the pressure-temperature relationship. By rearranging the exponential function, the temperature, T_{eq}, can be set as the subject,

$$T_{eq} = \frac{\ln(P_{eq}/d)}{b} \quad \text{Eq. 54}$$

The preceding equation includes constants d and b, which are the standard parameters in all exponential relationships. Constants a and b contribute to the empirical factors derived. Using the rearranged expression, substitution of Eq. 54 into Eq. 53 results in the following general relation,

$$T_{eq}(P_{eq}, x_i \ldots x_n) = \left(\frac{\ln(P_{eq}/d)}{b}\right)_{ref} + \sum_{i=1}^{n} \left(\frac{x}{x_{ref}} \frac{\ln(P_{eq}/d)}{b}\right)_i \quad \text{Eq. 55}$$

To compensate for the varied weightings of the studied components towards a change in hydrate equilibrium conditions, a weighting factor, c, is applied (Eq. 56). This factor is proportional to the substituted component's composition and its corresponding gas mixture's area relative to M0 (discussed further below).

$$T_{eq}(P_{eq}, x_i \ldots x_n) = \left(\frac{\ln(P_{eq}/d)}{b}\right)_{ref} + \sum_{i=1}^{n} \left(\frac{cx}{x_{ref}} \frac{\ln(P_{eq}/d)}{b}\right)_i \quad \text{Eq. 56}$$

The derivation of the correlation parameters pertaining to each species involved integrating about the y-axis, hence the rearrangement of the exponential fitted equation. An integration was performed from the pressure range of 30-200 bar, where the calculated area for of the substituted natural gases was compared to the reference M0. A difference between these areas was representative of the magnitude of the deviation in equilibrium temperature, $\Delta T_{eq,i0}$. An area of 3142 was integrated for M0, which is relatively greater than 2813 for M2 with propane substituted. Such a reduction in area is proportional to $\Delta T_{eq,i0}$, and is translated from the fractional change in area, designated c_i for component i. For convenience, the c_i, b_i and $x_{ref,i}$ are combined to produce a collective constant, a. Both a and d parameters are summarised in Table 17.

Table 17 – Collective Empirical Terms (Smith, et al., 2016)

Component	a	d
Ethane	1.009	1.620
Propane	26.92	4.945
i-Butane + n-Butane	12.45	3.892
i-Pentane + n-Pentane	0.432	1.350
Carbon dioxide[a]	8.653	19.22
Nitrogen[a]	-5.058	25.24
Reference	3.602	1.659

[a] From Chapter 4

Provided the higher sensitivity of T_{eq} at lower pressures and lower sensitivity at higher pressures, 2.0 °C is added when the pressure is below 40 bar and subtracted when above 75 bar. The assumed linearity between Δx_i and $\Delta T_{eq,i}$ for the interpolation is not particularly valid, since the gradient $dT_{eq,i}/dx_i$ is not constant. The addition/subtraction of 2.0 °C is sufficient to counteract the assumed linearity and varying sensitivities with pressure.

5.4.2 Application

The relation established in the previous section along with the empirical constants may be used to estimate T_{eq} for a natural gas at specified pressure. Equilibrium temperatures predicted based on the theoretical model proposed by van der Waals and Platteeuw (vdWP) (1959) is compared to the produced experimental correlation. The vdWP data is generated using Aspen HYSYS (v. 8.1) and Calsep PVTsim (v. 20), where both programs apply similar variations of the vdWP model. Experimental work on natural gas hydrate equilibria collected by Nixdorf and Oellrich (1997), and Tohidi, et al. (2000) are also compared to the calculations of the correlation. The reported compositions of these synthetic natural gases are tabulated in Table 18.

Table 18 – Composition of Gases in Literature

Component	x_i[b]	x_i[c]
Methane	0.8636	0.9502
Ethane	0.0543	0.0398
Propane	0.0149	0.0100
i-Butane	0.0018	-
n-Butane	0.0031	-
i-Pentane	0.0006	-
n-Pentane	0.0006	-
Carbon-dioxide	0.0112	-
Nitrogen	0.0499	-

[b] Tohidi, et al. (2000); [c] Nixdorf and Oellrich (1997)

The reported compositions and pressures for both literature natural gases were applied with the experimental correlation to produce values for T_{eq} at their specified pressures. Values were also evaluated with HYSYS and PVTsim using the SRK EoS and compared to literature and this work's formulation (Table 19).

Table 19 – Equilibrium Temperature (°C) Conditions of Literature Gases (Smith, et al., 2016)

Reference	P (bar)	Reported	Calculated	PVTsim (SRK)	HYSYS (SRK)
Tohidi, et al. (2000)	45.0	13.25	13.01	13.14	12.97
Nixdorf and Oellrich (1997)	39.9	11.15	10.08	10.98	9.56
	69.6	15.41	16.23	15.19	13.87
	109.4	18.45	17.98	18.13	16.92
	173.6	20.89	19.77	20.73	19.77

There is agreement between the experimental model's application and the reported literature T_{eq} for the selected natural gases in literature. For the temperatures noted by Tohidi, et al. (2000) and Nixdorf and Oellrich (1997), there is an average difference of 5.3% and 6.0% respectively when compared the formulation's predicted temperature. Similarly, calculated equilibrium conditions generally agree with the

vdWP thermodynamic model implemented in PVTsim, although at several pressures, HYSYS produces values in considerable disagreement with literature, PVTsim and the correlation. Both vdWP models differ in some key areas (Smith, et al., 2015), however, such large variations between software predictions are unusual. These discrepancies between software models and their evaluating procedures are discussed in more detail in Chapter 7.

5.5 Conclusion

A shift in hydrate equilibrium conditions has been demonstrated after replacing several hydrocarbons in natural gas individually with helium, a hydrate-inert gas. This process is synonymous with a desired separation procedure of a specific natural gas hydrocarbon, allowing measurement of the new hydrate equilibrium conditions for the parent natural gas after separation. This study showed extreme influences that both propane and i-butane have on the equilibrium profile of natural gas. Both components, i-butane more-so than propane, were the primary sources of hydrate equilibrium promotion, and when combined, work synergistically in stabilising the hydrate. Compared to pure methane, the hydrate equilibria shifted by approximately 7 °C, a very considerable promotion, which highlights the necessary separation of these hydrocarbons in early downstream processing to avoid hydrate plugging. Comparatively, ethane and i-pentane, which can form sI and sH hydrates with methane respectively, did not contribute significantly to the hydrate phase as evidenced by the minute change in equilibria. Propane and i-butane are thermodynamically favoured as the preferred occupants, as they offer greater stability to their sII hydrate cavities, which results in sII being the preferred structure. These gas species in addition to other present non-sII formers such as carbon dioxide are not capable of filling sII cages and therefore remain gaseous, diluting the propane and i-butane sII formers. This study recommends careful consideration of the separating processes in natural gas refinement, since the separation of particular hydrocarbons have considerable variability in hydrate equilibrium temperature reduction if an aqueous phase is also present.

The experimental hydrate equilibria for the synthetic natural gases are in good agreement with literature and theoretical vdWP thermodynamic models, particularly the PVTsim model, by way of a correlation derived from experimental measurements. This indicates reliable hydrate equilibrium measurements and the assurance that equilibrium temperatures and pressures are well represented by the correlation. Except for some equilibrium conditions computed by HYSYS, the results calculated

using this study's experimental correlation usually differed by less than 1 °C with literature, equating to a 5.3% and 6.0% disagreement with reported values by Tohidi, et al. (2000) and Nixdorf and Oellrich (1997).

New information and data concerning the heat of dissociation for natural gas hydrates has been reported, and will aid in the determination of energy requirements to dissociate a hydrate plug and maintain thermodynamic conditions that ensure the gas-water system remains outside of the hydrate stability zone. The Clausius-Clapeyron equation was used to provide enthalpy changes, where higher values were reported for the natural gases containing both propane and i-butane. Lower slopes in addition to lower heat of dissociation values were associated with the natural gases that had either of these components substituted with helium. This observation relates to the extensive capabilities of propane and i-butane to occupy the large sII cages, given their high molecule/cavity size ratios, providing additional stability to the hydrate. Relative to methane, the natural gas hydrate dissociation enthalpy changes were far greater, often exceeding 100 kJ/mol given that 60.0 kJ/mol was determined for methane hydrates. More energy is therefore necessary to dissociate a highly stabilized sII hydrate phase than sI. Another reason for the observed variation between heats of dissociation was attributed to the different P_{eq} that correspond to 15.0 °C for each gas. In summary, the heats of dissociation calculated with the Clausius-Clapeyron equation are accurate within no more than 10% (Sloan & Koh, 2008), and have provided a reasonable engineering approximation for the heat of dissociation of natural gas, and are consistent with the expected hydrate stabilities.

Chapter 6

6. Hydrates of Propane, i-Butane and n-Butane

The proceeding study focuses primarily on the role propane, i-butane and n-butane in natural gas hydrate formation in response to their substantial contribution to promoting the hydrate equilibria of the studied synthetic gases in Chapter 5. Experimentally, propane demonstrated that it was most influential in stabilisation of the hydrate phase. The butanes, whose hydrate equilibria contributions were not individually characterised, but collectively they imposed a very high degree of equilibria promotion. Consultation with literature informed that i-butane was a far more effective sII hydrate-former than n-butane in the presence of methane, leading to the conclusion that propane and i-butane were responsible for the transition to a highly stabilized sII hydrate phase (Deaton & Frost, 1946); (Ng & Robinson, 1976a); (Wu, et al., 1976); (Sloan & Koh, 2008). Hydrate equilibria promotion due to these hydrocarbons was in proportion to their concentration in the natural gas mixtures, which was fixed except for their respective helium substituted mixtures. For better characterisation, this chapter investigates propane, i-butane and n-butane hydrates in methane gas to establish the varied extent of their individual capacity to promote the hydrate equilibrium boundary with composition.

In previous chapters, it was mentioned that the hydrate structure type may be determined from equilibrium data when applied with the Clausius-Clapeyron equation. As mentioned previously, the slope of the equation and the enthalpy of dissociation are relatively constant for each structure type (Sloan & Fleyfel, 1992); (Sloan & Koh, 2008), which is agreeable from a conceptual point of view and from results presented in the preceding chapters. However, it is theorised that for a binary methane-propane/i-butane/n-butane gas mixture, this may not be true on the basis that a non-negligible change is proposed, resulting from differing degrees of stabilisation associated with varying compositions of the sII former. Logically, the slope/ΔH_d for hydrate equilibria corresponding to the composition where the hydrate transitions to sII compared to slope/ΔH_d for a gas mixture with higher concentration will not be insignificant and therefore cannot be assumed constant for more accurate applications. The composition of the hydrocarbon in the presence of methane necessary to induce a change from sI to sII is approximated by establishing connections between the slope of the Clausius-Clapeyron equation, ΔH_d and the composition of propane/i-butane/n-butane in methane. The identification of trends

correlating slope/ΔH_d to composition would be particularly helpful in estimating the extent of hydrate stability, and whether hydrates of a natural gas constituting low propane, i-butane and/or n-butane contents will manifest as sI or sII.

6.1 Methodology

6.1.1 Equipment and Instrumentation

The sapphire PVT cell apparatus and flow loop located at the CGTA hydrate laboratory in Bentley used in the previous chapters is again the sole means of acquiring experimental hydrate measurements. Only minor modifications to the apparatus were made – several valves were leaking at higher pressures and were replaced with identical parts and internal tubing connecting the sapphire cell to the piston pump were replaced because a deformed capping, also causing leaks. Additionally, electrical wiring and cables connecting the piston pump controller to the computer were renewed because of communication malfunctions that disabled any form of control over the pump. Because of the extensive use of the PVT cell, the magnetic actuator was subject to degradation. Due to its degrading state, it was feared that small rust particles and corrosion products may escape from the mixer, enter the solution and possibly affect results. A new and identical mixer was installed at the Future Engineering workshop as a precautionary measure.

6.1.2 Application of Apparatus

Most equipment utilized in the previous chapter is applied in an identical manner for the experimentation in this section. The settings related to pressure and temperature control (Mint Workbench and FALCON) have remained unchanged and the replacing of tubing, valves and magnetic mixer have not had any influence on the operation of the hydrate PVT cell plant. The purpose of the gas booster pump is not specifically to increase the pressure as it was in Chapter 5, but instead to ensure the prepared gas composition does not change when released into the system. Each gas is separately contained in a steel gas sample canister (500 mL) – i.e. not mixed – so their release into the plant is driven only by the canister's pressure, where a large proportion can remain in the canister. The booster pump transfers the remaining gas so that the desired composition in the system is achieved.

6.1.3 Experimental Procedure

Overall, the experimental procedure also remained largely unchanged. Pressurising the system was far less tedious than in Chapter 5, as cylinder pressure was not an issue. The experimentation process is essentially identical to methane-nitrogen/carbon dioxide hydrate testing.

6.1.4 Gas Mixture Preparation

Gas mixtures were prepared using a method identical to that in the preparation of the methane-nitrogen/carbon dioxide mixtures in Chapter 4. Gas mixtures of methane-propane/i-butane/n-butane and methane-nitrogen-propane/i-butane/n-butane were experimented with, where each gas mixture was synthesized on a weight basis. A Shimadzu weighing balance (±0.0005g) weighed the empty and filled gas sample canisters to quantify the contents of each canister. Each gas canister was vacuumed prior to pressurisation so that the possibility of contamination was minimised. Two or three gas canisters were usually required (two for binary mixtures and three for ternary) – one for each gas species. The gas components in low composition (i.e. propane, i-butane, n-butane and nitrogen) were released into the piston pump and extracted with the booster pump first, followed by the high-pressure methane. All gases were supplied by BOC Australia and were classed as high purity (99.99%).

6.2 Experimental Observations

The hydrates of methane with propane/i-butane/n-butane and in some instances nitrogen were all observed to have relatively similar physical characteristics to the natural gas hydrates in Chapter 4 and Chapter 5. The lighting in the air bath chamber that ensures observation is possible was improved to capture better quality images of the experimental proceedings. A folded white sheet of paper was placed behind the sapphire cell and wrapped around the unit, leaving the front exposed for visualisation. The stirrer was also periodically stopped for short moments to provide less blur and a clearer picture of the various phases of matter. Images of the phase transitions are shown in Figure 49.

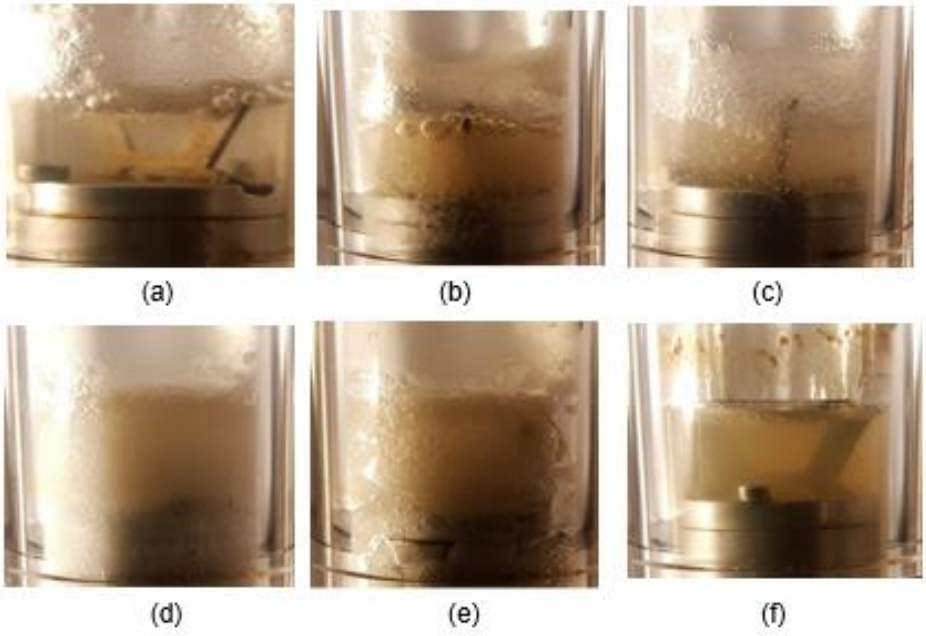

Figure 49 – Experimental Observations

Interestingly, the initial formation of hydrates not only occurred at the gas-water phase interface, but often deposited as a clearly visible thin layer. This phenomenon is illustrated in (a), and became visible at the same time as the small interfacial hydrate crystals. The 5.0 mL of water is syringed through the top of the cell through a separate inlet to the gas which is capped during operation of the apparatus. This inlet is not located directly above the centre of the cylindrical cell, but rather to the side where it is common for the water to trickle down and swirl along the inside wall of the glass during and after injection. Small droplets of water consequently adhere to the glass surface immediately above the bulk water. Essentially, the surface of the aqueous phase is extended. Hydrocarbon gas hydrate formation will occur at phase interfaces because of the very low water solubility of these gases, and tend to grow as films (Wu, et al., 2013). The surface of the aqueous phase is always disturbed by the magnetic actuator, so a film does not synthesize. However, the layer of water adhering to the glass is not disturbed, and subsequently forms a hydrate film. Whether this observation was only noticed because of the improved visualisation of the fluids and had been present in hydrate experiments in Chapters 4 and 5, or was unique to these gas mixtures cannot be confirmed. As demonstrated in (b), the hydrate formation extends from the interface (heterogeneous nucleation) to the bulk of the solution (homogeneous nucleation). The liquid phase has completely lost its transparency and becomes cloudy due to the emergence of many microscopic crystals that result from homogeneous nucleation. This clarified depiction of the early hydrate formation stage illustrates the early development of stabilized hydrate

clusters. Being less dense than water, these clusters succumb to buoyancy forces causing them to rise and collect near the surface of the solution (Sloan, 1998). Eventually, the clusters united and began to form a continuous hydrate solid (c), which gradually occupied greater volumes with further addition of clusters to the structure. Strain on the stirrer was evident, and often became stuck for short periods. Previous observations regarding the rate of formation are consistent with these – there was a definite decrease in hydrate formation rate with time, and is explained by the constant decrease in chemical potential driving force ($\Delta\mu^{driv}$). A lessening of the hydrate nucleation rate consequently occurs, and is exponentially proportional to $\Delta\mu^{driv}$ (Anklam & Firoozabadi, 2004).

As commonly encountered in previous studies, most of the liquid phase transformed into a large, singular crystallized plug (d). At this point, there is essentially no more significant enclathration of gas molecules at the present thermodynamic conditions and the phase transformation to hydrate is complete with no fluids flowing. Due to the non-stoichiometric nature of gas hydrates, not all the water cages necessarily are required to be filled by a guest (Sloan & Koh, 2008). In fact, the extent of cage-filling has been shown to be proportional to not only the guest species, but also the operating conditions (Anderson, 2003); (Ravipati & Punnathanam, 2013).

The crystallized hydrate mass is extremely similar in appearance to the natural gas structures of Chapter 5. Hydrates in this study are also sII and their equilibria indicate very stable hydrates as they generally have high equilibrium temperatures. This manifested physically, as their appearance shows more definition compared to the type I hydrates of methane-nitrogen/carbon dioxide, which at a glance appeared to be softer.

Dissociating the formed hydrates involved significant heating. This indicated considerable stability of the hydrate structure, and agrees with the somewhat similar hydrates of natural gas in the preceding section. Dissociation of the hydrate was again identified by the melting of the solid, causing the reformation of the liquid, and crevices to emerge (e). Complete dissociation induced by continued heating expectedly melted the entire hydrate, reforming the gas and liquid, sometimes leaving the solution murky (f). It is possible these observations correspond to “nano-bubbles” – agglomerated methane gas in solution that manifest due to slow methane diffusion velocities (Bagherzadeh, et al., 2015). The required heating for complete dissociation was quite substantial, where temperatures approximately 6-7 °C higher than the equilibrium temperature were necessary. This stability of natural gas hydrates even

after exceeding the equilibrium point is an important aspect in studies related to storage of gas as their hydrate (Gudmundsson, et al., 1997). A metastable state can be achieved, provided that the surrounding gas solution remains supersaturated (Buffett & Zatsepina, 1999), prolonging the hydrate state at those specific conditions. This was proved by Buffett & Zatsepina (1999) who undertook experiments that confirmed hydrates can be heated several degrees above the dissociation temperature and remain relatively stable.

6.3 Results and Discussion

6.3.1 Equilibrium Results

Natural gases almost always produce sII hydrates in the presence of liquid water because of the propane and butanes, especially i-butane, that are commonly produced (Kini, et al., 2004). With the help of methane, a 'help gas', the smaller cages are also filled and the equilibrium conditions are drastically elevated. One of the expected findings in Chapter 5 was that propane and the butanes were the greatest contributors to the equilibrium stability of the studied natural gas hydrates. Whilst there is knowledge of the phase behaviour of these hydrocarbons with water as singular components as well as in binary mixtures with methane and other gases, there is little information that focuses on small quantities of propane/butane in the presence of methane. There can often be very small compositions of these gases in produced natural gases, where a reasonable assumption would be that such small concentrations have no significant influence on the hydrate equilibrium profile. The following equilibria illustrate that this assumption is not valid in some cases, and the opposite is in fact true.

6.3.1.1 Methane and Propane

Hydrate equilibria for methane-propane systems have been established by several studies in literature, one of the first being Deaton and Frost (1946). Other works have confirmed the promoting influence of propane with methane, such as Mcleod & Campbell (1961) and Song & Kobayashi (1982). However, there is little establishment of very low propane compositions (<1 mol%) and whether such a small quantity will have any influence on the hydrate profile with methane. Furthermore, there is very little literature material on the possible impact of the addition of nitrogen to methane-propane gases. Figure 50 demonstrates the change in conditions brought about by varying propane concentrations and also includes equilibria of a ternary methane-propane-nitrogen gas mixture.

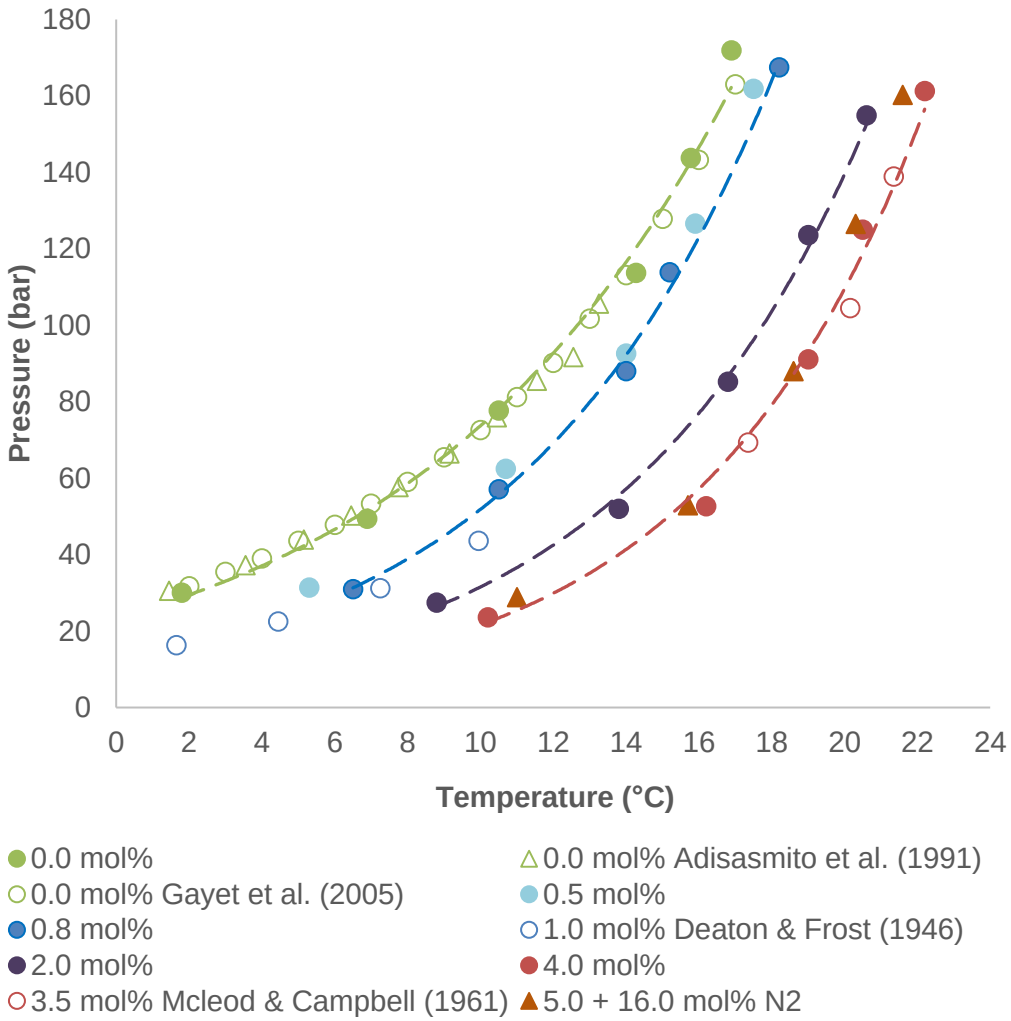

Figure 50 – Methane-Propane Hydrate Equilibria (Smith, et al., 2017)

Possibly the most striking aspect of the methane-propane hydrate equilibria is the major increase in the equilibrium conditions considering propane constituted less than 1.0 mol% of the combined gases (0.8 mol%). Throughout the range of operating pressures, T_{eq} for 0.8% propane is often greater than T_{eq} for 0.0% (pure methane), and is even more considerable at lower pressures. Measurements are consistent with the 1 mol% propane data reported by Deaton and Frost (1946), which despite the limited range of their tested pressure conditions, display slightly greater equilibrium conditions than this work's 0.8% propane curve. Interestingly, increasing the propane composition to 2.0 mol% amplifies the promoting influence substantially, and is consistently more than 4 °C higher than the equilibrium conditions for methane. Further increasing the composition to 4.0 mol% expectedly elevates the equilibrium curve but not to the same extent. The rate of hydrate equilibrium promotion relative to methane reduces with higher propane concentrations, and is indicative of diminishing returns. This may be rationalized by considering the concept of fractional

occupancy, θ_{ij}, of cavity type i by gas species j, mentioned in Chapter 4. The equation is reiterated below:

$$\theta_{ij} = \frac{C_{ij} f_i}{1 + \sum_i C_{ij} f_i}$$

A greater occupancy of hydrate lattice cavities generally implies that the hydrate is more stable and requires more energy to dissociate, which is synonymous with promoted equilibrium conditions. Considering the occupancy of the large $5^{12}6^4$ cavities for sII hydrates, with a very small propane the $\sum_i C_{ij} f_i$ term would not be as great compared to higher propane partial pressures. Although θ_{ij} for propane in the $5^{12}6^4$ cage will increase because of the increase in its corresponding $C_{ij} f_j$ term at a certain pressure, the rate of increase will reduce because $C_{ij} f_j$ approaches $\sum_i C_{ij} f_i$ as the propane mol% rises. This explains the seemingly reduced hydrate promoting effect for 2.0-4.0 mol% compared to 0.0-2.0 mol%.

For the methane-propane-nitrogen hydrate profile, there is a relatively small but noticeable depression of the equilibrium curve with 16.0 mol% nitrogen. From Figure 50, the equilibria exhibit very high sensitivity to propane. Observably, given a propane composition of 5.0 mol%, dilution with 16.0 mol% nitrogen suppresses the curve so that it overlaps the 4.0 mol% line. Nitrogen is diluting the methane, which is at least 96.0 mol% in the other analysed gas mixtures, compared to 79.0 mol% in this example. From the other methane-propane gases, there is an obvious correlation between the fillings of sII $5^{12}6^4$ cavities with propane, which evidently overshadows any effect resulting from reduced methane occupation of the small 5^{12} cavities. The reduction in methane content to 79.0 mol% is far more significant, and undoubtedly has reduced the occupancy of the small cages. This confirms methane is an effective 'help gas' with propane sII hydrates (Sloan & Koh, 2008).

6.3.1.2 Methane and i-Butane

Phase equilibria for methane, i-butane and water have also been documented in several studies in literature. Deaton and Frost (1946) provided hydrate equilibrium data for i-butane amongst many other hydrocarbon gas hydrates. Another important contribution was by Wu, et al. (1976), who experimented with three and four-phase conditions for i-butane in methane. Wu and co-workers experimented with various i-butane compositions and also stated equilibria for concentrations less than 1.0 mol%, although these were only single data points rather than a complete profile. The

experimentally established hydrate equilibrium curves for i-butane in methane are summarised in Figure 51 in addition to a ternary mixture with nitrogen.

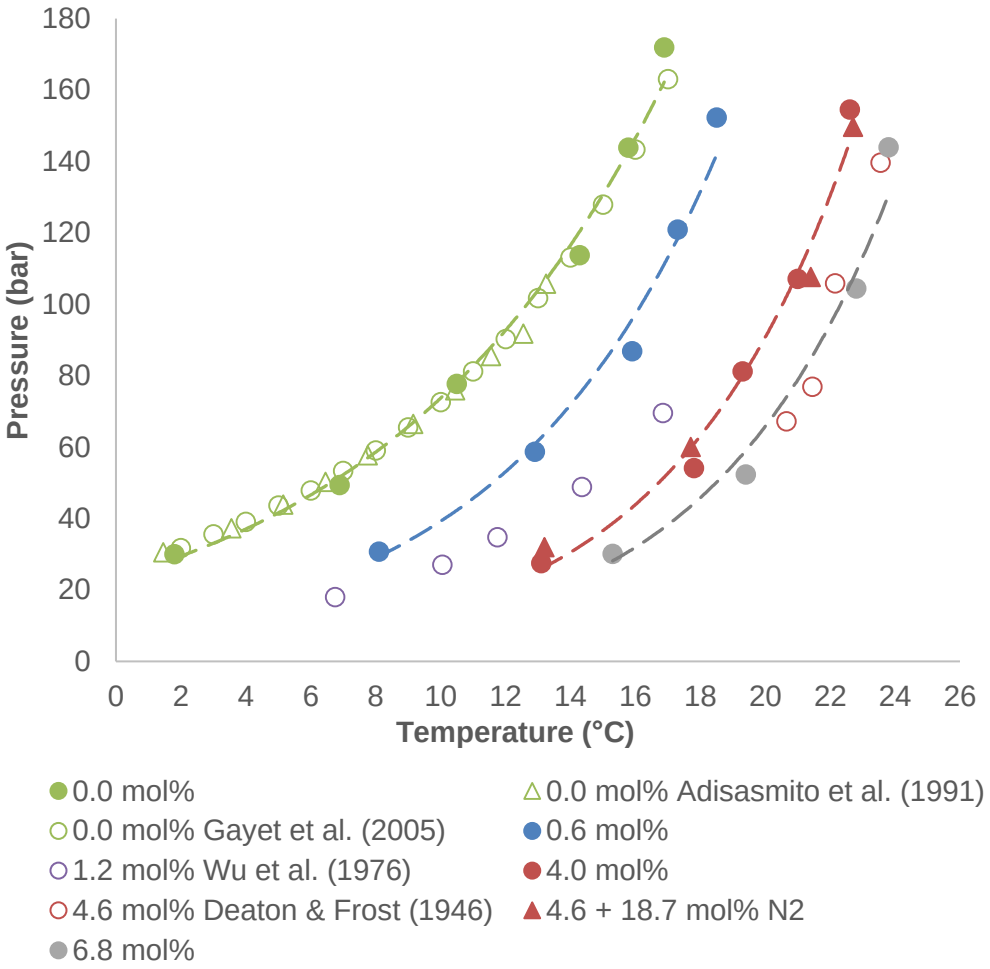

Figure 51 – Methane-i-Butane Hydrate Equilibria (Smith, et al., 2017)

Similar to the methane-propane hydrate profile (Figure 50), the addition of i-butane to methane results in a considerable shift in the hydrate equilibrium conditions, perhaps even slightly more-so. This is apparent by observing the considerable increase in T_{eq} for only 0.6 mol% i-butane, which is consistently 3-4 °C above the methane hydrate equilibrium conditions. Such a considerable increase for a very small quantity of i-butane is indicative of the highly stabilising impact i-butane has on the sII hydrate structure. Given 0.6 mol% is enough to induce a very significant shift of the equilibrium line, it is implied that less than 0.6 mol% is necessary for the hydrate to transition from sI to sII throughout the working pressure range. Naturally, increasing the i-butane concentration shifts the curve further to the right substantially and is now approximately 8 °C higher than methane's T_{eq}, often reaching 10 °C+ at lower pressures. However, a similar effect observed with methane-propane also occurs here: beyond 4.0 mol%, there is a far less drastic increase in T_{eq}. A similar logic may

be applied here regarding the theoretical relationship between occupancy, composition and fugacity of i-butane at a specified pressure. The reduced rate of hydrate equilibria promotion with composition also appears to be more evident at higher compositions than the methane-propane equilibria, where diminishing returns became observably prominent after 2.0 mol% propane. With methane-i-butane, this phenomenon becomes apparent from about 4.0 mol% i-butane and onwards, however, the region from 0.6-4.0 mol% also exhibits this effect, albeit to a far less extent compared to 4.0-6.8 mol%. This is also marked by the 1.2 mol% data by Wu, et al. (1976), which although were collected with a different and older apparatus, are consistent with the likelihood of a reduced rate of hydrate equilibria promotion with i-butane concentration at less than 4.0 mol% i-butane.

The sensitivity of increasing i-butane concentration in methane on the sII hydrate equilibrium conditions is reasonably greater than propane with methane. This is very recognizable by comparing Figure 50 and Figure 51. Considering the heightened sensitivity of hydrate equilibria promotion with i-butane, dilution with nitrogen logically would have less of an effect because the influence of i-butane on structural stabilisation outweighs methane to a greater extent than propane does. In Figure 51, experimental measurements agree with this rationale. With 4.6 mol% i-butane, the addition of 19.0 mol% nitrogen depressed the equilibrium curve to the 4.0 mol% curve's location. Hydrate equilibria depression by nitrogen dilution is lessened with respect to dilution of the methane-nitrogen system, despite methane being of lower partial pressure and a greater dilution factor in this instance. It would therefore be more beneficial to remove or separate i-butane from natural gas production streams rather than introducing nitrogen, unless a vast quantity of nitrogen is introduced.

6.3.1.3 Methane and n-Butane

The role of n-butane in hydrate formation was long-thought to be minimal and possibly non-existent altogether. Byk & Fomina (1968) state that n-butane does not form hydrates in their extensive review on gas hydrates. Musaev (1966) reportedly had similar views on the subject of n-butane hydrates. Parrish & Prausnitz (1972) confirmed the inability of n-butane hydrates theoretically by stating that the n-butane molecule is too large to fit into either sI or sII cavities. However, Mcleod and Campbell (1961) were successful in synthesizing n-butane hydrates with methane as the help gas. They compared the equilibrium line for methane and methane-n-butane gases and came to the conclusion that n-butane in methane slightly promotes the hydrate equilibria at lower pressures, however at higher pressures, the methane-n-butane line crosses the methane line where it may even be considered as an inhibitor at such

pressures. The following experimental hydrate equilibria presented in Figure 52 for methane-n-butane are consistent with the mentioned findings.

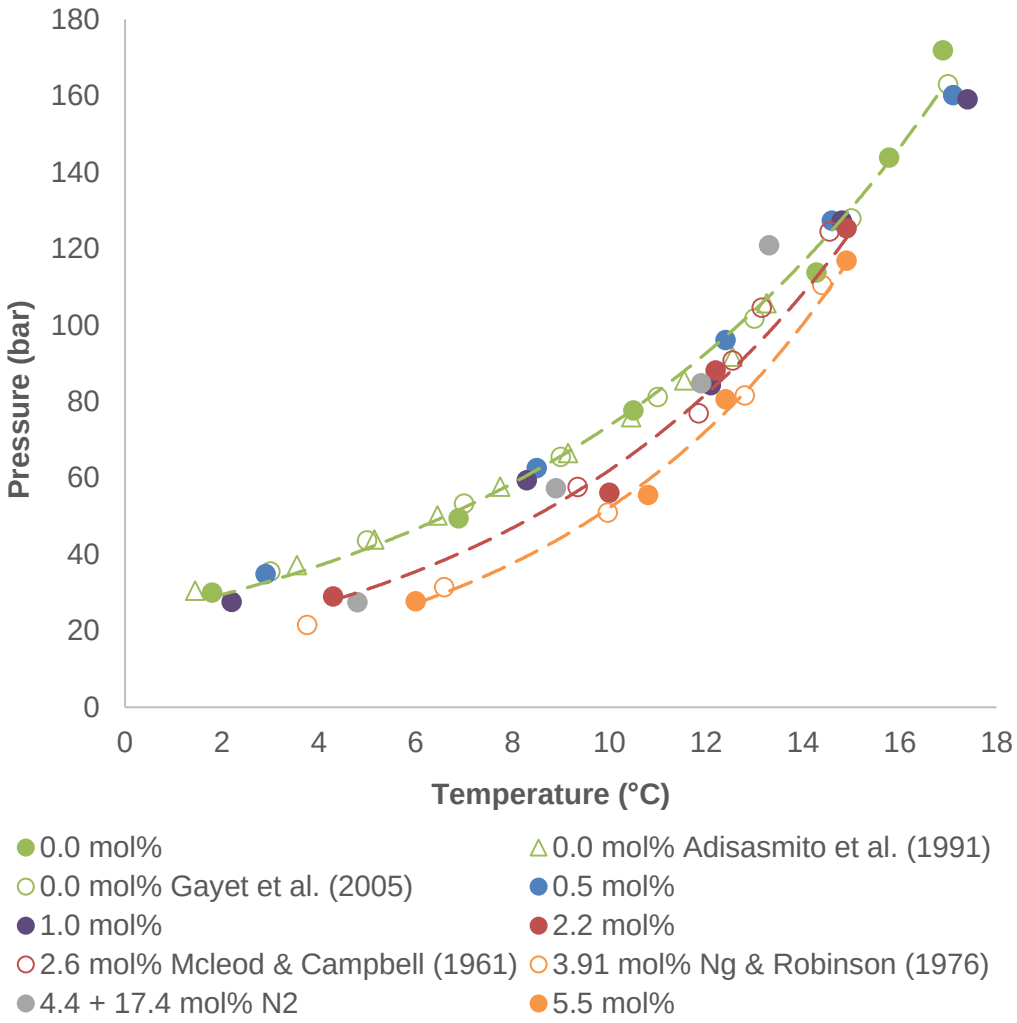

Figure 52 – Methane-n-Butane Hydrate Equilibria (Smith, et al., 2017)

The experimental hydrate measurements for methane-n-butane follow a somewhat similar trend to the previous propane and i-butane, although the extent of equilibrium shift is far inferior. Equilibrium data from earlier works in literature compare favourably with the measurements acquired in this thesis. Possibly the biggest discrepancy lies with the 3.9 mol% n-butane line corresponding to data from Ng and Robinson (1976a), which is on par with this study's 5.5 mol% curve. Provided that there is a smaller margin of error required for perfect clarity and resolution on account of the considerably lower sensitivity of the above profile, overlap is not entirely unexpected. The improved equipment available today is also likely to contribute to any perceived differences between the literature works for which experimental error may not account for.

A common trait amongst all tested gas mixtures is the elevated equilibrium conditions accompanied with the increasing composition of the additive. A noteworthy observation is the significantly smaller impact of n-butane in methane on the hydrate equilibria compared to propane and i-butane. This is also true according to the presented literature measurements. Interestingly, there is a sharp decline in ΔT_{eq} (between the pure methane line and methane-n-butane line) with increasing pressure between methane and its mixtures with n-butane, approaching the methane T_{eq}. For the tested compositions, there is a crossover point at which point T_{eq} is equal with methane, where a further rise in pressure moves the methane-n-butane line into pure methane's hydrate stability region. For all gas mixtures, this phenomenon occurs approximately between 80-120 bar. This confirms the observations of Mcleod and Campbell (1961), who noted that methane-n-butane gases exhibit equilibrium conditions to the left of methane consistently from approximately 100 bar and continued up to the 680 bar limit in their illustrations. The cause of this effect relates to minor distortions of the hydrate lattice due to higher pressures, ultimately changing the size of the cavities (Ng & Robinson, 1976a); (Claussen & Frost, 1951); (Stackelber & Muller, 1951). The molecule/cavity ratio for n-butane in its designated sII cavity is 1.081, hence its occupation of the cavity is already strained. Slight changes in lattice structure brought about by increased pressures will therefore inevitably have a large detrimental effect on stability. Furthermore, Ng and Robinson (1976a) also concluded from their measurements that there is a transition zone that occurs between 100-138 bar where the behaviour of n-butane is gradually resemblant of a hydrate non-former, although their compositions were slightly higher than this work's.

Observably, n-butane's hydrate stability increases relative to methane are considerably inferior to propane and i-butane, i.e. its hydrate profile is generally less sensitive to composition. Diluting methane with nitrogen therefore has a greater effect relative to methane-propane/i-butane mixtures, particularly at pressures above 80 bar where n-butane essentially has no effect on the equilibrium curve. Sloan and Koh (2008) mention that only a 0.5% change in lattice size may change the equilibrium pressure at a specified pressure by 15%. From Figure 52, the 4.4 mol% n-butane with 17.4 mol% nitrogen curve is initially in line with the experimental 2.2 mol% curve, evidently a result of dilution. However, after 80 bar, the curve deviates across the methane line rather substantially. This confirms the heightened influence of nitrogen dilution for the methane-n-butane system at elevated pressures.

6.3.1.4 Equilibrium Data

Table 20 summarises the raw equilibrium data in addition to the temperature's expanded uncertainty (95%, k = 2). There was no pressure scatter; hence its expanded uncertainty (95%, k = 2) is simply the instrument's uncertainty of ±0.25 bar.

Table 20 – Experimental Vapour-Liquid-Hydrate Equilibrium Data (Smith, et al., 2017)

C_1 (100.0)		C_1/C_3 (99.5/0.5)		C_1/C_3 (99.2/0.8)	
P/bar	**T/°C**	**P/bar**	**T/°C**	**P/bar**	**T/°C**
31.25	1.8 ± 0.1	31.34	5.3 ± 0.1	31.00	6.5 ± 0.1
49.38	6.9 ± 0.1	62.45	10.7 ± 0.1	57.10	10.6 ± 0.1
77.66	10.5 ± 0.1	92.61	14.0 ± 0.2	88.01	14.0 ± 0.1
113.71	14.3 ± 0.1	126.57	15.9 ± 0.2	113.88	15.3 ± 0.2
143.80	15.8 ± 0.1	161.84	17.5 ± 0.1	167.50	18.2 ± 0.1
171.89	16.9 ± 0.1				
C_1/C_3 (98.0/2.0)		**C_1/C_3 (96.0/4.0)**		**$C_1/C_3/N_2$ (79.0/5.0/16.0)**	
P/bar	**T/°C**	**P/bar**	**T/°C**	**P/bar**	**T/°C**
27.43	8.8 ± 0.1	23.60	10.2 ± 0.1	28.90	11.0 ± 0.2
52.02	13.8 ± 0.2	52.62	16.2 ± 0.2	52.89	15.7 ± 0.1
85.20	16.8 ± 0.1	91.09	19.0 ± 0.1	87.96	18.6 ± 0.2
123.61	19.0 ± 0.1	124.98	20.5 ± 0.2	126.56	20.3 ± 0.1
154.92	20.6 ± 0.1	161.30	22.2 ± 0.1	160.27	21.6 ± 0.1
C_1/iC_4 (99.4/0.6)		**C_1/iC_4 (96.0/4.0)**		**C_1/iC_4 (93.2/6.8)**	
P/bar	**T/°C**	**P/bar**	**T/°C**	**P/bar**	**T/°C**
30.68	8.1 ± 0.1	27.45	13.1 ± 0.1	30.11	15.3 ± 0.1
58.65	12.9 ± 0.1	54.10	17.8 ± 0.2	52.31	19.4 ± 0.2
86.83	15.9 ± 0.2	81.20	19.3 ± 0.1	104.42	22.8 ± 0.1
120.90	17.3 ± 0.1	107.11	21.0 ± 0.1	143.93	23.8 ± 0.1
152.27	18.5 ± 0.1	154.51	22.6 ± 0.1	155.24	24.3 ± 0.1
$C_1/iC_4/N_2$ (76.7/4.6/18.7)		**C_1/nC_4 (99.5/0.5)**		**C_1/nC_4 (99.0/1.0)**	
P/bar	**T/°C**	**P/bar**	**T/°C**	**P/bar**	**T/°C**
31.91	13.2 ± 0.1	34.83	2.9 ± 0.1	27.52	2.2 ± 0.1
60.01	17.7 ± 0.1	62.57	8.5 ± 0.1	59.37	8.3 ± 0.1
107.65	21.4 ± 0.1	96.05	12.4 ± 0.1	84.22	12.1 ± 0.2
149.63	22.7 ± 0.1	127.33	14.6 ± 0.2	127.31	14.8 ± 0.1
		160.14	17.1 ± 0.1	159.06	17.4 ± 0.1
C_1/nC_4 (97.8/2.2)		**C_1/nC_4 (94.5/5.5)**		**$C_1/nC_4/N_2$ (78.2/4.4/17.4)**	
P/bar	**T/°C**	**P/bar**	**T/°C**	**P/bar**	**T/°C**
29.00	4.5 ± 0.1	27.70	6.0 ± 0.1	27.45	4.8 ± 0.1
56.07	9.9 ± 0.2	55.51	10.8 ± 0.1	57.30	8.9 ± 0.1
88.13	12.0 ± 0.1	80.61	12.4 ± 0.2	84.83	11.9 ± 0.1
125.30	14.9 ± 0.1	116.84	14.9 ± 0.1	120.90	13.3 ± 0.2

6.3.2 Structural Transition Estimation

An important theme of the foregoing section with the hydrate equilibrium results was that very small amounts of a favourable hydrate-former can shift the equilibrium curve drastically. Therefore, it is important to quantify the concentration of the sII hydrate-former necessary to induce the transition from sI methane hydrates to the more stable methane-propane/i-butane/n-butane (n-butane only at lower pressures) type II hydrates.

It has been stated in literature that 1 mol% of propane in methane is sufficient to induce the formation of sII hydrates (Deaton & Frost, 1946); (Sloan & Koh, 2008). This is certainly agreeable and is demonstrated by the methane-propane hydrate data in this thesis. Provided that compositions less than 1 mol% were tested, all of which were clearly identified as sII as evidenced by their considerable hydrate equilibrium promotion, there is an implication that sII hydrates of these components with methane are possible with compositions below even the minute gas concentrations studied. To approximate concentrations where there is a transition to sII, the Clausius-Clapeyron equation will be used, and is reiterated as follows:

$$\frac{d\ln P}{d(1/T)} = \frac{\Delta H_d}{ZR}$$

The slope of the equation, dlnP/d(1/T), is directly related to the structure type of the hydrate, where steeper slopes are indicative of sII and stability (Sloan & Fleyfel, 1992). As mentioned in previous chapters, the slope and ΔH_d are the same for all hydrates that are of the same structure type, regardless of the guest species (Sloan & Koh, 2008). Any changes that occur are attributed to how well the guest species fits into the cavity, i.e. its molecule/cavity ratio, and the magnitude of the van der Waal attractive forces between the guest and caging water molecules (Sloan & Koh, 2008). To the author's knowledge, there are no complete studies that relate composition with the Clausius-Clapeyron slope and ΔH_d. Using the experimental hydrate equilibrium data presented in the previous sections, lnP was plotted against 1/T and the slope and ΔH_d evaluated for each composition. Trend-lines for dlnP/d(1/T) and ΔH_d versus composition are arbitrarily placed which take into account calculated values from the experimental data. For the proceeding results, slopes/ΔH_d values were computed at 100 bar and the corresponding T_{eq} with the SRK EoS (for ΔH_d) . Should the PR EoS be preferred, ΔH_d can be converted by multiplication with a conversion factor, (Z_{PR}/Z_{SRK}).

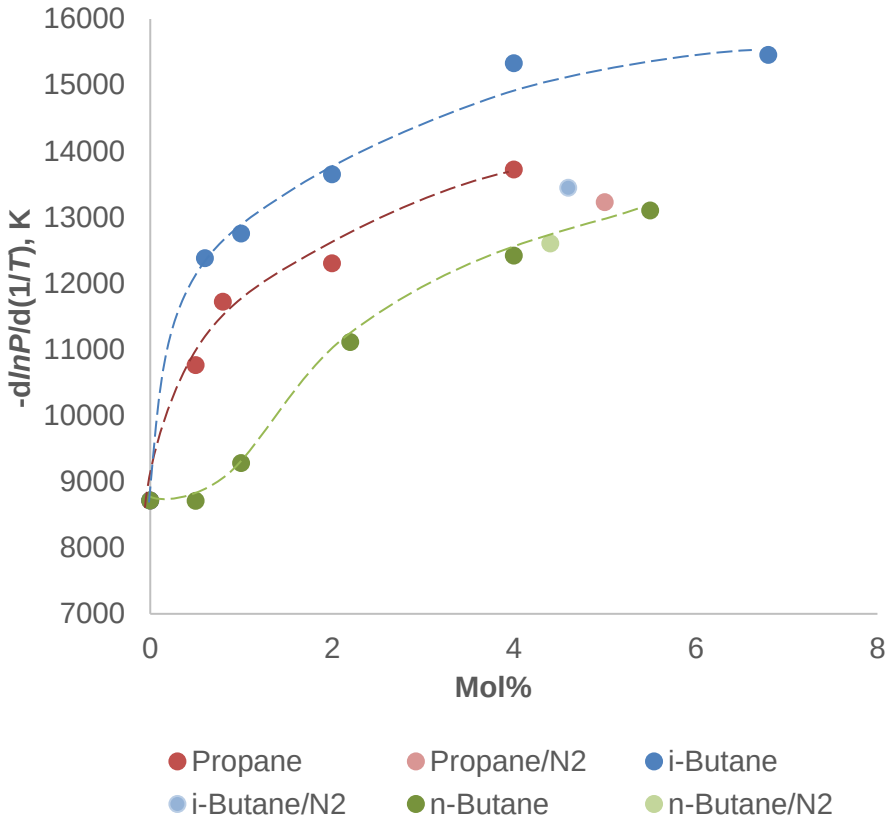

Figure 53 – dlnP/d(1/T) Sensitivity (0.0 – 8.0 mol%) (Smith, et al., 2017)

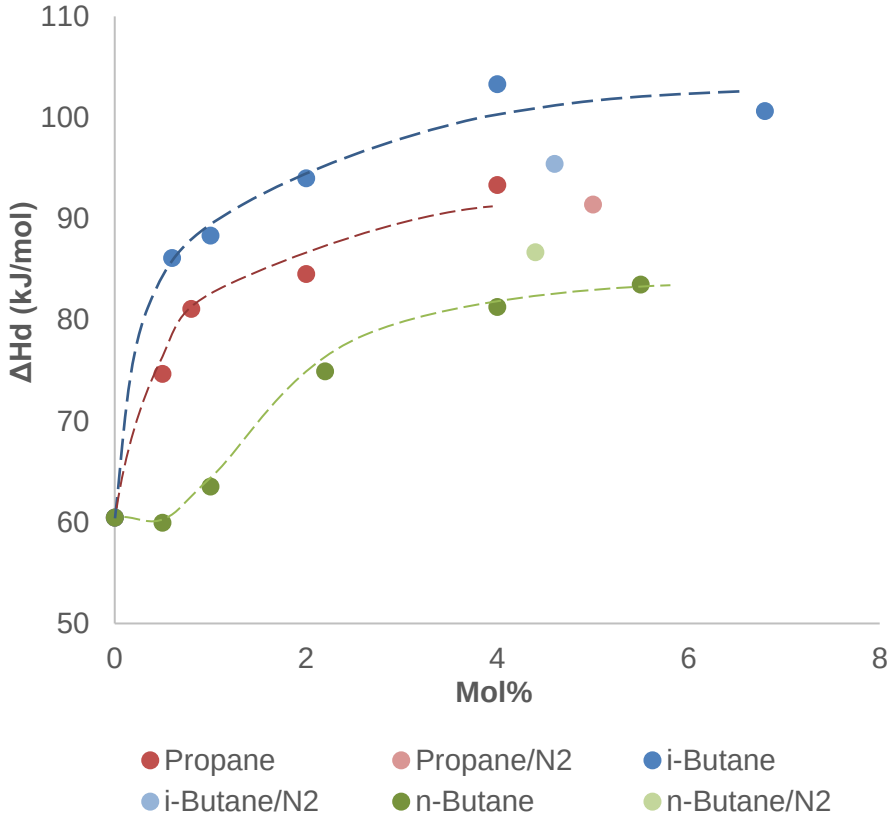

Figure 54 – ΔH_d Sensitivity (0.0 – 8.0 mol%) (Smith, et al., 2017)

The Clausius-Clapeyron slopes and ΔH_d relationships with composition are generally what would be expected – there is an increase in slope and ΔH_d, therefore hydrate stability, with higher concentrations of propane, i-butane or n-butane in methane. Steeper slopes are associated with methane-i-butane mixtures followed by methane-propane and lastly methane-n-butane. This agrees conceptually with the phase equilibrium diagrams and the characteristic information they portray regarding stability and its correlation with promoted thermodynamic conditions. Increased stability of the hydrate phase offered by i-butane correlated with promotion of the equilibrium conditions to the greatest extent, and this is also reflected in the preceding two illustrations.

With an increase in composition, the Clausius-Clapeyron slope and ΔH_d rise at a greater rate and sustain values of higher magnitude for i-butane. A similar profile exists for propane, which is also able to maintain a constant positive gradient in Figure 53, although not of the same magnitude as i-butane. While it is stated by Sloan & co-workers that the slope and heat of dissociation is relatively constant and only varies significantly between structure type, this is not entirely true according the trends in Figure 53 and Figure 54. It is certainly agreeable that both ΔH_d and dlnP/d(1/T) does not change significantly for most compositions, but the same cannot be said for low compositions, where both parameters can change in excess of 20% (varies depending on the guest).

An interesting observation is the nature of n-butane's relationship with ΔH_d and its composition. For instance, except for the initial flat region, its relationship with dlnP/d(1/T) is similar to the propane and i-butane lines, which increase rapidly, until the relationship becomes more linear. Propane and i-butane continue to increase with a small gradient, whereas n-butane's gradient is essentially 0. Similarly, with ΔH_d, the n-butane curve exhibits an initial relationship similar to propane and i-butane, but rather than becoming linear and maintaining a positive gradient, ΔH_d remains steady after approximately 4.0 mol%. This is an indication of declining stability of the hydrate phase. It was previously noted in the methane-n-butane equilibrium diagram (Figure 52) that there is a transition where n-butane's role in contributing to the hydrate phase becomes non-existent and provides no added stability on its part (Mcleod & Campbell, 1961); (Ng & Robinson, 1976a). This is consistent with Figure 54, which illustrates no increase in stability after the initial rise in ΔH_d with composition.

From the previous figures, the regions of greatest sensitivity for propane, i-butane and n-butane composition increases are 0.0-0.5, 0.0-0.6 and 0.5-2.2 mol%

respectively. Each methane additive (propane, n-butane and i-butane) also clearly have varying levels of sensitivity towards increasing the sII-like nature of the hydrate phase when their composition is increased in these identified ranges (as indicated by increase in slope/ΔH_d with composition). Table 21 numerically describes and summarises the sensitivity of composition of the slope/ΔH_d versus mol% relationship by listing their gradients.

Table 21 – Equilibria Promotion Sensitivity (Smith, et al., 2017)

Additive	d(slope)/d(mol%), K/mol%	d(ΔH_d)/d(mol%), kJ/mol.mol%	Range, mol%
Propane	4232 ±36	26.64 ±0.23	0.0 – 0.5
i-Butane	6223 ±49	43.50 ±0.34	0.0 – 0.6
n-Butane	1808 ±20	11.66 ±0.13	0.5 – 2.2

The values given in Table 21 are indicative of their propensity to assume a sII hydrate configuration and promote the hydrate equilibrium conditions. Standard uncertainties were calculated using the RMS average of pressure and temperature standard uncertainty, given that the parameters listed in Table 21 were evaluated using slope, which incorporates pressure and temperature. Expanded uncertainties (95%, k = 2) are given in Table 21. Since the provided values were derived from a collective of data sets, each with its own attributed uncertainty, the worst-case (highest uncertainty) uncertainties are used. Additionally, each sensitivity parameter is unique for each additive. In the circumstance that the slope/ΔH_d has been experimentally determined from hydrate pressure-temperature equilibria for a gas mixture with known composition (within the tabulated range), the provided gradients can be used to mathematically generate equilibrium data for another supposed gas mixture (provided its composition is within the nominated range).

Upon the addition of a sII hydrate-former to a sI former, there will be a brief period where the addition of said sII guest will not impact the overall structure of the hydrate phase. In the previous figures, this would correspond to a flat region extending from 0.0 mol% to a certain small composition where a sharp increase in gradient occurs. It is hypothesized that determining the approximate composition where there is a structural transition from type I to II may be accomplished by examining the trends

illustrated in such diagrams. A turning point where there this transition manifests is illustrated by the sudden increase in gradient in Figure 55.

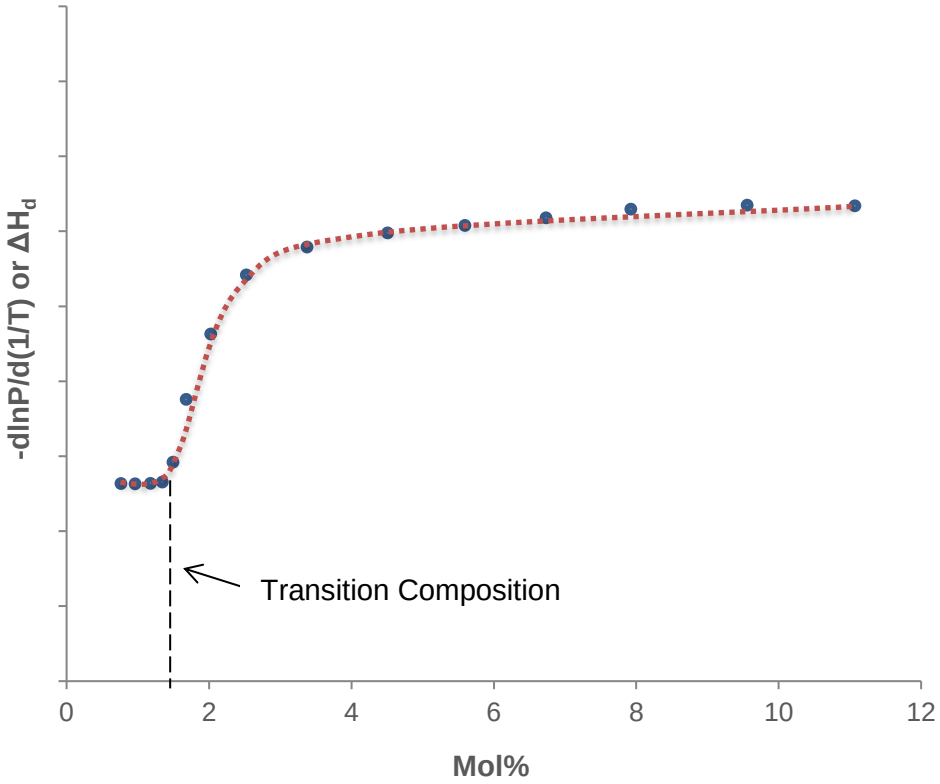

Figure 55 – Structure Transition Composition

Unfortunately, no flat region was detectable with the available experimental data sets for propane and i-butane. Prior to experimentation, it was expected that compositions of 1.0 mol% would suffice, which evidently was not low enough to exhibit the proposed effect. However, there is an observable turning point for n-butane in Figure 54. Without the proper instrumentation to prepare gas compositions lower than 0.5 mol%, an alternative method using PVTsim was employed. By using equilibrium data generated by the vdWP thermodynamic model implemented in PVTsim, the dlnP/d(1/T) and ΔH_d for compositions lower than the experimented compositions, the Clausius-Clapeyron slopes and ΔH_d can be computed. These results are displayed in the proceeding figures.

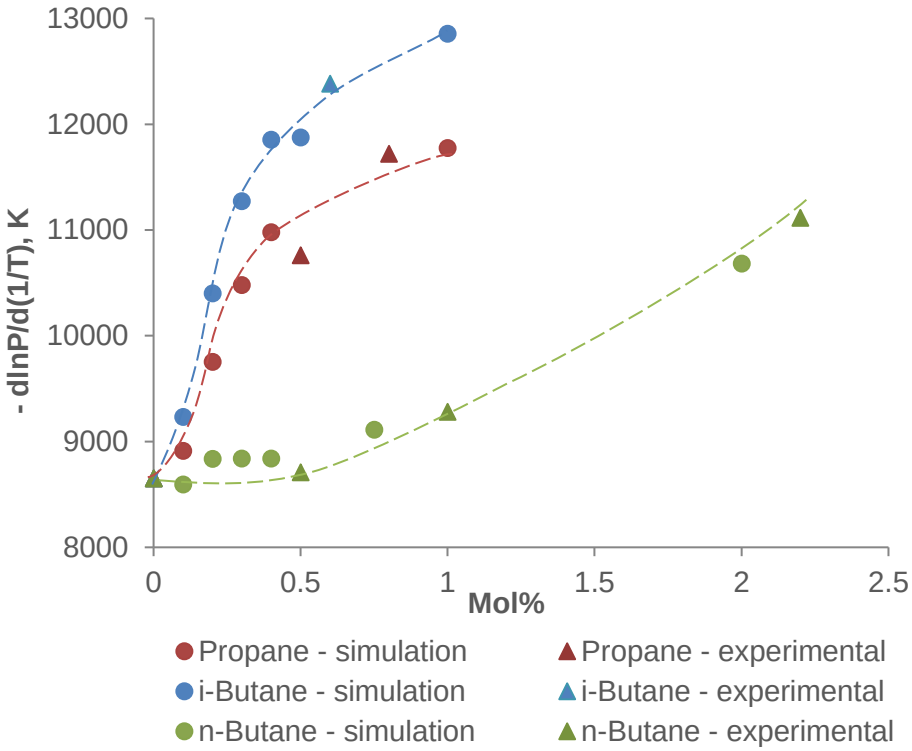

Figure 56 – dlnP/d(1/T) Sensitivity (0.0 – 2.5 mol%) (Smith, et al., 2017)

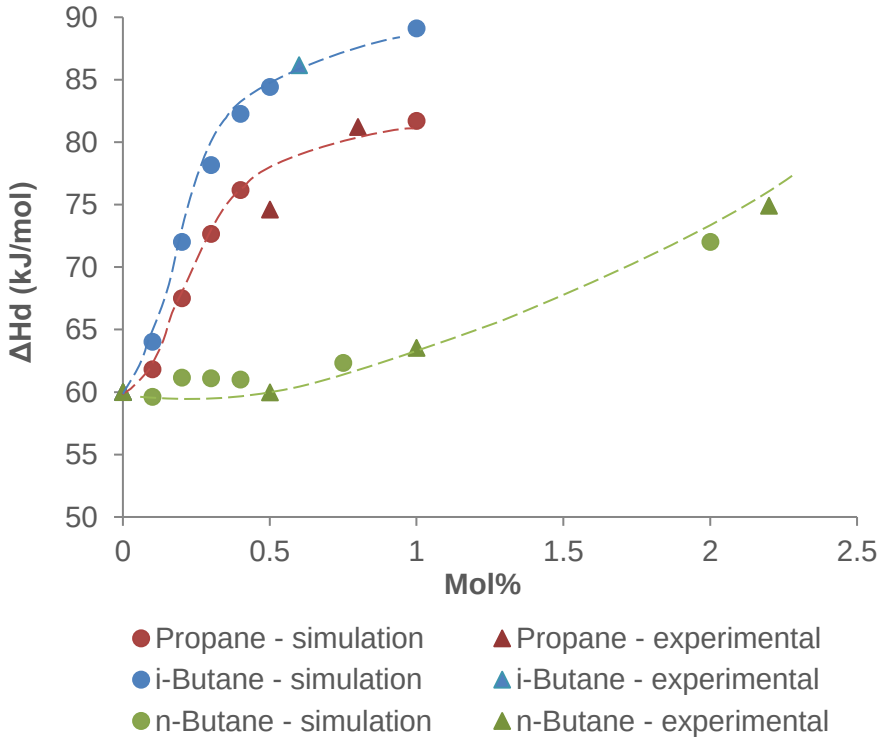

Figure 57 – ΔH_d Sensitivity (0.0 – 2.5 mol%) (Smith, et al., 2017)

To aid in identifying the range where propane/i-butane are initially inert, PVTsim with the PR EoS was consulted. Unfortunately, it was not possible to synthesize gas

mixtures with the desired (low) compositions because of the extreme delicacy required and excessive uncertainty associated with the composition. More accurate and precise instrumentation was not available. To accommodate, pressure-temperature equilibrium data for the intended gas mixture was used to calculate Clausius-Clapeyron slopes and ΔH_d.

Calculations for the Clausius-Clapeyron slope and ΔH_d for methane-propane/i-butane/n-butane gas mixtures were executed in increments of 0.1 mol% up to 1.0 mol% for propane and i-butane and 2.0 mol% for the less sensitive n-butane. Understandably, Figure 56 and Figure 57 exhibit very similar relationships with composition. Because the composition is increased in such small increments, the compressibility practically remains constant, meaning that Z has minimal effect on the increasing ΔH_d. The experimental values closest to the small range of compositions have also been included. As demonstrated by the previous illustrations, the experimental data points fit well with the theoretical values for the Clausius-Clapeyron slope and ΔH_d, providing validation of this unique method in estimating the structural transition point.

The transition composition for n-butane was somewhat observable from the larger ranged plots in Figure 53 and Figure 54, where a flat region constituting two data points existed for slope and ΔH_d. A transition between 0.5-0.75 mol% was visible in both cases. The additional points from PVTsim are confirmation of the existence of a flat region of 0 gradient where an increase in composition exhibits no stabilising or structural transitioning effect on the hydrate phase. All points in this region are relatively constant with only small deviations, however at 0.75 mol% n-butane, there is a small but characteristic positive deviation. The continued increase from 0.75-1.0 mol% justifies the previous increase, where further increases in concentration continue the trend. It can therefore be concluded that from 0.5-0.75 mol%, the n-butane concentration is significant enough to initiate increased stability on its behalf. At this point, the fugacities of methane and n-butane in the gas phase are sufficient to form sII hydrates.

In relation to propane, the vastly reduced composition range does not adequately describe the exact period where propane enters the hydrate phase (as inferred by the Clausius-Clapeyron equation) – certainly not as clearly as n-butane's curve. However, there is a minor improvement in resolution, where an increasing gradient followed by a decreasing gradient, i.e. an inflection point, is depicted as opposed to a straight line in Figure 53 and Figure 54. This observation implies there is a period

where a small enough quantity of propane will not result in favouritism of the sII hydrate, i.e. a region of very low gradient may exist. Observably, the cut-off for this period is clearly between 0.0-0.1 mol% propane. Propane can provide far greater stability to the sII large cage than methane which may also occupy said cage (Sloan & Koh, 2008), with a ratio of 0.957 to 0.664 for propane and methane respectively (Lederhos, et al., 1993). Also, NMR measurements on methane-propane hydrates indicate that the rate of propane filling the large cages is approximately twice that of methane filling the small cages at low pressures (Kini, et al., 2004). These reasons support the very low propane content in methane that apparently results in a more stable hydrate structure.

Table 22 – Structure (I to II) Transition Composition (Smith, et al., 2017)

Hydrate System	Composition, mol%
Methane-Propane	0.0 – 0.1
Methane-i-Butane	0.0 – (<0.1)
Methane-n-Butane	0.5 – 0.75

For methane-i-butane, a very similar slope and ΔH_d profile to methane-propane exists at very small compositions, although in i-butane's circumstance, the relationships are stronger and even more sensitive. Consequently, the composition range where i-butane exhibits no effect on the hydrate phase could be estimated. An inflection point manifests at very small concentrations, like the propane system, indirectly confirming a very narrow composition region (0.0-x mol%) exists where i-butane essentially has no synergistic impact with methane on hydrate stability and equilibrium promotion. Given the steeper initial gradient of the methane-i-butane system in both Clausius-Clapeyron and ΔH_d plots than methane-propane, the i-butane hydrate-inert composition range is smaller: 0.0-(<0.1) mol%. The i-butane molecule is only capable of filling the sII large cavity like propane (Sloan & Koh, 2008), although its greater molecule/cavity size ratio of approximately 0.99 (Lederhos, et al., 1993) implies a better fit. Therefore, a smaller composition resulting in a sI to sII transition is required. Wu, et al. (1976) experimentally studied the phase behaviour of methane-i-butane-water systems, and noted that the transition composition is "exceedingly small," as their hydrate equilibrium results for 0.23 mol% i-butane yielded a decrease in equilibrium pressure at a certain temperature relative to 100 mol% methane. This supports the extremely low calculated theoretical compositions required for a

transition in this study. Table 22 summarises the approximate concentration range where a structure change occurs.

6.4 Conclusion

This chapter has extended the findings in Chapter 5 by analysing the methane hydrates of the gas species that were deemed to be responsible for the highly stable natural gas hydrates as expressed by their hydrate equilibria. It was confirmed that these natural gas components significantly promote the hydrate equilibrium conditions with methane, more-so with increasing composition. This was especially true for propane and i-butane binary mixtures with methane, although n-butane was substantially less effective at shifting the equilibrium curve. The unfavourable >1.00 n-butane molecule/cavity ratio meant the sII large cavity had to be slightly distorted to accommodate the n-butane guest, and was the primary source of the relatively ineffective contribution of n-butane gas. Such unfavourable lattice interactions were far more prominent with pressure, resulting in an apparent transition where n-butane behaved as a hydrate non-former by intercepting with the methane curve. Depending on composition, this transition was observed from 80-120 bar and continued further to the left of methane's line which implicated an inhibiting effect. Increased deformation of the sII hydrate crystal structure with pressure was suspected to be the source of the transition and has also been noted in literature by Ng and Robinson (1976a) with similar reasoning. Comparatively, propane and i-butane both provided considerably more stability to the hydrate phase than n-butane. This was evident from all the presented and discussed parameters: hydrate equilibria, Clausius-Clapeyron slope, heat of dissociation and molecule/cavity size ratio. The magnitude and higher sensitivity of these parameters with composition in the methane-i-butane gas system confirmed that i-butane imposes the greatest amount of added hydrate stability when coupled with methane.

Perhaps of greatest significance is the determination of the approximate quantity of propane, i-butane or n-butane necessary to cause a change in hydrate crystal structure from sI to sII. Because the slope of the Clausius-Clapeyron equation and ΔH_d are indicative of structure type and stability, their determination at various compositions permitted the estimation of this quantity. It was proposed that a flat region with a gradient of 0 exists at the origin of the Clausius-Clapeyron slope and ΔH_d plots against composition which represents this phenomenon. However, without access to the necessary instrumentation and excessive uncertainty, the aid of theoretical vdWP equilibrium data generated in PVTsim was required to extrapolate.

Fortunately, Clausius-Clapeyron slopes and ΔH_d evaluated from experimental equilibria agreed with the trends associated with theoretical values and composition. A very clear transition region was observed for n-butane, where it was found that an n-butane composition of 0.5-0.75 mol% in methane results in a structural transition. Despite greater resolution and reduced propane and i-butane compositions, no composition range of inactivity was observed, although it was implied via an inflection point. The estimated concentrations for propane and i-butane were 0.0-1 mol% and 0.0-(<1) mol% respectively, with the methane-i-butane system being notably more sensitive to i-butane concentration.

Chapter 7

7. Hydrate Software Analysis

An integral part in analysing hydrate equilibria presented in this thesis was the utilisation of simulation software programs that have implemented hydrate prediction utilities. These utilities were consulted for the purpose of comparing experimental hydrate equilibrium measurements as a guide when considering the validity and reproducibility of the acquired results. Software computations were also used in the preparation stages of a hydrate equilibrium experiment, and were particularly useful in estimating the temperature range where the cooling/heating rate should be reduced or increased. Because more accurate equilibrium measurements correlate strongly with reduced heating rates during the dissociation period (Tohidi, et al., 2000), having an approximate value beforehand led to better reliability in the measurement and reduced the possibility of gross error. Hydrate simulation software also permitted speedier experimental procedures without the loss of confidence in the measurement because higher cooling and heating rates were possible outside the metastable region (between formation and dissociation/equilibrium conditions). Simulation software was involved with all studies, and generally provided equilibrium conditions that were consistent with experimental measurements.

The software programs available were Aspen HYSYS (v. 8.1) and Calsep PVTsim (v. 20), both of which were used comparatively with experimental results in addition to each other. HYSYS is a chemical process simulating program which includes several utilities and packages, one of those of course focusing on hydrate formation and equilibrium. PVTsim is a more specialised program which is predominantly used in analysing petroleum fluids. In addition to phase behaviour analysis of hydrate-forming systems, PVT operations such as flash operations and other flow assurance utilities are also available. Naturally, the hydrate utilities included in both programs are the centrepiece of this chapter. Differences between software equilibrium computations and experimental equilibria are comparatively quantified as a means of expressing the degree of consistency. Hydrate computations are executed using several settings, such as altering the EoS and water quantities with any significant differences investigated in the proceeding sections.

7.1 Software Computations

There are a variety of different settings available in HYSYS and PVTsim that enable comprehensive customisation of their hydrate computations. A common option

between both utilities is the choice of EoS, which in later sections is discovered to provide reasonably dissimilar equilibrium data. The Peng-Robinson (PR) and Soave-Redlich-Kwong (SRK) EoS were the most suitable because of their suitability and better applicability to hydrocarbon systems.

7.1.1 Equations of State

Although many EoS were available in HYSYS and PVTsim, the most suitable options were the Peng-Robinson (PR) and Soave-Redlich-Kwong (SRK) EoS. HYSYS even aids in the selection of an appropriate EoS model by prompting the user to specify the types of components (hydrocarbon, electrolyte, amines, sour water etc.) that constitute the chemical system and the type of process (chemical, hydrate, mineral, petrochemical, electrolyte etc.). The program offers recommendations that are best suited to the selected options. PVTsim does not offer such a service, presumably because it is specific to petroleum fluids and only a select-few EoS are reliably applicable. Consequently, the only options available in PVTsim are the PR and SRK EoS.

The SRK EoS is a modification of the Redlich-Kwong (RK) equation, which is of a comparatively simple form due to its empirical nature. It was introduced in 1949 and is similar to the van der Waals equation except with corrections made to the attractive pressure term of the equation (i.e. a), which was previously not assumed to be temperature dependent (Redlich & Kwong, 1949). Several modifications to RK EoS have been suggested, the Soave modification being one example. The acentric factor (ω), which considers the shape of a molecule, is introduced and enables better compatibility with non-polar substances (Soave, 1972). This is particularly valid in natural gas hydrate phase behaviour calculations.

The PR EoS is relatively similar to SRK, and is capable of slightly enhanced liquid phase density predictions (Peng & Robinson, 1976). Like the SRK EoS, it is also relatively simple and includes its own version of the empirically derived attractive pressure term. With these modifications, reasonably similar PVT predictions to those using SRK are generally predicted. The application of the PR and SRK EoS in HYSYS and PVTsim is of course important and understandably can influence predictions in phase behaviour analysis and consequently produce different hydrate equilibrium values despite using the same EoS. This was found to be true to some extent, but is sensitive to the thermodynamic conditions (Smith, et al., 2015). The breakdown of the EoS equations and parameters acquired from HYSYS and PVTsim are summarised in Table 23.

Table 23 – PVTsim and HYSYS EoS Parameters (Smith, et al., 2015)		
	Peng-Robinson	**Soave-Redlich-Kwong**
Critical Values	*The Properties of Gases and Liquids* (Reid et al. 1977)	
Equation of State	$P = \frac{RT}{V - b} - \frac{a(T)}{V(V + b) + b(V - b)}$ $Z^3 - (1 - B)Z^2 + (A - 2B - 3B^2)Z$ $- (AB - B^2 - B^3) = 0$	$P = \frac{RT}{V - b} - \frac{a(T)}{V(V + b)}$ $Z^3 - Z^2 + (A - B - B^2)Z - AB = 0$
A	$\frac{aP}{(RT)^2}$	$\frac{aP}{(RT)^2}$
B	$\frac{bP}{RT}$	$\frac{bP}{RT}$
a_i or a_j	$a_c\alpha$	$a_c\alpha$
a_c	$0.45724\frac{R^2T_c^2}{P_c}$	$0.42748\frac{R^2T_c^2}{P_c}$
α	$\left[1 + m\left(1 - \left(\frac{T}{T_c}\right)^{0.5}\right)\right]^2$	$\left[1 + m\left(1 - \left(\frac{T}{T_c}\right)^{0.5}\right)\right]^2$
a	$\sum_{i=1}^{n}\sum_{j=1}^{n} x_i x_j (a_i a_j)^{0.5}(1 - k_{ij})$	$\sum_{i=1}^{n}\sum_{j=1}^{n} x_i x_j (a_i a_j)^{0.5}(1 - k_{ij})$
m	$0.37464 + 1.54226\omega - 0.269922\omega^2$	$0.480 + 1.574\omega - 0.176\omega^2$
m (if ω ≤ 0.49)	$0.37464 + \omega(1.48503 - 0.164423\omega + 0.01666\omega^2)$	-
ω	$-\log_{10}P_r^{Sat}$ at $T_r = 0.7$	$-\log_{10}P_r^{Sat}$ at $T_r = 0.7$
b	$0.07780\frac{RT_c}{P_c}$	$0.08664\frac{RT_c}{P_c}$

The “a” term, which semi-empirically describes attractive pressure, turns out to be slightly different between the two because the different experimental measurements and fluid species used in their derivation that ultimately lead to different constants in the a_c equation. An α term is also included in both, and replaces the $1/\sqrt{T}$ in the van der Waals EoS, accounting for non-sphericity of the molecule with ω dependence. Moreover, the semi-empirical term describing molar volume, b, as a function of critical temperature (T_c) and pressure (P_c) also slightly differs for similar reasons to a. The use of reliable critical values for pure species is imperative in solving a cubic EoS or

any form of thermodynamic state equation for that matter. Consultation with each program's documentation revealed that the critical properties used in PVT calculations are acquired from the comprehensive study by Reid, et al. (1977); a large collection of experimental critical property measurements for many pure species was provided. To compare the outcomes of applying the SRK and PR equations, critical properties were computed for methane-nitrogen and methane-carbon dioxide mixtures by Smith, et al. (2015) by HYSYS and PVTsim with their predictions tabulated in Table 24 and Table 25.

Table 24 – PR Critical Property Calculations (Smith, et al., 2015)

Critical Property	0.95 CH_4 - 0.05 CO_2		0.9 CH_4 - 0.1 N_2	
	HSYS	PVTsim	HSYS	PVTsim
P_c, bar	49.87	48.93	48.69	48.23
T_c, °C	-76.47	-77.27	-87.52	-87.58
v_c, cm^3/mol	100.7	102.2	100.3	101.23
Z_c	0.3070	0.3071	0.3166	0.3164

Table 25 – SRK Critical Property Calculations (Smith, et al., 2015)

Critical Property	0.95 CH_4 - 0.05 CO_2		0.9 CH_4 - 0.1 N_2	
	HSYS	PVTsim	HSYS	PVTsim
P_c, bar	50.05	49.04	48.60	48.21
T_c, °C	-76.19	-77.10	-87.40	-87.45
v_c, cm^3/mol	109.2	110.9	109.2	110.5
Z_c	0.3336	0.3336	0.3435	0.3436

The generated critical PVT data for the specified gas mixtures reveals that between both EoS, there is very little discrepancy, most of which is speculated to be rounding embedded in the program's coding. However, there is what may be considered a non-negligible difference between the critical molar volumes, v_c, which differ by more than 10% in both HYSYS and PVTsim calculations. This is primarily attributed to the b term in each model, which is responsible for molar volume corrections (Soave, 1972) and

modified differently by Peng and Robinson (1976) and Soave (1972). However, it can be concluded that HYSYS and PVTsim property calculations with both EoS agree with one another.

7.1.2 Hydrate Equilibrium Computations

In addition to the selection of EoS, there are other manageable options pertaining to hydrate equilibrium computations in HYSYS and PVTsim. For HYSYS, in addition to selecting the EoS, many more options are available to tune and a custom property package associated with the selected EoS is supplied. Some of these options include the EoS solution method (analytical or numerical), density evaluation (EoS, Costald or Lee-Kesler), surface tension method (HYSYS or API 10A3.2) and whether to use the standard EoS or a HYSYS modified version. Many of these options were irrelevant when using the hydrate equilibrium utility and had no impact on the predicted equilibrium conditions. Additionally, extremely little difference between predicted values was noticed when experimenting with density evaluation methods and other solution methods that may influence the overall outcome. The only discernible factor seemingly capable of producing variation in predicted hydrate equilibria was the selected EoS and the calculation method. The default option is “Assume Free Water”, although another method developed, namely the CSM model by the Colorado School of Mines (CSM), is available. This method was developed by Sloan and co-workers and is packaged with Clathrates of Natural Gas (2008) as a DOS executable. The default option was selected in all hydrate predictions as CSM is more of an alternative thermodynamic model to HYSYS’s, rather than a calculation mode.

There are far less optional features associated with the hydrate formation utility in PVTsim, although thermal conductivity and viscosity evaluation methods are customisable. Changing these methods had no effect on hydrate calculation outcomes as they are not factors that constitute the PR or SRK EoS or the statistical thermodynamic vdWP model that is the foundation of the HYSYS and PVTsim hydrate equilibrium calculations. An option not offered by HYSYS is the relative quantity of water to gas. Different pressure conditions were of course necessary to develop a hydrate equilibrium curve for a particular gas-water system. The relative amount, or gas/water molar ratio therefore changed with pressure because of the constant 5.0 mL water used across all experimental procedures and the varied operating pressures. These relative quantities were calculated by the following simple procedure at the lowest and highest operating pressures in this study,

1. Calculate moles of water in 5.0 mL assuming a density of 1000 g/mL: 0.278 mol
2. Calculate moles of gas at 30 bar and 200 bar using $n = \frac{PV}{ZRT}$ where V is the cell volume (105.8 cm^3 including internal tubing) and temperature set to 15.0 °C: 0.143 and 1.121 mol respectively
3. This equates to a gas/water molar ratio ranging from approximately 0.5-4.0

Throughout the entirety of this project, PVTsim's hydrate equilibrium predictions usually did not differ at all between the above gas/water molar ratios, and only experienced extremely minute variations on some occasions (<0.03 °C difference) which were considered negligible. All predictions were therefore taken at the average gas/water ratio of about 2.3.

7.1.2.1 Methane-Nitrogen and Methane-Carbon Dioxide

All HYSYS and PVTsim hydrate equilibrium temperature computations for both PR and SRK EoS were compared to the experimental equilibrium measurements as shown in Table 26 and Table 27. Comparisons are made based on their average deviation from each set of experimental equilibrium pressure-temperature point in the form of the average % and temperature difference.

Table 26 – Experimental-Computation Difference: Methane-Nitrogen

	HYSYS (SRK/PR)		PVTsim (SRK/PR)	
Gas	%	°C	%	°C
Methane	3.5/3.0	0.44/0.19	3.0/3.5	0.33/0.42
1.0 mol%	5.5/6.4	0.73/0.94	6.7/5.7	0.61/0.50
3.0 mol%	15.1/10.7	1.65/1.13	3.6/3.5	0.39/0.38
25.0 mol%	9.3/5.3	1.11/0.61	4.4/3.9	0.38/0.39
Average	8.4/6.4	0.98/0.72	4.4/4.2	0.43/0.42

Table 27 – Experimental-Computation Difference: Methane-Carbon Dioxide

	HYSYS (SRK/PR)		PVTsim (SRK/PR)	
Gas	%	°C	%	°C
7.0 mol%	3.9/3.9	0.58/0.58	2.5/1.3	0.34/0.18
10.0 mol%	10.5/6.5	0.73/1.16	3.5/6.3	0.36/0.70
14.0 mol%	3.5/1.6	0.54/0.18	2.2/2.7	0.25/0.30
19.0 mol%	3.8/1.6	0.55/0.20	1.5/2.2	0.20/0.28
Average	5.4/3.4	0.60/0.53	2.4/3.1	0.29/0.37

In general, HYSYS and PVTsim equilibrium temperature predictions differed to moderate extents with the same EoS applied. However, in some isolated instances, there was considerable disagreement between computations, particularly with 3.0 mol% nitrogen. HYSYS predictions deviate quite significantly from the 3.0 mol% experimental measurements for both EoS models, whereas PVTsim exhibited very reasonable consistency. Similarly, another discrepancy is observed for 10 mol% carbon dioxide where there also some inconsistency between predictions. HYSYS predictions differed by an average of 10.5% for this gas mixture with the SRK EoS, whereas PVTsim deviated by only 3.5%. In many cases, both programs are relatively consistent with one another. However, the generated PVT data in Table 24 and Table 25 suggest that with the same EoS, hydrate equilibria predictions should be nearly identical. Another factor must therefore be the source of these observations and almost certainly resides in the specific vdWP thermodynamic model that HYSYS and PVTsim use in their hydrate calculations (Smith, et al., 2015); (Smith, et al., 2016).

There is an apparent favourability between experimental results and software computations using the PR EoS. In 3 out of 4 occurrences, the overall average experimental-computation deviation for PR is less than the corresponding SRK average. Both PR and SRK are based on the van der Waals EoS and include the same modifications to molar volume and attractive pressure, except the empirical nature of their associated terms differ because different fitting parameters. These fitting parameters were designed to be specifically compatible with natural gas

systems (Peng & Robinson, 1976), and are likely a key element in the slightly better hydrate predictions (relative to this study's experimental values).

7.1.2.2 Natural Gas

Overall, HYSYS and PVTsim are approximately on par with their predictions for natural gas hydrate equilibria relative to experimental values. The natural gas experimental-computation deviations were calculated identically to the methane-nitrogen/carbon dioxide hydrate results, and are certainly more consistent with each other overall. Equilibrium predictions for individual natural gases are occasionally not in good agreement, with one program being reasonably more favourable with experimental results than the other for one gas, yet the opposite may occur for another. This prominently manifests in M3 and M1 (Table 28), where HYSYS thoroughly outperforms PVTsim in M3 but PVTsim is the more accurate in M1. Like the methane-nitrogen/carbon dioxide computational predictions, this is likely sourced from each simulation software's unique modifications to the vdWP model.

Table 28 – Experimental-Computation Difference: Natural Gas

	HYSYS (SRK/PR)		PVTsim (SRK/PR)	
Gas	%	°C	%	°C
M0	5.0/3.5	1.00/0.68	3.5/3.8	0.68/0.74
M1	5.3/2.0	1.04/0.42	1.5/2.0	0.29/0.39
M2	3.2/3.0	0.53/0.50	4.6/4.5	0.76/0.74
M3	2.8/3.5	0.49/0.67	7.0/7.0	1.23/1.23
M4	6.2/4.0	1.22/0.79	4.5/4.6	0.89/0.91
Average	4.5/3.2	0.85/0.61	4.2/4.4	0.77/1.0

The reference M0 hydrate equilibrium curve from the natural gas studies in Chapter 5 are compared to the predictions made by PVTsim and HYSYS with the PR and SRK EoS (Figure 58). Computational predictions generally indicate a reasonable degree of agreement, particularly at higher pressures. The duplicate measurements at lower pressures had a higher standard deviation than measurements at greater pressures (indicated by error bars) as they were less precise. Lower measurement precision

and variability in software algorithms (discussed in Chapter 7.2) are explanations for this observation.

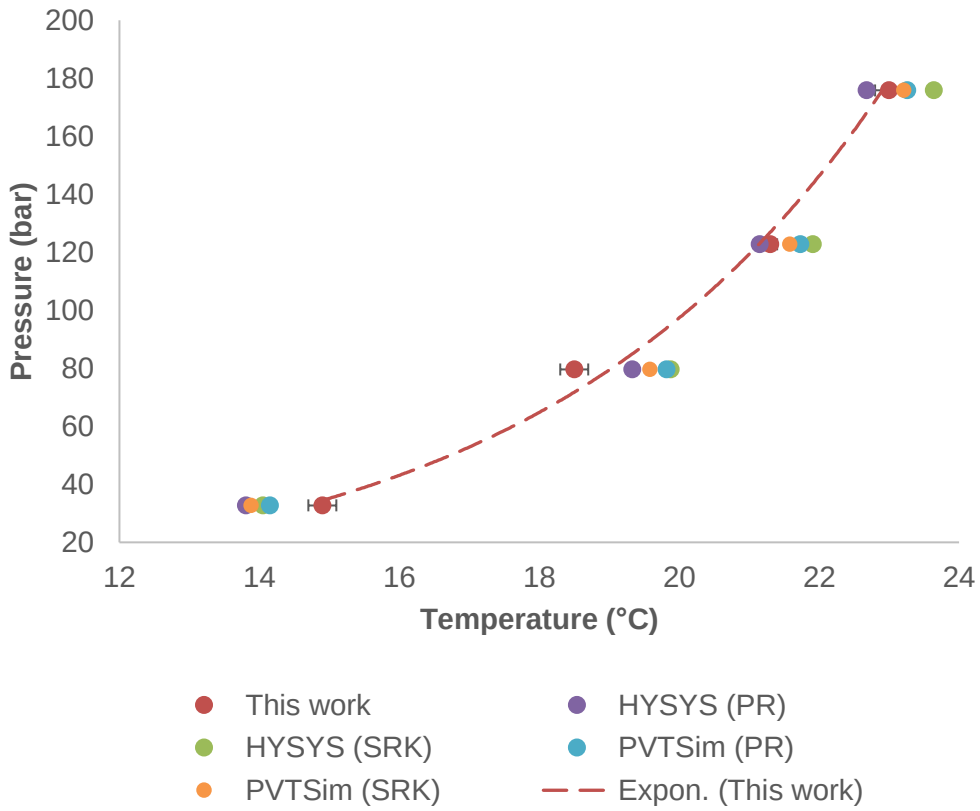

Figure 58 – M0 Hydrate Equilibria (Smith, et al., 2016)

PVTsim and HYSYS were also used to generate hydrate equilibrium points for natural gas mixtures (M0-M4 including methane). Each set of equilibrium points was individually analysed via linear regression with the Clausius-Clapeyron equation to provide values for their slopes. Data sets were generated with PR and SRK thermodynamic models, which displayed slightly different slopes (Figure 59). The slopes determined for the experimental work in Chapter 5 are compared against those based on software equilibrium computations. The illustration includes 95% confidence intervals for the experimental slopes and were consistently minor. This translates to relative uncertainties in the range of ±1.45 to ±3.17%.

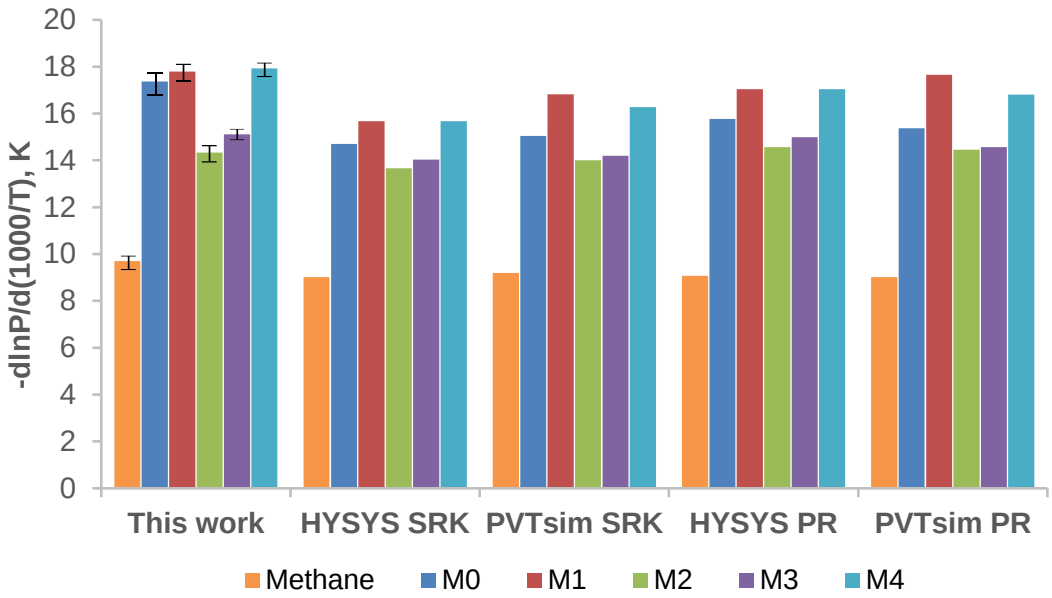

Figure 59 – Clausius-Clapeyron Equation Slopes (Smith, et al., 2016)

The clear majority of the tested natural gas samples were found to have very good agreement with HYSYS and PVTsim in terms of their Clausius-Clapeyron Slopes. In some cases, more specifically M4, the slope appears to be underestimated. However, the general trend/hierarchy of slopes agrees with results based on experimental data. This gives validity and confirmation of the experimental slopes and thus their dissociation enthalpies as well as HYSYS's and PVTsim's hydrate thermodynamic models.

7.1.2.3 Methane-Propane, Methane-n-Butane and Methane-i-Butane

Experimental-computational equilibrium deviations relating to the propane, i-butane and n-butane study were again similar between HYSYS and PVTsim for each type of gas (Table 29 – Table 31). Average deviation in the form of temperature difference is slightly higher than methane-nitrogen/carbon dioxide, and sometimes reaches 1 °C. Much like the natural gas experiments, far greater equilibrium temperatures are acquired, particularly with the propane and i-butane gases. Therefore, similar % differences will correspond to a greater absolute deviation, i.e. equilibrium temperature difference. Calculated temperature deviations for methane-n-butane mixtures averaged less than propane and i-butane, which corresponded to similar, perhaps slightly higher, % deviation. The considerably lower temperature range for methane-n-butane equilibria is responsible for this.

Table 29 – Experimental-Computation Difference: Methane-Propane

	HYSYS (SRK/PR)		PVTsim (SRK/PR)	
Gas	%	°C	%	°C
0.8 mol%	6.2/3.1	0.83/0.38	6.6/11.5	0.79/1.33
2.0 mol%	2.1/4.1	0.28/0.61	1.1/3.9	0.19/0.54
4.0 mol%	6.5/5.6	1.06/0.85	5.6/5.1	0.98/0.97
5.0 mol%[a]	3.2 /0.9	0.62/0.15	5.1/6.9	0.91/1.16
Average	4.5/3.4	0.70/0.50	4.6/6.9	0.72/1.00

Table 30 – Experimental-Computation Difference: Methane-n-Butane

	HYSYS (SRK/PR)		PVTsim (SRK/PR)	
Gas	%	°C	%	°C
2.2 mol%	6.3/6.2	0.61/0.46	6.0/5.0	0.48/0.42
5.5 mol%	3.8/2.5	0.48/0.25	2.6/3.1	0.30/0.39
4.4 mol%[a]	8.4/5.9	0.79/0.43	6.8/6.5	0.58/0.56
Average	6.2/4.9	0.63/0.38	5.1/4.9	0.45/0.46

Table 31 – Experimental-Computation Difference: Methane-i-Butane

	HYSYS (SRK/PR)		PVTsim (SRK/PR)	
Gas	%	°C	%	°C
0.6 mol%	3.5/3.3	0.54/0.42	7.0/2.1	0.91/0.26
4.0 mol%	6.1/2.9	1.20/0.58	2.4/5.4	0.47/1.04
6.8 mol%	3.8/1.0	0.80/0.19	0.5/3.5	0.10/0.69
4.6 mol%[a]	4.4 /1.7	0.79/0.28	1.4/4.4	0.23/0.75
Average	4.5/2.2	0.83/0.37	2.8/3.9	0.43/0.69

[a]With 16.0, 18.7 and 17.4 mol% nitrogen respectively

An unusual trend linked to hydrate simulations for methane-propane/i-butane/n-butane gases is that with the PR EoS selected in HYSYS, the predicted values are more agreeable with experimental data than SRK, whereas this is the exact opposite for PVTsim – more consistent values are produced with SRK. It is difficult to conclude exactly what is the source of this phenomenon, as it has been established that both EoS are very consistent between each simulation program and that the same critical properties are used. The bias therefore cannot be attributed to the selected PVT model, and must therefore be coincidental or related to the embedded thermodynamic hydrate model. If this observation is caused by different thermodynamic hydrate models, a similar effect should be identifiable in the previous natural gas and methane-nitrogen/carbon dioxide tables, which exhibit no such occurrences.

The PR and SRK EoS are best applied to systems containing non-polar species, such as hydrocarbons (Twu, et al., 1998). Of note is the fact that the methane-propane/i-butane/n-butane mixtures are the only gas mixtures composed entirely of hydrocarbons that were studied in this research. Natural gas mixtures contained carbon dioxide as well the gases tested in the nitrogen and carbon dioxide dilution study. The inclusion of non-hydrocarbon gas species possibly had some influence on the application of the EoS. The absence of this influence associated with hydrate equilibria computations for methane-propane/i-butane/n-butane systems likely contributed to the opposing biases between the applied EoS in HYSYS and PVTsim with the hydrate simulations.

7.2 Variation in Software Hydrate Models

From the experimental-software hydrate equilibrium deviations in the preceding tables, there is on some occasions a source of disagreement between the computed values which undoubtedly cannot be attributed to the EoS when the same model is in use. Different equilibrium values are sometimes delivered. As previously mentioned, both simulation programs apply modifications to the fundamental statistical thermodynamic model proposed by van der Waals and Platteeuw (1959). To understand the nature of these modifications applied by HYSYS and PVTsim, it is necessary to provide the foundation of the clathrate vdWP thermodynamic model.

7.2.1 Theoretical Hydrate Equilibrium

7.2.1.1 Fluid Phases

The fugacity is calculated as per the usual expression for a gas, f_i^g,

$$f_i^g = \varphi_i x_i P \qquad \text{Eq. 57}$$

The fugacity coefficient, φ_i, is evaluated using the applied EoS, and will differ depending on whether PR or SRK is selected. The fugacity of i is given upon the multiplication of its mole fraction, x_i, and the operating pressure, P, i.e. its partial pressure.

Similarly, the fugacity of i in a liquid phase, f_i^l, is evaluated by,

$$f_i^l = \gamma_i x_i \hat{f}_i^l \qquad \text{Eq. 58}$$

The activity coefficient, γ_i, represents the non-ideal nature of i in the liquid and $\hat{f}_i^l$ is the fugacity of i in an ideal liquid phase (superscript l). The ideal liquid phase fugacity is described by the well-established thermodynamic equation,

$$\hat{f}_i^l = F_i^{sat} P_i^{sat} \exp\left[v_i^l \left(P - P_i^{sat}\right)/RT\right] \qquad \text{Eq. 59}$$

The fugacity of i in the ideal liquid phase is expressed in terms of its fugacity when saturated, F_i^{sat}, its saturation pressure, P_i^{sat}, specific volume of i, v_i^l, overall system pressure, P, and temperature, T. Apart from F_i^{sat}, all other parameters can be easily acquired as they are simple fluid properties. Like ϕ_i, F_i^{sat} is evaluated using an EoS, thereby authorizing the finding of f_i^l.

7.2.1.2 Hydrate Phase

The review by van der Waals and Platteeuw on Clathrate statistical thermodynamics was not the first work to take such an approach toward hydrate equilibrium determination. A similar model was proposed by Barrer & Stuart (1957), but was improved by van der Waals and Platteeuw (1959) who are mostly credited for the model's conception. The model describes the formation of hydrates in terms of the chemical potential difference between the several phase transitions of the water phase. Given a liquid water phase is present, initially the water exists in its natural liquid state (α) and transforms to the hydrated state (H), provided thermodynamic conditions permit a phase change. This requires the assembly of water molecules in the form of a crystal lattice, in addition to the filling of the crystal lattice cavities by guest molecules. To account for the restructuring of water molecules required to achieve the crystal lattice, a hypothetical empty lattice state (β) is considered, which then progresses to H. The complete free energy change from α to H can therefore be expressed as the sum of these two transitions:

$$\mu^H - \mu^\alpha = (\mu^H - \mu^\beta) + (\mu^\beta - \mu^\alpha) \qquad \text{Eq. 60}$$

The chemical potential difference between the hydrate (μ^H) and normal water (μ^α) state is the sum of the difference between the hypothetical lattice (μ^β) and water (μ^α) state, and the difference between the hydrate (μ^H) and hypothetical lattice (μ^β) states. At the equilibrium point, the chemical potential of water in all states will be equal. Therefore,

$$0 = (\mu^H - \mu^\beta) + (\mu^\beta - \mu^\alpha) \qquad \text{Eq. 61}$$

$$(\mu^H - \mu^\beta) = (\mu^\beta - \mu^\alpha) \qquad \text{Eq. 62}$$

The $\mu^H - \mu^\beta$ term represents the stabilisation of the hypothetical empty lattice by the adsorption of guest molecules. Van der Waals and Platteeuw (1959) derived an expression that enables its resolution,

$$(\mu^H - \mu^\beta) = -RT\sum_j v_j \ln\left(1 - \sum_i \theta_{ij}\right) \qquad \text{Eq. 63}$$

The $\mu^H - \mu^\beta$ term is demonstrated to be a function of the combined occupancy, θ, for all cavity types (j) and their compatible guest species (i). The equation is formulated on a molar basis, and therefore the chemical potential difference will be proportional to the relative amount of water molecules per cavity. The v_j component is a constant and represents the number of type j cavities per mole of water. Values for v_j are

listed in Table 32 for sI, sII and sH hydrates, and can even be calculated from Table 3.

Table 32 – Cavities per Mole of Water (v_j) Values

Cavity, j	Structure I	Structure II	Structure H
5^{12}	1/23	2/17	3/34
$5^{12}6^2$	3/23	-	-
$5^{12}6^4$	-	2/17	-
$5^{12}6^8$	-	-	2/34
$4^3 5^6 6^3$	-	-	1/34

The occupancy of component i in cavity type j, θ_{ij}, as introduced in previous chapters, is one of the most valuable parameters in the vdWP theory because it provides information regarding hydrate composition and the hydration numbers of a hydrate. It is also known as the Langmuir isotherm because it uses the Langmuir adsorption model to describe the occupancy of adsorbing sites/cavities in the hydrate lattice at a specific temperature (isotherm) as a function of pressure/fugacity (or partial pressure of the guest in multi-component gases) (Langmuir, 1916). The Langmuir isotherm, i.e. fractional occupancy, is described again as,

$$\theta_{ij} = \frac{C_{ij} f_i}{1 + \sum_i C_{ij} f_i}$$

Applying the Langmuir isotherm affords the fraction of type j cavities that are filled by a specific component, i. For a non-ideal gas, the fugacity of component i, f_i, is substituted for its partial pressure.

The Langmuir adsorption constant is defined from rigorous statistical thermodynamics. It is a collective term that incorporates the absolute chemical activity of guest molecule i and the statistical partition function of molecule i in cavity j. The previous two equations are incredibly useful in hydrate equilibrium calculations because the specified pressure-temperature settings relate to the chemical potential of a guest molecule in different states (Sloan & Koh, 2008). C_{ij} is also a function of the guest-host molecule attractive energy which is described by the Lennard-Jones 6-12 pair potential, $\varphi(r)$. It is presented as a function of r, the distance between guest and host molecules,

$$\varphi(r) = 4\varepsilon\left[\left(\frac{\sigma}{r}\right)^{12} - \left(\frac{\sigma}{r}\right)^{6}\right] \quad \text{Eq. 64}$$

The Lennard-Jones potential approximates the interaction between molecules by assuming spherical molecules and cores and is described by the maximum potential, ε, and the distance where the guest-water molecule potential approaches zero, σ (Lennard-Jones, 1924). These constants are also known as Kihara parameters and are fitted to experimental data. Kihara parameters have been refined by several researchers since its implementation into the vdWP theory (Kihara, 1951); (Danon & Pitzer, 1962); (Mckoy & Sinanoglu, 1963). Parameters ε and σ (more than one ε/σ value possible) are also unique for each guest molecule, which is conceptually justified because each guest species is shaped differently and have different electromagnetic field strengths and polarity. With the correctly fitted parameters, the Lennard-Jones potential can be used to calculate the Langmuir constant for component i in cavity j:

$$C_{ij} = \frac{4\pi}{kT}\int_0^R \exp\left(-\frac{\varphi(r)}{kT}\right) r^2 dr \quad \text{Eq. 65}$$

The Langmuir constant is evaluated by summing over the entire radius (R) of the cavity. Values for R are listed in Table 3 for all hydrate cavity types. The equation shows that the Langmuir constant is dependent on temperature only. The fractional occupancy, θ_{ij}, and change in chemical potential for the hydrate state, $\mu^H - \mu^\beta$, can be resolved for a simple hydrate system.

Although the fundamental aspects of the vdWP model have been presented, hydrate equilibrium conditions cannot be determined solely on this information. Importantly, the fugacity of all species present in the hydrate state must be acquired. This is not as simple as fugacity computations for fluids because a hydrate is a crystallized solid phase. There are several approaches to perform this task, one of which is applying an expression derived by Michelsen (1991) for the guest and Ballard and Sloan (2002) for water,

$$f_i = \frac{N_i}{N_o C_{i,2}(1 + \alpha_i(1 - l))} \quad \text{Eq. 66}$$

$$f_w^H = f_w^o \exp\left(\frac{\mu^H - g^o}{RT}\right) \quad \text{Eq. 67}$$

The first equation (Eq. 66) is used for evaluating the fugacity of the guest species i in the hydrate phase. The stoichiometric ratio of guest i to water in the hydrate phase is

represented by N_i, N_o is the stoichiometric ratio of empty lattice cavities to water, l is the fraction of large empty (subscripted 2) lattice cavities, $C_{i,2}$ is the Langmuir constant for guest i in the large cavity and α_i is the ratio of the Langmuir constants for i in the small (subscripted 1) and large cavity, $C_{i,1}/C_{i,2.}$ For larger molecules, α_i is set to zero because they cannot enter the small cavity. The second equation determines the fugacity of water in its hydrate state. It uses the ideal fugacity of water at 1.0 bar, f_w^o, as a reference point. The deviation from this reference point to the fugacity of water in hydrate, f_w^H, is determined by the difference between the chemical potential of water in the hydrate state, μ^H, and the Gibbs free energy of water in the ideal reference state, g^o, at a specified T. The μ^H may be resolved using Eq. 67.

Initially, the fugacity values for all fluids are estimated by firstly assuming that the water and gas phases are ideal. Using the estimated values, a multi-phase pressure-temperature flash will provide the compositions of all each component in each phase as well as the overall phase fractions. With this information, their respective fugacities are re-calculated. This involves the application of a selected EoS, usually PR or SRK. An overall system fugacity for each component can then be determined by averaging the mole-weighted fugacity for each species in each phase (k),

$$f_i^T = \sum_i \frac{n_i^k f_i^k}{n_T^k} \qquad \text{Eq. 68}$$

The total (superscript and subscript T) averaged fugacity for component i, f_i^T, is calculated by taking the molar average fugacity over all present phases. The total moles in phase k is designated n_T^k, the moles of component i in phase k is n_i^k and its corresponding fugacity is f_i^k. The fugacity of a component constituting the hydrate phase, f_i^H, may be in terms of f_i^T,

$$\ln f_i^H = \ln f_i^T + \Theta \qquad \text{Eq. 69}$$

At equilibrium, the fugacity of each component in each phase is equal to its average fugacity across all phases, f_i^T, because the fugacity of this component won't be different between phases. Therefore, $\ln f_i^H$ should equal $\ln f_i^T$ at equilibrium, but this will not be the case based on the initial assumption of ideal fluids. This is corrected by Θ, and utilised with the equation detailed by Michelsen (1991),

$$(\ln f_w^T - \ln f_w^\beta) + \Theta = v_1 \ln\left[\frac{N_o(1 - l)}{v_1}\right] + v_1 \ln\left[\frac{N_o\, l}{v_2}\right] \qquad \text{Eq. 70}$$

Using the evaluated fugacity from Michelsen's equation, the occupancy of the hydrate lattice cavities can be resolved by determining the Langmuir constant with experimentally fitted Kihara parameters and substituting both into the Langmuir isotherm relationship. The composition in the hydrate phase may be deduced from the acquired θ_{ij} values.

With this information, a multi-phase equilibrium flash will provide the compositions in all phases and the phase fractions. These values will not be equal to the values produced from the previous flash as they were based on the assumed ideal fluids. The procedure is simply repeated until all parameters converge, resulting in the hydrate equilibrium conditions. It should be noted that there are many other calculation procedures available for hydrate equilibria, some of which vary in the method of flash equilibrium calculations. For example, PVTsim uses a multi-phase equilibrium flash algorithm developed by Michelsen (1989) for their hydrate flash calculations, which is reportedly quicker and more reliable.

7.2.2 Software Hydrate Model Differences

The reliance on the vdWP model for theoretical hydrate equilibrium calculations is common between the HYSYS and PVTsim programs as well as the development of modifications that enhance the accuracy of the model. In the versions of HYSYS and PVTsim used to fulfil the hydrate equilibrium approximations requirements necessary in this thesis, versions 8.1 and 20 respectively, there is sometimes a noticeable difference in their computations. As previously mentioned, it was discovered that the difference in computed values was largely attributed to the choice of modifications each program applied to the base vdWP model. The subsequent paragraphs summarise the procedures HYSYS and PVTsim adhere to in their hydrate calculations.

7.2.2.1 Aspen HYSYS

The method in HYSYS uses an improved version of the work of van der Waals and Platteeuw (1959) by incorporating modifications by Parrish & Prausnitz (1972). Parrish and Prausnitz provided modifications that better enabled the model to characterise the aqueous interactions in a potential hydrate-forming system. Experimental hydrate dissociation data from various literature sources were used to derive Kihara parameters that were better representative of the gas-water interactions (Parrish & Prausnitz, 1972). The observed differences between calculated and experimental chemical potentials of water enabled more reliable Kihara parameters

for several natural gas constituents including methane, ethane, propane, i-butane, nitrogen and carbon dioxide.

The determination of the Langmuir constant is based on the proposed method of Ballard & Sloan (2002). They explain that the interactions between the water and guest molecules is better represented by employing what they describe is a “multi-layered” approach (Ballard & Sloan, 2002). The cage size is therefore not considered constant with pressure and temperature and is subject to change with the number of water “shells”. Water molecule radii data was collected from Mak & McMullan (1965) and McMullen & Jeffrey (1965), who acquired crystal diffraction data for hydrated water molecules in sI and sII hydrates.

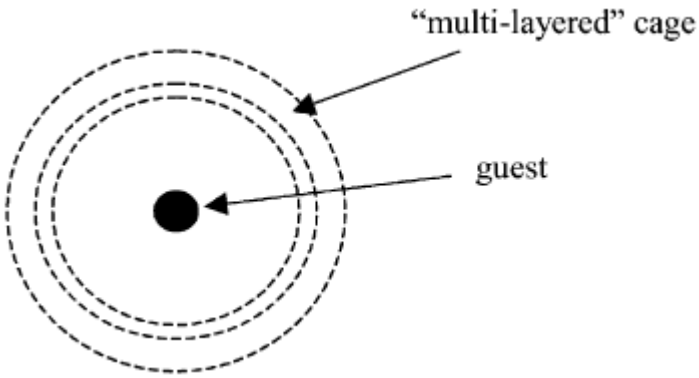

Figure 60 – Multi-layered Water Cage (Ballard & Sloan, 2002)

The radius for each shell was provided for all types of lattice cages in sI and sII hydrates as well as the number of water molecules in each shell. Data is based on sI ethylene oxide hydrate and sII tetrahydrofuran-hydrogen sulphide hydrate (Table 33).

Table 33 – Hydrate Structure I Shell Layer Radius (nm) (Ballard & Sloan, 2002)

	Structure I		Structure II	
Layer	($5^{12}6^2$)	($5^{12}6^2$)	($5^{12}6^2$)	($5^{12}6^4$)
a	-	-	0.375	-
e	-	-	-	0.473
c	-	0.425	-	-
e	-	-	0.385	-
g	-	-	0.396	0.472/0.464
i	0.383	0.447	-	-
j	-	-	-	-
k	0.396	0.406/0.465	-	-

Each type of water shell/layer type was assigned a certain number of water molecules. The sum of water molecules over all the shells for a specific cavity equates to the total quantity of water molecules that constitute that particular cavity; 20 for the small $5^{12}6^2$ cage for example. Based on this alternative and more in-depth approach to the relative positions of water molecules to the guest, Ballard and Sloan (2002) provided the following adjusted Langmuir constant equation:

$$C_{ij} = \frac{4\pi}{kT}\int_0^{R_1-a_i} \exp\left(-\frac{\omega_{i,n}(r)}{kT}\right) r^2 dr \qquad \text{Eq. 71}$$

Ballard and Sloan's Langmuir isotherm equation incorporates several alterations to the previously described equation. Instead of using the average radius of cavity, C_{ij} is evaluated up to R_1-a_i, where R_1 is the radius up to the smallest shell and a_i is the spherical core radius of guest i. The upper limit therefore, in Layman's terms, is the distance between the outer edge of the guest to the nearest water shell. The Lennard-Jones potential is also replaced with the Lennard-Jones-Devonshire equation which averages the cell potential between the guest and water molecules (Lennard-Jones & Devonshire, 1937). This potential is assigned ω(r), and is described by,

$$\omega(r) = 2z\varepsilon\left[\frac{\sigma^{12}}{R^{11}r}\left(\delta^{10} + \frac{a}{R}\delta^{11}\right) - \frac{\sigma^6}{R^5 r}\left(\delta^4 + \frac{a}{R}\delta^5\right)\right] \qquad \text{Eq. 72}$$

where,

$$\delta^N = \frac{1}{N}\left[\left(1 - \frac{r}{R} - \frac{a}{R}\right)^{-N} - \left(1 + \frac{r}{R} - \frac{a}{R}\right)^{-N}\right] \quad \text{Eq. 73}$$

This is a far more sophisticated model to the simple 12-6 Lennard-Jones model. As pointed out by Ballard and Sloan, the implementation of these adjustments to the Langmuir isotherm allow high levels of accuracy at lower pressures, but become less reliable at high pressure-temperature conditions for methane hydrates (Ballard & Sloan, 2002). This was a consequence of assigning temperature and pressure dependencies to the water shell radii, which ultimately contract at such extremities forcing the guest out of the cage. A large improvement over the current model at the time however was achieved.

In terms of the procedural algorithm that HYSYS follows in its hydrate equilibrium computations, the algorithm described by Parrish and Prausnitz (1972) is applied. The subsequent flow chart is reproduced from Parrish and Prausnitz (1972), illustrating the overall procedure for determining if hydrate formation is possible for a specified system.

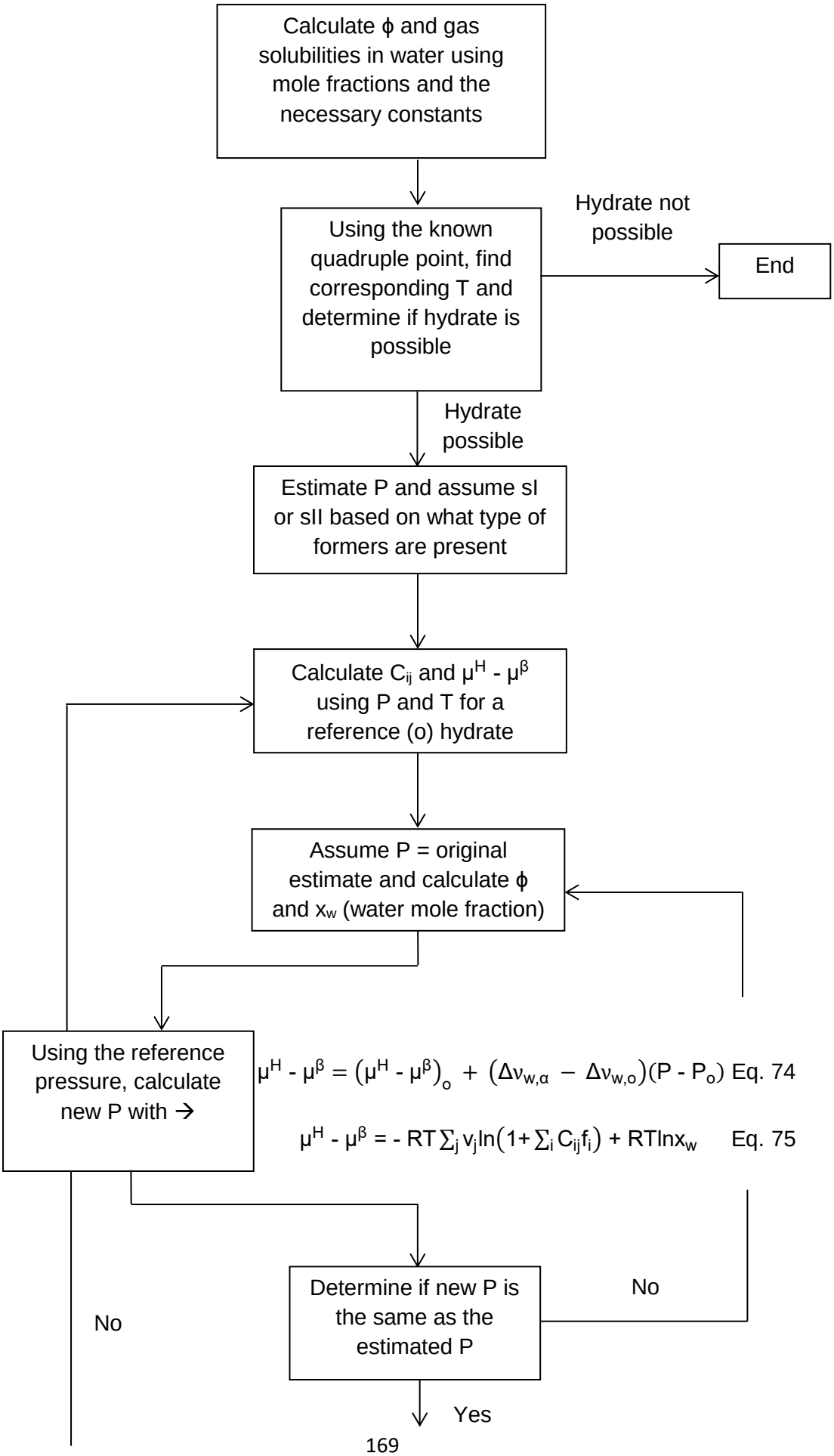
Calculate ϕ and gas solubilities in water using mole fractions and the necessary constants
Using the known quadruple point, find corresponding T and determine if hydrate is possible
Hydrate not possible
End
Hydrate possible
Estimate P and assume sI or sII based on what type of formers are present
Calculate C_{ij} and $\mu^H - \mu^\beta$ using P and T for a reference (o) hydrate
Assume P = original estimate and calculate ϕ and x_w (water mole fraction)
Using the reference pressure, calculate new P with →
$\mu^H - \mu^\beta = (\mu^H - \mu^\beta)_o + (\Delta v_{w,\alpha} - \Delta v_{w,o})(P - P_o)$ Eq. 74
$\mu^H - \mu^\beta = -RT\sum_j v_j \ln(1+\sum_i C_{ij} f_i) + RT\ln x_w$ Eq. 75
Determine if new P is the same as the estimated P
No
No
Yes

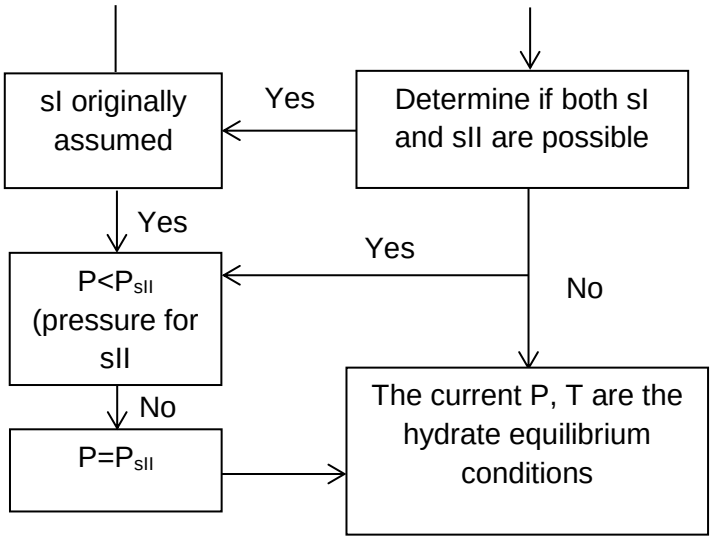

Figure 61 – HYSYS Hydrate Equilibrium Algorithm (Parrish & Prausnitz, 1972)

It is mentioned in Aspen HYSYS's documentation that the Parrish-Prausnitz algorithm is modified in such a way that allows for the prediction hydrates in aqueous systems, however, it is not specified what these modifications are. It is also mentioned that the contributions of Ng & Robinson (1976;1980) are implemented, particularly their work on the fugacity of components in the aqueous phase and Kihara potential parameters. Different modifications of the semi-empirical hydrate fugacity expressions derived by Ng and Robinson are used for two-phase (gas-hydrate) and three-phase (gas-hydrate-water) equilibrium. As Ng & Robinson founded their fugacity equations with the use of the PR EoS for the resolution of their fugacity coefficients, it would be expected that HYSYS's predictions compared with this study's experimental data would be more consistent with the PR equation selected. As mentioned in the preceding sections, this is indeed the case as evidenced from Table 26-Table 31. It should be therefore be noted that the overall HYSYS model depends on the applied EoS and the phases present in the specified process stream.

7.2.2.2 Calsep PVTsim

Similar to HYSYS, PVTsim builds upon the classic vdWP statistical thermodynamic model by incorporating modifications and changes proposed by various proven works in literature. An initial investigation into the methodology behind the hydrate utility in PVTsim established that the Langmuir constant was calculated via a different method (Smith, et al., 2015); (Smith, et al., 2016). The work of Munck, et al. (1988) delivered a far simpler and convenient temperature dependent expression for $C_{i,j}$ based on a

square-well cell potential (Parrish & Prausnitz, 1972). Munck's Langmuir expression is of the form,

$$C_{ij} = (A_{ij}/T)\exp(B_{ij}/T) \qquad \text{Eq. 76}$$

This simpler relationship depicts the Langmuir constant as only dependent on temperature. Such an expression clearly demonstrates that the parameters A_{ij} and B_{ij} are empirical constants which are formulated from databases of experimental hydrate equilibrium data that were acquired from many literature sources. Each constant is specific not only to guest i, but also the corresponding hydrate cage, j. Because there are many hydrate formers, several which have the capability of filling more than one cavity type (e.g. methane), numerous studies were required to account for the many combinations of i and j for A and B. Munck, et al. (1988) calculated A and B parameters for the primary natural gas constituents methane, ethane, propane, n-butane, i-butane, carbon dioxide, nitrogen and hydrogen sulphide. This was supported by the work of Rasmussen & Pedersen (2002) – they calculated additional A and B parameters for sI and sII formers. Several parameters for sH formers have also been documented. Some examples include i-pentane, n-hexane, methylcyclopentane, methylcyclohexane and cycloocatane (Madsen, et al., 2000).

The highly empirical nature of this method of Langmuir constant evaluation can be advantageous or disadvantageous, depending primarily on the gas species present and the hydrate structure type that ultimately forms with water. An advantage is that the model is founded on real experimental equilibrium measurements and may therefore be interpreted as realistic. The fact that many measurement points were often used/available in the numerical modeling adds to its statistical value by reducing random error. However, the disadvantage is that experimental data is not collected from a single source, but instead relies upon results from many literature studies which in turn use different equipment. The absence of quality assurance may indeed contribute heavily to inconsistencies with PVTsim's hydrate model. Moreover, the SRK was the choice of EoS for the calculation of fugacities and other properties during the derivation of A and B and should therefore be selected in PVTsim for reliable hydrate predictions. This is confirmed by this study's experimental equilibrium measurements, as there is in fact better overall consistency in most cases with PVTsim's predictions when the SRK equation applied.

Regarding the overall algorithm used in computing the hydrate equilibrium conditions, the general procedure is somewhat similar to HYSYS. PVTsim utilises the fugacity

equations offered by Michelsen (1991) in addition to his work on multi-phase equilibrium flash calculations. The algorithm is presented in pictorial form in Figure 62.

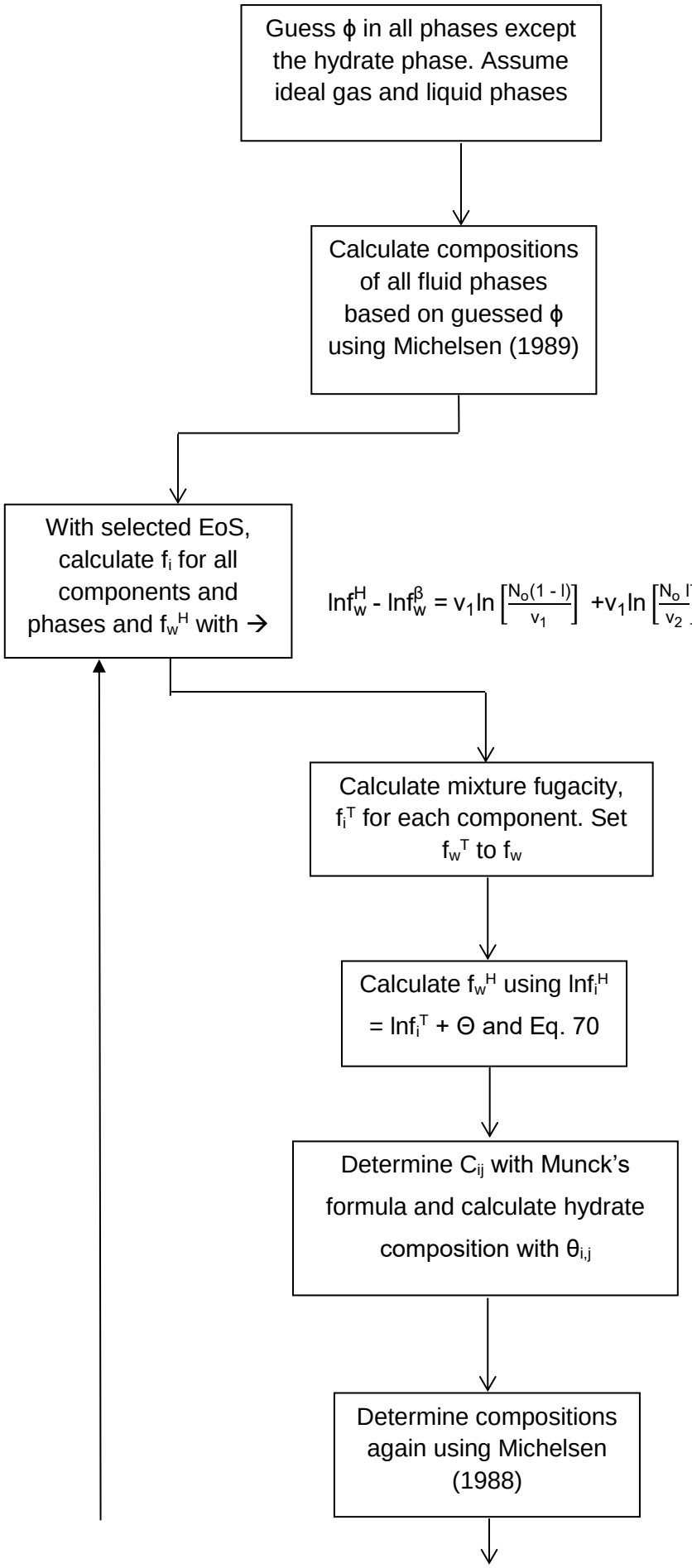
Guess ϕ in all phases except the hydrate phase. Assume ideal gas and liquid phases
Calculate compositions of all fluid phases based on guessed ϕ using Michelsen (1989)
With selected EoS, calculate f_i for all components and phases and f_w^H with →
$\ln f_w^H - \ln f_w^\beta = v_1 \ln\left[\frac{N_o(1-l)}{v_1}\right] + v_1 \ln\left[\frac{N_o\, l}{v_2}\right]$
Eq. 77
Calculate mixture fugacity, f_i^T for each component. Set f_w^T to f_w
Calculate f_w^H using $\ln f_i^H = \ln f_i^T + \Theta$ and Eq. 70
Determine C_{ij} with Munck's formula and calculate hydrate composition with $\theta_{i,j}$
Determine compositions again using Michelsen (1988)

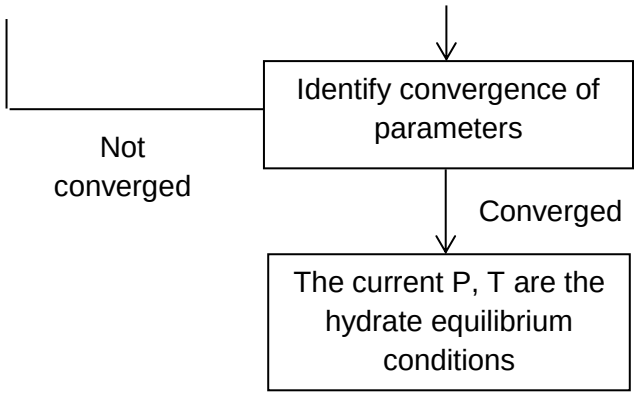

Figure 62 – PVTsim Hydrate Equilibrium Algorithm

Like the Parrish and Prausnitz algorithm in HYSYS, an iterative procedure is required. It ultimately converges to a set of constant parameters which reflect the equilibrium point. The listed equation in Figure 62 determines the fugacity of water in its hydrate state according to Michelsen (1991). It considers the small cages, as represented by the first term on the right side, and the added effect of the large cages in the second term, both as a function of their respective occupancies and v_i values. The fugacity of guest-occupied hydrated water, f_w^H, is resolved with respect to the hypothetical empty lattice, f_w^β.

From a general outlook, PVTsim determines the equilibrium conditions and phase compositions via a simpler procedure. The evaluation of the Langmuir isotherm is a far simpler process and only requires knowledge of the temperature. Calculation of cell potentials and Kihara parameters are not necessary, and are not even mentioned in PVTsim's documentation. However, their algorithm does not specify how the structure type of the hydrate is identified. In a separate document, it is mentioned that the type of hydrate PVTsim specifies is determined from which structure type has the lowest chemical potential in the presence of the gas components that may potentially contribute to the hydrate phase. PVTsim documents Eq. 63 for $\mu^H - \mu^\beta$ and the following equation for $\mu^\beta - \mu^\alpha$:

$$\frac{\mu^\beta - \mu^\alpha}{RT} = \frac{(\mu^\beta - \mu^\alpha)_o}{RT_o} - \int_{T_o}^{T} \frac{\Delta H}{RT^2} dT + \int_{P_o}^{P} \frac{\Delta v}{RT} dP \qquad \text{Eq. 78}$$

Although it is not directly mentioned at which step chemical potential changes are calculated, they are an important parameter in the flash calculation procedure for two flashes mentioned in Figure 62. The transition of water from α to β is represented as the deviation from a reference (subscript o) point. This point is described by the first

term on the right where changes in pressure and temperature from the reference point will influence $\mu^{\beta} - \mu^{\alpha}$. The change in enthalpy, ΔH, and molar volume, Δv, account for such changes, which themselves are also relative to a reference point. Reference points are simply constants and vary depending on the hydrate structure type and whether liquid water or ice is contained in the system. The values used in PVTsim are from Erickson (1983) for sI and sII, and Mehta & Sloan (1994) for sH.

7.3 Conclusion

This chapter discussed the level of agreement between the hydrate computations of process and PVT simulation software, HYSYS and PVTsim respectively and with all the experimental work presented in this thesis. The PR and SRK EoS were the two equations applied because of their applicability to non-polar hydrocarbon systems. Results showed that the predicted hydrate equilibrium temperature for one EoS was occasionally different to the other and this was partly due to the difference in the attractive term for each equation. The b term responsible for describing molar volume also differs by way of the empirical constant and the effects of this is apparent based on the presented sample of critical properties calculated by each program and EoS. Generally, HYSYS and PVTsim were consistent with the experimental work and performed roughly on par overall with a slight edge towards PVTsim. PVTsim provided slightly more consistent values with methane-nitrogen/carbon dioxide hydrate experimental measurements.

Despite the essentially identical physical property calculations between the two programs for a given EoS, their hydrate predictions sometimes did not agree when applying the same EoS. This chapter attributed these observations to the different modifications to the vdWP thermodynamic model HYSYS and PVTsim implement. The most significant difference relates to the evaluation of the Langmuir adsorption constant, where HYSYS uses the approach by Ballard and Sloan with their proposed multi-layered water shell model when determining the Kihara potential. Naturally, this still required the use of fitted Kihara parameters. In contrast, the much simpler and more empirically derived Langmuir expression by Munck is used in PVTsim and depends only on temperature. Its fitted empirical parameters are specific for each guest-cavity possibility and are founded from experimental data from various resources. The SRK EoS was applied for the determination of these parameters which explains the better agreement of this project's experimental equilibria with PVTsim's predictions with the SRK EoS selected. Likewise, for HYSYS, fugacity models by Ng and Robinson were founded from the PR EoS and explains HYSYS's

improved consistency with experimental results with the PR equation. It is therefore recommended that PR be the choice of EoS for HYSYS's hydrate utility, and the SRK EoS for PVTsim.

Chapter 8

8. Conclusions and Recommendations

Throughout this dissertation, there has been an extensive evaluation of how common natural gas components influence the equilibrium of the hydrate phase with water and the gas mixture itself. One of the primary objectives of this project was to investigate the possible inhibiting power of nitrogen gas on the formation and dissociation conditions of natural gas hydrates as well as other gases such as carbon dioxide. This led to the use of helium where it was validated that it could be used to experimentally investigate the dominant hydrate phase occupants and which constituents are promoting or stabilising the hydrate phase relative to a reference gas mixture. The helium substitution was followed up by a more extensive enquiry into the promoting effects of propane, i-butane and n-butane.

8.1 Hydrates of Nitrogen and Carbon Dioxide with Methane

Nitrogen gas was investigated on the basis that it can provide a hydrate inhibiting effect when added to natural gas via dilution of the hydrate-forming natural gas constituents. At small concentrations of nitrogen (<3.0 mol%), inhibition of hydrate formation could not be detected based on its water-gas-hydrate equilibria profiles, however, increasing its concentration to 25.0 mol% demonstrated respectable inhibition (via dilution) of hydrates and reduced hydrate temperatures by approximately 2-4 °C from a 40-80 bar pressure range. No change in the hydrate structure occurred due to nitrogen's neutrality in this pressure range. The slope of the Clausius-Clapeyron equation confirmed that the hydrate structure remained type I. The heat of dissociation evaluated using the slope did not have an obvious trend associated with nitrogen composition at lower concentrations (believed to be within experimental error like its hydrate equilibria). However, an increase in ΔH_d for 25.0 mol% nitrogen hydrates relative to methane implied they were more stable. This was attributed to the higher pressure at which it was evaluated, causing greater occupancy of hydrate cavities despite methane's lower concentration.

Methane gas was used as a representative of natural gas due to most natural gases being dominated by the methane content. It was later determined that pure methane gas was not such a good option because of the large differences in hydrate equilibrium conditions and structure type of most natural gases. Methane exists as a sI hydrate with water whereas most natural gases are sII. From a review of earlier literature studies and the results presented in Chapter 5, natural gas hydrates tend to

form more easily than simple methane hydrates. In fact, the clear majority of natural gas components promote natural gas hydrate phase equilibria in the presence of methane, so a good assumption is that essentially all natural gases have dissociation temperatures greater than methane hydrates, as shown in the various hydrate equilibria presented. However, nitrogen dilution of natural gas is still expected to have similar effects to those observed in Chapter 4, since it is the reduction in partial pressure of hydrate-forming constituents that inhibits hydrate formation. A future study could focus on using various natural gas compositions and adding specific quantities of nitrogen to observe reductions in hydrate equilibrium temperatures and relate these observations relative to nitrogen dilution of methane gas hydrates.

Like nitrogen, the dilution effects of carbon dioxide gas on methane hydrates was influential. This influence was consistent with literature and increased the hydrate equilibrium temperature (at a certain pressure) by stabilising the large sI cavity. The temperature increase, i.e. promotion of the equilibrium curve, became greater with higher proportions of carbon dioxide. At 19.0 mol%, the equilibrium temperature was elevated by 2 °C, enough to make a distinguishable difference and an influence on processing conditions. Like nitrogen dilution, an indication of sI hydrate formation was provided using the Clausius-Clapeyron equation, whose slope was characteristic of typical sI hydrates. A more consistent trend was notable, which slightly increased in magnitude with carbon dioxide concentration. Increasing slope and ΔH_d therefore indicated the increased stability of the hydrate phase with carbon dioxide concentration, although the increase was quite gradual. To the author's knowledge, most studies are inexact when heats of dissociation and their slopes are a topic of interest and do not attempt to establish a connection with gas composition, even though there are notions that these values may change, and only change depending on the hydrate structure type. A more detailed study involving these connections would be worth undertaking.

8.2 Helium Substitution of Hydrocarbons in Natural Gas

While methane is the most abundant component in natural gas, its phase behaviour in the presence of water and other hydrocarbons changes dramatically. This is not unknown, but it was necessary to establish this notion to pave the way for the substitution effect of helium. Their contrasting hydrate phase conditions are summarized in Figure 63.

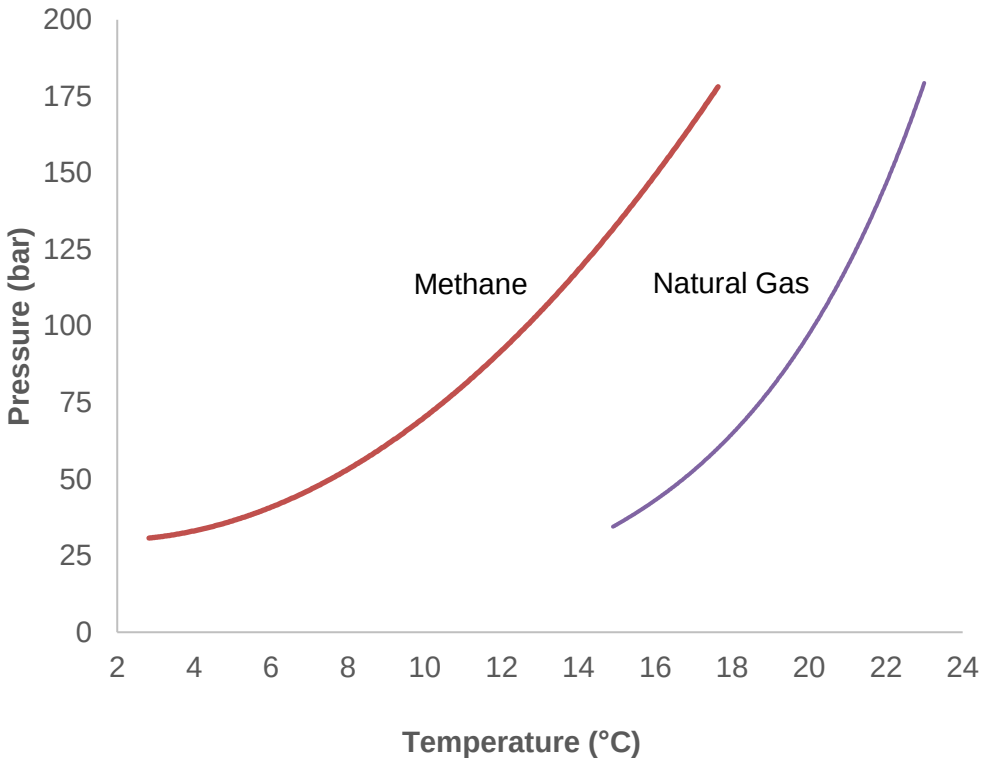

Figure 63 – Methane versus Natural Gas Hydrate Equilibrium

Substituting hydrocarbons in a natural gas mixture one-by-one with helium allowed the identification of the extent the substituted hydrocarbon was contributing to the stability of the hydrate phase. It was imperative that the substituting component (helium) not be hydrate-forming. In the chosen natural gas (M0), helium substitution found that propane and i-butane in combination with methane were stabilising the hydrate phase significantly, thus promoting the equilibrium conditions. This method of helium substitution also simulated the industrial processing consequences of a simple separation procedure (e.g. removal of propane) on the hydrate equilibrium conditions of the post-separated gas relative to the pre-separated gas. By removing selected hydrocarbons from natural gas, the equilibrium conditions shifted towards the methane curve, reducing the risk of hydrate formation.

The changes in stability of the hydrate phase after helium substitution were determined according to their relative dissociation enthalpies. The greatest reductions in ΔH_d were caused by the absence of propane and i-butane, similar to their respective hydrate equilibrium profiles. Furthermore, empirical quantification in the form of an empirical correlation captured these influences, making it possible to predict hydrate equilibrium conditions of natural gas. Using interpolation techniques, the correlation could reproduce equilibrium temperatures of literature gases (within its pressure and compositional range) reasonably well. It proved a useful alternative

to thermodynamic models, which have been shown to deliver contradictory results on occasion.

8.3 Hydrates of Propane, i-Butane and n-Butane

The conclusion of the study conducted in Chapter 5 prompted further investigation into the influences of propane and the butanes on natural gas hydrate stability. Because of the significant amount of stability offered by these hydrocarbons towards the hydrate phase with methane, each hydrocarbon was separately studied in various concentrations with methane as binary gas mixtures. Relatively small concentrations were used to pin-point when the transformation from sI to the more stable sII hydrate occurs and the corresponding minimum concentration required.

Although concentrations less than 1 mol% were tested, the transition composition could not be accurately quantified because the effect on the hydrate equilibria was still too significant. It was also too difficult to prepare gas mixtures with such small compositions without more delicate equipment. For aid, equilibria of <1 mol% mixtures were acquired from PVTsim to increase resolution and identify (or at least infer) the inert region from 0.0-x mol% and the structural transition composition. Methane-n-butane did not require any more resolving since 0.0-0.5 mol% and 0.5-0.75 mol% were already identified as the inert and structural transition composition ranges. Methane-propane and methane-i-butane profiles were still too sensitive, but their transition concentrations were approximated to be 0.0-0.1 and 0.0-(<0.1) mol% respectively based on inflection points of their Clausius-Clapeyron slope/ΔH_d versus mol% gradients within this range. The low concentrations of propane/i-butane that are suspected to result in a structural transition demonstrated the propensity of propane/i-butane to fill the sII cavities and cause a change in the crystal structure.

The sensitivity of the increase in hydrate stability with propane/i-butane addition to methane was evident from ΔH_d calculations. Enthalpies were shown to increase more rapidly at lower concentrations. The case with n-butane was different in that the highest point of sensitivity was from 0.5-0.75 mol% (transition range), since n-butane had begun hydrate cavity occupation within this much later range (compared to propane and i-butane). Profiles for propane and i-butane addition to methane were similar to one another. The experimental enthalpies followed the ΔH_d-mol% trends calculated using PVTsim and HYSYS equilibria and demonstrated a gradual decrease in sensitivity with a continued increase in concentration. Decreases in sensitivity were deemed a consequence of hydrate sII cavities becoming increasingly occupied. Further studies and research regarding the relationship between hydrate

structural transitions and concentration of the transition-inducing component is necessary to accurately determine the minimum required concentration.

References

Abay, H. & Svartaas, T., 2011. Multicomponent Gas Hydrate Nucleation: The Effect of the Cooling Rate and Composition. *Energy & Fuels,* pp. 42-51.

Adisasmito, S., Frank, R. & Sloan, E., 1991. Hydrates of Carbon Dioxide and Methane Mixtures. *Journal of Chemical Engineering Data,* pp. 68-71.

Adisasmito, S. & Sloan, E. D., 1992. Hydrates of Hydrocarbon Gases Containing Carbon Dioxide. *Journal of Chemical Engineering Data,* pp. 343-349.

Anderson, G., 2003. Enthalpy of Dissociation and Hydration Number of Carbon Dioxide Hydrate from the Clapeyron Equation. *The Journal of Chemical Thermodynamics,* pp. 1171-83.

Anklam, M. & Firoozabadi, A., 2004. Driving Force and Composition for Multicomponent Gas Hydrate Nucleation from Supersaturated Aqueous Solutions. *The Journal of Chemical Physics,* pp. 11867-75.

Archer, D., Buffett, B. & Brovkin, V., 2008. *Ocean Methane Hydrates as a Slow Tipping Point in the Global Carbon Cycle.* s.l., s.n., pp. 20596-20601.

Bagherzadeh, S., Alavi, S., Ripmeester, J. & Englezos, P., 2015. Formation of Methane Nano-bubbles during Hydrate Decomposition and their effect on Hydrate Growth. *Journal of Chemical Physics,* p. 214701.

Bai, Y. & Bai, Q., 2005. *Subsea Pipelines and Risers.* s.l.:Elsevier.

Ballard, A. L. & Sloan, E., 2002. The Next Generation of Hydrate Prediction: I. Hydrate Standard States and Incorporation of Spectroscopy. *Fluid Phase Equilibria 194-197,* pp. 371-383.

Barrer, R. & Stuart, W., 1957. *Non-Stoichiometric Clathrate Compounds of Water.* London, Proceedings of the Royal Society of London.

Battino, R., 1982. *IUPAC Solubility Data Series, Vol. 10.* Oxford: Pergamon Press.

Belosludov, R. et al., 2014. Stability and Composition of Helium Hydrates Based on Ices Ih and II at Low Temperatures. *The Journal of Physical Chemistry,* pp. 2587-93.

Belosludov, V. et al., 2011. *Prediction of Structure, Composition and Phase Behaviour of Helium Hydrates.* Edinburgh, Heriot Watt University.

Boswell, R. & Collett, S., 2011. Current Perspectives on Gas Hydrate Resources. *Energy and Environmental Science,* pp. 1206-15.

Buffet, B., 2000. Clathrate Hydrates. *Annual Review of Earth and Planetary Science, Volume 28,* pp. 477-509.

Buffett, B. & Zatsepina, O., 1999. Metastability of Gas Hydrate. *Geophysical Research Letters,* pp. 2981-84.

Byk, S. & Fomina, V., 1968. Gas Hydrates. *Russian Chemical Reviews,* pp. 469-91.

Cady, G., 1983. Composition of Gas Hydrates: New Answers to an Old Problem. *Journal of Chemical Education,* pp. 915-18.

Carrol, J., 2002. *Natural Gas Hydrates: A Guide for Engineers.* s.l.:Elsevier Science & Technology Books.

Chandra, V., 2006. *Fundamentals of Natural Gas: An International Perspective.* s.l.:PennWell Corporation.

ChemicaLogic, 1999. *Carbon Dioxide: Temperature - Pressure Diagram,* s.l.: CO2Tab V1.0.

Cheng, Y., 2015. Pipeline Corrosion. *Corrosion Engineering, Science and Technology,* pp. 161-62.

Christiansen, R. & Sloan, E., 1994. Mechanisms and Kinetics of Hydrate Formation. *Annals New York Academy of Sciences,* pp. 283-305.

Chuvilin, E., Yakushev, V. & Perlova, E., 1998. Gas and Possible Gas Hydrates in the Permafrost of Bovanenko Gas Field, Yamal Peninsula, West Siberia. *Polarforschung,* pp. 215-19.

CIA, 2013. *The World Factbook.* [Online]
Available at: https://www.cia.gov/library/publications/the-world-factbook/fields/2117.html
[Accessed 1 February 2016].

Claussen, W. & Frost, E., 1951. Suggested Structures of Water on Inert Gas Hydrates. *Journal of Chemical Physics,* pp. 259-60.

Claussen, W. & Polglase, M., 1952. Solubilities and Structures in Aqueous Aliphatic Hydrocarbon Solutions. *Hournal of the American Chemical Society,* pp. 4817-19.

Clever, H. & Young, C., 1987. *IUPAC Solubility Data Series, Vol. 27/28.* Oxford: Pergamon Press.

Clever, H. & Young, C., 1988. *IUPAC Solubility Data Series, Vol. 32.* Oxford: Pergamon Press.

Crovetto, R., 1991. Evaluation of Solubility Data for the System CO2 - H2O. *Journal of Physical and Chemical Reference Data,* p. 575.

Dahlberg, E. & Bruno, T., 1985. Analysis of Gas Pipeline Failure. *Journal of Metals,* pp. 71-2.

Danesh, A., 1998. *PVT and Phase Behaviour of Petroleum Reservoir Fluids.* s.l.:Elsevier.

Danon, F. & Pitzer, K., 1962. Volumetric and Thermodynamic Properties of Fluids. VI. Relationship of Molecular Properties to the Acentric Factor. *Journal of Chemical Physics,* pp. 425-30.

Davidson, D., 1983. *Natural Gas Hydrates: Properties, Occurrence and Recovery.* Boston: Butterworth.

Davidson, D. et al., 1986. Crystallographic Studies of Clathrate Hydrates. Part I. *Molecular Crystals and Liquid Crystals,* pp. 141-9.

Davies, S. et al., 2006. Hydrate Plug Dissociation. *AIChE Journal,* pp. 4016-27.

Davy, H., 1811. On a Combination of Oxymuriatic Gas and Oxygen Gas. *Philosophical Transactions of the Royal Society,* p. 155.

de Forcrand, R., 1902. *Compt. Rend.,* p. 959.

de Forcrand, R., 1923. *Compt. Rend.,* p. 355.

de Forcrand, R., 1925. *Compt. Rend.,* p. 15.

de Roo, J., Peters, C., Lichtenthaler, R. & Diepen, G., 1983. Occurrence of Methane Hydrate in Saturated and Unsaturated Solutions of Sodium Chloride and Water in Dependence of Temperature and Pressure. *AIChE Jounral,* Volume 29, pp. 651-57.

Deaton, W. & Frost, E., 1946. *Gas Hydrates and Their Relation to the Operation of Natural Gas Pipelines,* s.l.: U.S. Bureau of Mines.

Deaton, W. M. & Frost, E., 1946. *Gas hydrates and Their Relation to the Operation of Natural Gas Pipelines,* s.l.: U.S. Beureau of Mines Monograph 8.

deForcrand, R. & Thomas, S., 1897. *Compt. Rend.,* p. 109.

Dicharry, C. et al., 2013. Carbon Dioxide Gas Hydrate Crystallisation in Porous Silica Gel Particles Partially Saturated With a Surfactant Solution. *Chemical Engineering Science,* pp. 88-97.

Dickens, G., 2011. Down the Rabbit Hole: Toward Appropriate Discussion of Methane Release from Gas Hydrate Systems During the Paleocene-Eocene Thermal Maximum and Other Past Hyperthermal Events. *Climate of the Past,* pp. 831-46.

Dyadin, Y. & Aladko, E., 1996. *Proceedings of the Second International Conference on Natural Gas Hydrates.* Toulouse, Monfort, J.P..

Dyadin, Y., Aladko, E. & Larionov, E., 1997. Decomposition of Methane Hydrates up to 15 kbar. *Mendeleev Communications,* pp. 34-5.

Dyadin, Y., Larionov, E. & Manakov, A., 1999. Clathrate Hydrates of Hydrogen and Neon. *Medelev Communications,* pp. 209-10.

EGIG, 2011. *Gas Pipeline Incidents: 8th Report of the European Gas Pipeline Incident Data Group,* s.l.: European Gas Pipeline Incident Data Group.

EIA, U., 2008. *About U.S. Natural Gas Pipelines.* [Online]
Available at: https://www.eia.gov
[Accessed 29 January 2016].

EIA, U., 2015. *International Energy Statistics.* [Online]
Available at:
https://www.eia.gov/cfapps/ipdbproject/IEDIndex3.cfm?tid=3&pid=26&aid=24
[Accessed 29 Januay 2016].

Ellision, B. & Gallagher, C., 2001. *Baker Petrolite Flow Assurance Course.* Houston: s.n.

Engel, M. & Macko, S., 2013. *Organic Geochemistry: Principles and Applications.* s.l.:Springer Science & Business Media.

English, N. & Tse, J., 2010. Perspectives on Hydrate Thermal Conductivity. *Energies,* pp. 1934-42.

Erickson, D., 1983. *Development of a Natural Gas Hydrate Prediction Computer Program,* s.l.: Colorado School of Mines.

Falabella, B., 1975. *A Study of Natural Gas Hydrates,* University of Massachusetts: Ph.D Thesis.

Faraday, J., 1823. On Fluid Chlorine. *Philosophical Transactions of the Royal Society,* pp. 160-89.

Fateen, S.-E. K., Khalil, M. & Elnabawy, A., 2013. Semi-empirical Correlation for Binary Interaction Parameters of the Peng–Robinson Equation of State with the van der Waals Mixing Rules for the Prediction of High Pressure Vapor–liquid Equilibrium. *Journal of Advanced Research,* Volume 4, pp. 137-45.

Franks, F. & Reid, D., 1973. *In Water: A Comprehensive Treatise, Vol. 2.* New York: Platinum Press.

Freyss, H. et al., 1989. PVT Analysis for Oil Reservoirs. *Reservoir Engineering,* pp. 4-15.

Gabitto, J. & Tsouris, C., 2010. Physical Properties of Gas Hydrates: A Review. *Journal of Thermodynamics,* pp. 1-12.

Galloway, T., Ruzka, W., Chappelear, P. & Kobayashi, R., 1970. Experimental Measurement of Hydrate Numbers for Methane and Ethane and Comparison with Theoretical Values. *Industrial & Engineering Chemistry Fundamentals,* Volume 9, p. 237.

Garverick, L., 1994. *Corrosion in the Petrochemical Industry.* s.l.:ASM International.

Gayet, P. et al., 2005. Experimental Determination of Methane Hydrate Dissociation Curve up to 55 MPa by Using a Small Amount of Surfactant as Hydrate Promoter. *Chemical Engineering Science,* pp. 5751-58.

Giarvarini, C. & Hester, K., 2011. *Gas Hydrates: Immence Energy Potential and Environmental Challenges.* New York: Springer.

Giavarini, C., Maccioni, F., Politi, M. & Santarelli, M., 2007. CO2 Hydrate: Formation and Dissociation Compared to Methane Hydrate. *Energy & Fuels,* pp. 3284-91.

Gibbs, W., 1876. On the Equilibrium of Heterogeneous Substances. *Transactions of the Connecticut Academy of Arts and Sciences,* pp. 108-524.

Ginsburg, G., 1969. Hydrogeology of the North Yenisei Region. *Natural Gas Crystalline Hydrate Formation in the Interior of the Earth,* pp. 109-28.

Green, D. & Perry, R., 2008. *Perry's Chemical Engineers' Handbook.* s.l.:McGraw-Hill.

Gudmundsson, J., Anderson, V. & Levik, O., 1997. *Proceedings of the Offshore Mediterranean Conference.* Ravenna, s.n.

Gudmundsson, J. & Borrehaug, A., 1996. *Frozen Hydrate for Transport of Natural Gas.* Toulouse, Second International Conference on Natural Gas Hydrate.

Gupta, A., 2007. *Methane Hydrate Dissociation Measurements and Modeling: The Role of Heat Transfer and Reaction Kinetics,* Golden: Colarado School of Mines.

Gupta, A. et al., 2004. *Modeling Methane Hydrate Dissociation X-ray Computer Tomography Data Using a Heat Transfer Model.* Trondheim, s.n.

Hammerschmidt, E., 1934. Formation of Gas Hydrates in Natural Gas Transmission Lines. *Industrial and Engineering Chemistry,* pp. 851-855.

Handa, Y., 1986a. Compositions, Enthalpies of Dissociation and Heat Capacities in the Range 85 to 270 K for Clathrate Hydrates of Methane, Ethane and Propane and Enthalpy of Dissociation of Isobutane Hydrate, as determined by a Heat-flow Calorimeter. *Journal of Chemical Thermodynamics,* pp. 915-21.

Handa, Y., 1986b. Calorimetric Determinations of the Compositions, Enthalpies of Dissociation and Heat Capacities in the range 85 to 270 K for Clathrate Hydrates of Xenon and Krypton. *The Journal of Chemical Thermodynamics,* pp. 891-902.

Handa, Y., Hawkins, R. & Murray, J., 1984. Calibration and Testing of a Tian-Calvet Heat-flow Calorimeter: Enthalpies of Fusion and Heat Capicities for Ice and Tetrahydrofuran Hydrate in the Range of 85 to 270 K. *The Journal of Chemical Thermodynamics,* pp. 623-32.

Hatley, H., 1969. Pipeline Coatings and Corrosion Prevention. *Anti-Corrosion,* pp. 22-3.

Hayduk, E., 1982. *IUPAC Solubility Data Series, Vol. 9.* Oxford: Pergamon Press.

Hayduk, E., 1986. *IUPAC Solubility Data Series, Vol. 24.* Oxford: Pergamon Press.

Henry, W., 1803. Experiments on the Quantity of Gases Absorbed by Water, at Different Temperatures, and Under Different Pressures. *Philosophical Transactions of the Royal Society of London,* pp. 29-276.

Herri, J. et al., 2011. Gas Hydrate Equilibria for CO2-N2 and CO2-CH4 Gas Mixtures - Experimental Studies and Thermodynamic Modelling. *Fluid Phase Equilibria,* pp. 171-90.

Hester, K. et al., 2007. Direct Measurement of Multi-component Hydrates on the Seafloor: Pathways to Growth. *Fluid Phase Equilibria,* pp. 396-406.

IEA, 2015. *Key World Energy Statistics 2015.* [Online]
Available at:
https://www.iea.org/publications/freepublications/publication/KeyWorld_Statistics_2015.pdf
[Accessed 28 January 2016].

IPCC, 2001. *Climate Change 2001: The Scientific Basis,* New York: Cambridge University Press.

IPCC, 2007. *Climate Change 2007: The Physical Basis,* New York: Cambridge University Press.

ISO, 2008. *Evaluation of Measurement Data — Guide to the Expression of Uncertainty in Measurement.* s.l.:JCGM.

Jensen, L., 2010. Experimental Investigation and Molecular Simulation of Gas Hydrates. *DTU.*

Jhaveri, J. & Robinson, D., 1965. Hydrates in the Methane-Nitrogen System. *The Canadian Journal of Chemical Engineering,* pp. 75-8.

John, V. & Holder, G., 1985. Langmuir Constants for Spherical and Linear Molecules in Clathrate Hydrates. Validity of the Cell Theory. *The Journal of Physical Chemistry,* pp. 3279-85.

Juan, Y. et al., 2015. Measurements for the Equilibrium Conditions of Methane Hydrate in the Presence of Cyclopentanone or 4-Hydroxy-4-methyl-2-pentanone Additives. *Fluid Phase Equilibria, Vol 386,* pp. 162-167.

Kalikmanov, V., 2013. *Nucleation Theory.* s.l.:Springer.

Kang, S., Lee, H. & Ryu, B., 2000. Enthalpies of Dissociation of Clathrate Hydrates of Carbon Dioxide, Nitrogen, (Carbon Dioxide + Nitrogen), and (Carbon Dioxide + Nitrogen + Tetrahydrofuran). *Journal of Chemical Thermodynamics,* pp. 513-21.

Kaschiev, D. & Firoozabadi, A., 2002b. Driving Force for Crystallization of Gas Hydrates. *Journal of Crystal Growth,* pp. 220-230.

Kashchiev, D. & Firoozabadi, A., 2002a. Nucleation of Natural Gas Hydrates. *Journal of Crystal Growth,* pp. 476-89.

Keshavarz, L., Javanmardi, J., Eslamimanesh, A. & Mohammadi, A., 2013. Experimental Measurement and Thermodynamic Modeling of Hydrate Dissociation Conditions in the Presence of Aqueous Solution of Ionic Liquid. *Fluid Phase Equilibria,* pp. 312-18.

Kihara, T., 1951. Determination of Intermolecular Forces from the Equation of State of Gases. II.. *Journal of the Physical Society of Japan,* pp. 184-88.

Kini, R., Dec, S. & Sloan, E., 2004. Methane + Propane Structure II Hydrate Formation Kinetics. *Journal of Physical Chemistry,* pp. 9550-56.

Kobayashi, R. & Katz, D., 1949. Methane Hydrate at High Pressure. *Journal of Petroleum Technology,* Volume 1, pp. 66-7.

Kobayashi, R. & Katz, D., 1953. Vapour-Liquid Equilibria for Binary Hydrocarbon-Water Systems Correlation of Data. *Industrial Engineering Chemistry,* pp. 446-51.

Kuhs, W., Chazallon, B., Radaelli, P. & Pauer, F., 1997. Cage Occupancy and Compressibility of Deuterated Nitrogen-Clatherate Hydrate by Neutron Diffraction. *Journal of Inclusion Phenomena and Molecular Recognition in Chemistry,* pp. 65-77.

Kvamme, B., 1996. *Proceedings of the Second International Conference on Natural Gas Hydrates.* Toulese, s.n., p. 139.

Kvenvolden, K. & McMenamin, M., 1980. *Hydrates of Natural Gas: A Review of Their Geologic Occurrence,* s.l.: U.S. Geolical Survey.

Landolt, D., 2007. *Corrosion and Surface Chemistry of Metals.* Lausanne: EPFL Press.

Langmuir, I., 1916. The Constitution and Fundamental Properties of Solids and Liquids. Part I. Solids. *Journal of the American Chemical Society,* pp. 2221-95.

Larson, S., 1955. *Phase Studies of the Two-Component Carbon Dioxide-Waterr System Involving the Carbon Dioxide Hydrate,* University of Illinois: Ph.D Thesis.

Lederhos, J. P., Christiansen, L. & Sloan, E. D., 1993. A First Order Method of Hydrate Equilibrium Estimation and its Use With New Structures. *Fluid Phase Equilibria,* pp. 83-445.

Lennard-Jones, J., 1924. *On the Determination of Molecular Fields.* London, Proceedings of the Royal Society of London A.

Lennard-Jones, J. & Devonshire, A., 1937. *Critical Phenomena in Gases-I.* s.l., Proceedings of the Royal Scoiety London A.

Løken, K., Li, X. & Austvik, T., 1999. *The Hydrate Control Strategy for the Asgard Field and Hydrate Plug Melting using the Bundle Heating Method.* Cannes, s.n.

Long, J., 1994. *Gas Hydrate Formation Mechanism and Its Kinetic Inhibition,* Golden: Colarado School of Mines.

Löwig, C., 1828. Über einige Bromverbindungen und über Bromdarstellung. *Magazine für Pharmacie,* pp. 31-6.

MacDonald, I. et al., 2005. Thermal and Visual Time-series at a Seafloor Gas Hydrate Deposit on the Gulf of Mexico Slope. *Earth and Planetary Science Letters,* pp. 45-59.

Madsen, J., Pdersen, K. & Michelsen, M., 2000. Modeling of Structure H Hydrates Using a Langmuir Adsorption Model. *Industrial & Engineering Chemistry Research,* pp. 1111-14.

Makogon, Y., 1965. A Gas Hydrate Formation in the Gas Saturated Layers Under Low Temperature. *Gas Industry,* pp. 14-15.

Makogon, Y., 1988. *Natural Gas Hydrates: The State of Study in the USSR and Perspectives for its Use,* Toronto: Third Chemical Congress of North America.

Makogon, Y., 1997. *Hydrates of Hydrocarbons.* s.l.:PennWell Books.

Makogon, Y. & Holditch, S., 1998. *Measurement of Gas Solubility in Water Under High Pressure and Low Temperature,* Texas: A&M University.

Makogon, Y., Holditch, S. & Lee, S., 2000. *Solubility of Natural Gas in Water and its Role in the Formation of Gas Hydrates,* s.l.: The Korea Gas Union.

Makogon, Y., Holditch, S., Perry, K. & Holste, J., 2004. *Gas Hydrate Deposits: Formation and Development.* Houston, s.n.

Makogon, Y., Kobolova, I. & Chalikov, G., 1971. Solubility of Gases in Water at Phase Transition Conditions. *Mining Business.*

Makogon, Y., Makogon, T. & Holditch, S., 2000. Kinetics and Mechanisms of Gas Hydrate Formation and Dissociation with Inhibitors. *Annals of the New York Academy of Sciences,* pp. 777-796.

Mak, T. & McMullan, R., 1965. Polyhedral Clathrate Hydrates. X. Structure of the Double Hydrate of Tetrahydrofuran and Hydrogen Sulfide. *Journal of Chemical Physics,* pp. 2732-37.

Marshal, D., Saito, S. & Kobayashi, R., 1964. Hydrates at High Pressures. Methane-Water and Argon-Water Systems. *AIChE Journal,* Volume 10, pp. 202-05.

Marshall, D., Saito, S. & Kobayashi, R., 1964. Hydrates at High Pressures: Part 1. Methane-Water, Argon-Water and Nitrogen-Water Systems. *AIChE Journal,* Volume 10, pp. 202-05.

Max, M., Johnson, A. & Dillon, W., 2006. *Economic Geology of Natural Gas Hydrates.* s.l.:Springer.

McGinnis, D. G. J., Artemov, Y., Beaubien, S. & Wuest, A., 2006. Fate of rising methane bubbles in stratified waters: How much methane reaches the atmosphere?. *Journal of Geophysical Research.*

Mckoy, V. & Sinanoglu, O., 1963. Theory of Dissociation of Some Gas Hydrates. *The Journal of Chemical Physics,* pp. 2946-56.

Mcleod, H. & Campbell, J., 1961. Natural Gas Hydrates at Pressures to 10,000 psia. *Journal of Petroleum Technology,* pp. 590-94.

McMullen, R. & Jeffrey, G., 1965. Polyhedral Clathrate Hydrates. IX. Structure of Ethylene Oxide Hydrate. *Journal of Chemical Physics,* pp. 2725-32.

Mehta, A. & Sloan, E., 1994. A Thermodynamic Model for Structure-H Hydrates. *AIChE Journal,* pp. 312-320.

Mehta, A. & Sloan, E., 1996. Improved Thermodynamic Parameters for Prediction of Structure H Hydrate Equilibria. *AIChE Journal,* pp. 2036-2046.

Mei, D.-H., Liao, J., Yang, J.-T. & Guo, T.-M., 1996. Experimental and Modeling Studies on the Hydrate Formation of a Methane + Nitrogen Gas Mixture in the Presence of Aqueous Electrolyte Solutions. *Industrial and Engineering Chemistry Research,* pp. 4342-47.

MHAC, 2002. *Report for the Methane Hydrate Advisory Committee on Methane Hydrate Issues and Opportunities Including Assessment of Uncertainty of the Impact of Methane Hydrate on Climate Change,* s.l.: U.S. Department of Energy.

Michelsen, M., 1989. Calculation of Multiphase Ideal Solution Chemical Equilibrium. *Fluid Phase Equilibria,* pp. 73-80.

Michelsen, M., 1991. Calculation of Hydrate Fugacities. *Chemical Engineering Science,* pp. 1192-93.

Miller, S. & Smythe, W., 1970. Carbon Dioxide Clathrate in the Martian Ice Cap. *Science 170,* pp. 531-33.

Mohammadi, A., Tohidi, B. & Burgass, R., 2003. Equilibrium Data and Thermodynamic Modeling of Nitrogen, Oxygen and Air Clathrate Hydrates. *Journal of Chemical Engineering Data,* pp. 612-16.

Mori, Y., 1998. Clathrate Hydrate Formation at the Interface Bewtween Liquid CO2 and Water Phases - A Review of Rival Models Characterizing "Hydrate Films". *Energy Conservation and Management,* pp. 1537-1557.

Mork, M., 2002. *Formation Rate of Natural Gas Hydrate,* s.l.: s.n.

Mraw, S., Hwang, S.-C. & Kobayashi, R., 1978. Vapor-Liquid Equilibrium of the CH4-C02 System at Low Temperatures. *Journal of Chemical Engineering Data,* Volume 23, pp. 135-39.

Mullin, J., 2001. *Crystallization, 4th Edition.* s.l.:Butterworth Heinemann.

Mullin, J. & Jancic, S., 1979. Interpretation of Metastable Zone Widths. *Trans I Chem Eng,* pp. 188-93.

Munck, J., Skjold-Jorgensen, S. & Rasmussen, P., 1988. Computations of the Formation of Gas Hydrates. *Chemical Engineering Science Vol. 43,* pp. 2661-2672.

Musaev, R., 1966. *Candidate's Thesis,* Moscow: All-Union Scientific Research Institute for Gas.

Namiot, A., 1991. *Solubility of Gas in Water.* Moscow: NEDRA.

Ng, H.-J. & Robinson, D., 1976a. The Role of n-Butane in Hydrate Formation. *AIChE Journal,* pp. 656-61.

Ng, H.-J. & Robinson, D., 1976b. The Measurement and Prediction of Hydrate Formation in Liquid Hydrocarbon-Water Systems. *Industrial and Engineering Chemistry Fundamentals,* pp. 293-298.

Ng, H.-J. & Robinson, D., 1980. A Method for Predicting the Equilibrium Gas Phase Water Content in Gas-Hydrate Equilibrium. *Industrial Engineering Fundamentals,* pp. 33-36.

Ng, H.-J. & Robinson, D., 1983. *Equilibrium Phase Compositions and Hydrating Conditions in Systems Containing Methanol, Light Hydrocarbons, Carbon Dioxide and Hydrogen Sulfide: Research Report,* Tulsa, OK: Gas Processors Association.

Nixdorf, J. & Oellrich, L., 1997. Experimental Determination of Hydrate Equilibrium Conditions for Pure Gases, Binary and Ternary Mixtures and Natural Gases. *Fluid Phase Equilibria,* pp. 325-333.

NOAA, 2015. *Monthly Mean Methane Concentrations for Cape Grim, Australia.* [Online]
Available at:
ftp://ftp.cmdl.noaa.gov/data/trace_gases/ch4/flask/surface/ch4_cgo_surface-flask_1_ccgg_month.txt
[Accessed 27 January 2016].

Obanijesu, E., 2012. *Corrosion and Hydrate Formation in Natural Gas Pipelines,* Perth: Curtin University.

Obanijesu, E., Akindeju, M., Pareek, V. & Tade, M., 2011. *Modeling the Natural Gas Pipeline Internal Corrosion Rate as a Result of Hydrate Formation.* Neos Marmaras, s.n.

Obanijesu, E. et al., 2014. The Influence of Corrosion Inhibitors on Hydrate Formation Temperature along the Subsea Natural Gas Pipelines. *Journal of Petroleum Science and Engineering,* pp. 239-52.

Obanijesu, E., Pareek, V., Gubner, R. & Tade, M., 2011. Hydrate Formation and its Influence on Natural Gas Pipeline Corrosion Rate. *NAFTA Journal,* pp. 164-73.

Østergaard, K. et al., 2001. Hydrate Equilibrium Data of Multicomponent Systems in the Presence of Structure-II and Structure-H Heavy Hydrate Formers. *Journal of Chemical Engineering Data,* pp. 703-708.

Pahlavanzadeh, H., Kamran-Pirzaman, A. & Mohammadi, A., 2012. Thermodynamic Modeling of Pressure-Temperature Phase Diagrams of Binary Clathrate Hydrates of Methane, Carbon Dioxide or Nitrogen + Tetrahydrofuran, 1,4-Dioxane or Acetone. *Fluid Phase Equilibria,* pp. 32-7.

Parrish, W. & Prausnitz, J., 1972. Dissociation Pressures of Gas Hydrates Formed by Gas Mixtures. *Ind. Eng. Chem. Process Des. Delep.,* pp. 26-34.

Pederson, K., Christensen, P. & Shaikh, J., 2015. *Phase Behaviour of Petroleum Reservoir Fluids.* Boca Raton: CRC Press.

Peekma, R., 2013. Causes of Natural Gas Pipeline Explosive Ruptures. *Journal of Pipeline Systems Engineering and Practice,* pp. 74-80.

Peng, D.-Y. & Robinson, D., 1976. A New Two-Constant Equation of State. *Industrial and Engineering Chemistry: Fundamentals,* pp. 59-64.

Rachold, V., Bolshiyanov, D. & Grigoriev, M., 2007. Nearshore Arctic Subsea Permafrost in Transition. *EOS, Transactions of the American Geophysical Union,* pp. 149-56.

Rasmussen, C. & Pedersen, K., 2002. *Challenges in Modeling of Gas Hydrate Phase Equilibria.* Yokohoma, Proceedings of the 4th International Conference on Gas Hydrates.

Ravipati, S. & Punnathanam, N., 2013. Calculation of Chemical Potentials and Occupancies in Clathrate Hydrates through Monte Carlo Molecular Simulations. *The Journal of Physical Chemistry.*

Redlich, O. & Kwong, J., 1949. On the Theromodynamics of Solutions. V. And Equation of State. Fugacities of Gaseous Solutions. *Chemical Reviews,* pp. 233-44.

Reid, R., Prausnitz, J. & Sherwood, T., 1977. *The Properties of Gases and Liquids.* s.l.:Mcgraw-Hill.

Ripmeester, J. A., Tse, J. S., Ratcliffe, C. I. & Powell, B. M., 1987. A New Clathrate Hydrate Structure. *Nature,* pp. 325, 135.

Ripmeester, J. & Davidson, D., 1980. *Bulletin of Magnetic Resonance,* p. 139.

Ripmeester, J., Ratcliffe, C., Klug, D. & Tse, J., 1994. Molecular Perspectives on Structure and Dynamics in Clathrate Hydrates. *Annals New York Academy of Sciences,* pp. 161-76.

Roberts, O., Brownscombe, E. & Howe, L., 1940. Constitution Diagrams and Composition of Methane and Ethane Hydrates. *Oil and Gas Journal,* Volume 39, pp. 37-43.

Robinson, D. & Mehta, B., 1971. Hydrates in the Propane - Carbon Dioxide - Water System. *Technology,* pp. 33-5.

Ross, R., Andersson, P. & Backstrom, G., 1981. Unusual PT Dependence of Thermal Conductivity for a Clathrate Hydrate. *Nature,* pp. 322-23.

Rowley, J., 1994. *Statistical Mechanics for Thermophysical Property Calculations.* s.l.:Prentice Hall.

Ruppel, C., 2011. Methane Hydrates and Contemporary Climate Change. *Nature Education Knowledge,* p. (10):29.

Ruppel, C. & Noserale, D., 2012. *Gas Hydrates and Climate Warming—Why a Methane Catastrophe Is Unlikely.* [Online]
Available at: http://soundwaves.usgs.gov/2012/06/
[Accessed 28 January 2016].

Sabil, K., Witkamp, G. & Peters, C., 2010. Estimations of Enthalpies of Dissociation of Simple and Mixed Carbon Dioxide Hydrates from Phase Equilibrium Data. *Fluid Phase Equilibria,* pp. 109-14.

Schicks, J. M., 2010. Natural Gas Hydrates. *Handbook of Hydrocarbon and Lipid Microbiology,* pp. 67-77.

Shin, H. et al., 2009. Thermodynamic Stability, Spectroscopic Identifaction and Cage Ocupation of Binary CO2 Clathrate Hydrates. *Chemical Engineering Science,* pp. 5125-30.

Sloan, E., 1998. Gas Hydrates: Review of Physical/Chemical Properties. *Energy & Fuels,* pp. 191-196.

Sloan, E. & Fleyfel, F., 1991. A Molecular Mechanism for Gas Hydrate Nucleation from Ice. *AIChE Journal,* pp. 1281-92.

Sloan, E. & Fleyfel, F., 1992. Hydrate Dissociation Enthalpy and Guest Size. *Fluid Phase Equilibria,* pp. 123-140.

Sloan, E. & Fleyfel, F., 1994. Reply to "comments on: hydrate dissociation enthalpy and guest size". *Fluid Phase Equilibria,* pp. 233-235.

Sloan, E. & Koh, C., 2008. *Clathrate of Natural Gas Hydrates, Third Edition.* s.l.:Taylor & Francis Group.

Smith, C., Barifcani, A. & Pack, D., 2015. Gas Hydrate Formation And Dissociation Numerical Modelling with Nitrogen and Carbon Dioxide. *Journal of Natural Gas Science and Engineering,* pp. 1118-28.

Smith, C., Barifcani, A. & Pack, D., 2016. Helium substitution of natural gas hydrocarbons in the analysis of their hydrate. *Journal of Natural Gas Science and Engineering,* pp. 1293-1300.

Smith, C., Pack, D. & Barifcani, A., 2017. Propane, n-Butane and i-Butane Stabilization Effects on Methane Gas Hydrates. *The Journal of Chemical Thermodynamics,* pp. 293-301.

Soave, G., 1972. Equilibrium Constants from a Modified Redlich-Kwong Equation of State. *Chemical Engineering Science,* pp. 1197-1203.

Song, K. & Kobayashi, R., 1982. Measurement and Interpretation of the Water Content of a Methane-Propane Mixture in the Gaseous State in Equilibrium with Hydrate. *Industrial & Engineering Chemistry Fundamentals,* pp. 391-95.

Stackelber, M. & Muller, H., 1951. On the Structure of Gas Hydrates. *Journal of Chemical Physics,* pp. 1319-20.

Subramanian, S., Kini, R., Dec, S. & Sloan, E., 2000. Structural Transition Studies in Methane + Ethane Hydrates Using Raman and NMR. *Annals of the New York Academy of Sciences,* pp. 873-86.

Sun, Z. et al., 2004. Investigation on Gas Storage in Methane Hydrate. *Journal of Natural Gas Chemistry,* pp. 107-12.

Tohidi, B. et al., 2000. Improving the Accuracy of Gas Hydrate Dissociation Point Measurements. *Annals New York Academy of Sciences,* pp. 924-931.

TRB, T. R. B., 2004. *Transmissionn Pipelines and Land Use: A Risk-Informed Approach,* Washington: Transportation Research Board.

Twu, C., Coon, J. & Bluck, D., 1998. Comparison of the Peng-Robinson and Soave-Redlich-KwongEquations of State Using a New Zero-Pressure-Based Mixing Rule for the Prediction of High-Pressure and High-Temperature Phase Equilibria. *Industrial Engineering Chemistry Research,* pp. 1580-85.

Unruh, C. & Katz, D., 1949. Gas Hydrates of Carbon Dioxide - Methane Mixtures. *Pet. Trans. AIME,* pp. 83-6.

USGS, 2014. *U.S. Geological Survey Gas Hydrates Project.* [Online] Available at: http://woodshole.er.usgs.gov/project-pages/hydrates/primer.html [Accessed 15 December 2015].

van Cleef, A. & Diepen, G., 1960. Gas Hydrates of Nitrogen and Oxygen. *Recueil des Travaux Chimiques des Pays-Bas,* pp. 582-86.

van der Waals, J. & Platteeuw, J., 1959. Clathrate Solutions. *Advances in Chemical Physics,* pp. 1-59.

Verma, V., 1974. *Gas Hydrates from Liquid Hydrocarbon-Water Systems,* University of Michigan: Ph.D Thesis.

Villard, P., 1888. *Compt. Rend.,* p. 1602.

Villard, P., 1890. *Compt. Rend.,* p. 302.

Villard, P., 1896. *Compt. Rend.,* p. 337.

Volmer, M. & Weber, A., 1926. Keimbildung in übersättigten Gebilden (Nucleation of Supersaturated Structures). *Physik. Chem.,* pp. 277-301.

von Stackelberg, M. & Müller, H., 1951. On the Structure of Gas Hydrates. *Journal of Chemical Physics,* p. 1319.

Wang, X. & Economides, M., 2009. *Advanced Natural Gas Engineering.* Houston: Gulf Publishing.

Wilcox, W., Carson, D. & Katz, D., 1941. Natural Gas Hydrates. *Industrial & Engineering Chemistry,* pp. 662-65.

Wittenstein, J. & Wolfson, L., 2010. *Gas Explosion Engulfs Homes in San Francisco Suburb.* [Online]
Available at: http://www.bloomberg.com/news/articles/2010-09-10/san-francisco-neighborhood-engulfed-by-fire-after-gas-pipeline-explosion
[Accessed 1 February 2016].

Wu, B., Robinson, D. & Ng, H., 1976. Three- and Four-Phase Hydrate Forming Conditions in Methane + Isobutane + Water. *The Journal of Chemical Thermodynamics,* pp. 461-69.

Wu, Q. & Zhang, B., 2010. Memory Effect on the Pressure-Temperature Condition and Induction Time of Gas Hydrate Nucleation. *Journal of Natural Gas Chemistry,* pp. 446-51.

Wu, R. et al., 2013. Methane-Propane Mixed Gas Hydrate Film Growth on the Surface of Water and Luvicap EG Solutions. *Energy & Fuels,* pp. 2548-54.

Zare, M., Hagtalab, A., Ahmadi, A. & Nazari, K., 2013. Experiment and Thermodynamic Modeling of Methane Hydrate Equilibria in the Presence of Aqueous Imidazolium-based Ionic Liquid Solutions Using Electrolyte Cubic Square well Equation of State. *Fluid Phase Equilibria,* pp. 61-9.

Zarenezhad, B., Mottahedin, M. & Varaminian, F., 2015. A New Approach for Determination of Single Gas Hydrate Formation Kinetics in the Absence or Presence of Kinetic Promoters. *Chemical Engineering Science,* pp. 447-457.

Every reasonable effort has been made to acknowledge the owners of copyright material. I would be pleased to hear from any copyright owner who has been omitted or incorrectly acknowledged.

Appendix A: Uncertainty Calculations

To determine the combined uncertainty and expanded as contributed by instrumental and consumable uncertainty, the ISO Guide to the Expression of Uncertainty in Measurement (GUM) was consulted (ISO, 2008). The procedure for finding the uncertainty for individual sources (e.g. pressure, temperature) and propagating them was followed in accordance with their standard uncertainty calculation methods. Each step is listed in the proceeding paragraphs.

Pressure Reading

Sources (i) to be accounted for:

- Transmitter uncertainty (± 0.5%)
- Stability (± 0.1%)
- Temperature effect (± 1%)
- Calibration uncertainty (± 0.5%)

Other sources such as current leakage can be considered, but such minor factors are often insignificant and are sometimes not provided in instrumental data sheets as in this case.

At the 95% confidence level, the divisor (k_i) is 2 and the degrees of freedom (v_i) is $20^2/2 = 200$, as there is a 1/20 chance that the chosen uncertainty range is an underestimate.

The procedure for evaluating the uncertainty associated with the pressure reading is as follows:

- Calculate standard uncertainty (u_i) from the uncertainty interval (a_i) and k_i: $u_i = a_i/k_i$
- Calculate sensitivity (c_i) weighted standard uncertainty, u_ic_i
- Calculate $(u_i \times c_i)^2$
- Calculate $(u_i \times c_i)^4/v_i$
- Uncertainty (u_c) is calculated: $u_c = \text{sqrt} \sum_i(u_ic_i)^2$
- The effective degrees of freedom (v_{eff}) is calculated: $\sum_i(u_ic_i)^2/\sum_i(u_ic_i)^4/v_i$
- From the t-distribution, the coverage factor (k) is given by corresponding v_{eff} for the 95% confidence level
- Calculate expanded uncertainty at the 95% confidence limit (U_{95}): $U_{95} = u_ck$

The proceeding table summarises these steps numerically for the pressure reading uncertainty.

Source	Value, %	k_i	v_i	u_i	c_i	$u_i c_i$	$(u_i c_i)^2$	$(u_i c_i)^4/v_i$
Transmitter	± 0.5	2	200	0.25	1	0.25	0.0625	1.95E-05
Stability	± 0.1	2	200	0.05	1	0.05	0.0025	3.13E-08
Temperature effect	± 1.0	2	200	0.50	1	0.50	0.2500	3.136E-04
Calibration	± 0.5	2	200	0.25	1	0.25	0.0625	1.95E-05
						Sum	0.3775	3.52E-04
						u_c, %	0.6144	
						v_{eff}	405.32	
						k	1.9658	
						U_{95},%	1.2078	
						Total uncertainty = 1.21 %		

Temperature Reading

Sources (i) to be accounted for:

- Transmitter uncertainty (±0.5%)
- Calibration uncertainty (±0.4%)
- Stability (±0.1%)

An identical procedure is applied to the temperature reading with the selected sources of uncertainty. As with the pressure reading, possible sources of error such as the effect of ambient temperature and current leakage have been neglected. These sources are very likely to be insignificant compared to the uncertainty pertaining to stability and the calibration.

Source	Value, %	k_i	v_i	u_i	c_i	u_ic_i	$(u_ic_i)^2$	$(u_ic_i)^4/v_i$
Transmitter	± 0.5	2	200	0.25	1	0.25	0.0625	1.95E-05
Stability	± 0.1	2	200	0.05	1	0.05	0.0025	3.13E-08
Calibration	± 0.4	2	200	0.20	1	0.20	0.0400	8.00E-06
						Sum	0.1050	2.76E-05
						u_c, %	0.3240	
						v_{eff}	400.00	
						k	1.9659	
						U_{95}, %	0.6370	
						Total uncertainty = 0.64 %		

Propagated Uncertainty

The propagated uncertainty consisting of both pressure and temperature is calculated by considering their sources of uncertainty and totalled. With reference to ISO's GUM, the procedure is as follows:

- Sum all individual $(u_ic_i)^2$, combining the sources for pressure and temperature, i.e. $\sum_i(u_ic_i)^2$
- Combined uncertainty (u_c) is calculated: $u_c = \text{sqrt } \sum_i(u_ic_i)^2$
- The quantity, $\sum_i(u_ic_i)^4/v_i$, is calculated across all sources (pressure and temperature)
- v_{eff} is calculated: $\sum_i(u_ic_i)^2/\sum_i(u_ic_i)^4/v_i$
- From the t-distribution, k is given by the calculated v_{eff} for the 95% confidence level
- Total U_{95} encompassing all pressure and temperature sources is calculated: u_ck

These steps provide the following table of results.

Source	Value, %	k_i	v_i	u_i	c_i	$u_i c_i$	$(u_i c_i)^2$	$(u_i c_i)^4/v_i$
Pressure								
Transmitter	± 0.5	2	200	0.25	1	0.25	0.0625	1.95E-05
Stability	± 0.1	2	200	0.05	1	0.05	0.0025	3.13E-08
Temperature effect	± 1.0	2	200	0.50	1	0.50	0.2500	3.136E-04
Calibration	± 0.5	2	200	0.25	1	0.25	0.0625	1.95E-05
Temperature								
Transmitter	± 0.5	2	200	0.25	1	0.25	0.0625	1.95E-05
Stability	± 0.1	2	200	0.05	1	0.05	0.0025	3.13E-08
Calibration	± 0.4	2	200	0.20	1	0.20	0.0400	8.00E-06
						Sum	0.4825	3.79E-04
						u_c, %	0.6946	
						v_{eff}	614.01	
						k	1.9638	
						U_{95}, %	1.3641	
						Total uncertainty = 1.36 %		

Upon consideration of the major sources of uncertainty with pressure and temperature, a propagated uncertainty at the 95% level of confidence yields a relative error of ±1.36%.

Appendix B: PR EoS Application

For a methane-nitrogen binary mixture, critical and other thermodynamic parameters are provided by Perry's Chemical Engineers' Handbook (2008), (Fateen, et al., 2013) and (Mraw, et al., 1978):

- Methane T_c = 190.60 K; Nitrogen T_c = 126.20 K
- Methane P_c = 45.99 bar; Nitrogen P_c = 34.00 bar
- Methane ω = 0.0115; Nitrogen ω = 0.0390
- x_{C1} = 0.50; x_{N2} = 0.50
- P = 100 bar, T = 150 K
- Binary coefficient for methane-nitrogen: k ≈ 0

The PR EoS is expressed with P as the subject,

$$P = \frac{RT}{V - b} - \frac{a(T)}{V(V + b) + b(V - b)}$$

Or in its cubic form,

$$Z^3 - (1 - B)Z^2 + (A - 2B - 3B^2)Z - (AB - B^2 - B^3) = 0$$

Firstly, the mixing parameters are evaluated:

$m_i = 0.37464 + 1.54226\omega - 0.269922\omega^2$

$m_{C1} = 0.3923$

$m_{N2} = 0.4344$

$$a_{ci} = 0.45724 \frac{R^2 T_{ci}^2}{P_{ci}}$$

$a_{cC1} = 2495779\ cm^6.bar/mol^2$

$a_{cN2} = 1480628\ cm^6.bar/mol^2$

$$\alpha_i = \left[1 + m\left(1 - \left(\frac{T}{T_{ci}}\right)^{0.5}\right)\right]^2$$

$\alpha_{C1} = 1.0905$

$\alpha_{N2} = 0.9232$

$a_i = \alpha_i a_{ci}$

$a_{C1} = 2722872\ cm^6.bar/mol^2$

$a_{N2} = 1366846\ cm^6.bar/mol^2$

$a_{i,j} = (a_{C1}a_{N2})^{0.5}(1 - k_{ij})$

$a_{i,j} = 1929182\ cm^6.bar/mol^2$

$a = a_{C1}x_{C1}^2 + 2a_{i,j}(x_{C1}x_{N2}) + a_{N2}x_{N2}^2$

$a = 1987021\ cm^6.bar/mol^2$

$$b_i = 0.07780\frac{RT_{ci}}{P_{ci}}$$

$b_{C1} = 26.81\ cm^3/mol$

$b_{N2} = 24.01\ cm^3/mol$

$b = x_{C1}b_{C1} + x_{N2}b_{N2}$

$b = 25.41\ cm^3/mol$

The coefficients of the cubic polynomial form can now be resolved:

$$A = \frac{aP}{(RT)^2}$$

$A = 1.277$

$$B = \frac{bP}{RT}$$

$B = 0.204$

Given the polynomial function $Z^3 - (1 - B)Z^2 + (A - 2B - 3B^2)Z - (AB - B^2 - B^3) = 0$,

$Z = 0.357$

The calculated Z value is close to 0.363 (the value computed in PVTsim and HYSYS with the PR EoS) given the inaccuracies involved with hand calculations. It can be concluded that the computed values are reliable.

Appendix C: SRK EoS Application

The same gas mixture (x_{C1} = 0.50; x_{N2} = 0.50) from Appendix B is used for the SRK EoS calculations. Physical and critical property data for methane and nitrogen is therefore carried through for this hand calculation.

The SRK EoS is expressed with P as the subject,

$$P = \frac{RT}{V - b} - \frac{a\,(T)}{V(V + b)}$$

Or in its cubic form,

$$Z^3 - Z^2 + (A - B - B^2)Z - AB = 0$$

Firstly, the mixing parameters are evaluated:

$$m_i = 0.48508 + 1.55171\omega_i - 0.15613\omega_i^2$$

$$m_{C1} = 0.5029$$

$$m_{N2} = 0.5454$$

$$a_{ci} = 0.42748\frac{R^2T_{ci}^2}{P_{ci}}$$

$$a_{cC1} = 2334318\ cm^6.bar/mol^2$$

$$a_{cN2} = 1384259\ cm^6.bar/mol^2$$

$$\alpha_i = \left[1 + m\left(1 - \left(\frac{T}{T_{ci}}\right)^{0.5}\right)\right]^2$$

$$\alpha_{C1} = 1.1168$$

$$\alpha_{N2} = 0.9040$$

$a_i = \alpha_i a_{ci}$

$a_{C1} = 2606860\ cm^6.bar/mol^2$

$a_{N2} = 1251386\ cm^6.bar/mol^2$

$a_{i,j} = (a_{C1}a_{CO2})^{0.5}(1 - k_{ij})$

$a_{i,j} = 1806153\ cm^6.bar/mol^2$

$a = a_{C1}x_{C1}^2 + 2a_{i,j}(x_{C1}x_{CO2}) + a_{CO2}x_{CO2}^2$

$a = 1867638\ cm^6.bar/mol^2$

$b_i = 0.08664\frac{RT_{ci}}{P_{ci}}$

$b_{C1} = 29.85\ cm^3/mol$

$b_{N2} = 26.74\ cm^3/mol$

$b = x_{C1}b_{C1} + x_{N2}b_{N2}$

$b = 28.30\ cm^3/mol$

The coefficients of the cubic polynomial form can now be resolved:

$A = \frac{aP}{(RT)^2}$

$A = 1.201$

$$B = \frac{bP}{RT}$$

$B = 0.227$

Given the polynomial function $Z^3 - Z^2 + (A - B - B^2)Z - AB = 0$,

$Z = 0.399$

The calculated Z value is close to 0.404 (the value computed in PVTsim and HYSYS with the PR EoS) given the inaccuracies involved with hand calculations. It can be concluded that the computed values are reliable.

Appendix D: HYSYS Hydrate Simulation Procedure

Step 1: After creating a new case, a component list is created. The desired gas mixture components are selected from the library offered by HYSYS.

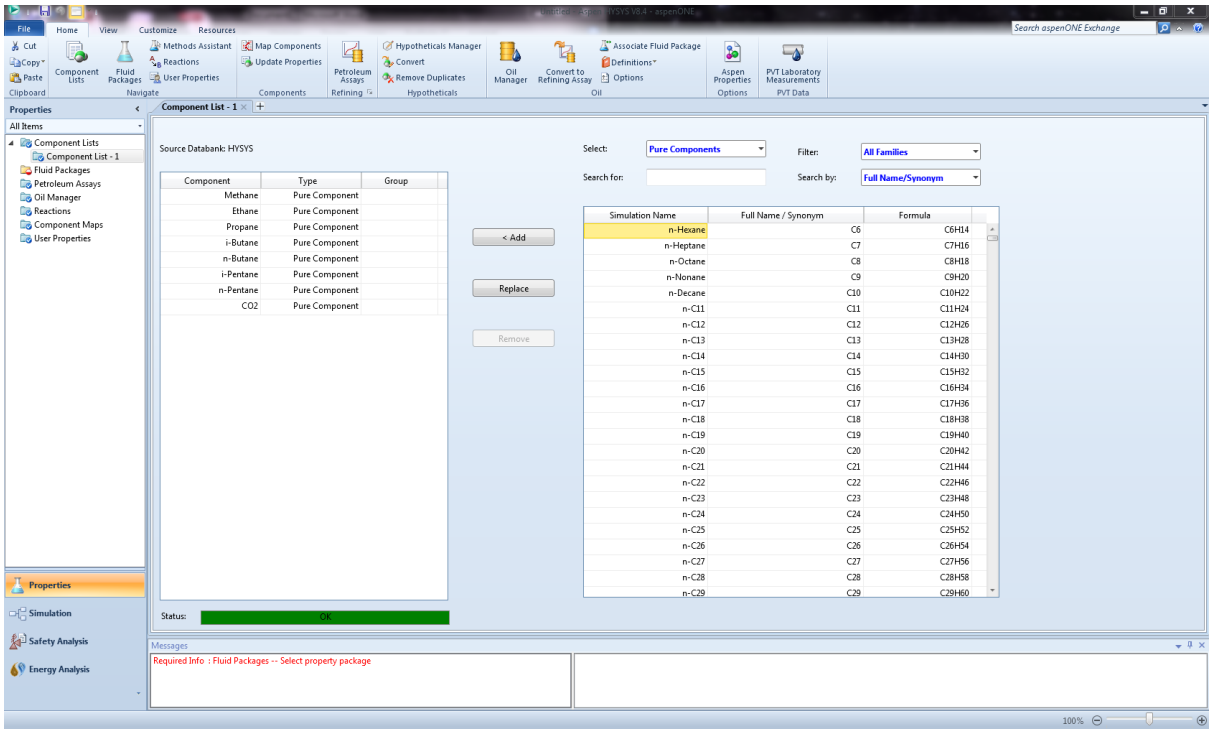

Step 2: An appropriate fluid package was selected for the component mixture, i.e. Peng-Robinson or Soave-Redlich-Kwong.

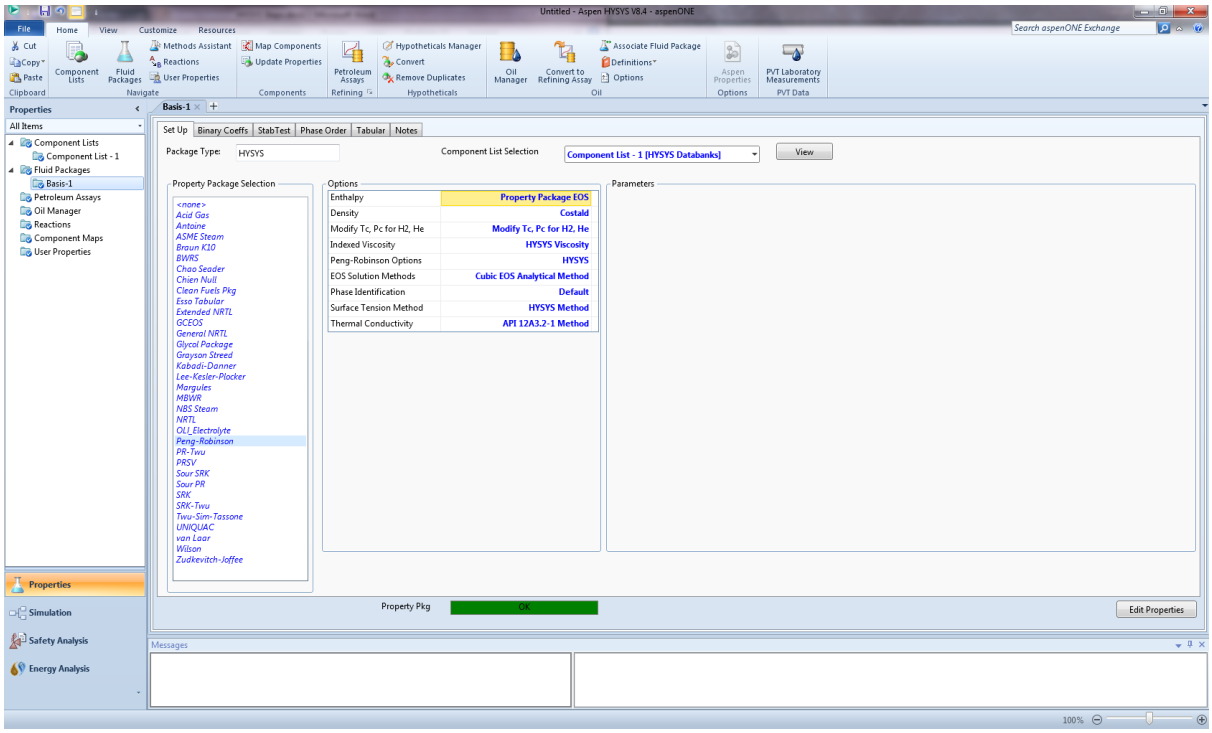

Step 3: Simulation mode was selected and a material stream created for the gas mixture.

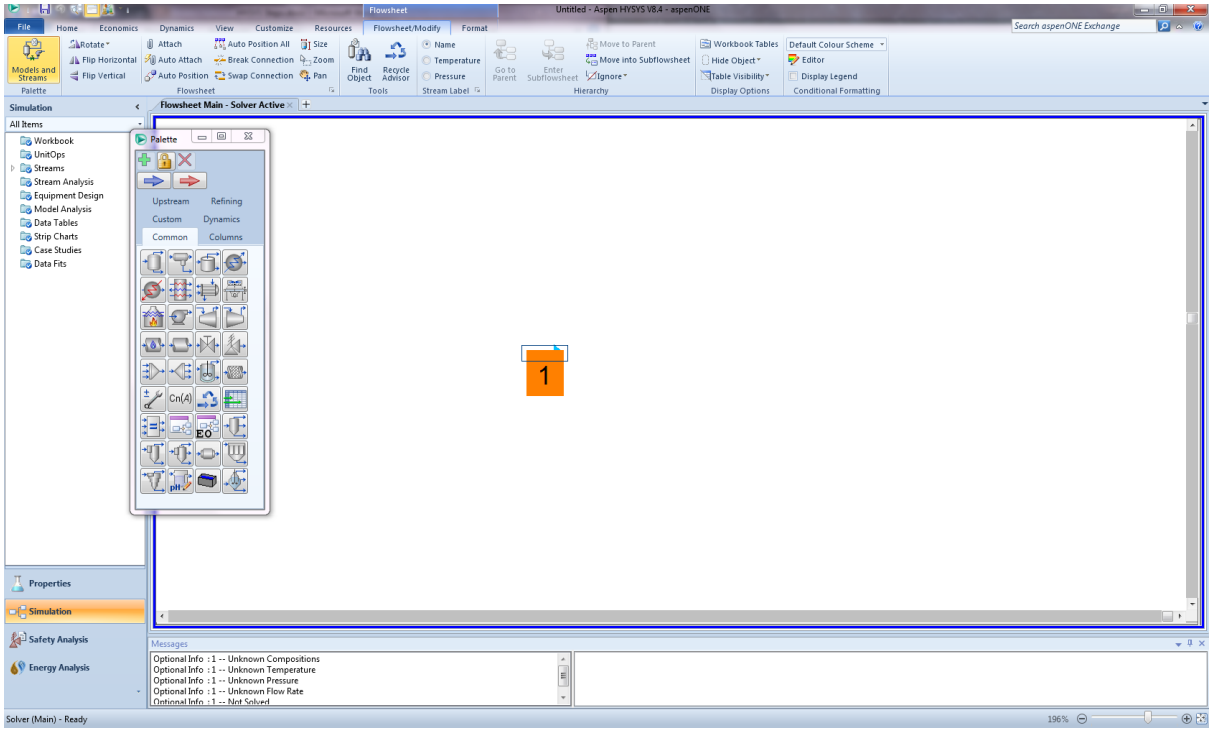

Step 4: The composition of the gas was entered into the created material stream's worksheet ("Composition" tab).

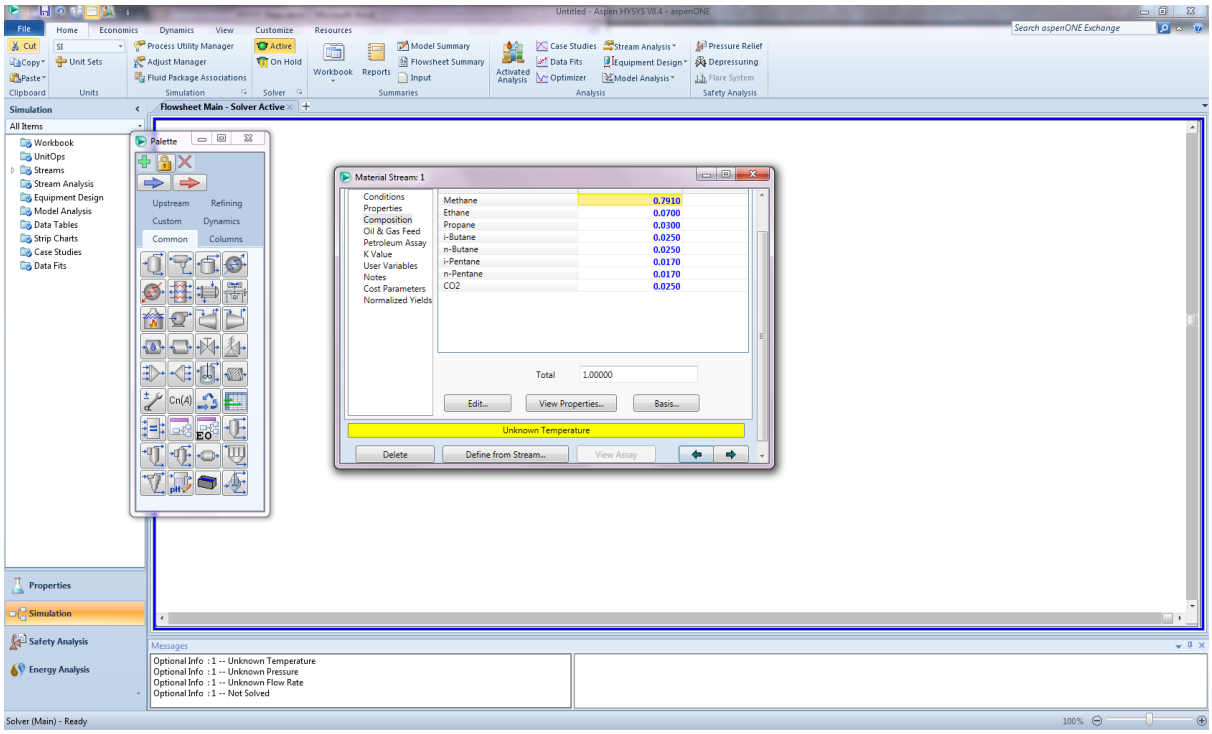

Step 5: The required information was entered for the simulation to solve. For the vapour phase fraction, a value of 1 was set . The desired pressure (e.g. 100 bar) was also input. Arbitrary numbers were input for temperature and mass/molar flow because the hydrate utility requires the simulation to be solved and have no impact on the computed hydrate equilibrium temperature.

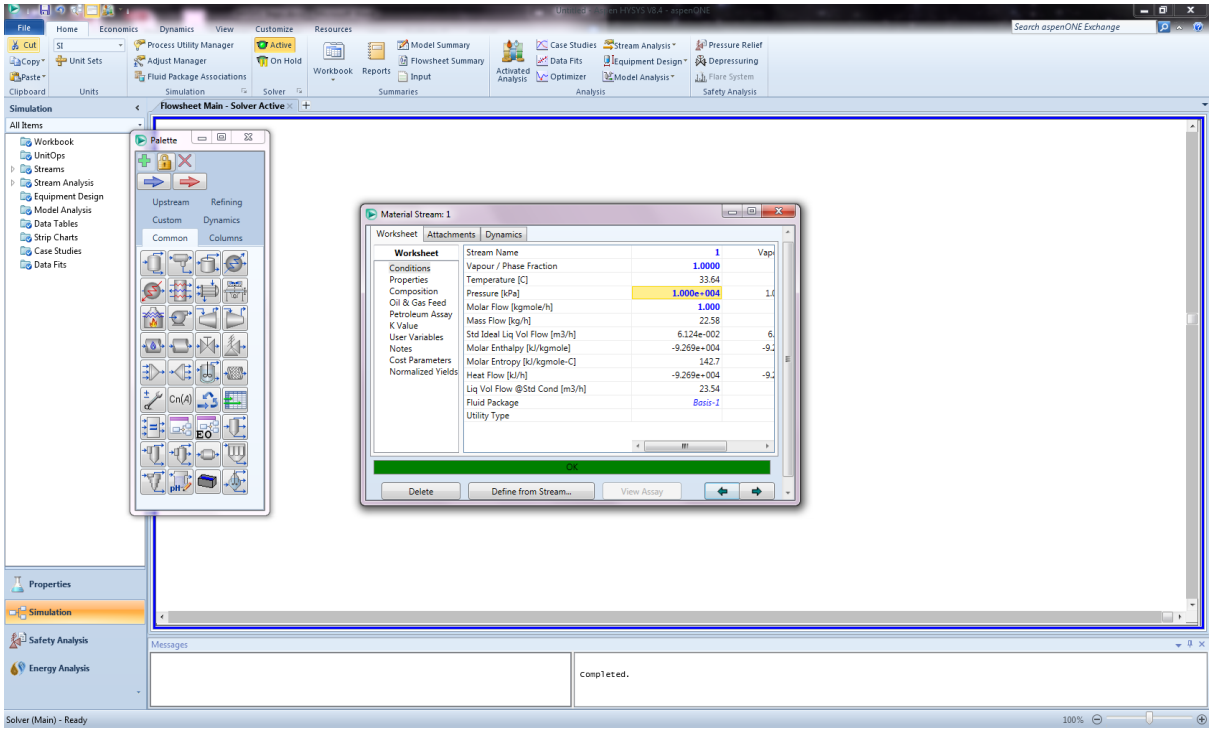

Step 6: Using the hydrate stream analysis utility, the equilibrium temperature is provided for the pressure specified in Step 5. An equilibrium temperature of 20.08 °C was evaluated in this example.

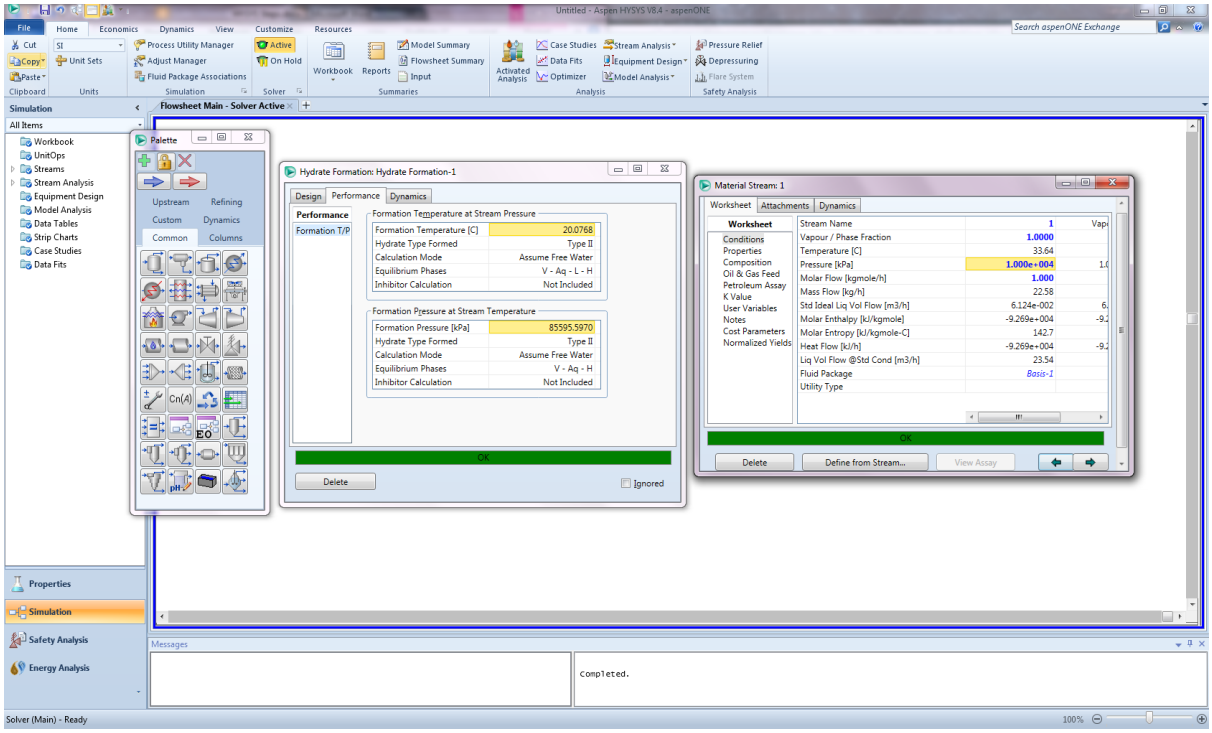
Untitled - Aspen HYSYS V8.4 - aspenONE
Flowsheet Main - Solver Active
Palette
Hydrate Formation: Hydrate Formation-1
Design
Performance
Dynamics
Formation T/P
Formation Temperature at Stream Pressure
Formation Temperature [C] 20.0768
Hydrate Type Formed Type II
Calculation Mode Assume Free Water
Equilibrium Phases V - Aq - L - H
Inhibitor Calculation Not Included
Formation Pressure at Stream Temperature
Formation Pressure [kPa] 85595.5970
Hydrate Type Formed Type II
Calculation Mode Assume Free Water
Equilibrium Phases V - Aq - H
Inhibitor Calculation Not Included
OK
Delete
Ignored
Material Stream: 1
Worksheet
Attachments
Dynamics
Conditions
Properties
Composition
Oil & Gas Feed
Petroleum Assay
K Value
User Variables
Notes
Cost Parameters
Normalized Yields
Stream Name 1
Vapour / Phase Fraction 1.0000
Temperature [C] 33.64
Pressure [kPa] 1.000e+004
Molar Flow [kgmole/h] 1.000
Mass Flow [kg/h] 22.58
Std Ideal Liq Vol Flow [m3/h] 6.124e-002
Molar Enthalpy [kJ/kgmole] -9.269e+004
Molar Entropy [kJ/kgmole-C] 142.7
Heat Flow [kJ/h] -9.269e+004
Liq Vol Flow @Std Cond [m3/h] 23.54
Fluid Package Basis-1
Utility Type
OK
Delete
Define from Stream...
View Assay
Messages
completed.
Solver (Main) - Ready

Appendix E: PVTsim Hydrate Simulation Procedure

Step 1: A new fluid was constructed based on mol%. For all instances, “no plus fraction” was checked because the composition of the heavier components were known and didn’t require extrapolation. The desired EoS (PR or SRK) for hydrate calculations had to be selected prior to entering the details of the new fluid as conflictions sometimes occurred.

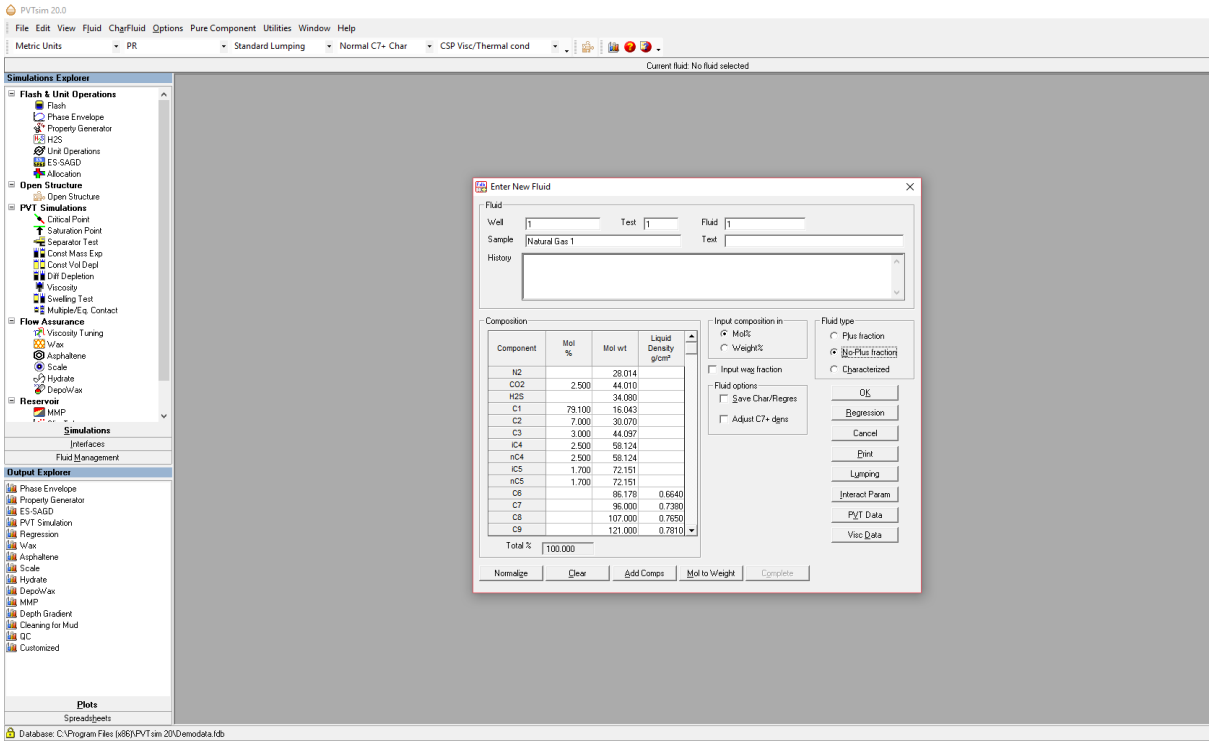

Step 2: Under the Hydrate simulation tab, the water: gas molar ratio, water composition, amount of inhibitor and inhibitor concentration was entered.

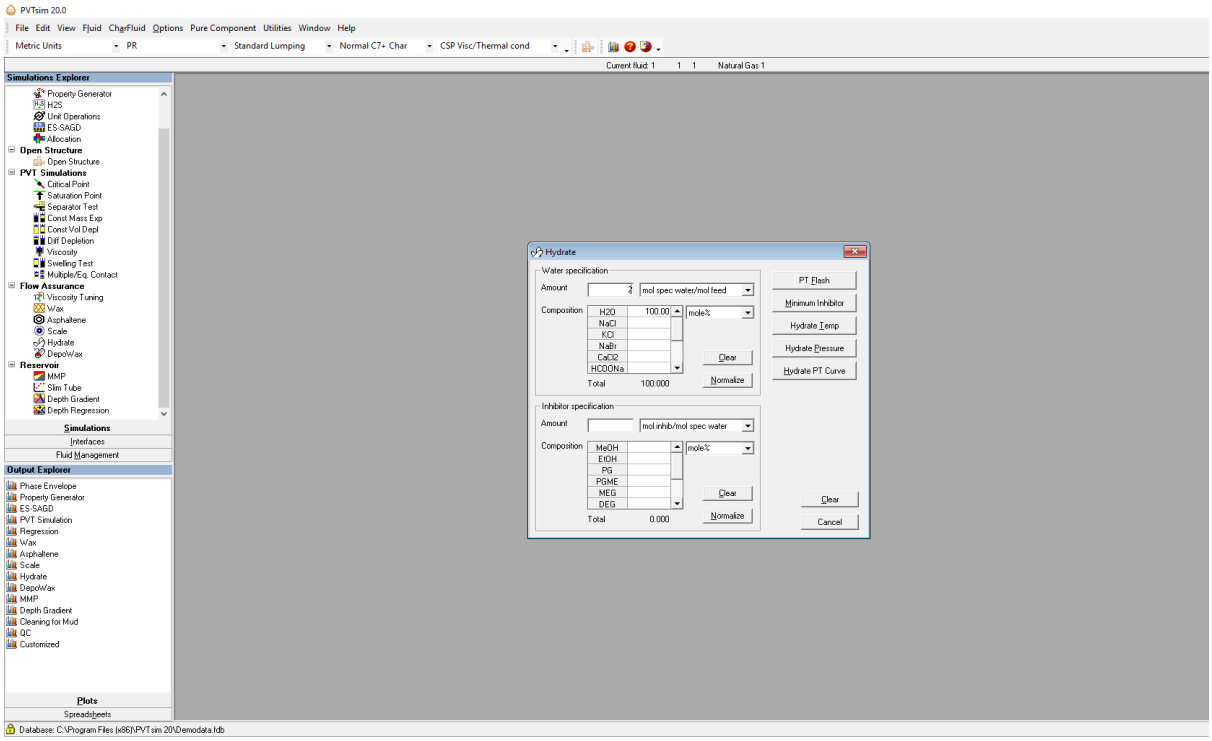

Step 3: The hydrate temperature was of primary interest; PVTsim returns values when given a value for gas pressure.

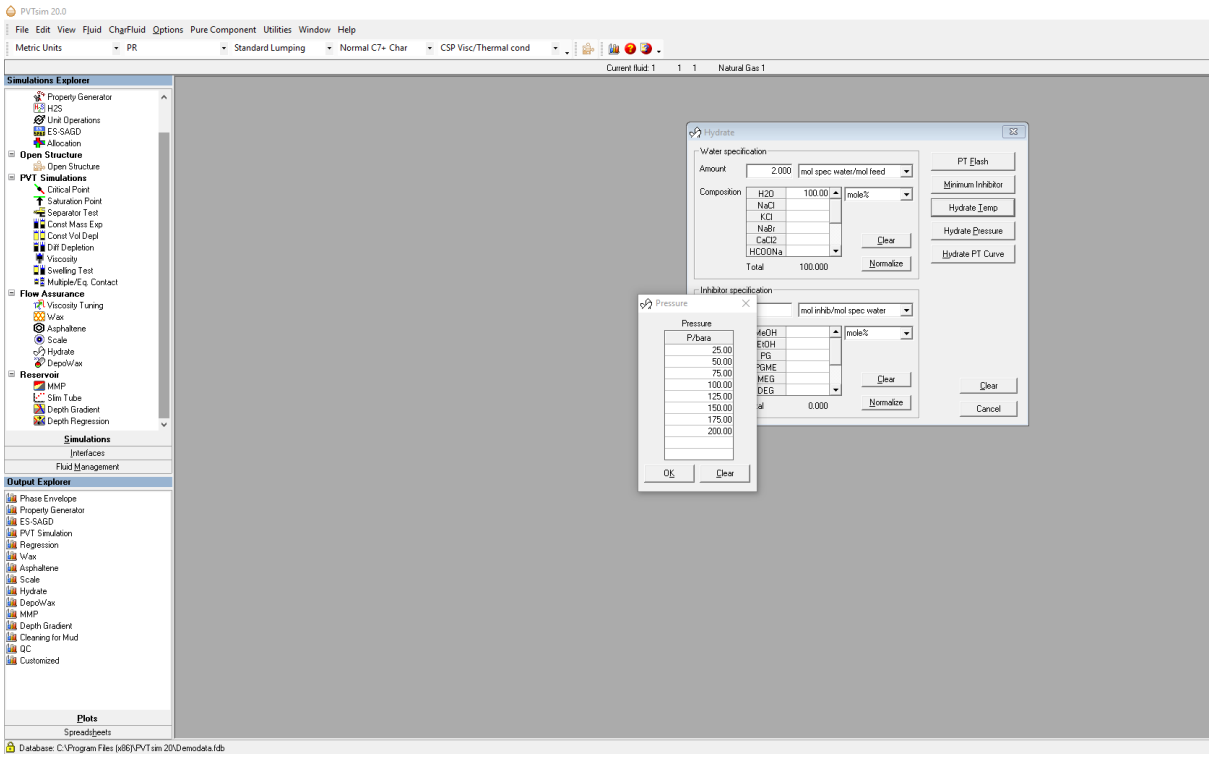

Step 4: The computed hydrate equilibrium temperatures for the prescribed EoS are listed for each pressure fed to the program in Step 3.

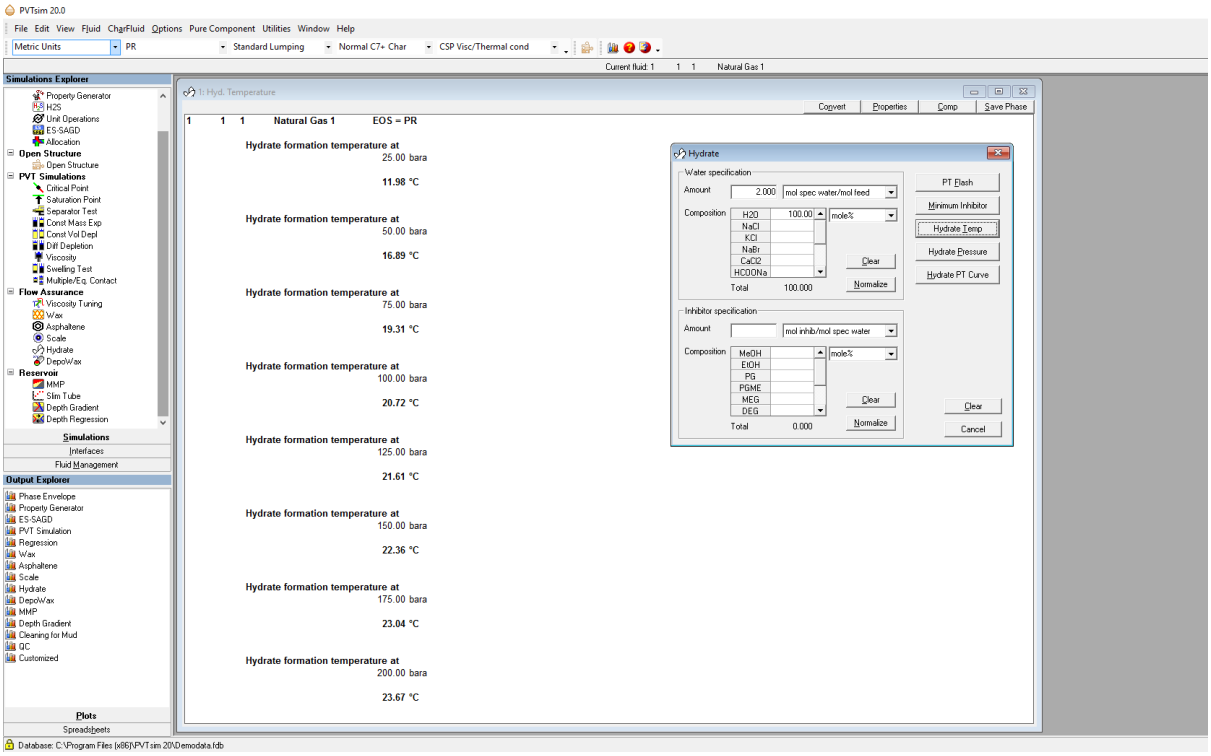

Step 5: Other useful information such as phase compositions and other properties of the system were given by selecting the “Properties” and/or “Comp” tabs.